DOCTOR OF PHILOSOPHY

Sedimentological, geophysical and oceanographic studies of postglacial and contemporary sedimentary processes of the NE Menai Strait and Conwy Bay (Wales, U.K.)

Ali, Asgharali

Award date:
1992

Awarding institution:
Bangor University

SEDIMENTOLOGICAL, GEOPHYSICAL AND OCEANOGRAPHIC STUDIES OF POSTGLACIAL AND CONTEMPORARY SEDIMENTARY PROCESSES OF THE NE MENAI STRAIT AND CONWY BAY (WALES, U.K.)

by

ASGHAR ALI

B.Sc, M.Sc (Punjab)

A thesis submitted in accordance with the requirements of the University of Wales for the degree of **Philosophiae Doctor**.

University of Wales
Bangor
School of Ocean Sciences
Marine Science Laboratories
Menai Bridge, Gwynedd
WALES, U.K.

MCMXCII

I would like to dedicate this thesis to:

My Father, MUHAMMAD HUSSAIN AWAN *(Rahmt Allah Alyh)*

My Mother

Sister Shahnaz, brothers; Zulfiqar, Qamar, Yousaf,

Akhtar, Moien, wife Tahira and son Umar

ABSTRACT

Various sedimentological, geophysical and oceanographic techniques have been used to study postglacial and contemporary sedimentary processes in the NE Menai Strait and Conwy Bay.

Seismic records show three main reflectors, which delineate three depositional sequences (glacial, post-glacial and modern). The maximum recorded depth of the Pre Quaternary bedrock is 99m O.D. Newlyn, northeast of Puffin Island in a channel-filled structure which is probably an extension of the Dinorwic Fault. Variations in thickness of modern sediment deposits indicate the dynamic nature of sedimentation in the area.

Tidal currents have been measured over spring/neap cycles at several stations. It is shown that residual currents in the NE Menai Strait are to the southwest though near Great Ormes Head (in the northern part of the study area) they are to the northeast. It is shown that sedimentation in this macrotidal coastal area is controlled primarily by tidal currents.

Most of the seabed is covered by sands with local occurrences of gravelly sands, muddy sands, and sandy muds. The area can be subdivided into 5 subareas on the basis of sediment type, statistical grain size parameters, configuration of grain size distribution curves, and percentages of organic matter and carbonate. In *Area A* (near Bangor Pier) the sediments are very fine sands to medium silts, poorly and very poorly sorted, very positive skewed. The sediments are dominated by intermittent suspension and suspension populations. The sediments of *Area B* are: unimodal, fine and very fine sands, very well sorted, positively skewed, leptokurtic, and the dominant mode of transport is intermittent suspension. In the main channel area of the Menai Strait (*Area C*), mean grain size ranges from gravel to fine sands, sorting is spatially very variable, skewness is very negative, and sediment transport modes are surface creep and intermittent suspension. Northeast of Puffin Island (*Area D*) sediments are: poorly to very poorly sorted, negative and very negative skewed, and sediment transport modes are surface creep, intermittent suspension and suspension. Near Great Ormes Head (*Area E*), sediments are poorly to very poorly sorted, very positively skewed and the dominant transport mode is suspension.

Small-scale ripples are the most abundant surficial bedforms in the intertidal areas where the sediments are fine grained and current velocities are relatively low. More than 80% of the observed megaripples are found in those areas where the water depth is between 9m and 11m and mean grain size >3.0ϕ. Sandwaves predominate in those areas with water depth >11m, where the grain size is <2.75ϕ. Sandwaves also occur in intertidal areas where water depths are 4-6m at high water and sediment size is 2.0-2.5ϕ.

Calculated sediment transports at 12 hydrographic stations (subtidal area) vary from 1 to 136 kg cm^{-1} per tide depending mainly on sediment grain size and current velocity. In intertidal areas, the rate of flood dominant sediment transport increases away from the Arfon coastline towards the main channel in the Menai Strait and increases to the southwest as the Menai Strait narrows. Residual sediment transport is generally in the flood direction.

It is shown that the net sediment transport in the area is to the southwest since: (1) bedform asymmetries are in the flood direction; (2) trends of grain size fining, regionally improved sorting, and a change from negative to positive skewness are to the southwest; (3) calculated residual transport vectors are also to the southwest.

ACKNOWLEDGMENTS

I would like to express special thanks and gratitude to Dr Colin Jago for proper guidance, constructive criticism, useful suggestions, enduring patience and continual inspiration, throughout my study period. His supervision and help enabled me to achieve this target.

I am highly grateful to all members of the technical staff for their help in the field and in laboratory, in particular, Gwyn Jones, Alan Nield, Geraint Williams, Frank Dewes; William Rowntree for the photography of box cores and duplicating aerial photographs.

Thanks to the captains and crews of the research vessels Prince Madog and Lewis Morris of UCNW Bangor.

Many thanks to Dr Jim Bennell for his help and support in the collection of geophysical data, and his expert advice in the interpretation and processing of this data. I would also thank Dr Garry Reid for his help in the sediment sampling programme.

I would like to acknowledge Dr Sarah Jones for her help in grain size analysis, computation of statistical parameters by computer programmes and sediment transport calculations.

Thanks to all those colleagues who helped me at various stages of my studies in the School and in the field, in particular Reginaldo Durazo, Dei Huws, Dr Ian McDermott, Fajin and A. Al-Barkati. Thanks to all my country fellows; Saleem Khan, Abdus Salam, Saeed Soomro, Tanwir, Murtaza, Ayub, and Khalid at UCNW Bangor for their companionship and moral support.

Thanks also to Drs Toby Sherwin, Alan Elliott, Dave Bowers and Prof. John Simpson for assistance in understanding the current meter data; Dr Ivor Rees for providing information about Lavan Sands; Dr John Matthews for interpretation of aerial photographs and Landsat imagery of the area.

I would like to say thanks to Prof. Denzil Taylor Smith (Head of School) for providing facilities to carry out this research.

Back at home, with the support and help of M. Hussan, M. Arif, M. Yaqoob, M. Shareef, M. Rafiq, M. Rashid and Dr A. Awan, I was enabled to fully concentrate on studies. I must say thank you to you all. Thanks also to my friends; Riaz Tahir, Col. Wahid, M. Saeed, Arshid, Auranzeb, Tariq and Dr Raza Yasin for good wishes. Iftikhar Ahmad (Late), you are in my mind now.

Finally I wish to acknowledge the financial support of the Ministry of Science and Technology, Government of Pakistan.

CONTENTS

CHAPTER - 4

HYDROGRAPHIC STUDIES OF THE AREA

CHAPTER - 5

SEABED SEDIMENTS: SIZE DETERMINATION AND INTERPRETATION

CHAPTER - 6

SEDIMENT TRANSPORT

CHAPTER - 7

BEDFORM OBSERVATIONS AND SEDIMENTARY STRUCTURES

Part-I:

Bedform Observations from Photographs and Surveys

Part - II:

Bedform Sedimentary Structures from Box Cores

CHAPTER ONE

INTRODUCTION

Studies of tidal sedimentary environments began when Kindle [1917] made a descriptive summary of ripple mark occurrence from several environments and included data and illustrations from the tidal flats of the Bay of Fundy. Subsequently, Krumbein [1932, 1934, 1938, 1939, 1953] studied the sedimentary processes of the Gulf of Mexico Coast, and was one of the first to show that the grain size distributions of modern sediments are sensitive to hydrodynamic conditions. Inman & Chamberlain [1955] working on nearshore sediments, concluded that the different forms of grain size distribution curves are due to different transport mechanisms, and to varying amounts and types of sediment supply. The detailed results of grain size studies by Steward [1958] showed how textural and compositional properties are closely linked to environmental processes.

There was an upsurge in tidal flat sedimentological research in the late 1950's and 1960's. Van Straaten conducted major sedimentological studies of intertidal areas [Van Straaten, 1952, 1954, 1959, 1961; Van Straaten & Kuenen, 1957]. Similar studies were carried out along the northwest coast of Germany by Reineck [1963, 1967, 1972] and Reineck & Wunderlich [1968], and along the coast of eastern England (the Wash) by Evans [1965, 1976], Evans & Collins [1975], and McCave & Geiser [1978]. These studies emphasised the importance of sedimentary structures and the spatial distribution of different sediment textural groups.

Variations of tidal current velocities and their duration were recognised as being the major control for sediment distribution across tidal flats.

More recently Visher [1969], Middleton [1976] and Sagoe & Visher [1977] have emphasised the effects of the transporting fluid on sediment grains and have provided a base for the interpretation of hydrodynamic conditions from grain size distributions. Several techniques have been used to interpret sedimentary environments from grain size distributions such as scatter plots of sorting against skewness [Friedman, 1961], analysis of log-probability cumulative weight percentage frequency curves [Visher, 1969] and plots of quartile-deviation versus median-diameter on double-logarithmic graph paper [Buller & McManus, 1972a, b; 1973a, b, c].

Bedforms in intertidal coastal areas have received particular attention in the literature [Collinson, 1970; Klein, 1970; Costello, 1974; Allen & Friend, 1976; Dalrymple, Knight & Lambiase, 1978; Terwindt, 1971, 1981; Costello & Southard, 1981; Collinson & Thompson, 1982; Terwindt & Brouwer, 1986]. From the wide range of hydrodynamic conditions encountered in these studies, it has been shown that tidal current velocity, flow depth, and grain size are the controlling parameters for the occurrence of the different bedforms in tidal environments. The shape, size and rate of migration of tidal bedforms is determined by the degree of time-velocity asymmetry of the

tidal currents. Study of the internal structures of bedforms formed by tidal currents shows that the prevailing structure developed is cross-stratification demarked by sharp set boundaries. A common structure is in the form of herringbone cross-bedding which forms in response to diurnal inequality of tidal flows. According to Reineck [1963, 1970], the internal organisation of the cross-bedding may be simple or complex depending mainly on the hydrodynamic conditions and surficial sediment grain size.

The aims of this project were to study prevailing hydrodynamic processes, postglacial and contemporary sedimentary processes in the North Eastern Menai Strait and Conwy Bay (Fig. 1.1). For this purpose data from the area have been collected using various sedimentological, geophysical and oceanographic techniques; the results have been compared and integrated to produce a sedimentary model of the area.

Previous work in the study area has included various M.Sc. projects undertaken in particular areas of the Strait. Those of a relevant sedimentological or geophysical nature which have provided some background information on some parts of the study area are given here. Fouere [1966] studied the textural parameters of surface sediments between Menai Bridge and Beaumaris. From Bangor Pier toward Beaumaris, 35 sediment samples were collected on a grid of 100 meters to 1.5 kilometer. Hind [1974] carried out a sedimentological and geotechnical examination on the sediments of parts of the Lavan Sands. Walker [1977]

Fig: 1.1 Location Map

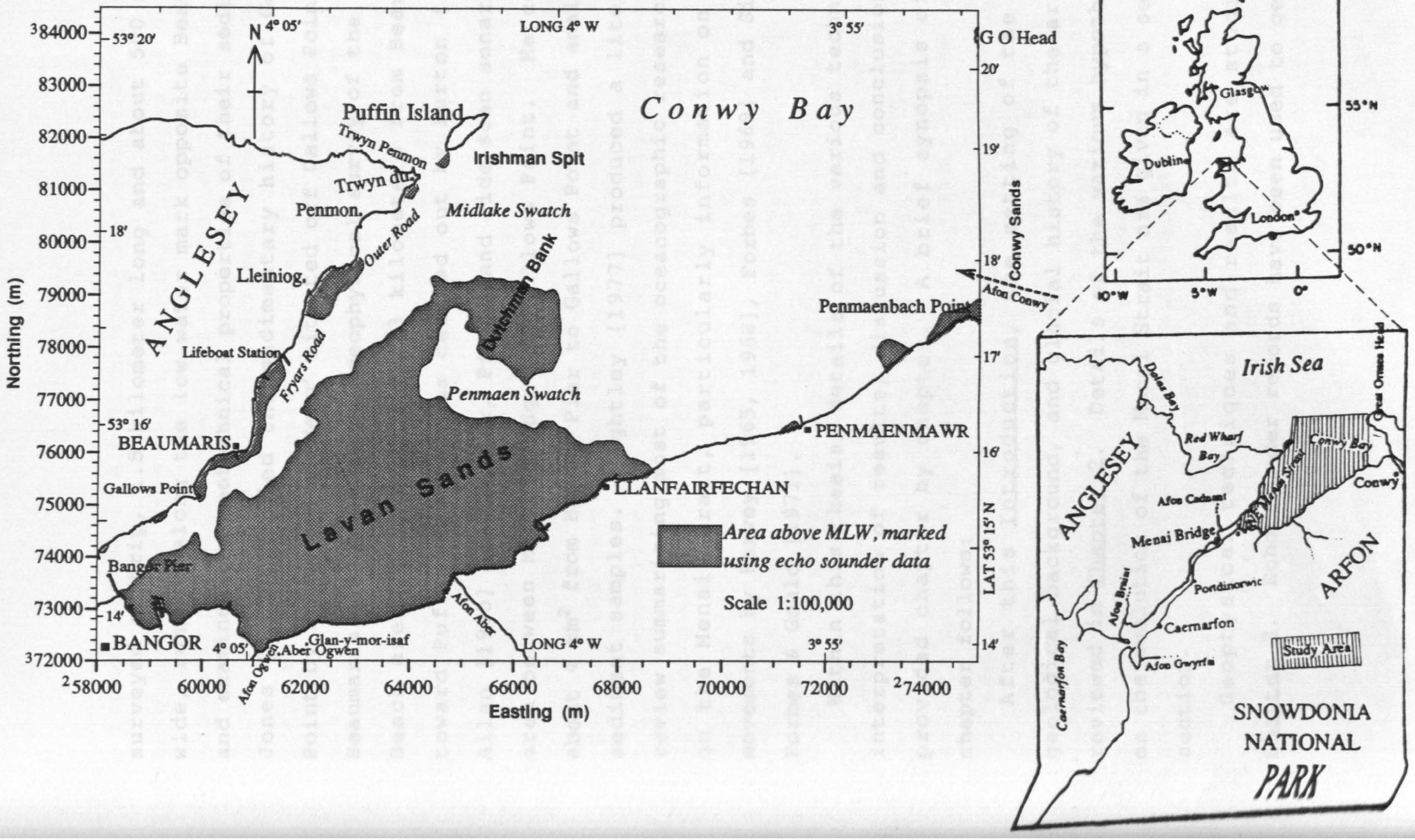

surveyed a strip, 1.5 kilometer long and about 500 meters wide, running along the low water mark opposite Beaumaris and examined the geotechnical properties of their sediments. Jones [1978] studied the sedimentary history of Gallows Point by examining a *'deep'* situated off Gallows Point near Beaumaris. A geotechnical/geophysical survey of the Penmon Beach area (about 1.3 km^2), 3 kilometers from Beaumaris toward Puffin Island, was carried out by Burton [1984]. Allan [1985] used Boomer, Pinger and side scan sonar in an area between Menai Bridge and Gallows Point. He covered about 4 km^2 from Bangor Pier to Gallows Point and analysed 9 sediment samples. Kightley [1977] produced a literature review summarising most of the oceanographic research work on the Menai Strait, particularly information on water movements by Harvey [1965, 1968], Forbes [1969] and Simpson, Forbes & Gould [1971].

Within this thesis, details of the various techniques, interpretation of results, discussion and conclusions are provided chapter by chapter. A brief synopsis of each chapter follows:

After this Introduction, the setting of the area, geological background, and glacial history of the area are reviewed in Chapter 2. Details of the various hypothesises on the evolution of the Menai Strait are given in a separate section.

Geophysical techniques and results are studied in Chapter 3. Echo sounder records have been used to generate

a bathymetric map. A bedform study was conducted using side scan sonar, and from these records, the types of bedforms and their migration directions are studied in details. The second part of this chapter comprises results obtained from different subbottom seismic sources i.e., sparker, boomer and pinger. From these seismographs, three seismic sequences deposited during the Holocene have been identified. A seismic stratigraphic analysis is given at the end of this chapter.

The results of hydrographic survey at 12 fixed stations from the study area are discussed in Chapter 4. At four stations the current meters were deployed for a complete lunar time series and from the other stations current data were obtained for a period of one tidal cycle. After analysis of current meter data, these results and previous available hydrographic information about the Menai Strait were used to predict a model of currents in the study area.

Chapter 5 is devoted to surficial sediment sampling and grain size determinations and distributions. Sediment grain size is an essential component of any study of sedimentary processes. In this study 235 sediment samples were grabbed during various cruises using the research vessels, Prince Madog, Lewis Morris and Robyn. Three laboratory techniques (sieving, fall tower and sedigraph) were used for grain size analysis of gravel, sand and mud fractions. Results from replicates of 46 samples used to calculate instrumental and procedural errors for different grain size parameters are also discussed in detail. A comprehensive examination of

the spatial distribution of sediment types and numerical descriptors are presented to differentiate zones of different sedimentary environments in the area. On the basis of surficial sediment types, the area has been divided into 5 subareas. Various methods were used to compare the grain size parameters of different subareas to discriminate their sedimentary processes. From the interpretation of particle size distribution curves, the modes of sediment transport in different subareas have been determined on the basis of the ideas of Visher [1969] and Sagoe & Visher [1977].

Sediment transport rates at various stations, calculated using physical parameters such as grain size and current velocity, are discussed in Chapter 6. The assessment of sediment transport rate involves the selection of suitable sediment transport rate formulae from the many formulae currently available. Transport rates in the study area were calculated from Engelund & Hansen's [1967] total load equation and Hardisty's [1983] bedload formula.

In Chapter 7, the relationships between surface processes and sedimentary features are presented; this is obviously significant to an understanding of depositional and transportation processes in such intertidal areas. The external shape and configuration of bedforms and their internal sedimentary structures depend mainly on current velocity, water depth, grain size and sedimentation rate. As such, bedforms are critical to an understanding of the

processes and conditions of sedimentation. The external shape and size of the bedforms in the intertidal area were examined using aerial and ground photographs, and in situ measurements through field visits of the area. Extensive box core sampling (using Senckenberg boxes) was carried out at low tide. In this chapter, the field procedure of box coring and the laboratory technique of impregnation to highlight the relief of internal sedimentary structures are explained in detail. From the internal sedimentary structures, the prevailing current regime in the area have been determined, the percentage of sediment movement in flood and ebb directions calculated, and the dominant transport directions on each coring position determined.

The final chapter is a summary of the work and some suggestions for future work are given.

CHAPTER TWO

SETTING, GEOLOGICAL AND GLACIAL BACKGROUND

2.1 Setting of the Area

The study area comprises Conwy Bay and the north-eastern part of the Menai Strait in the Irish Sea, North Wales (Fig. 1.1). The total area is about 115 square kilometres. In the south-western part of Conwy Bay is the Menai Strait; a long narrow stretch of water running in a NE-SW direction up to Caernarfon Bay, with a width of from 268 m to 6.4 km and length 24 km, with an average tidal flow of 30 * 10^6 m^3 in 12.5 hours in a south-westerly direction [Harvey, 1968]. The area is bounded on the south and south-east by the mainland of Gwynedd and on the south west by Anglesey; the north and north western boundary opens to the open sea (Irish Sea). Conwy Bay is entered between Trwyn-du and Great Ormes Head, 9.56 km east-north-eastward. Dutchman Bank and Lavan Sands (Traeth Lafan) occupy the south western part, and are most prominent features of the Bay. Lavan Sands, about 32 km^2, in area are sand and mud flats which are exposed at low tide. Dutchman Bank dries at low tide up to 3 m in places. Penmaen Swatch is a comparatively deep channel which does not dry at low tide and separates the Lavan Sands from the Dutchman Bank. Midlake Swatch separates the Irishman Spit from Dutchman Bank [Hydrographic Department, Admiralty 1960; Decca Chart nos. 1464, 1826, 1977 and 1978].

2.2 Geological Background

The shore areas adjacent to the study area contain rocks and geological structures of which range in age from Precambrian to Carboniferous. A geological map and a rock succession of the North Wales are shown in Fig. 2.1 and Fig. 2.2, respectively. Greenly [1919] comprehensively studied the area and is the main source of geological information. Among other prominent geological writers on this area are: Shackleton [1954, 1956, 1969], Maltman [1975], and Barber & Max [1979] for Precambrian studies; Bates [1968, 1972, 1974] on the Ordovician; and Allen [1965] on the Devonian.

On the Anglesey side of the Menai Strait, from Menai Bridge towards Puffin Island, the rocks are of Precambrian to Carboniferous age i.e., Gwyna Green schist (the Mona Complex) of the Precambrian, Arenig shales (Ordovician) and Lower Carboniferous Limestone. On the mainland side of the Menai Strait, from Bangor towards Conwy, the rocks are Carboniferous Limestone; Lower Cambrian tuff and sand stone; Arenig shales (Ordovician) over which Cegin river flows; on both sides of the mouth of the River Ogwen are andesites and again, Arenig shales up to Penmaenbach. Contemporaneous igneous rocks and Arenig shales lie between Penmaenbach and Conwy. The surface rocks on Great Ormes Head are Carboniferous Limestone. [Smith & George, 1961; BGS, South Sheet and Sheet 106, 1979].

The oldest rocks in the area are Precambrian and belong to the Mona Complex described by Matley [1928], Greenly [1928] and Shackleton [1954, 1956, 1969]. The

interpretation of the Mona Complex in tectonic terms is discussed by the Roberts [1979]. The Mona Complex contains various types of metamorphic and igneous rocks. The metamorphism and deformation which affect the Mona Complex were accompanied and thereafter followed by acid volcanism that gave rise to the Arvonian Series.

Marine Cambrian sediments ~~thus~~ begin with conglomerate which, in places, succeeds the Arvonian conformably. Elsewhere, as the sea broadened and deepened, conglomerates and sandstones rest unconformably upon the Arvonian and even, as at Trefdraeth on Anglesey, upon the Mona Complex. Uplift and folding in the Late Cambrian led to erosion and in west and north-west several thousand feet of Cambrian strata were stripped off. Thus on Anglesey and in Arfon in the north west, basal Arenig (Ordovician) sediments rest on various members of the Precambrian. The Caledonian Orogeny which took place at the end of the Silurian period provided major tectonic and orogenic disruption of most of the United Kingdom and its effect can be seen in North Wales in the dominant northeast-southwest trend. This trend was maintained by all subsequent deposition and indeed controlled the flow direction of the Pleistocene ice sheets to a large degree. Thus, deposition of Old Red Sandstone and Carboniferous rocks was largely controlled by this trend and took place in narrow gulfs, opening to the northeast, resulting in unconformity on lower Palaeozoic and Precambrian rocks; they are comprised of basal sandstones

Fig: 2.1

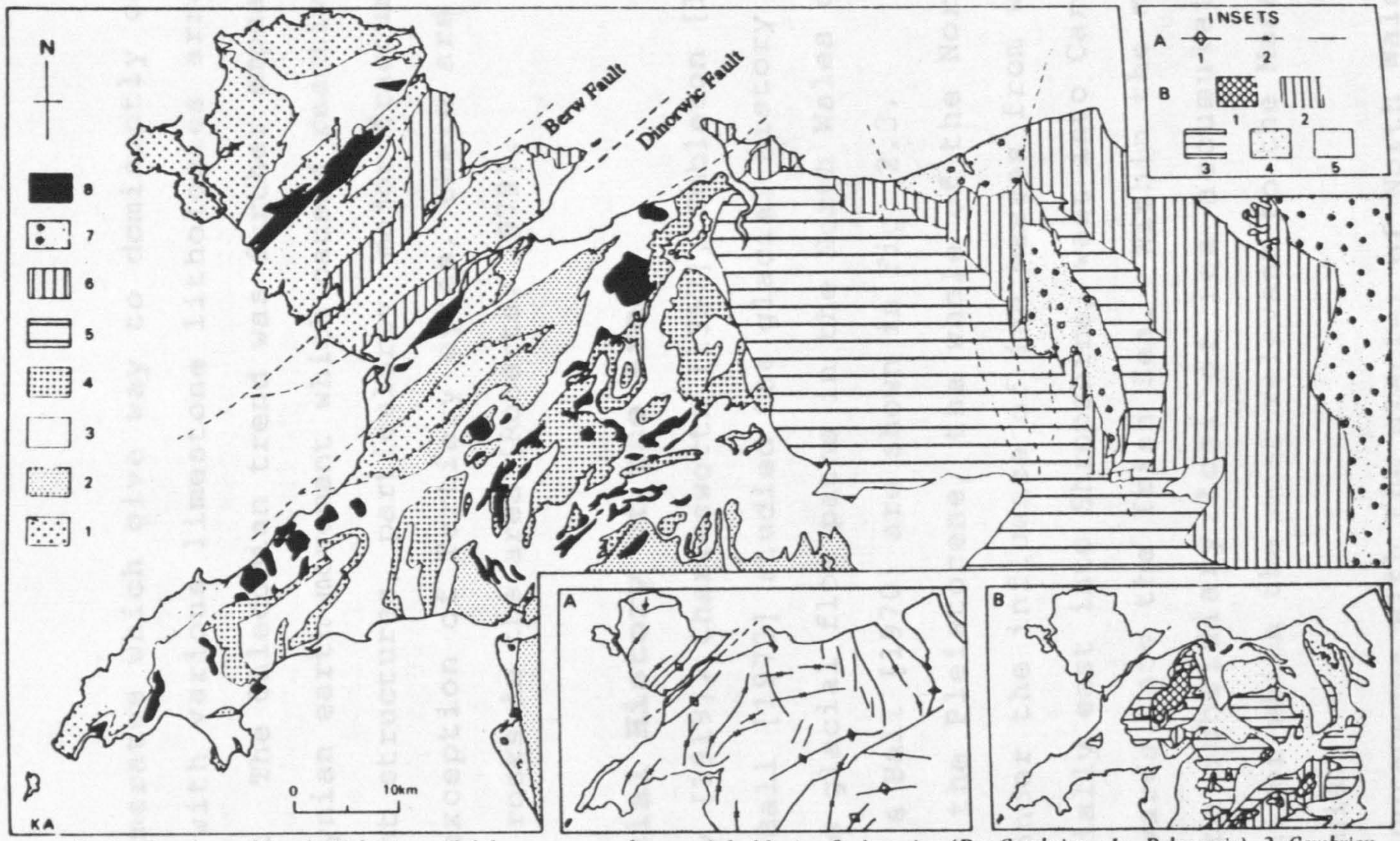

Regional geology of North Wales (compiled from a range of sources) 1, Monian & Arvonian (Pre-Cambrian→Lr. Palaeozoic). 2, Cambrian sediments. 3, Ordovician - primarily sediments. 4, Ordovician - primarily volcanics. 5, Silurian sediments. 6, Carboniferous sediments. 7, Triassic sediments. 8, Intrusive igneous rocks. Insets: (a) *Primary structures: 1, anticlines. 2, synclines. 3, faults (largely after Smith & George 1961).* (b) *Brown's (1960) erosion surfaces: 1, Monadnock group. 2, High Plateau. 3, Middle Peneplain. 4, Low Peneplain. 5, Platform remnant.*

NORTH WALES

Fig: 2.2 The thicknesses of the Pre-Cambrian rocks are not to scale; the rest of the section is on a scale of approximately 1 inch to 10,000 feet.

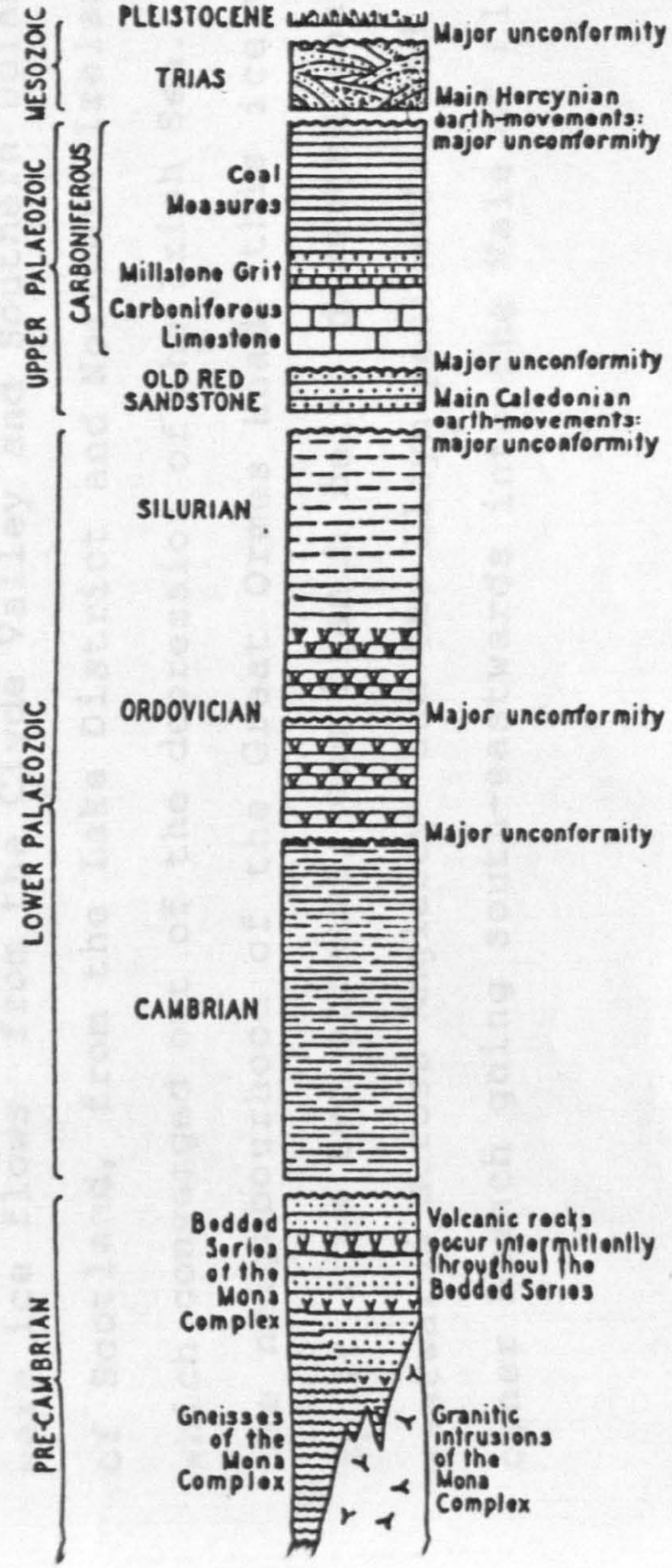

The rock succession in North Wales

and conglomerates which give way to dominantly carbonate sequences with various limestone lithologies arranged as cyclothems. The Caledonian trend was further emphasised by later Hercynian earth movement which caused reactivation of the basement structures, particularly major fracture lines. With the exception of Tertiary dykes, there are no post Palaeozoic rocks in the area [Roberts, 1979].

2.3 Glacial History of the Area

Greenly [1919], Charlesworth [1957], Embleton [1964] and Whittow & Ball [1970] studied the glacial history of North Wales. The glacial flow paths in the North Wales described by Whittow & Ball [1970] are shown in Fig. 2.3.

During the Pleistocene, the whole of the North Wales area was under the influence of ice masses from which ice flowed radially east into Shropshire, west into Cardigan Bay and northwards into the Irish Sea. Within the main area there were subsidiary loci of ice accumulation and development of which the most relevant to the Menai Strait was Snowdonia.

Contemporaneous with the glacier of North Wales, there were ice flows from the Clyde Valley and Southern Uplands of Scotland, from the Lake District and Northern Ireland, which converged out of the depression of the Irish Sea. In the neighbourhood of the Great Ormes Head, this ice was spilt into two streams; one branch being diverted south-westwards across Anglesey and the Lleyn peninsula, and the other branch going south-eastwards into the Vale of Clwyd

and Dee [Smith & George, 1961].

There were several advances and retreats of both ice sheets, evidence for which is seen by overlapping emplacement of boulder clays and glacial till; the Anglesey till being grey boulder clay containing shales and volcanic fragments, whereas the Irish Sea till contains erratics of northern rock types such as Lake District granite fragments, riebeckite microgranites (Ailsa Craig type) and has a definite kaolinite content which is not seen in the Anglesey clay [Whittow & Ball, 1970]

The most important post-glacial change which has affected this area is the eustatic rise of the sea level. Godwin [1943] stated that this post-glacial rise commenced at 10,300 B.P. and was completed during the Atlantic Period (7,500-5,000 years B.P.). This rise in sea level has resulted in the drowning of river valleys such as the Conwy. Since completion of the eustatic rise in sea level, minor isostatic oscillations have taken place, but it would appear that overall post-glacial submergence has not yet overtaken glacial emergence as the Anglesey and Caernarfon wave cut platform is still above sea level [Godwin, 1943].

Around the Anglesey and Mainland coasts, clay cliffs are situated in many areas. It appears that a large part of the sediment masses in Conwy Bay is the result of erosion and transportation of these cliffs as is currently taking place just east of the mouth of Ogwen river. Another source of sediment supply to this area could be the material eroded

Fig: 2.3

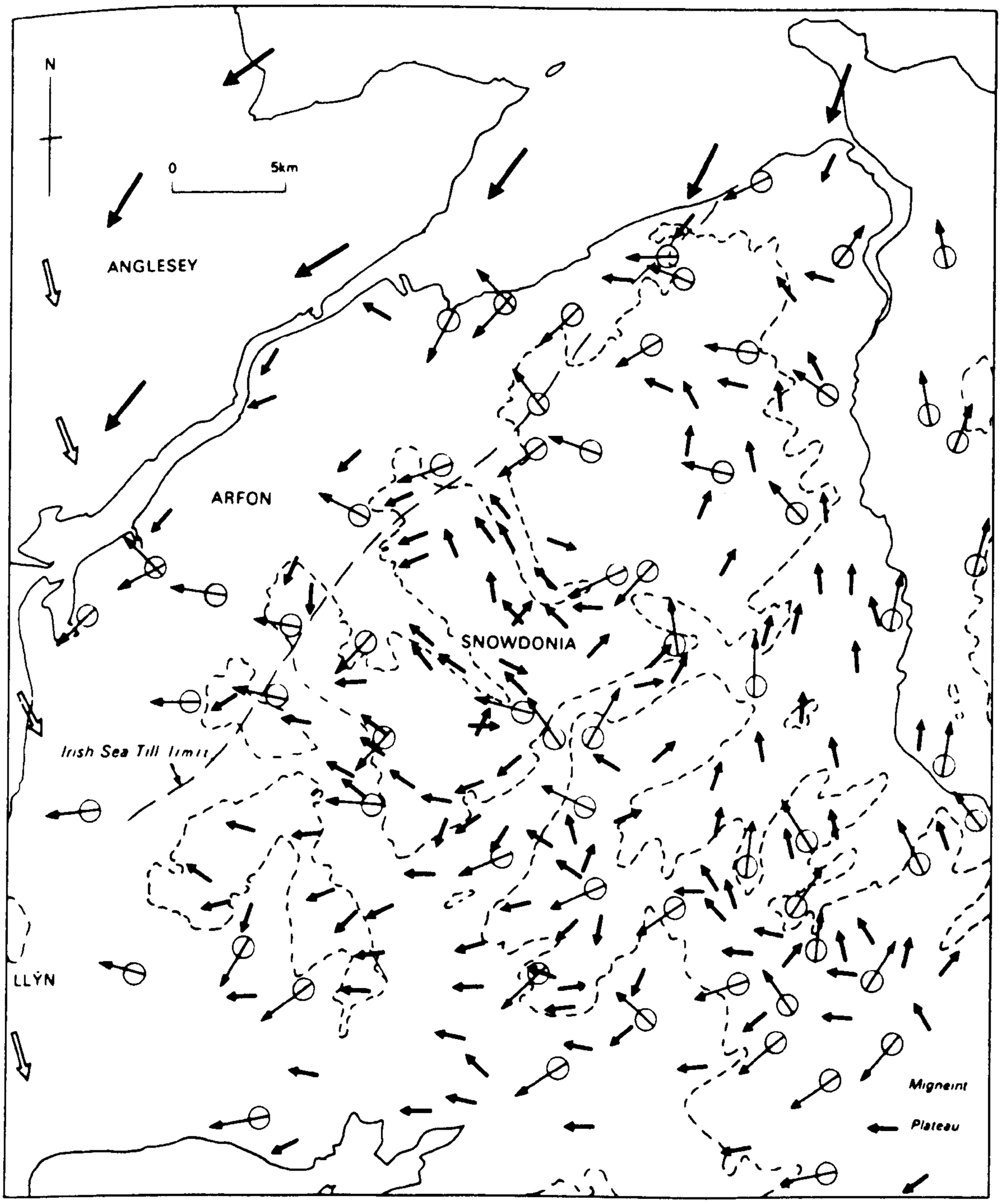

Regional ice-flow directions, north-west quadrant of the Late Devensian Welsh Ice-sheet based on striae & streamlined landforms → and till fabrics ⇉ Irish Sea Ice-sheet flow at first ⇦ and second ⬅ phases (after Whittow & Ball).

from the sea floor itself. Most of Conwy Bay is floored by in situ boulder clay and the Irish Sea and Celtic Sea are floored, in the main, with sand and lag-gravel deposits [Stride, 1963].

Finally, the most recent of all sediments in this area are the dune and marsh deposits, for example, the salt marsh area between Llanfairfechan Spit and the mainland, and the sand dunes of the Lavan Sands [Hind, 1974].

2.4 Formation of the Menai Strait

The Isle of Anglesey and the Arfon mainland comprise a series of parallel depressions, and the Menai Strait is believed to be one of these. These depressions coincide with faults of Caledonian origin and abrupt lithological changes and they were overdeepened due to erosion associated with the glaciation of the last ice sheet. The last widespread deglaciation caused a worldwide eustatic sea level rise and, as a result, many low lying areas were inundated by the sea. During the Holocene transgression, the Menai Strait depression was completely flooded. According to Embleton [1964], another 13m rise in the sea level would flood the Bangor-Dinorwic depression (Arfon mainland) and, similarly a rise of 30m would unite Malltraeth with Red Wharf Bay (Anglesey).

Several explanations have been put forward for the formation of the Menai Strait but the most likely are those of Ramsay [1860], Edwards [1905], Greenly [1919], Embleton [1964] and Embleton & King [1968].

Ramsay [1860] noticed that the trend of the Menai Strait coincided with his postulated ice movement direction of NE-SW, and concluded that the Menai Strait had overdeepened due to erosion during the last glaciation.

Edwards [1905] seems to have been the first to suggest an ice-dammed lake as an important factor in the evolution of the Strait. He stated that "The rivers of Caernarvonshire that now enter the Menai Strait have been factors working from very early periods of the direction of cutting off Anglesey from the mainland. The rivers, Conwy, Aber and Ogwen and other smaller streams, account for a large volume of water, which might account for the original breaking of the connection between Great Ormes Head and Penmon, and the River Seiont and others might account for the opening at Aber Menai. This would have left a narrow neck of low land, composed chiefly of various soft rocks, that would be eroded from both sides until the last connection was cut through in the neighbourhood of the present-day bridges, where the channel is today narrow, very shallow and studded with rocks. We are not without evidence in favour of the view that the Glacial Period left Menai Strait as a large lake, both ends being blocked by great mounds of drift."

Greenly [1919] mentioned that after the retreat of the Irish Sea Ice, the Llanberis and Ogwen glaciers emerged from the Snowdonia valleys, trapping a lake of meltwater between them over central Arfon. He divided the Strait into three

areas: the eastern reach and western reach separated by the shallow area of the middle reach (Fig. 2.4). He stated that the north-eastern (Beaumaris - Menai Bridge) and the south-western (Portdinorwic - Caernarfon) reaches of the Strait were normal river valleys draining respectively into Caernarfon and Beaumaris Bay. The river valleys were separated by an elevated watershed of harder Gwyna greenschists which stood out from the softer Ordovician to the north-east and limestone to the south-west. The river valley on the western side was once joined with the Bangor-Portdinorwic depression and ran along the Dinorwic fault into the Caernarfon Bay. The eastern reaches were formed from a river valley that ran in the opposite direction, along the edge of the Mona Complex and out into the Beaumaris Bay. Though the rivers followed the general structural trend of northeast-southwest, they had tributaries (the Cadnant and Braint) with about 90 degree confluences. The presence of boulder clay on the floor of the tributaries date their formation as pre-glacial. It is the lower reaches of the Braint which now forms the middle reaches of the Strait. It is believed that during the last glaciation there was deepening of the eastern reaches by the Irish Sea ice movement. Greenly argues that at the later stage the Irish Sea ice retreated and advanced, whilst the Welsh ice started to expand from the main valley glaciers (the Ogwen and the Llanberis valleys). He suggested that the Welsh ice advanced far enough to block the flow of the eastern reaches towards the Conwy area. With the eastern

reaches blocked by Welsh ice and the presence of the higher ground on the Llanfair and Vaynol side, meltwater continued to accumulate and resulted in the formation of an ice dammed lake. The evidence for this lake is a series of laminated clays found in the Bangor area [Greenly, 1941]. Continuous accumulation of meltwater forced the lake to overflow towards the southwest, where it was diverted to join the course of the river Braint which flowed out towards the western reaches and into Caernarfon Bay. Erosion and deepening continued until the eastern reaches had been drained to the watershed, and the middle reaches were formed. After deglaciation the Menai Strait remained as a dry valley until the subsequent rise in sea level drowned the valley and resulted in the formation of the present day feature.

Embleton [1964] agreed with some of the basic ideas forwarded by Greenly e.g., the formation of the pre-glacial river valleys, but he rejected the idea of an ice dammed lake and an advancing local glacier during an overall glacial retreat. To support his new interpretation, he put forward evidence of the Irish Sea ice esker and moraine deposits found at Penrhyn and around the mouth of the Ogwen river. He argued that any movement of a local glacier from the Ogwen would have removed the above evidence. Embleton also argued that the present day Braint river is too small for its lower reaches to have once been the middle reaches of the Strait.

Embleton [1964] believed that, either in the pre-glacial or in the last interglacial, there were two parallel rivers (Cadnant and Braint), both flowing south westwards. Later, the Cadnant changed its course and flowed northeast towards Beaumaris (Fig. 2.5). He postulated that the formation of the Menai Strait occurred during the downwasting of the last Irish Sea ice sheet, and pre-glacial river capture was responsible for determining the route. During deglaciation, as the ice thinned, parts of Anglesey and Arfon became ice free, and the resulting topography and ice sheet slope with a gradient of 1:200 to the SW, directed the meltwater toward the southwest. Initially the meltwater flowed through the Bangor-Dinorwic and Pentraeth-Malltraeth depressions. At later stages these were abandoned when the watersheds had been lowered to about 13m. The Braint river was overdeepened by the flow of meltwater and, when the ice was no longer continuous between the eastern and western reaches, the meltwater was forced to cut a divide between them forming the middle reaches. Once the Strait was formed it remained as a dry valley until it was submerged during the Flandrian transgression between about 6000 to 7000 years ago.

Although there is still controversy over the meltwater flow pattern of the Irish Sea ice and Welsh ice, it is generally agreed that parts of the Menai Strait were originally pre-glacial river valleys which were further deepened by erosion associated with the last deglaciation, and a subsequent transgression submerged the depressions,

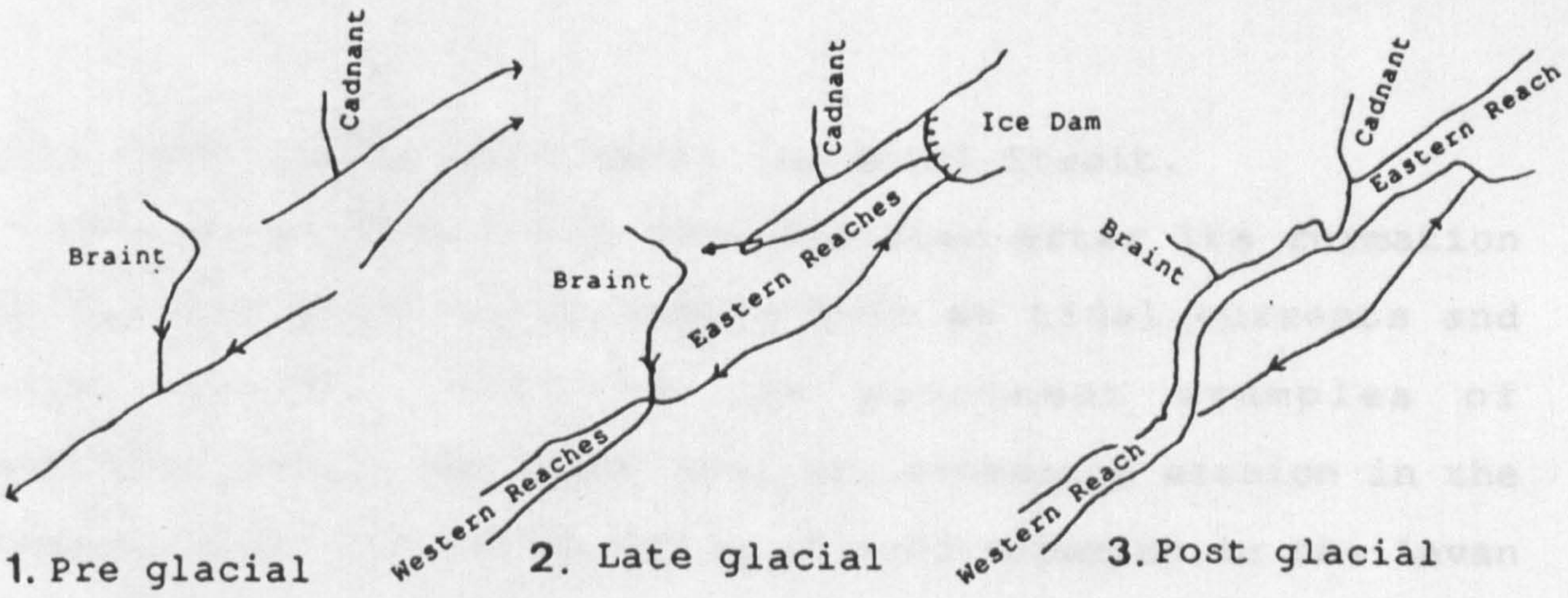

Fig: 2.4

The stages in the formation of the Menai Straits (after Greenly 1919)

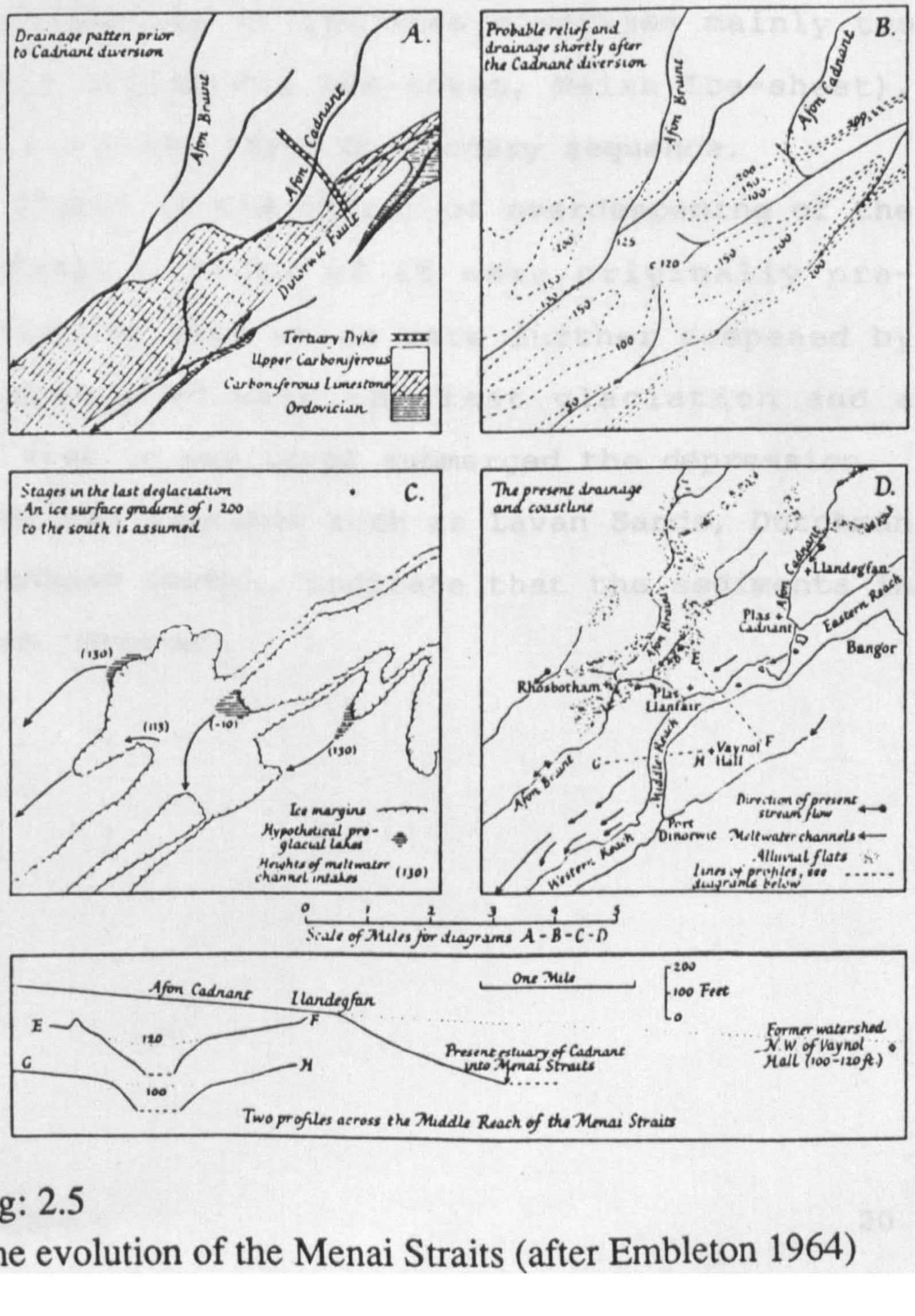

Fig: 2.5

The evolution of the Menai Straits (after Embleton 1964)

thus establishing the present day Menai Strait.

The Menai Strait has been modified after its formation by various physical processes such as tidal currents and wave action. Some of the prominent examples of modifications in the study area are extensive erosion in the Penmaen area, and accumulation of sand deposits in the Lavan Sands area.

2.5 Conclusions

(1) The glacial history of the area comprises mainly two ice advances (Irish Sea Ice-sheet, Welsh Ice-sheet), resulting in a three layer Quaternary sequence.

(2) The Menai Strait is the result of overdeepening of the Dinorwic Fault. Parts of it were originally pre-glacial river valleys which were further deepened by erosion associated with the last glaciation and a subsequent rise in sea level submerged the depression.

(3) Geomorphological features such as Lavan Sands, Dutchman Bank and Penmaen Swatch, indicate that the sediments in the area are 'active'.

CHAPTER THREE

GEOPHYSICAL STUDIES OF SEAFLOOR AND SUBBOTTOM FEATURES

The purpose of the geophysical survey was to collect more information about the seabed morphology and the subbottom sedimentary structure in the NE Menai Strait and Conwy Bay. A range of geophysical instruments (echo sounder, side scan sonar, pinger, boomer and sparker) was used for this objective. The plan of this marine geophysical study was to collect data about bottom topography, distribution of bedforms on the sea floor and the post-glacial sedimentary sequence. Integration of information about seabed morphology, current patterns and sediment grain size will also provide insights into sediment transport in the area.

3.1 Field Work

Field was carried out during the field seasons of 1988 and 1989. A summary is given in Table 3.1. The UCNW research vessel 'Prince Madog' was used in the comparatively deeper water of Conwy Bay on 24th, 25th May and 20th July 1988. Sparker, boomer, side scan sonar and echo sounder were used on this vessel for data collection. During the May 1988 cruise, the position of the ship was located at each turn and every 4 minutes when it was sailing on a straight course. On all other cruises, positions were fixed at an interval of about every 2 to 3 minutes.

Table: 3.1 Summery of Cruises for Geophysical Surveys.

No	Date	Cruise	Instrument Used	Fix No
1	24 May 88	Prince Madog	Boomer Side Scan Sonar Echo Sounder	1-80
2	25 May 88	Prince Madog	Boomer Side Scan Sonar Echo Sounder	81-164
3	6 June 88	Lewis Morris	Side Scan Sonar Echo Sounder	165-212
4	7 June 88	Lewis Morris	Side Scan Sonar Echo Sounder	213-293
5	20 July 88	Prince Madog	Sparker Side Scan Sonar Echo Sounder	294-425
6	9 Nov. 88	Lewis Morris	Echo Sounder	426-541
7	24 Nov. 88	Lewis Morris	Echo Sounder	542-636
8	3 July 89	Robyn	Echo Sounder	637-680
9	4 July 89	"	Echo Sounder	681-742
10	5 July 89	"	Echo Sounder	743-762
11	6 July 89	"	Echo Sounder	763-826
12	7 July 89	"	Echo Sounder	827-916
13	11 July 89	"	Side Scan Sonar	917-941
14	12 July 89	"	Side Scan Sonar	942-969
15	13 July 89	"	Side Scan Sonar	970-1040
16	14 July 89	"	Side Scan Sonar	1041-1071
17	18 July 89	"	Pinger	1072-1156
18	19 July 89	"	Pinger	1157-1222
19	20 July 89	"	Pinger	1223-1291
20	21 July 89	"	Pinger	1292-1361

About 35% of the study area is intertidal, so geophysical data in that shallow water area were collected during high tide using the Lewis Morris and Robyn. All position fixing coordinates (Lat. Long. and Trisponder ranges) were converted to the British National Grid. Survey tracks and graphic presentations were plotted using the UNIRAS graphic program [UNIRAS 1990] on the VAX mainframe computer.

3.2 Position Fixing

During the geophysical survey, positions of the data recording instrument on the ship/boat were fixed 1361 times. Two types of navigational systems (Decca Hifix and Trisponder) were used. Position fixing during one cruise (20th July 1988) was made using the Decca navigational system and, during all other surveys, a Trisponder position fixing system was used. The R V Prince Madog has the Decca Hifix system installed onboard. In this system, navigational error may be up to approximately ±100 metres depending on weather and terrain. For each fix the degrees and minutes (2 decimals) of latitude and longitude were recorded. These read-outs were converted into national grid coordinates (m). This conversion was cross checked manually on Ordnance Survey maps; Landranger 115, and Pathfinder 751, 752 and 753.

On the Prince Madog, during the May 1988 cruises, a Del Norte Technology, Inc. Model 542 Digital Distance Measuring Unit (Fig. 3.1-f) interfaced with Hewlett Packard (HP7550) graphic plotter, was used. Because of some missing

positions, the large scale and the poor plot quality, these plot outs were not used. The manual readouts of Trisponder ranges have been used for all position references. Trisponder Model 520 (Fig. 3.1-g) with the remote Transponders 217C (Del Norte Technology Inc.) system was used during the Lewis Morris and Robyn cruises (Table 3.1). This system consists of a master transceiver aboard the survey boat, and two or more remote (slave) sets fixed on land at known positions. The master Trisponder generates a microwave burst and simultaneously starts a timer. The remote Transponder receives these microwaves and transmits its own microwave burst. When these pulses return to the master, it internally calculates the distance in metres between the master and remote transponder positions by multiplying the half of the recorded time by the speed of light. It takes a finite length of time for the remote Trisponder to acquire the burst from master Trisponder, and then retransmit the burst. The accuracy of the system is ±1 metre. Resolution is 0.1 metre. Reynolds [1990] using a Trisponder system during a sparker and boomer survey in Plymouth Sound, determined a standard deviation between 0.5 and 1m on position fixings.

The positions of the remote Trisponders were fixed on a large scale map (1:10,000). The accuracy of estimating Easting and Northing of these remote stations is ±4m. During all cruises, 3 remote Trisponders were used at known positions. The positions of the remote Trisponders used are

Fig: 3.1 Some equipments on R.V. Prince Madog - May 1988 cruise.
a- Shipek grab sampler, b- Side scan sonar tow fish, c- Boomer transducer, d- Side scan sonar recorder,
e- EPC 4600 Griffith Recorder, f- Digital Distance Measuring Unit Model 542, g- Trisponder model 520 (master)

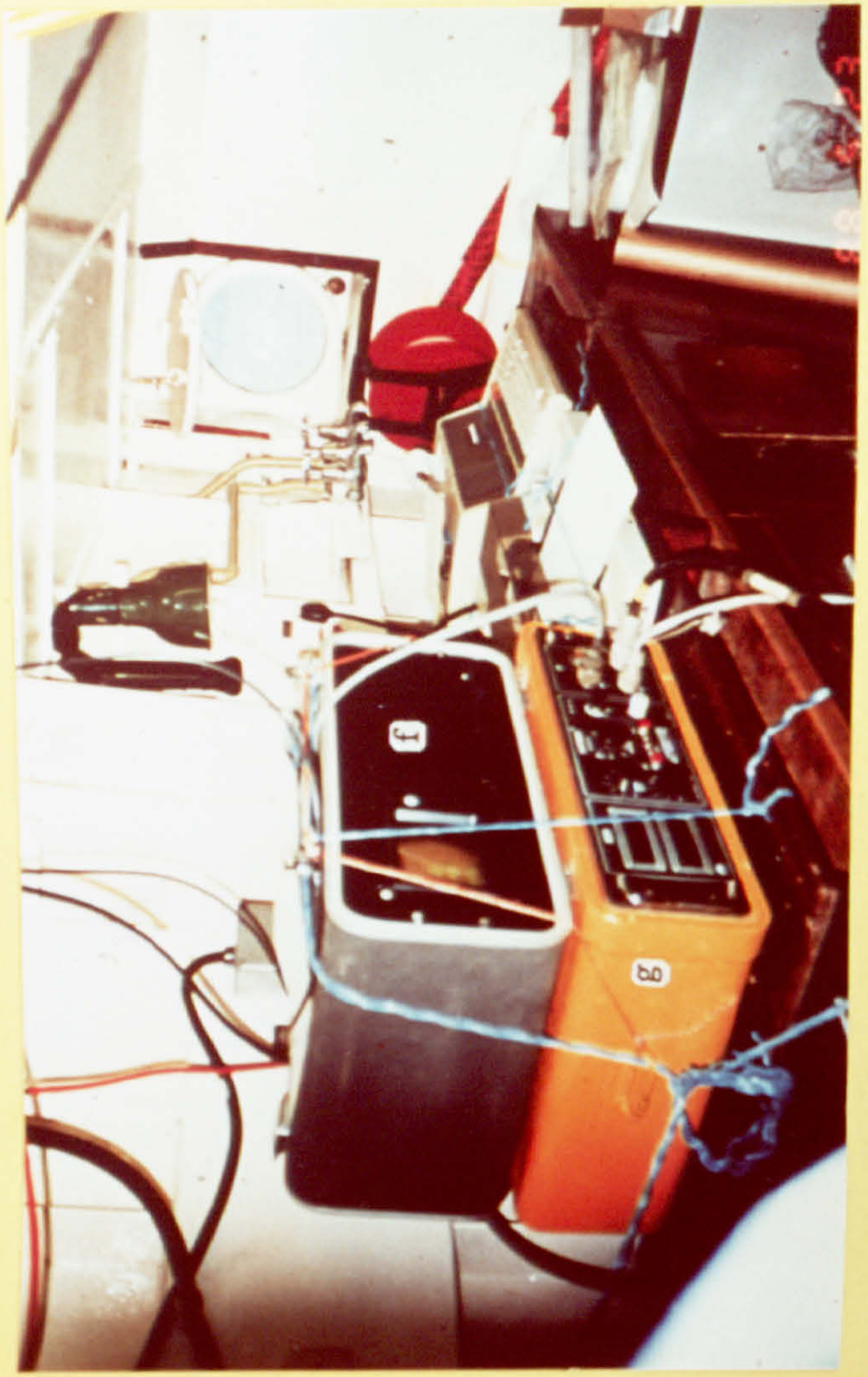

listed in Table 3.2. From the ranges of two stations on land, the position of the master Trisponder (ship/boat) at sea is calculated by the computer.

Table: 3.2 Positions of Remote Trisponders.

No.	Location	Easting(m)	Northing(m)	Height(m)
1	Bangor(Top College)	^{2}57952	^{3}72305	70
2	Llanfairfechan	^{2}68970	^{3}75197	120
3	Penmon (Coast Guard)	^{2}64003	^{3}81150	30
4	Bangor Pier	^{2}59975	^{3}75144	10
5	Llandudno, Anglesey Rd	^{2}77172	^{3}82548	65
6	Great Ormes Head	^{2}75509	^{3}83187	35
7	Penmaenmawr	^{2}73785	^{3}87056	10

The conversions of ranges to the national grid were manually counter checked by drawing circles at 500 metre intervals around each remote station on a 1:10,000 scaled map; all the position fixes were at a constant distance from the actual data points. This variation was about ±2m to ±15m depending on the size of vessel and nature of instrument installation.

3.3 Tidal Depth Correction

The tidal range in the area is 3.5m to 7.0m (Chapter 4). The water surface provides the base level from which elevation of the seabed is derived. In all the obtained geophysical data, a permanent reference height (bench mark) is required. All the depths are corrected with reference to Ordnance Datum (Newlyn). The Chart Datum at Beaumaris is used throughout the survey for depth correction, which is

-4m from O. D. Newlyn. Tidal depth for this purpose is obtained from the Hourly Tidal Prediction Model of UCES [Sherwin & Williams, 1988, 1989]. Tidal curves used for depth correction are shown in Fig. 3.2.

3.4 Seismic Study of the Seafloor

3.4.1 Bathymetry of NE Menai Strait and Conwy Bay

3.4.1.1 Equipment and Survey Procedure

A Raytheon DE-719 CM echo sounder was used for all bathymetric observations. Echo sounders were first developed in the early 1920s and most of its principles were well laid down by Shalowitz [1930], de Vanssay de Blavous [1930, 1933] and Hayes [1933]. During the forties, new types of recording fathometers were developed and specific features of the seafloor were being well surveyed, focusing interest on large features on the seafloor. Luskin & Israel [1956], developed the Precision Depth Recorder with which, for the first time, an accurate examination of small relief was possible.

The accuracy of depth determination depends on several variables, including sea state, the nature and shape of the bottom, and the velocity of sound, all of which differ from area to area. The speed of sound in water is 1460-1500 m s^{-1} depending on temperature, pressure and salinity. At 0°C, 1 atmospheric pressure and 34.8 ppm salinity, sound speed is 1445 m s^{-1}. Under the same conditions at 20°C, it increases to 1518.5 m s^{-1} [Groen, 1969]. The higher the temperature,

Fig: 3.2

Predicted tidal curves relative to O. D. Newlyn during surveys, used for depth correction of geophysical data.

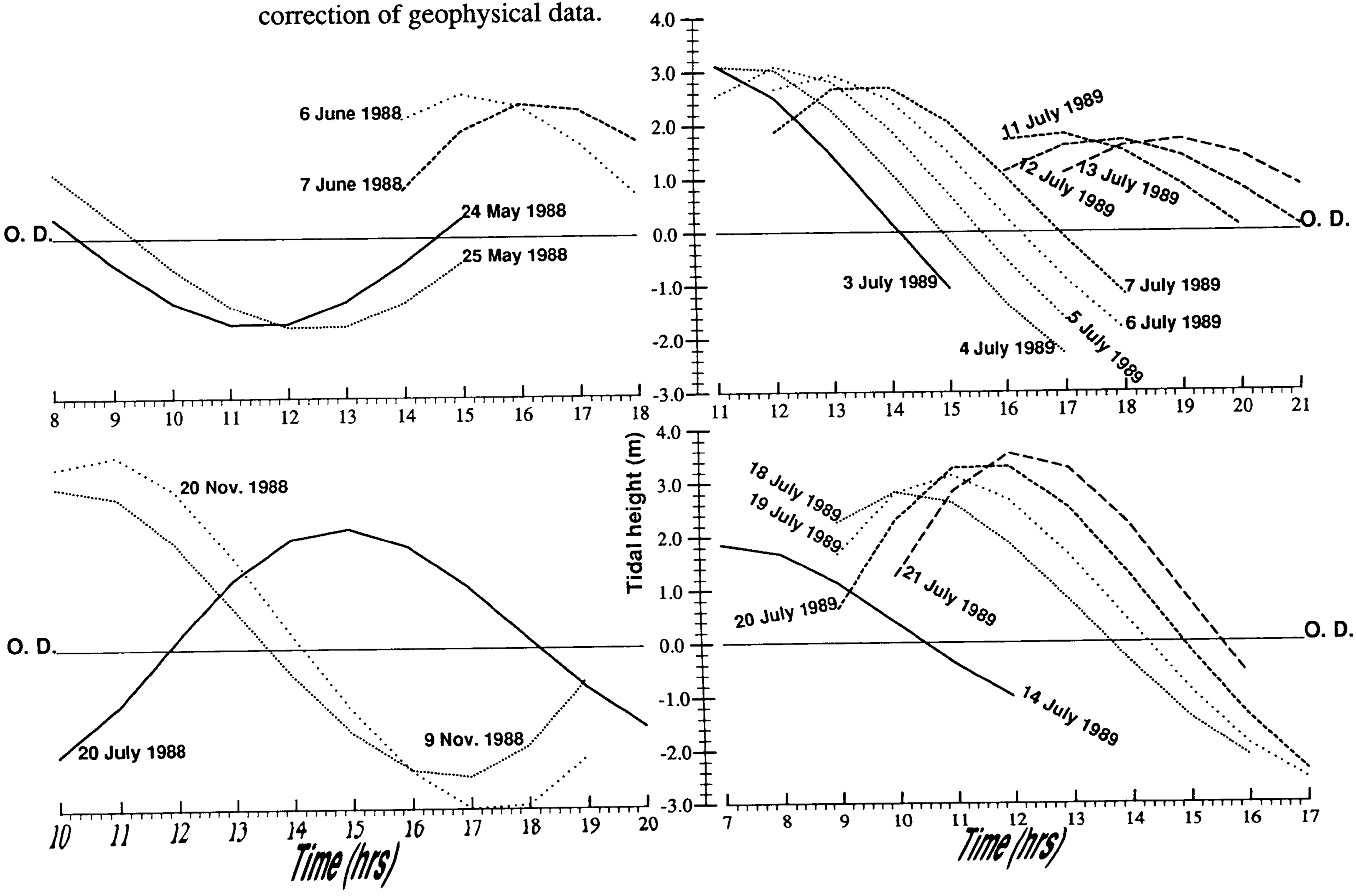

the higher the speed of sound in water, and the same in the case of salinity. The Raytheon echo sounder calculates the depth based on a 1500 m s^{-1} sound speed. A trace recorded by the Raytheon echo sounder is shown in Fig. 3.3.

3.4.1.2 Bathymetric Map

Each recorded depth was corrected for tidal variation, so all the soundings are with respect to O. D. Newlyn. On almost every one metre change in depth on the sounding paper, the grid coordinates and depth (m) were noted. The spot map (Fig. 3.4) shows 1178 positions on which bathymetric data are drawn. The topographic map (Fig. 3.5) is plotted by the UNIRAS graphic program. Those heights above Ordnance Datum (Newlyn) on the map are marked on the isobaths with + sign.

The minimum water depth of 2.5m above O. D. Newlyn is recorded near the Afon Aber mouth area. Overall relief in the area is 35m. In Conwy Bay, isobaths are almost parallel to the coastline up to 12m depth and the general trend of contours is NE-SW. Up to about 5 km from the shoreline, the bottom slope is 1:700 and beyond that it becomes comparatively steeper. In the Lavan Sands area, the slope is towards the NW at a gradient of about 1:1000. Water depth on the west margin of Dutchman Bank is less than on the eastern side.

A maximum depth of 33m was recorded about 800m N50°E from the north edge of Puffin Island. Isobaths around this

Fig: 3.3

Echo sounder traces showing water depth NE of Puffin Island (A) and maximum depth recorded in Penmaen Swatch (B). Positron fixes are indicated in Figure 3.6.

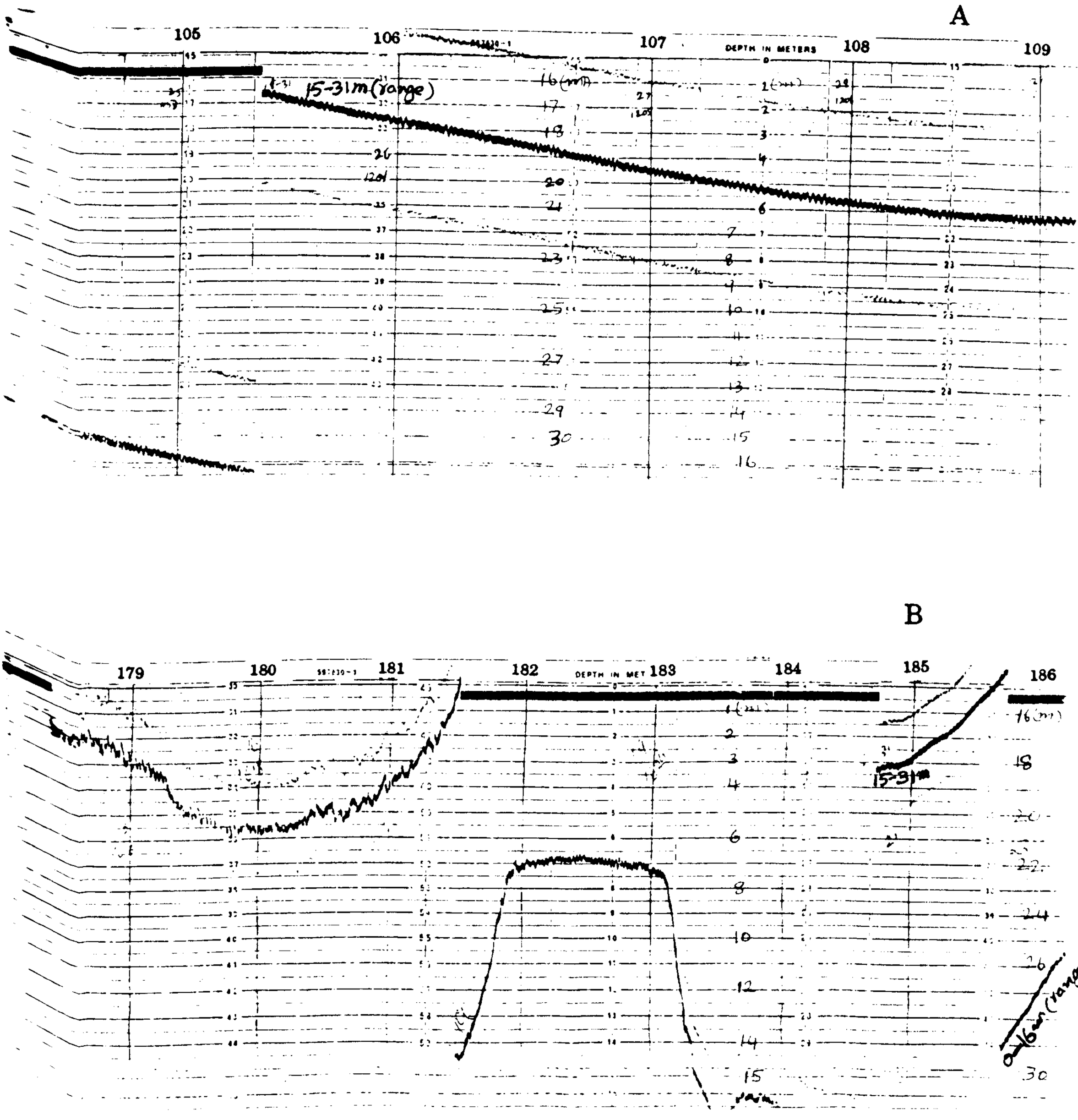

Fig: 3.4 Spot Map showing positions of c. 1 m change on Bathymetric records.

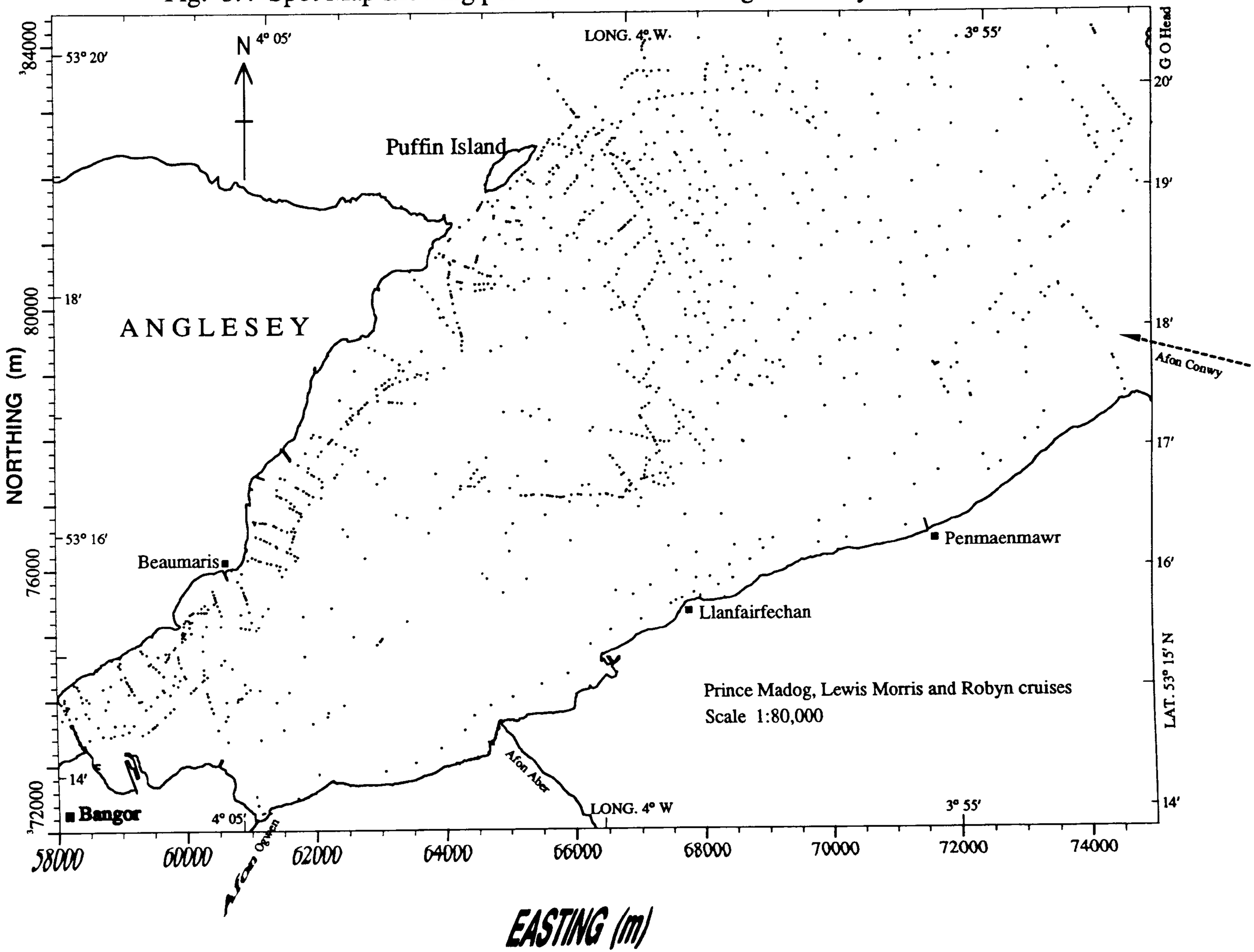

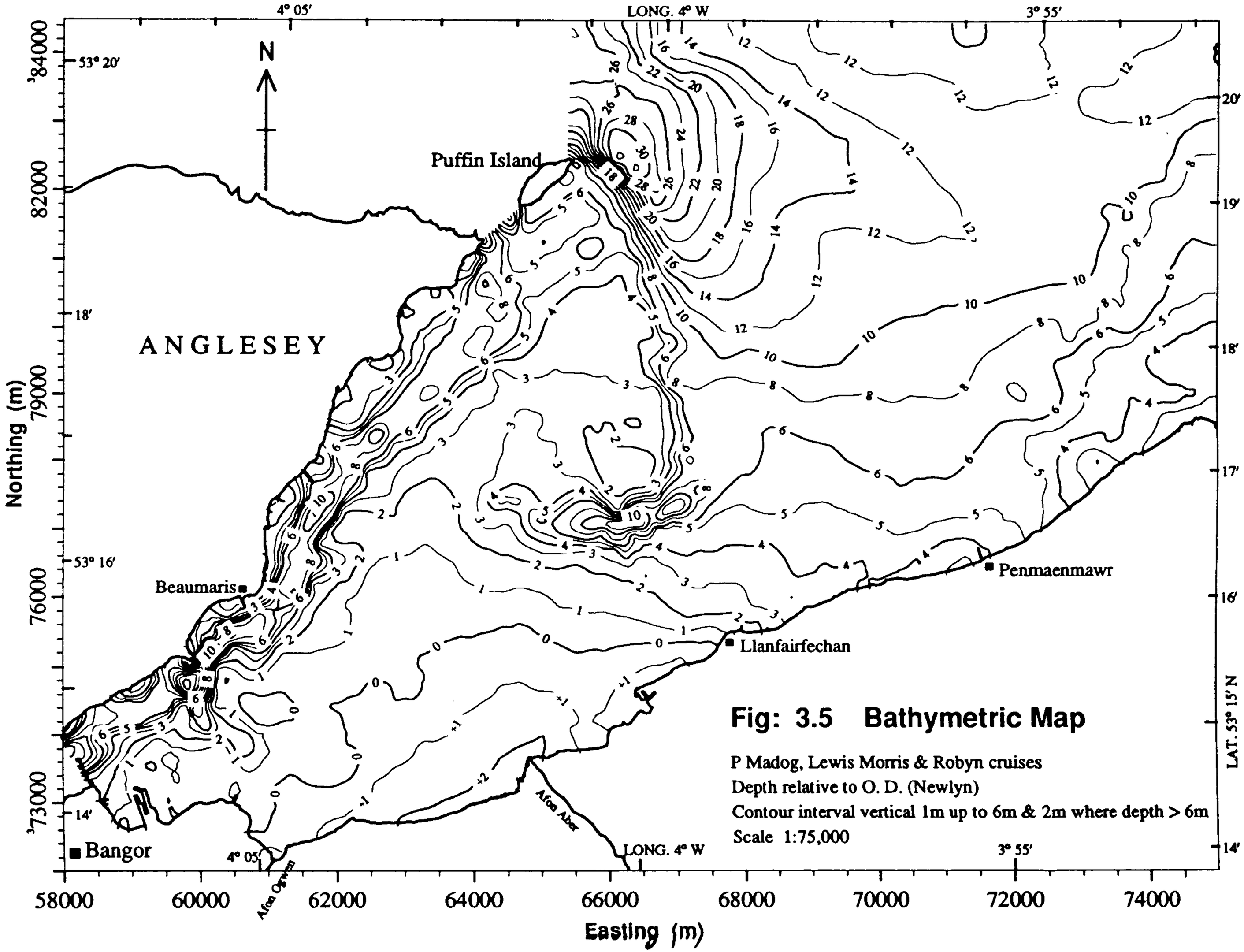

Fig: 3.5 Bathymetric Map

P Madog, Lewis Morris & Robyn cruises
Depth relative to O. D. (Newlyn)
Contour interval vertical 1m up to 6m & 2m where depth > 6m
Scale 1:75,000

depression are 'D' shaped at about 305°. To the south west of this point, the gradient is about -5% below 10m water depth, which is much steeper than on the other sides. One reason for the topographic configuration in this locality may be the pattern of currents (Chapter 4).

In Penmaen Swatch around grid coordinates 66500E 77000N, an elongated bowl shaped depression is recorded. Maximum depth at this point is 17m (Fig. 3.3B). Water flow in that area is comparatively strong during both flood and ebb tides (Current metre Station 2). As the flood tide starts, and water from the Conwy Bay reaches the Penmaen Swatch area, it is obstructed by the Dutchman Bank on its west side and by the Lavan Sands on its south and south east sides (both >3m above mean low water at this locality). This obstruction creates a temporary dam condition. During this period, the water rushes through the swatch and this is its most probable reason for the comparatively high depth at this location. Afon Aber enters at this point during almost all of the low water duration (Fig. 7.1, Ordnance Survey Sheet 752), and may be another cause of this deep channel.

In the Menai Strait, in the channel at Gallows Point (59900E 74750N), a local 'deep' is mapped, its depth at the centre being 14.5m. Jones [1978] is recommended for more information about this feature. Two other depressions (up to 10m deep), one near Bangor Pier and a second near the Life Boat Station, were observed during the echo sounding survey.

3.4.2 Seafloor Bedforms

3.4.2.1 Equipment and Survey Procedure

3.4.2.1.1 Side Scan Sonar

The first operable sideways-looking sonar was built by Tucker & Stubbs [1961] at the National Institute of Oceanography in England and since then the instrument has undergone rapid development and improvement. During the last two decades, it has played an important role in the field of marine geology and sedimentology. Side scan sonar provides information about the surface sediment distribution and bedforms, which can be integrated with subbottom, bathymetric and sediment sampling data and thus provide a detailed picture of the Recent geology and sedimentary processes. Some examples of detailed side scan sonar surveys are discussed by Belderson, Kenyon, Stride & Stubbs [1972]; Mckinney, Stubblefield & Swift [1974]; Werner & Newton [1975]; Bryant [1975]; Flemming [1976, 1982a, b]; Klein [1982], Key [1984], and Mazel [1985a, b].

The basic principle of side scan sonar is that a transducer (piezoelectric crystal) converts the oscillating electric field produced by the transmitter into mechanical vibrations. This vibration is transmitted into water as an oscillating pressure; the sound pulse. When sound strikes something such as the sea floor in the water, some of its outgoing sound is reflected back to the same transducer, and its receiver portion listens to the returning echoes. A recorder measures and displays the time it takes for the

pulse to reach the target (the seafloor) and to return. The colour shade of the print-out depends on the degree of the reflection. When stronger singles are received by the receiver, the print out is darker than when it receives weaker sound reflections.

A Mark 1B side scan sonar system was used for this purpose; this consists of a dual channel graphic recorder (EG & G Model 259-4: Fig. 3.1-d), a tow fish (EG & G Model 272: Fig. 3.1-b) and associated cables. The model 259-4 Recorder has two modes; Search and Survey with a Range scale of 50, 100, 125, 200, 250 and 500 metres. The resolution is 1/250 of full scale and two consecutive lines on the paper represent 25m slant distance.

Acoustic sound is transmitted and received through the tow fish. The operating frequency of Model 272 Saf-T-Link is 105±10 kHz with a pulse length of 0.1 millisec. The horizontal beam width of this model is 1.2°. The scale across the side scan sonar record is based on an assumed sonar velocity of 1500 m s^{-1}.

A survey of 226.4 km (Fig. 3.6) was conducted on different cruises (Table 3.1). On the R V Prince Madog, the tow fish was towed at about 10m behind the ship. The speed of the ship was 3-4.5 knots. In shallow areas (<10m) the Lewis Morris and Robyn were used for this survey. The speed of these boats was 3-4 knots. The survey was carried out at different side scan sonar ranges, i.e., from 100m to 200m. On the Prince Madog this range was 200m and on the Lewis Morris and Robyn cruises it was 100m and 125m depending on

Fig: 3.6 Side Scan Sonar Survey Tracks - NE Menai Strait & Conwy Bay.

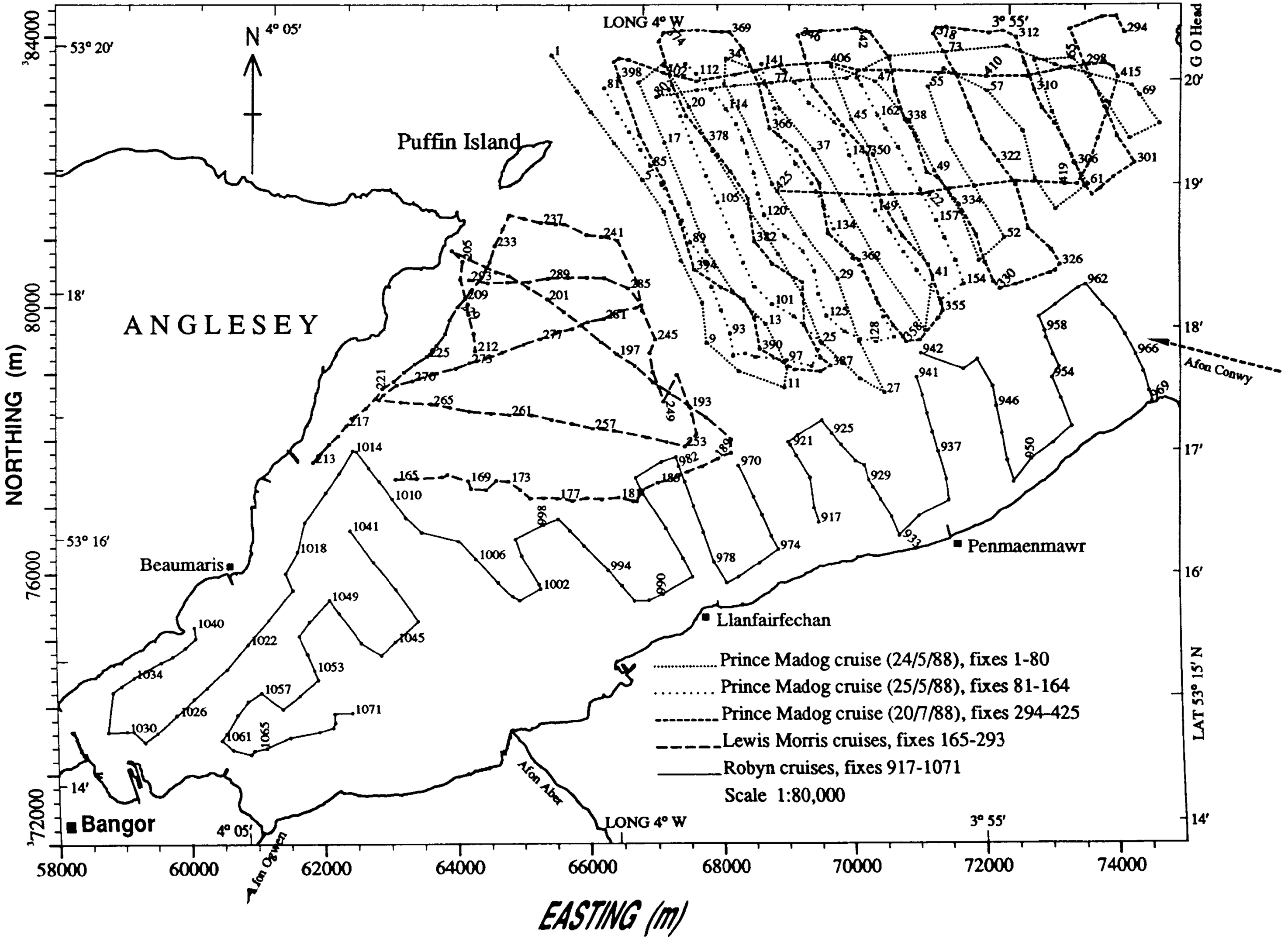

water depth. On the survey tracks with fixes 60-74, the side scan sonar range was 50 metres. Most of the surveys were started at the onset of high tide. On the Prince Madog, it was continued for 8-10 hours, but in intertidal area in small boats it was conducted around high water only to get maximum aerial coverage. So the bedform asymmetries indicated (Fig. 3.16) should be interpreted accordingly.

3.4.2.2 Bedform Terminology

Bedforms are undulations, restricted to cohesionless substrates, generated through dynamic interaction between the fluids and sediments in transport [Allen, 1980a].

An understanding of bedforms and primary sedimentary structures resulting from bedform migration and their relation to water dynamics may lead to greater understanding of the depositional environments. The formation of bedform type depend upon the following factors.

(i) Maximum flood and ebb velocities attained at a given locality

(ii) Velocity asymmetry

(iii) Velocity duration

(iv) Water depth

(v) Grain size

[Boothroyd & Hubbard, 1975].

According to Zarillo [1982], bedform heights depend upon the flow power, shear velocity, water depth and sediment grain size. In subtidal channels, bedform type and orientation

are controlled by the complex intertidal and subtidal topography. A sequence of bedforms in an area of sandy sediments indicates progressively changing flow velocities [Dyer, 1980].

The terminology used for the interpretation of sonograph records in the current study is based on various research workers, who conducted similar studies in intertidal environments. Many research workers have commented on the confusion over the classification and nomenclature of large flow-transverse bedforms present in tidal and fluvial environments [e.g., Allen, 1980a; Boersma & Terwindt, 1981a, b; Dyer, 1986; Terwindt & Brouwer, 1986; Mahamod, 1989; Larcombe, 1989; and Solangi, 1992]. The terminology for bedforms used by different research workers is summarised in Table 3.3.

In this study, the transverse bedforms are categorised into ripple, megaripple, small sandwave and large sandwave on the basis of the wavelength spacing. The hydraulic characteristics of transverse bedforms and longitudinal bedforms (sand ribbon) are described in the following section. The spatial distribution of bedforms in the intertidal area based on the aerial photographs, and field surveys will be discussed in Chapter 7. In that chapter, the analysis of internal sedimentary structures of bedforms through a box coring studies will be described in details.

Table: 3.3 Transverse bedforms terminology by different research workers based on wavelength spacing (m).

Research Workers	Terminology			
Cornish [1914]; Yalin [1972]	S.W (including antidunes)			
Coastal Res. Gp., Massachusetts University [1969]	S.R	M.R	S.W	
Hayes [1969]	R (<0.6)	M.R (0.6-6)	S.W (>6)	
Klein [1970]	Curr. R (<0.6)	Dunes (0.6-15)	S.W (>15)	
Boothroyd & Hubbard [1975]	R (<0.6)	M.R (0.6-6)	S.W (>6)	
Hine [1975]	R (<0.5)	M.R (0.5-5)	S.W (>5)	
Reineck & Singh [1973]	Small R (<0.6)	M.R (0.6-30)	Giant R (30-1000)	
Middleton & Southard [1978]	S.R	Dunes	S.W	
Dalrymple, Knight & Lambiase [1978]	R. (<0.3)	Type 1 M.R (.1-25)	Type 2 M.R (.05-14)	Red S.W (5-25)	M.Red S.W (10-215)
Allen [1980a, b]	Curr. R (<0.6)	Dunes (0.6-25)	S.W (25-1000)	
Belderson, Johnson & Kenyon [1982]	S.R	Small S.W	Large S.W	
Collinson & Thompson [1982]	Curr. R (<1.0)	Dunes (~1-5)	S.W (~5-100)	
Zarillo [1982]	S.R (<4)	M.R (4–15)	S.W (15–45)	
Pattiaratchi & Collins [1987]*		M.R (<30)	S.W (>30)	
Mahamod [1989]+	R (<0.6)	M.R (0.6-10)	S.W (>6)	
Larcombe [1989]#		M.R (0.2-50)	S.W (12-1000)	
Solangi [1992]£	R (<0.3)	type 1 M.R (0.1-25)	type 2 M.R (0.05-14)	S.W (5-215)	
Present Study	R (<0.6)	M.R (0.6-6)	Small S.W (6-25)	Large S.W (>25)	

R = ripple, M = mega, S = sand, W = wave

*= after McCave [1971].

+= after Hayes [1969]; Boothroyd & Hubbard [1975]; Harms, Southard, Spearing & Walker [1975]; and Dalrymple, Knight & Lambiase, [1978].

#= after Amos & King [1984].

£= after Dalrymple, Knight & Lambiase [1978]. Solangi further subdivided (his Fig. 4.19) type 1 megaripples into 'megaripples of 1-5m' and 'megaripples of 5-25m' wavelength.

3.4.2.2.1 Ripples

Ripples are small asymmetrical undulations produced by current flow on the bed surface with wavelength spacing <0.6 m [Allen, 1968a; Reineck, Singh & Wunderlich, 1971; Reineck & Singh, 1973]. The ripple index (the ratio of wavelength to summitpoint) of this category of bedform is always between 5-15. The shape of the crest depends upon the current speed. At relatively low velocities, the ripples are straight-crested (low-energy ripples of Harms, 1969]. The undulatory small ripples represents a transition form between low-energy straight-crested ripples and higher-energy lingoid ripples. The crest of these undulatory or wavy ripples can be traced for a distance of many metres. Undulatory small ripples of Reineck & Singh [1973] are analogous to Allen's [1968a] sinuous and catenary ripples. Lingoid ripples have discontinuous and broken crests and cannot be traced over a relatively long distance. The current velocity which forms these ripples is higher than for the straight-crested and undulatory ripples. Submarine sand ripples, whether on the continental shelf, in river, or in flumes, may be distinguished from sandwaves by having:

(a) a wavelength usually less than about 1600 times and usually greater than 600 times the median diameter of the sand in which they have been constructed.

(b) a height not greater than about 300 times the median diameter.

(c) both wavelength and height statistically independent

of water depth.

Sand ripple heights are in general between 1 and 5 cm. Wavelength are usually between 5 and 12 times sand ripple height.

3.4.2.2.2 Megaripples

Bedforms having wavelengths between 0.6 and 6m are referred to as megaripples. The lower limit (60 cm) is agreed upon by Allen [1968a], Simons, Richardson & Nordin [1965], Reineck & Singh [1973] and Hine [1975].

Megaripples are characterised by a sinous to highly cuspate crestline, usually with well developed scour pits downstream of the crestline. Some megaripples may have straight crests. Those megaripples whose crestline is not straight are three-dimensional megaripples. BY comparing the results in nine estuaries of New England, Boothroyd & Hubbard [1975] observed that megaripples are characterised by a high maximum flow velocity (80 cm s^{-1}) and little velocity asymmetry.

3.4.2.2.3 Sandwaves

Sandwaves are large, flow transverse bedforms produced under tidally oscillating flows [Allen, 1980b, c] and are widely recognised in modern and ancient deposits. Sandwaves with an internal structure of cross-bedding are common bedforms on the sea floor in the study area. The term sandwave refers to the lower regime transverse bedforms of

sand larger than the megaripples. A current speed only marginally above the threshold of grain movement forms sandwaves for sands coarser than 0.7 mm [Stride, 1988]. Sandwaves are further subdivided into small sandwaves (wavelength 6-25m) and large sandwaves (wave spacing >25m).

The divisions between megaripples, small sandwaves and large sandwaves are somewhat arbitrary.

3.4.2.2.4 Sand Ribbons

Among longitudinal bedforms, sand ribbons are identified on the sonographs. Sand ribbons are bands of mobile sand aligned with the current flow. The thickness of the internal bedding is often a few centimetres, but their width and length can be up to 200m and 15km, respectively. Sand ribbons are normally restricted to areas of coarse sediments and have high length/width ratio (up to 80), [Dyer, 1986]. They are essentially straight, although they may be slightly sinuous. Unlike transverse bedforms, the shape of sand ribbons does not show any transport direction, but the actual transport direction of sand transport can be found from associated ripples, megaripples and sandwaves [Klein, 1970]. Kenyon [1970] mentioned that mean current speeds of 100 cm s^{-1} can generate sand ribbons in areas of more than 0.7mm sediment mean grain size.

3.4.2.3 Sonograph Interpretations

The interpretation of sonographs is based on identification of shades of varying intensity and resolution

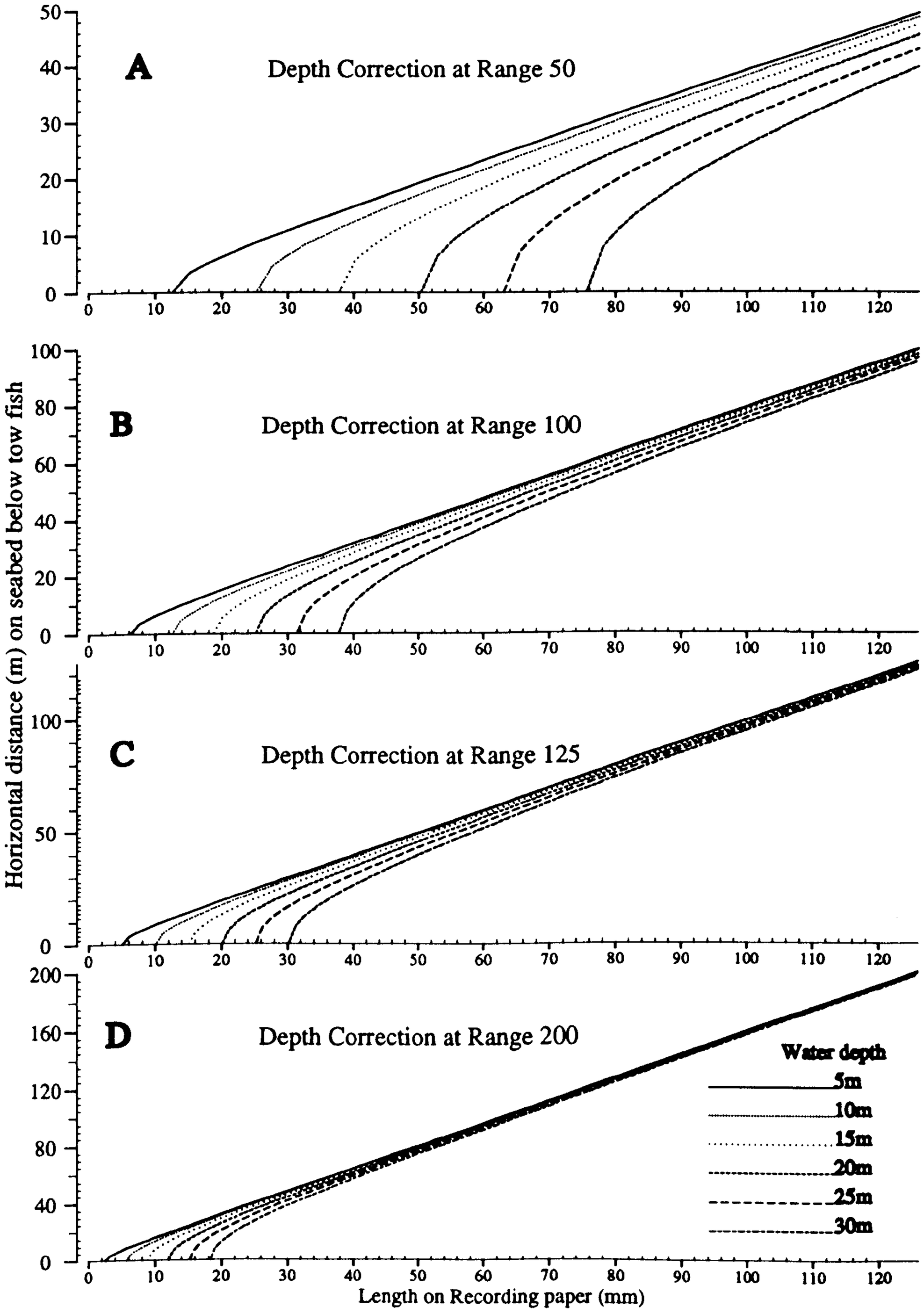

Fig: 3.7

Horizontal distance (m) on seabed at 5, 10, 15, 20, 25, and 30m depth at 50 (A), 100 (B), 125 (C) and 200 (D) metres side scan sonar range s.

on the printout paper. There are two main influences that may cause a darkening of the recording paper. One is purely electrical caused by the adjustments of the control settings of the recorder. These shades are always constant up to the new setting. The second is the incoming acoustic signals. Side scan sonar record interpretation is actually the recognition of the shades produced by these signals. Reflection of these signals depends on the type of 'material properties' and 'topographic features' of the seafloor. For example, rock and gravel are better reflectors than sand and will therefore record darker; a mud reflects weaker signals than sand. In the case of topographic features, the slopes facing the transducer reflect sound waves better than slopes lying oblique to the sound beam.

Two types of image distortion are encountered during the interpretation of acoustic pictures. The first is lateral distortion perpendicular to the line of travel. It depends on the height of the fish above the seabed. Correction of this distortion is shown in Fig. 3.7. The variable speed of the vessel produces the second type of distortion, which is parallel to the line of travel. The speed of ships during the survey was 2.5-4 knots. According to Newton, Seibold & Werner [1973] at about 2 knots virtually no distortion occurs parallel to the survey track.

Spatial distribution of seabed features recorded by the side scan sonar are shown in Fig. 3.16. On the basis of the characteristic acoustic returns, the sonograph is divided

into two patterns:

1 Bedforms patterns

2 Tonal patch patterns

3.4.2.3.1 Bedform Patterns

Different combinations of hydrodynamic conditions and sediment grain size create bedforms of different shape, size and orientation. The bedform patterns identified on the side scan sonar records are divided into ripples, megaripples, small sandwaves, large sandwaves and sand ribbons.

3.4.2.3.1.1 Ripples

Belderson, Johnson & Kenyon [1982] mentioned that sea floor sand ripples are not in general detectable by acoustic means. This finding was corroborated during the interpretation of side scan sonar records in the present study. Only on limited survey lines, it was possible to detect them, especially on records of the intertidal area using a small side scan range (100m). Ripples are observed on the Lavan Sands about 2.5 km east of Beaumaris Pier. To the NE of Puffin Island (fix 298) and on Dutchman Bank, these are found superimposed on small sandwaves and large sandwaves.

3.4.2.3.1.2 Megaripples

Megaripples are found in two modes, one as independent bedforms and the other as superimposed on sandwaves. To the

Fig: 3.8
Side scan sonar record showing megaripples. Position fixes are shown in Fig. 3.6.

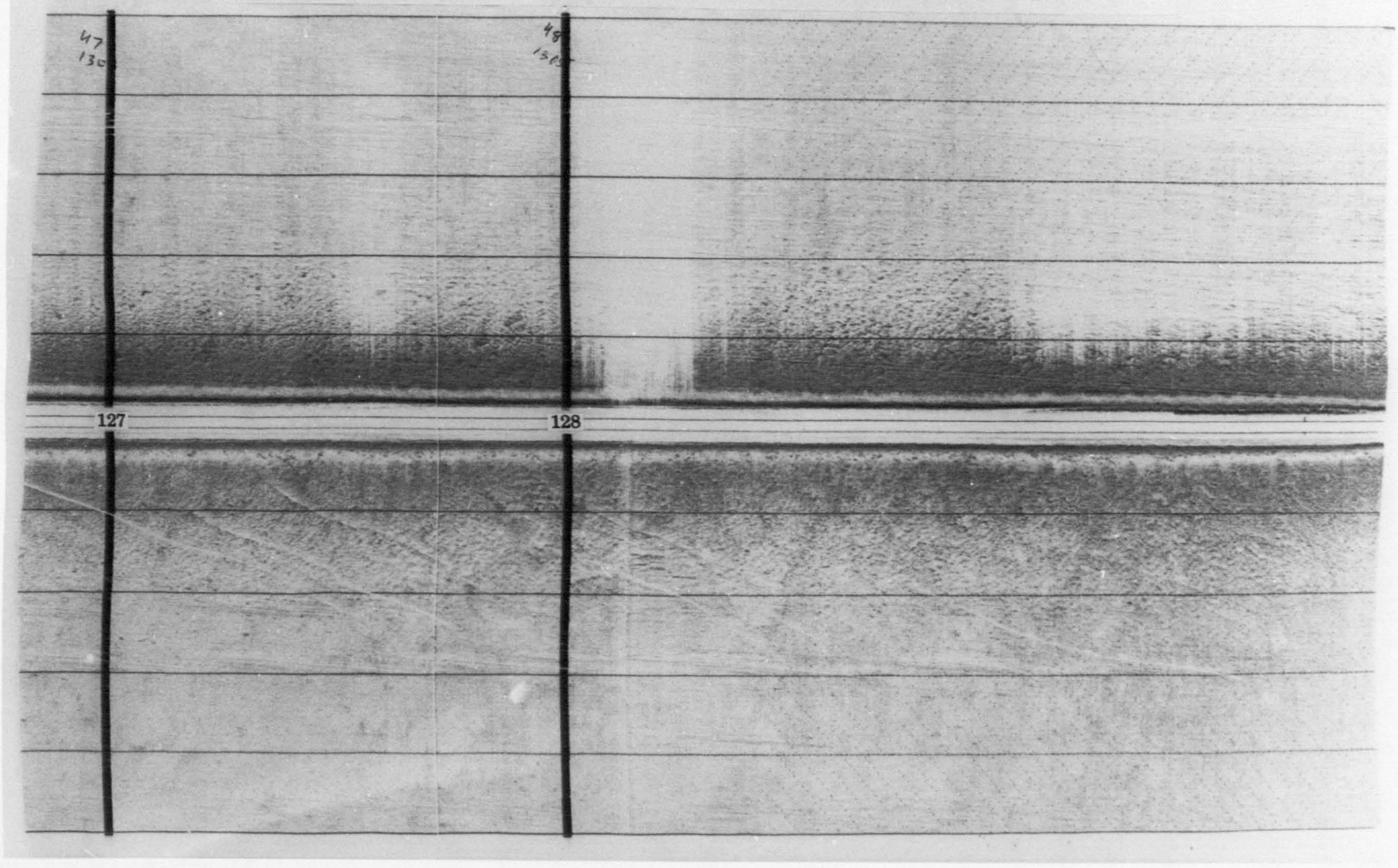

SW of Great Ormes Head (Fig. 3.8), these are the most commonly occurring seafloor feature. The other sites are on the Lavan Sands opposite Gallows Point and near Llanfairfechan. About 93% of the survey area that is covered by megaripples is between 9m and 11m water depth and the rest is intertidal. The mean grain size (see Chapter 5) in the megarippled area is more than 3.0 phi. Near Puffin Island, opposite the Lifeboat Station on Lavan Sands, and near Gallows Point on Lavan Sands, megaripples are found superimposed on the flanks of sandwaves. This is also observed on the aerial view and on ground photographs taken at low water (Chapter 7). On acoustic records the asymmetry of these bedforms was not recognised, may be because of their small size (<6m).

3.4.2.3.1.3 Small Sandwaves

Small sandwaves are the most abundant bedform observed in the side scan sonar surveys. These are nearly symmetrical (Fig. 3.9) to asymmetrical in shape. At some sites they are highly asymmetrical and clearly indicate the direction of movement (Fig. 3.10); these areas are NE of Puffin Island (1.5 to 2.4 km), Outer Road, and opposite the Lifeboat Station.

The crestlines of the small sandwaves between Puffin Island and Great Ormes Head are dominantly with an approximately NE-SW orientation. Almost all sandwaves in this area, where water depths are more than 11 metres, show

Fig: 3.9 Side scan sonar record showing patterns of small sandwaves.
Locations are shown in Fig. 3.6.

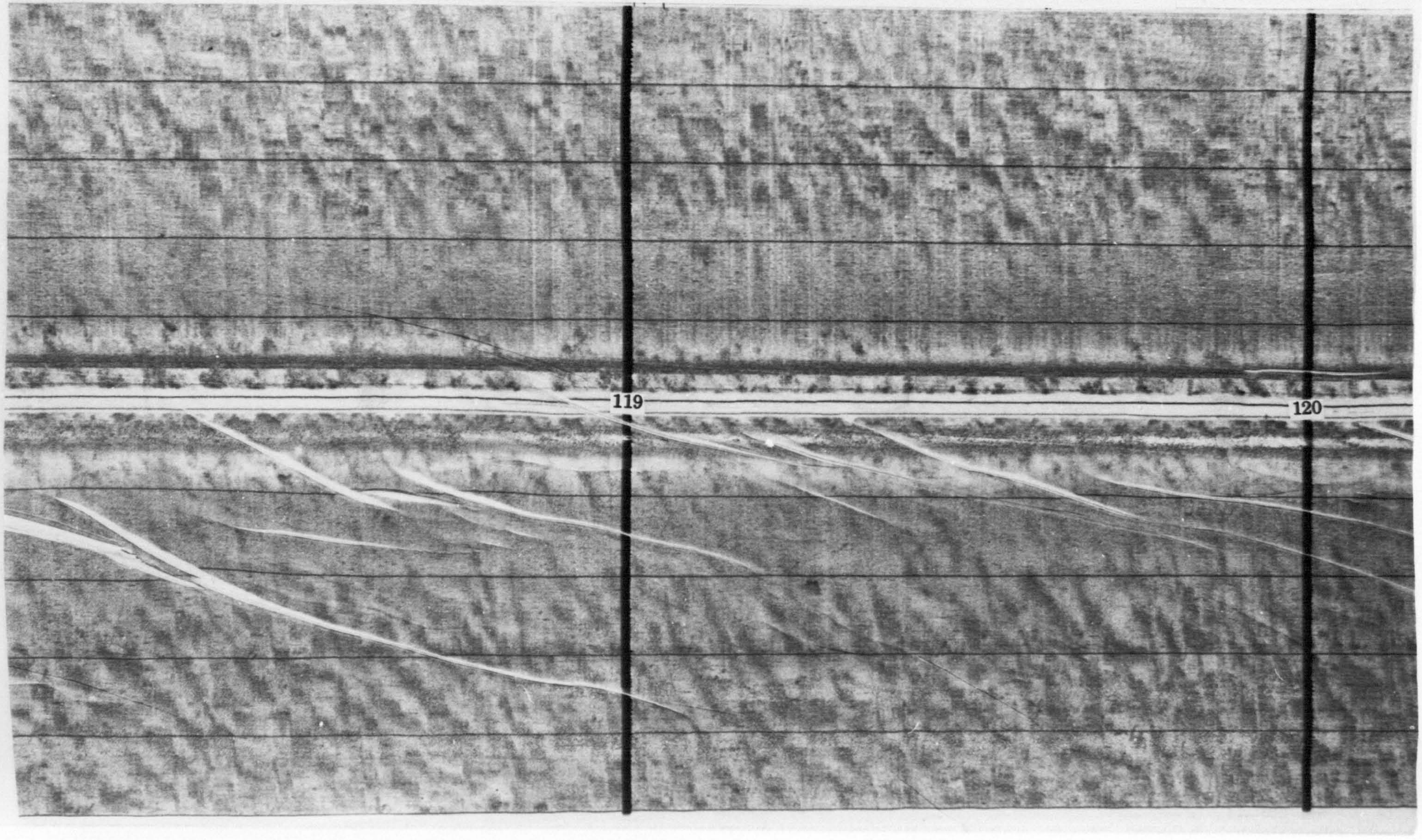

Fig: 3.10 Sonograph showing 2-D asymmetrical small sandwaves. Position fixes are shown in Fig. 3.6.

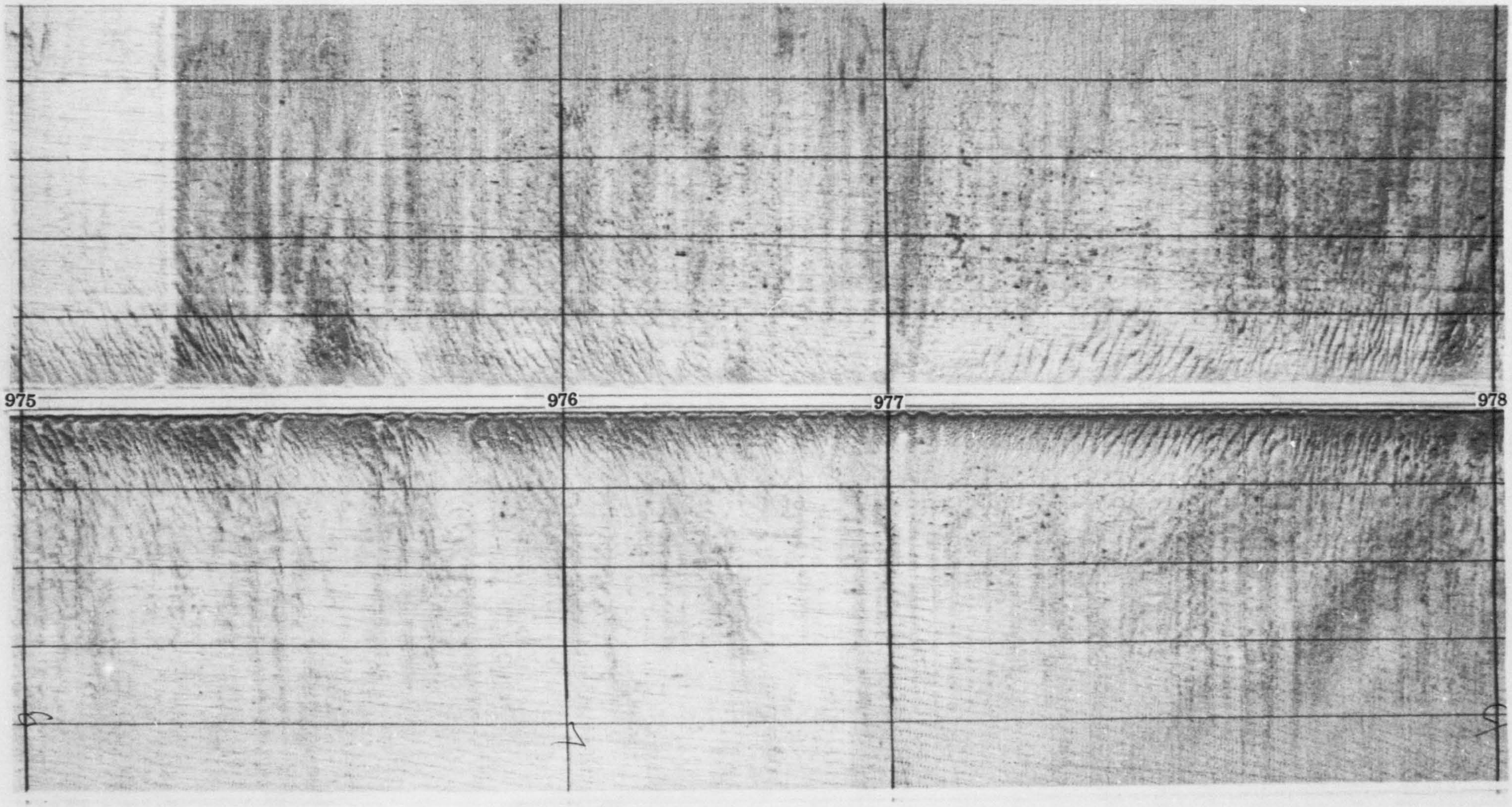

this character. Between Penmaenmawr and Llanfairfechan, their orientation is parallel to the coast, and crestlines are broken and sinous along most of the survey line. These broken and sinous crestlines most probably are due to comparatively more active hydrodynamic conditions. Near Llanfairfechan the small sandwaves are clearly 2-D (Fig. 3.10). Opposite Gallows Point (fix 1057) small sandwaves are revealed as a small field between megaripples and a tonal patches pattern. In places, ripples and megaripples are found on these bedforms.

3.4.2.3.1.4 Large Sandwaves

This category of transverse bedform is found in intertidal areas, at 2-4 metres water depth relative to O. D. Newlyn. The mean sediment grain size of more than 90% of the area having these bedforms is between 2 and 2.5 phi. Large sandwaves are recorded on both channels at fixes 235-240, and crestlines are about parallel to the survey line; megaripples and small sandwaves are superimposed at right angles to the crest of the large sandwaves (Fig. 3.11). Most probably the large sandwaves are the result of a north-south flow, while small sandwaves and megaripples are the result of flow between Puffin Island and Trwyn Penmon. In some areas, the migration direction can be easily identified e.g., south east of Puffin Island at fixes 237-241, and north of Penmaenbach Point. For spatial distribution of large sandwaves see Fig. 3.16. At some locations, megaripples and ripples are found superimposed on these

Fig: 3.11 Sonograph showing large sandwaves superimposed with small sandwaves south east of Puffin Island. Fixes are shown in Fig. 3.6.

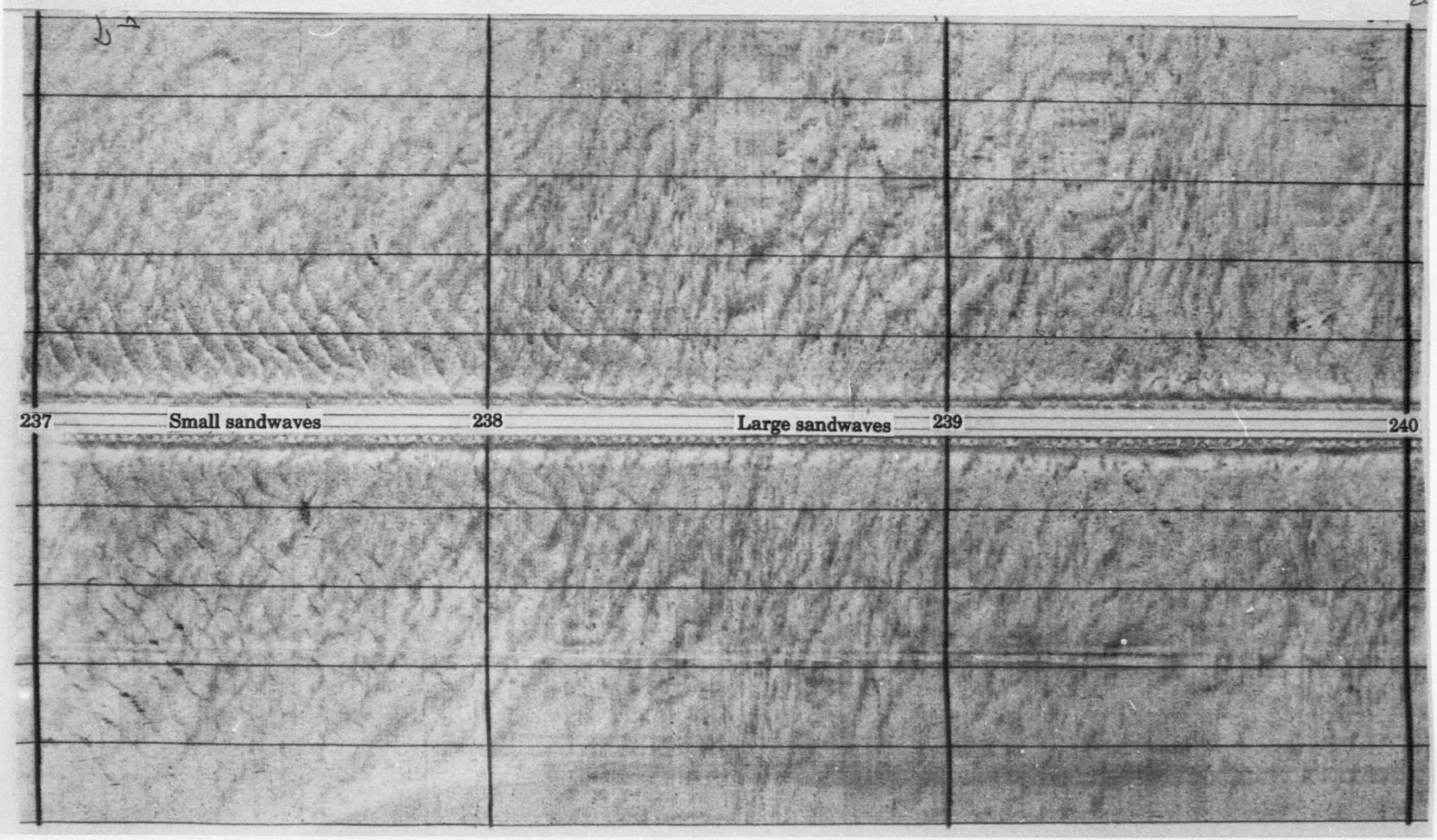

Fig: 3.12 Sonograph showing large sandwaves over Dutchman Bank area. Locations are shown in Fig. 3.6.

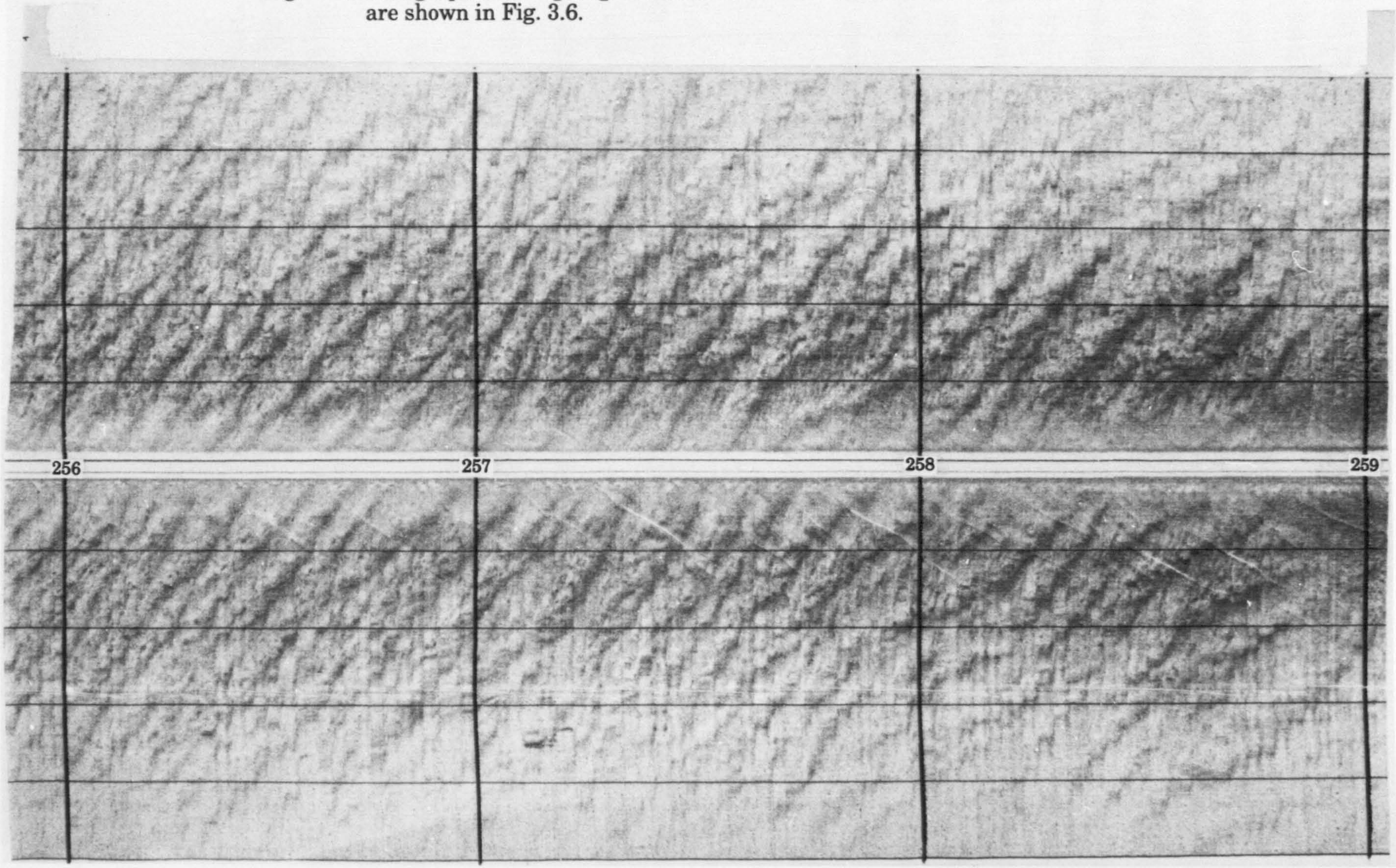

bedforms. Most of the central Dutchman Bank is covered by this pattern. An example is shown in Fig. 3.12.

3.4.2.3.1.5 Sand Ribbons

About 2 km offshore and parallel to the coast, between east of Penmaenmawr and Penmaenbach Point, longitudinal ridges or sand ribbons [Dalrymple, Knight & Lambiase, 1978; Amos & King, 1984] are the dominant seabed features (Fig. 3.13). Along the survey lines, their width ranges from about 80m to 400m. Megaripples are superimposed on these in a few places. The location and orientation of these sand ribbons shows that they are produced mainly under the influence of tidal flow adjacent to the mouth of the Conwy Estuary.

3.4.2.3.2 Tonal patch Patterns

The seafloor on the sonograph is sometimes depicted as a mosaic of light and dark patches, and isolated dark spots. These records are usually much darker than those of the surrounding area. Their appearance is sometimes subtlely mottled. This tonal patch pattern is analogous to the strong reflectivity and tonal patch pattern of Knebel, [1989]. The mosaic of light and dark patches is the result of a variation of grain size on the seafloor. The pattern is observed near Great Ormes Head; an example is shown in Fig. 3.14. The dark isolated and irregular patches are observed in Penmaen Swatch and on Lavan Sands in the course

Fig: 3.13 Fields of sand ribbons superimposed with megaripples, off Penmaenmawr Point. For fixes location see Fig. 3.6.

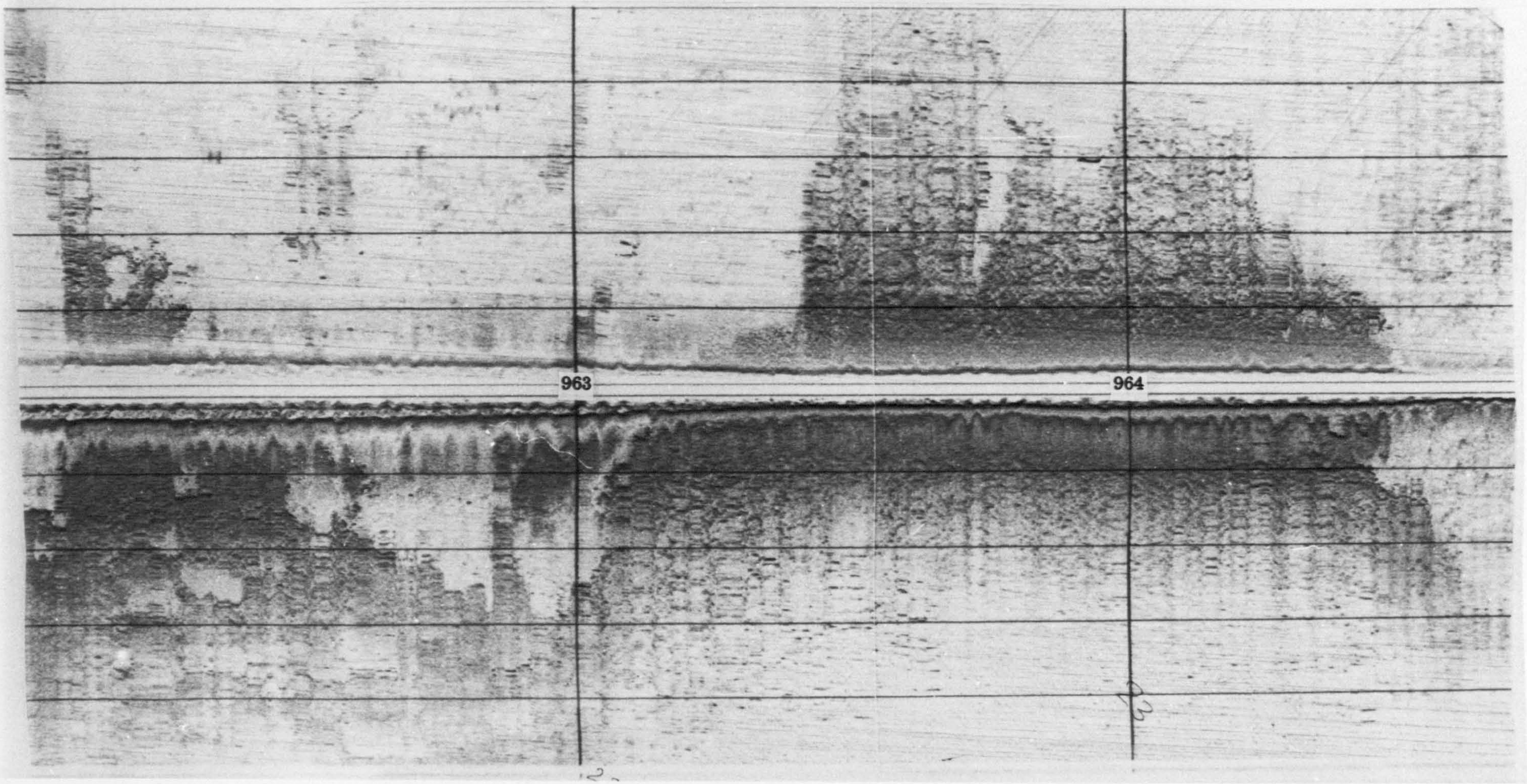

Fig: 3.14
Side scan sonar record showing tonal patches pattern near Great Ormes Head. Fixes are indicated in Figure 3.6.

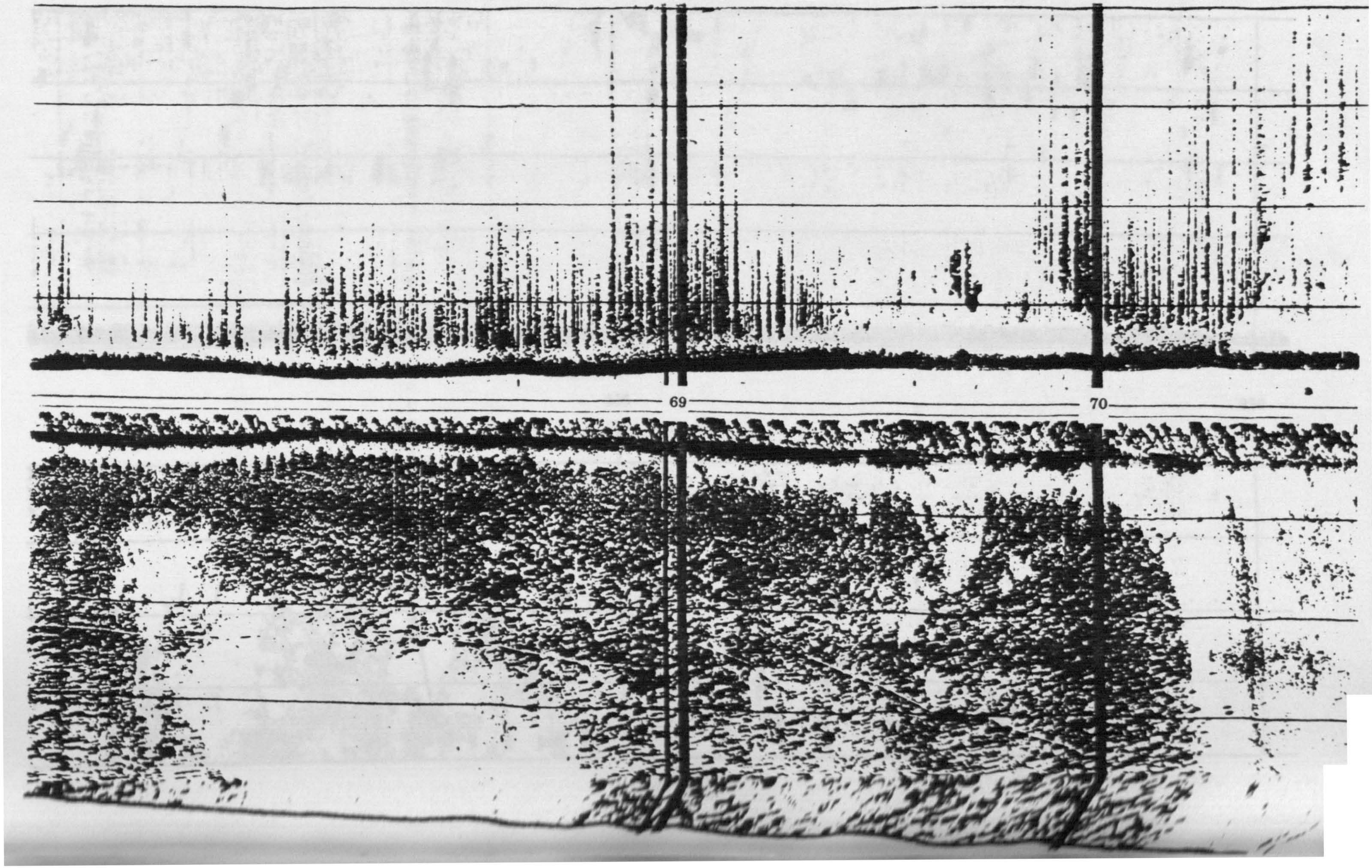

Fig: 3.15
Sonograph showing tonal patches pattern. Position fixes are shown in Figure 3.6.

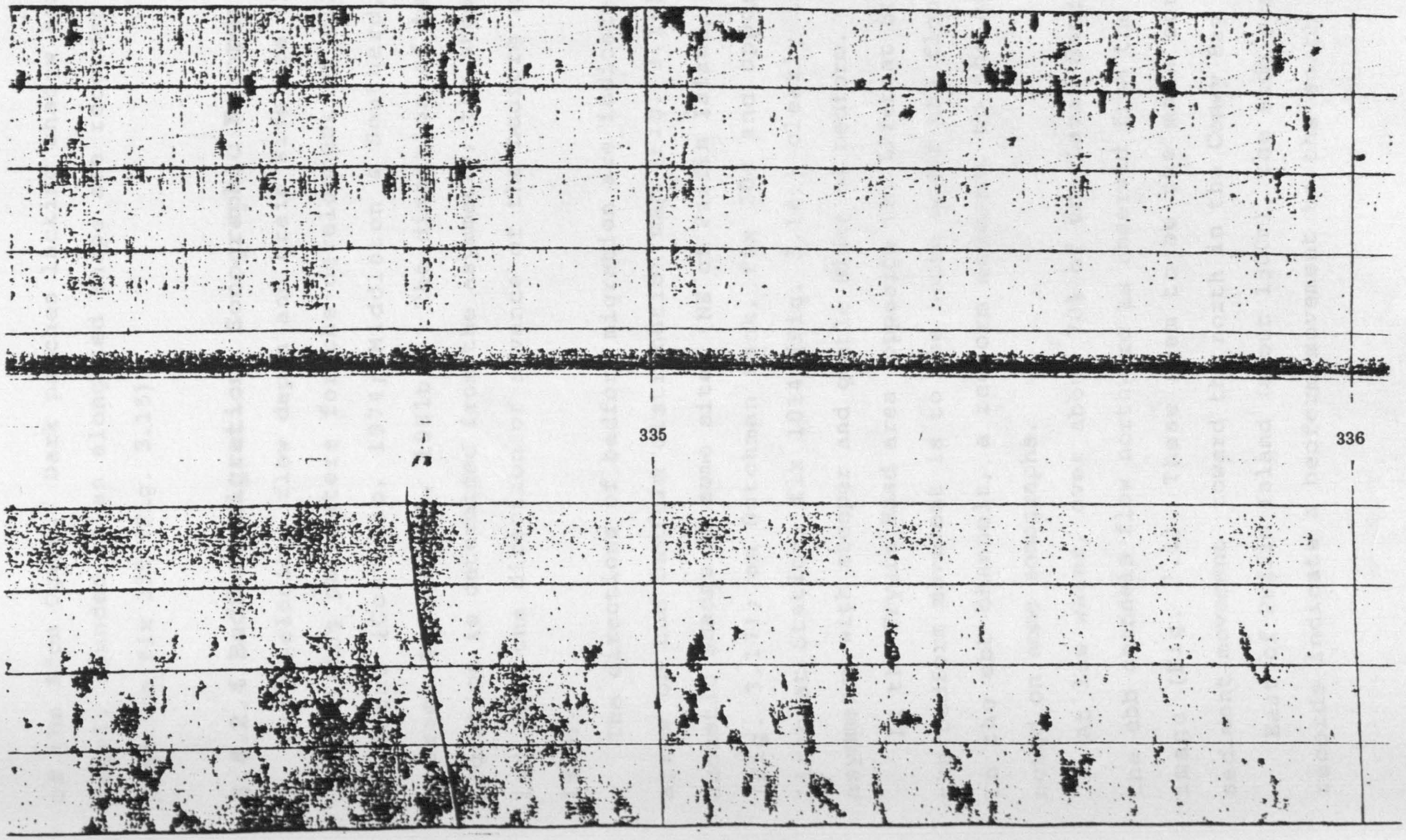

of the Afon Ogwen. Dark patches lacking shadow zones and nearly rounded to an elongated shape are recorded around position fix 335 (Fig. 3.15).

3.4.2.4 Bedform Migration: Sonographic Records

Flow velocity, flow depth and grain size are the main controlling parameters for the development of different bedforms [Costello, 1974; Middleton & Southard, 1978; Boersma & Terwindt, 1981b]. The direction of bedforms migration is determined from the asymmetry; the steep sides indicate the direction of advance of the bedform [Stride, 1963].

The directions of bedform migration are indicated by an arrow on the bedform distribution map (Fig. 3.16). The acoustic shades at some sites {NE of Puffin Island, fix 375 (Fig. 3.17); on Dutchman Bank, fix 204 and opposite to Lifeboat Station, fix 1014 (Fig. 3.18)} clearly indicate asymmetry with steeper and gentle sides of bedform.

In the Fryars Road area (opposite the Lifeboat Station), the bedform movement is to the south under the flood tide. In the ebb channels, a bedform movement to the north is noted on some sonographs.

At low water, over about 70% of the Lavan Sands area, the ebb channels flow northward as observed from the Landsat image (Fig. 7.1). These seem to be the main source of sediment movement toward the north in the Conwy Bay area.

East of Puffin Island (about 1300m), the side scan sonar records indicate a bedform movement to the south but the

Fig: 3.16 Distribution of seabed features recorded by side scan sonar.

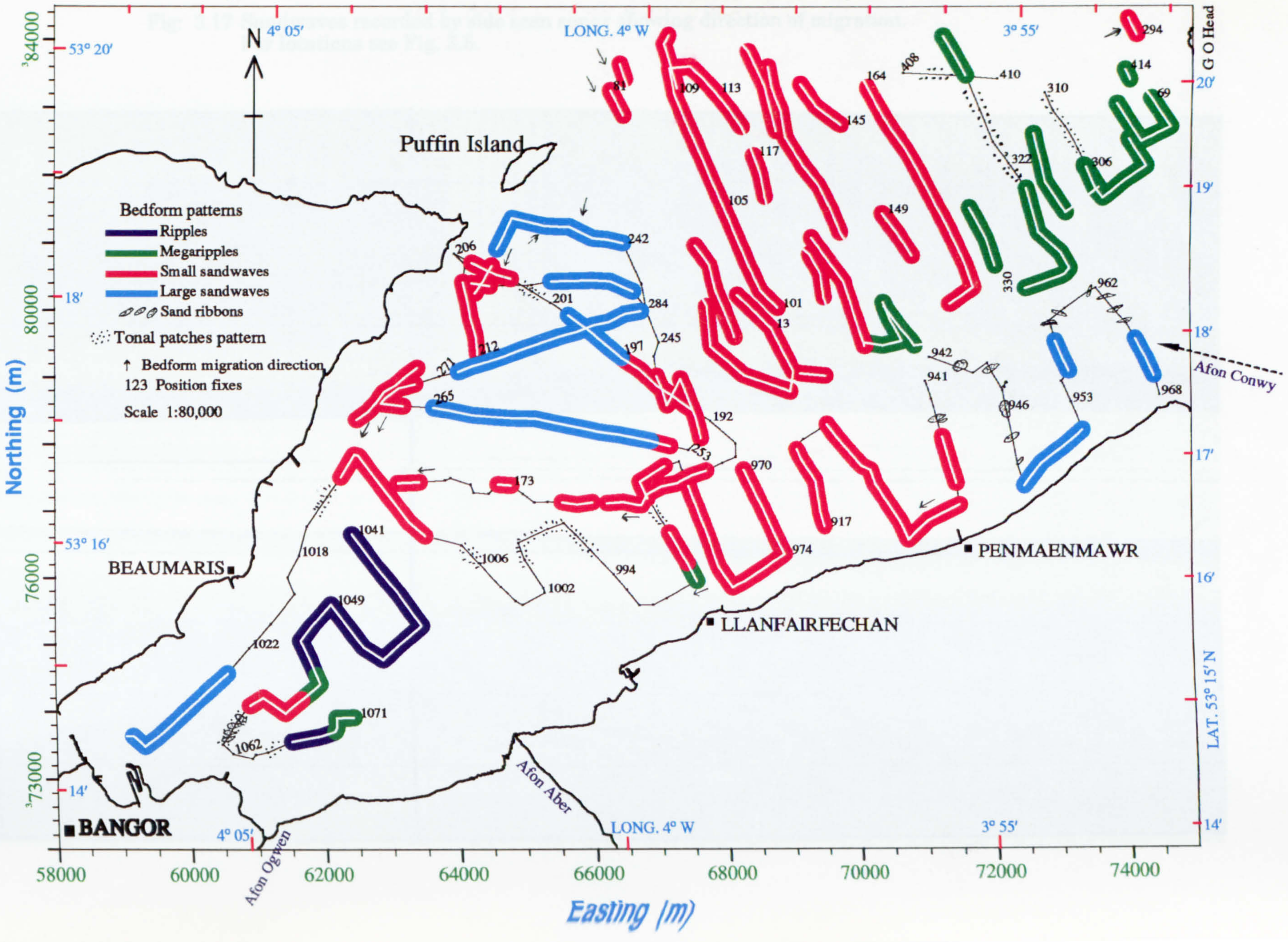

Fig: 3.17 Sandwaves recorded by side scan sonar showing direction of migration.
For locations see Fig. 3.6.

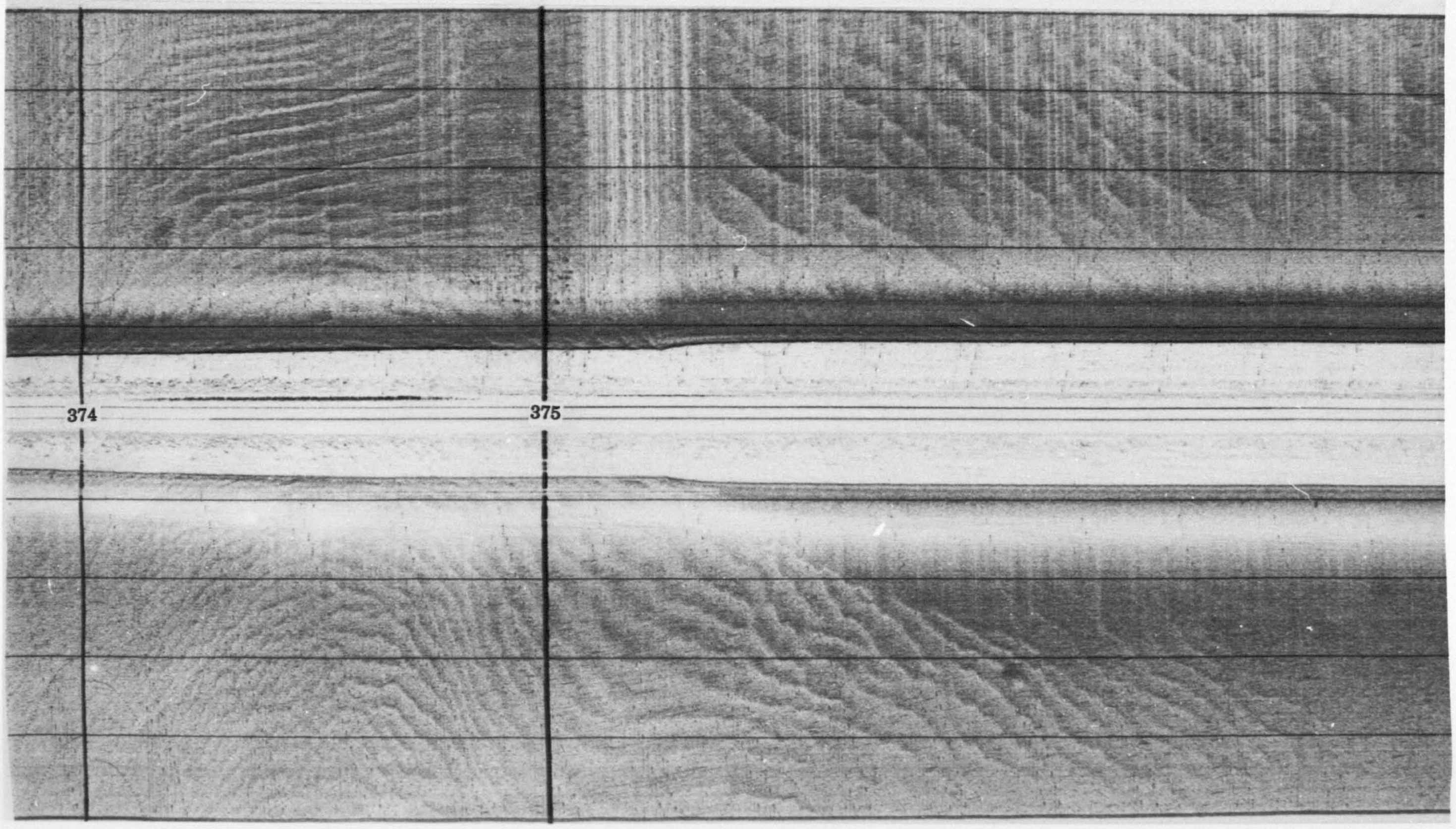

Fig: 3.18 Asymmetrical small sandwaves near Lifeboat Station showing direction of migration. Position fixes are shown in Fig. 3.6.

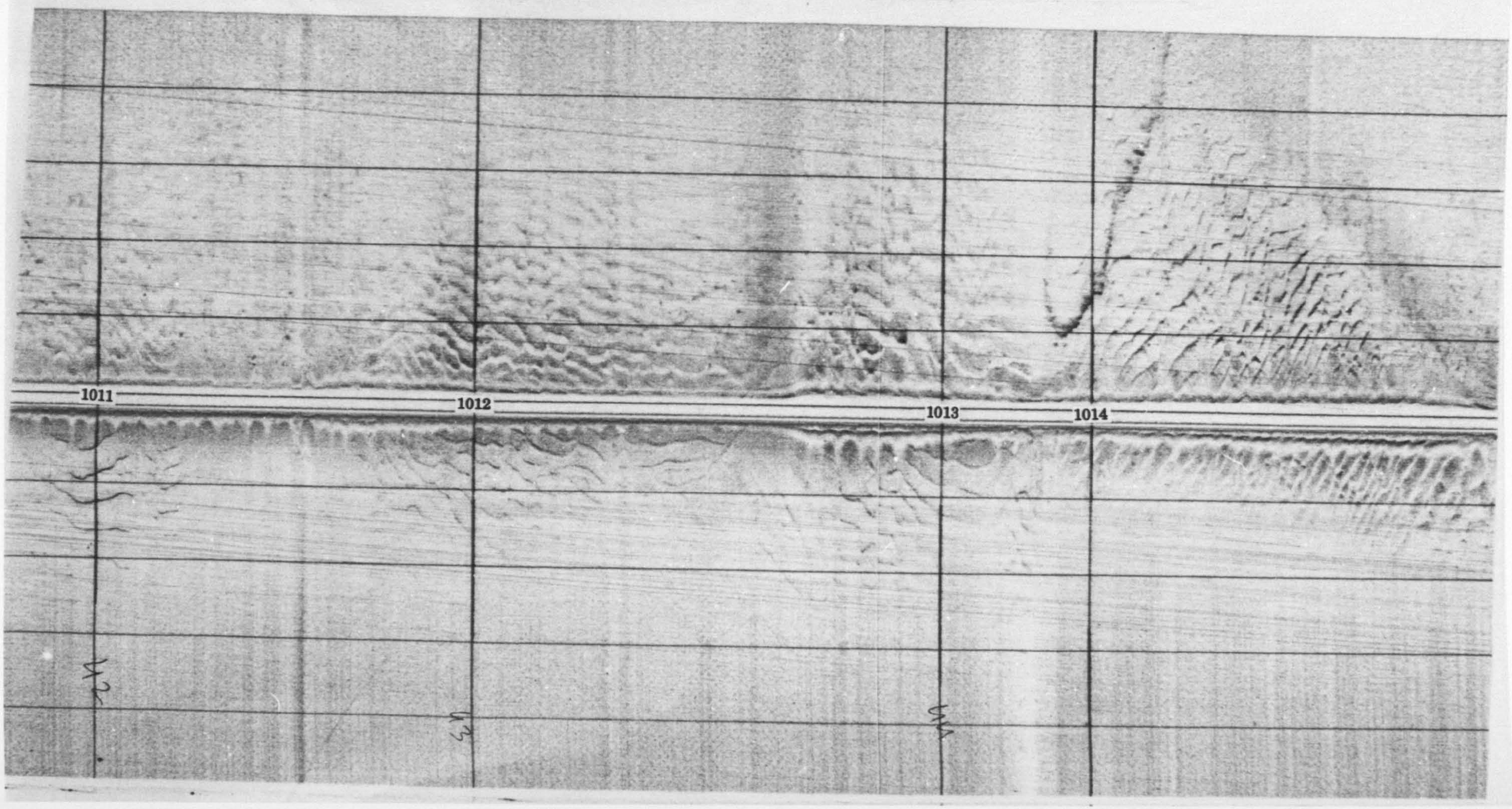

direction seen on aerial photographs is northward. The most probable reason for this reversal is the flood and ebb flow; because the side scan sonar survey was conducted during the flood tide and aerial photographs were taken at low water.

3.5 Subbottom Seismic Investigation

Sparker, boomer and pinger were used for the study of the distribution and thickness of recent sediment and the major structures of the consolidated rocks. Survey tracks are shown in Fig. 3.19. A short introduction of the equipment used for this purpose is given here.

3.5.1 Equipment and Survey Procedure

3.5.1.1 Sparker

This system was used on the Prince Madog on about 56.5km of survey line. On every ship turning and at about 2-3 minutes intervals, positions were located by a Decca Hifix. The sparker is a continuous seismic profiler using a low frequency, high energy sound source utilised for deep subbottom penetration in the marine environment. Anderson [1973], first studied the effect of an intensive electric spark between two electrodes located in the water. The heat generated by the discharge vaporises the water creating high-pressure bubbles. The explosion of these bubbles radiates the acoustic shock waves. Reflection of these sound waves from the boundaries of different density media

Fig: 3.19 Tracks of Subbottom Geophysical Surveys - NE Menai Strait & Conwy Bay.

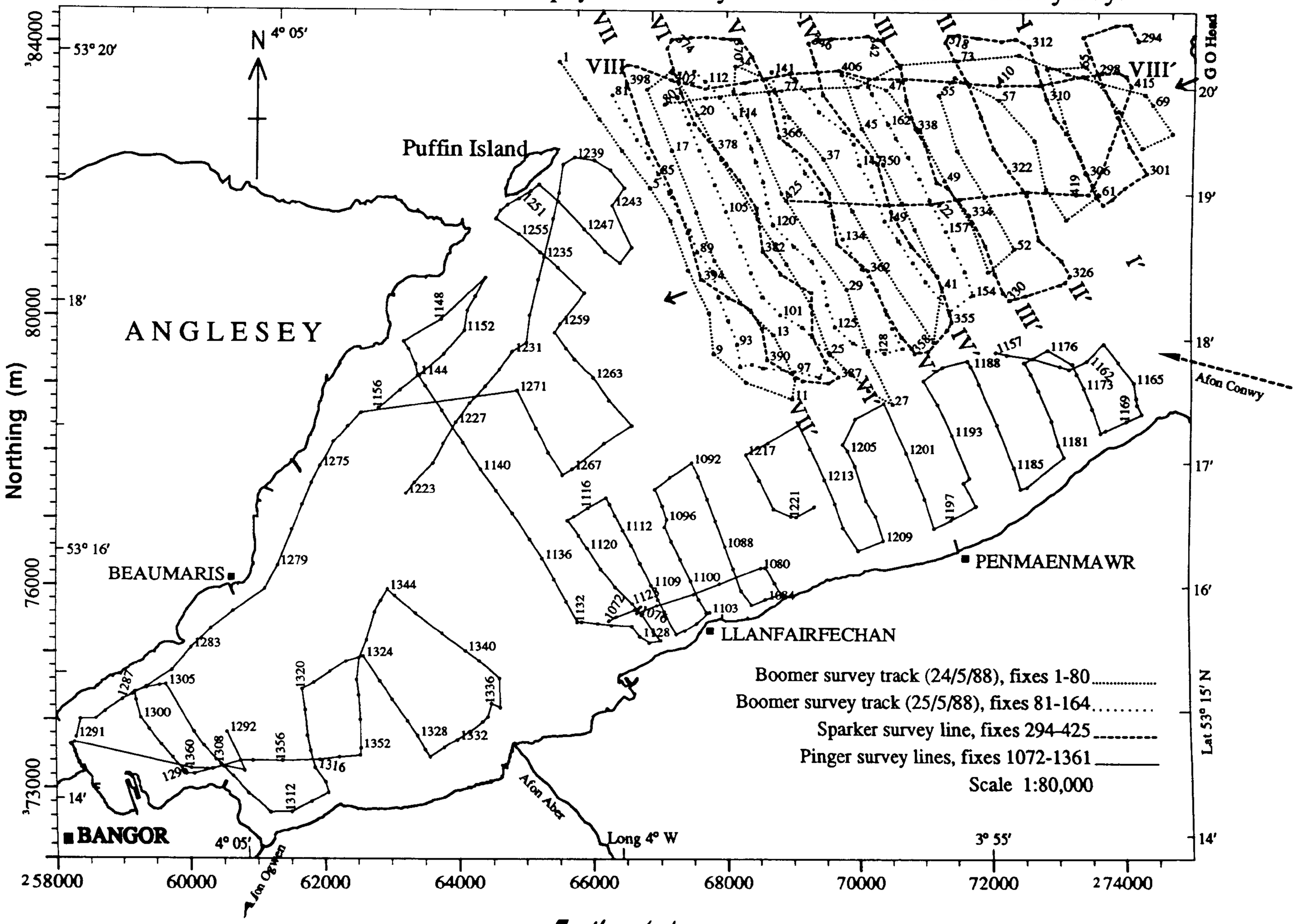

are picked up by a receiver and recorded graphically. Receiver EG & G hydrophone array model 265 is a modular array, which can be adjusted according to requirement by removal and addition of sections. Frequency range is 80-120 Hz. During the survey, the energy source unit was fixed for power outputs of 500 joules. A triggered capacitor bank (EG & G) model 231A, Power supply model 232, and EPC Model 4600 Griffith Recorder (Fig. 3.1-e) were used. The acoustic pulses of this system are capable of penetration up to 1000m. The resolution of the sparker model used is 2m or less, depending on operation power, frequency and subbottom materials.

3.5.1.2 Boomer

The boomer is an imploder which operates by creating a region of very low pressure. The collapse of water into that region generates seismic shock waves. Compared to the sparker, it is of higher frequency, lower energy and produces less penetration to the subbottom. It delivers about 200 joules of energy from about 400 Hz to a few kHz. The system consists of a transducer, electric power supply, capacitor storage bank, triggering device and recorder. EG & G Uniboom model 230 was used during two Prince Madog cruises. It provides a high resolution seismic profile of narrow section of the subbottom directly beneath the transducer. The sound-producing element (transducer) is a flat coil of wire which is magnetically coupled with insulated metal plate and rubber diaphragm. The transducer

is mounted on a catamaran (Fig. 3.1-c) towed behind the ship. An electrical capacitor discharges energy into the coil, causing induction currents in the plates that result in an outward force. The rubber diaphragm pushes the plate back slowly against the coil after each violent repulsion. The explosively forced plate generates a broad band of acoustic pulse toward the seabed. Reflections from seabed and subbottom boundaries are detected by a linear array of eight hydrophones, spaced at about 3.8m interval. An EPC Recorder 4600 was used to print acoustic reflections. A subbottom penetration limit of the model used is 50m.

3.5.1.3 Pinger

In intertidal and nearby adjacent areas, the O.R.E. Inc. Model 140 Pinger system was used to measure the thickness of modern sediments. This system consists of a fixed transducer comprising an array of 4 elements fixed on a plate at the end of vertical gimballed staff (Fig. 3.20). The staff is mounted vertically on the hull of the boat. Because of the assembly design, the transducer beam remains vertical towards the seabed despite any swing in the boat due to waves. The Pinger has a range of frequency between 3.5 ~~and~~ 7 kHz. A frequency of 3.5 kHz was chosen throughout the survey. A piezoelectric transducer produces a focused beam of sound directed vertically toward the seafloor. Power to the system was supplied by a generator (Fig. 3.20).

The ranges of frequency and energy required for the

Fig: 3.20 Robyn Cruise
Top: Pinger system (transducer & receiver)
Bottom: A- Generator for power supply to pinger, B- Master Trisponder Antenna

operation of the Pinger system provide suitable results for the mapping of surficial sediments [Leenhardt, 1967, 1969].

3.5.2 Reflector Depth from Acoustic Time

The travel time in millisec for an acoustic wave, from source to reflector and back to receiver, is marked on the acoustic records. The most common parameters, those involved in conversion of time to thickness of reflectors are; offset of source and receiver, and the velocity of sound in the sediment of the area. All water depths were calculated by echo sounder to minimise the effect of offset on depth and to avoid using two velocity scales. Depth measured by echo sounder will without doubt improve accuracy in determination of reflector depth. Subbottom two way travel time was converted into thickness of sediment layers. Sound velocity in sediments depends mainly on grain size, porosity, compaction, cementation and pore fluid salinity.

In recent years during a seismic study of glacial and surficial sediments, a seismic velocity of 1700-1800 m s^{-1} has been used in different parts of Irish Sea. Blundell, Davey & Graves [1971] calculated an average velocity of 1800 m s^{-1} for Quaternary sediments in the southern Irish Sea. Huws [1988] used a 1750 m s^{-1} seismic velocity in Traeth Lligwy Bay (Red Wharf Bay). Mahamod [1989] estimated sediment thickness by using a 1700 m s^{-1} sound velocity in the Dwyryd Estuary. Larcombe [1989] used a seismic velocity after Hamilton & Bachman, [1982] of 1710 m s^{-1} in the Mawddach Estuary where the mean grain size of the surficial

sediment is 2.5 phi. Solangi [1992] selected a sound velocity of 1750 m s^{-1} for medium to coarse sediment grain size in Caernarfon Bay. Other sources of information about this parameter are Taylor Smith [1975], Simpkin [1976], and Fenemore [1976].

Sound velocity in this area is calculated from the formula of Hamilton & Bachman [1982].

$$Vs = 1952.5 - 86.26\ d + 4.14\ d^2 \qquad (2.1)$$

Vs = Sound velocity in sediments (m s^{-1})

d = Sediment mean grain size (Ø)

After comparing the laboratory results with in situ velocity measurements, Hamilton & Bachman [1982] concluded that the prediction of an average seismic velocity at a standard error of 30 m s^{-1} could be made based on mean grain size. From Eq. 2.1 sound velocities for a representative mean grain size of 2.5Ø in the sparker and boomer survey area (1762 m s^{-1}) and 2.8Ø in the pinger survey areas (1743 m s^{-1}) have been calculated.

3.5.3 Depth Correction for Offset

The sound source and receiver were horizontally separated by a distance of about 12m during the sparker and boomer surveys. This offset may vary a few metres, because of rise, fall, and slew sideways of these instruments on turning of the ship. Because of this offset, the true thickness of reflection is less than the recorded thickness on the original record. Distortion is a maximum when the

reflector depth below source and receiver is of the order of their offset, so that a significant proportion of the sound travel time represents a horizontal component of ray path. Distortion decreases with an increase in depth of reflectors, when the angle of reflection at the acoustic boundary tends towards zero.

The area which requires correction in depth because of this offset has more than 10 metres water depth. So a correction in reflector thickness is made in water deeper than 10m (see Fig. 3.21.)

3.5.4 Subbottom Seismic Interpretation

A survey of about 240 km lines was conducted to collect information about the subbottom seismic sequence in the project area. Three main reflectors, defined as 1st, 2nd and 3rd reflectors from the seabed, were detected during the survey. These reflectors are parallel to sub parallel and are discontinuous in places. After necessary corrections (tidal depth, offset, time to velocity conversion) in seismic records, the interpretation is presented diagrammatically in four forms.

a- Interpretation as numerical values: in this presentation, the depths of records are shown as a spot map (Fig. 3.22). The position of the recorded depth is marked and labelled by value. The figure shows the comparison of data collected by different systems during different cruises.

b- Interpretation along survey lines: In these diagrams

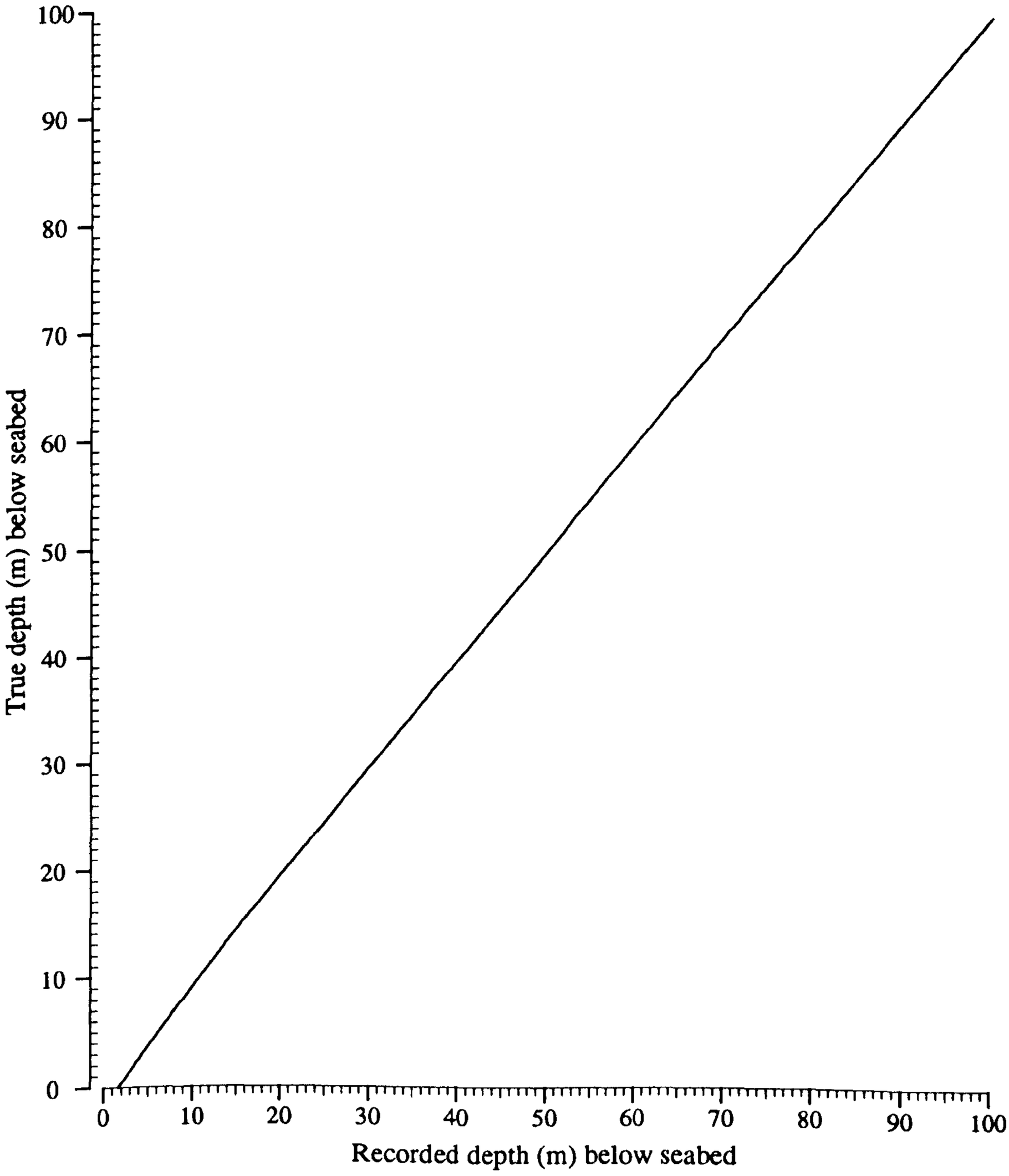

Fig: 3.21
Subbottom depth correction for sparker and boomer reflectors for water depth > 10 metres.

the records are interpreted along the survey tracks. The boomer and pinger data interpretations are shown in this form. From these diagrams the true positions with true seismic reflectors depth can be located by consulting the track chart. But the accuracy in comparisons of data from different survey lines depends on how parallel the lines are to each other. The boomer lines are almost parallel to each other. The reference positions are marked by arrows on each line.

c- Interpretation along x-sections: X-sections are straight lines along the survey lines and are parallel to each other (shown as I-I′ to VIII-VIII′ in Fig. 3.19). Those records that deviate more than 100m on either side of the x-sections are corrected. There are only few records (fixes 391, 392, 394 on VII-VII′, 382, 384 on VI-VI′ and 336 on III-III′), which are 200-400 metres apart from the survey lines. The data in x-sections can be readily compared and provide a quick visual trend of sedimentary layers in the study area. In x-sections, data from different cruises are integrated.

d- Contour map: The spatial distribution of the recorded seismic boundaries are shown as contour maps. A grid of 50m * 50m is selected in these maps during the data interpolation using the computer graphic programme.

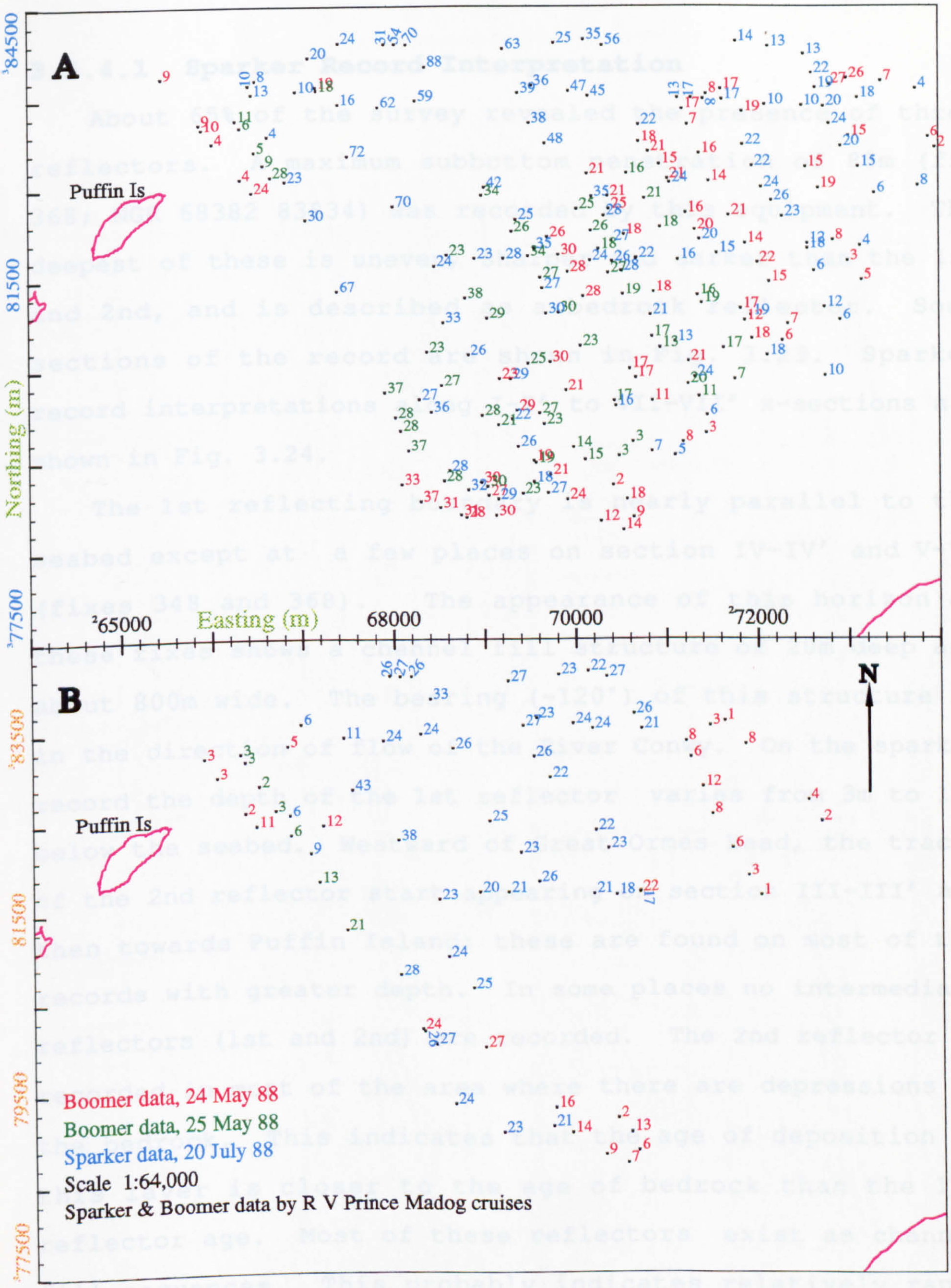

Fig: 3.22

Spot map showing depths (m) of 3rd (A) and 2nd (B) seismi c reflectors below seabed.

3.5.4.1 Sparker Record Interpretation

About 65% of the survey revealed the presence of three reflectors. A maximum subbottom penetration of 88m (fix 368; NGR 68382 83834) was recorded by this equipment. The deepest of these is uneven, sharper and darker than the 1st and 2nd, and is described as a bedrock reflector. Some sections of the record are shown in Fig. 3.23. Sparker record interpretations along I-I′ to VII-VII′ x-sections are shown in Fig. 3.24.

The 1st reflecting boundary is nearly parallel to the seabed except at a few places on section IV-IV′ and V-V′ (fixes 348 and 368). The appearance of this horizon at these fixes shows a channel fill structure of 20m deep and about 800m wide. The bearing (~120°) of this structure is in the direction of flow of the River Conwy. On the sparker record the depth of the 1st reflector varies from 3m to 12m below the seabed. Westward of Great Ormes Head, the traces of the 2nd reflector start appearing on section III-III′ and then towards Puffin Island; these are found on most of the records with greater depth. In some places no intermediate reflectors (1st and 2nd) are recorded. The 2nd reflector is recorded in most of the area where there are depressions in the bedrock. This indicates that the age of deposition of this layer is closer to the age of bedrock than the 1st reflector age. Most of these reflectors exist as channel fill sequences. This probably indicates relatively rapid deposition in sub- or pro-glacial environments, by meltwater from retreating ice sheet.

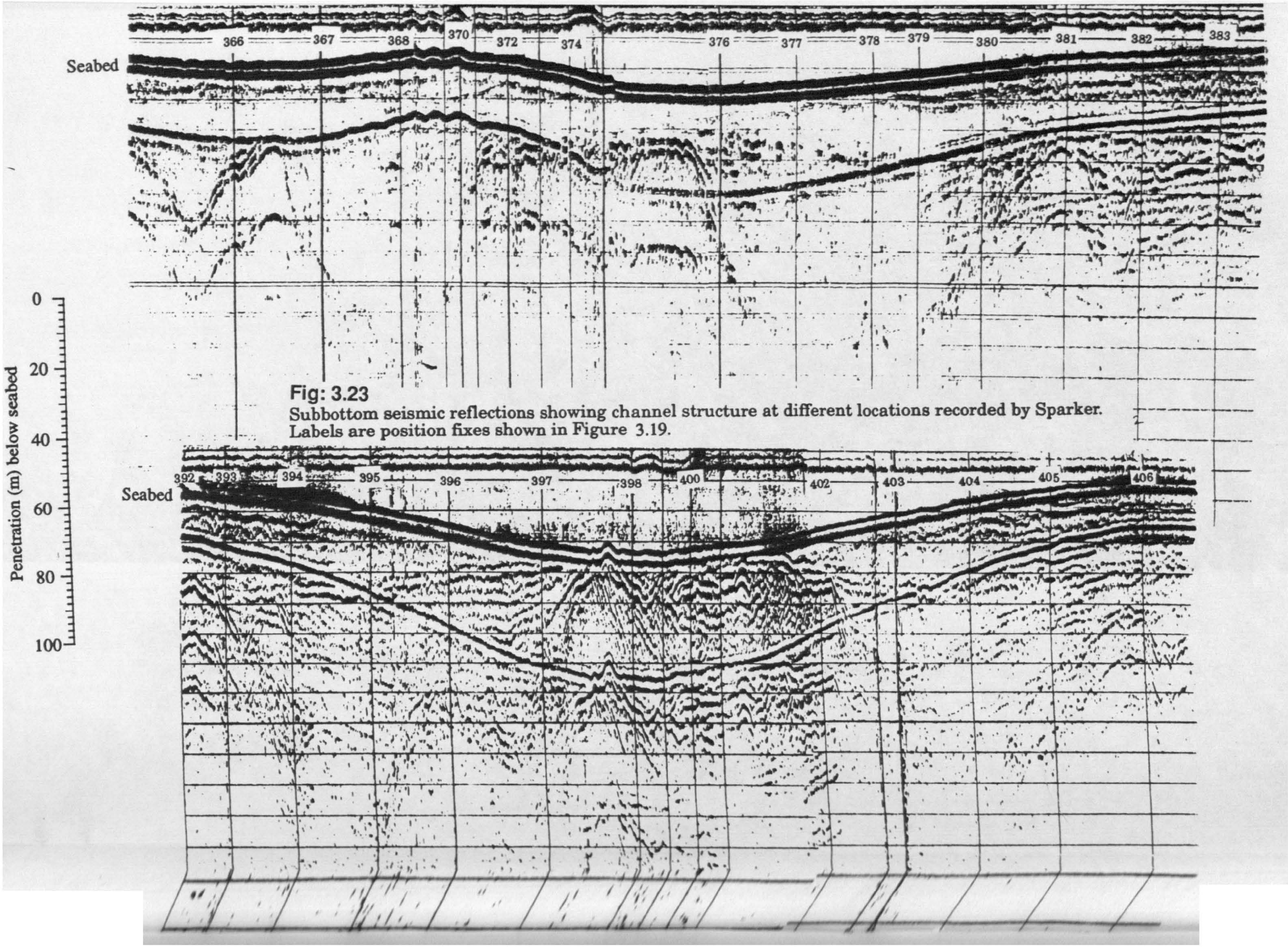

Fig: 3.23
Subbottom seismic reflections showing channel structure at different locations recorded by Sparker. Labels are position fixes shown in Figure 3.19.

Fig: 3.24

Interpretation of Sparker and Boomer subbottom seismic profiles along I-I′ to VIII-VIII′ x-sections. Depth below O. D. Newlyn. Position fixes (labels) and x-sections are shown in Fig. 3.19

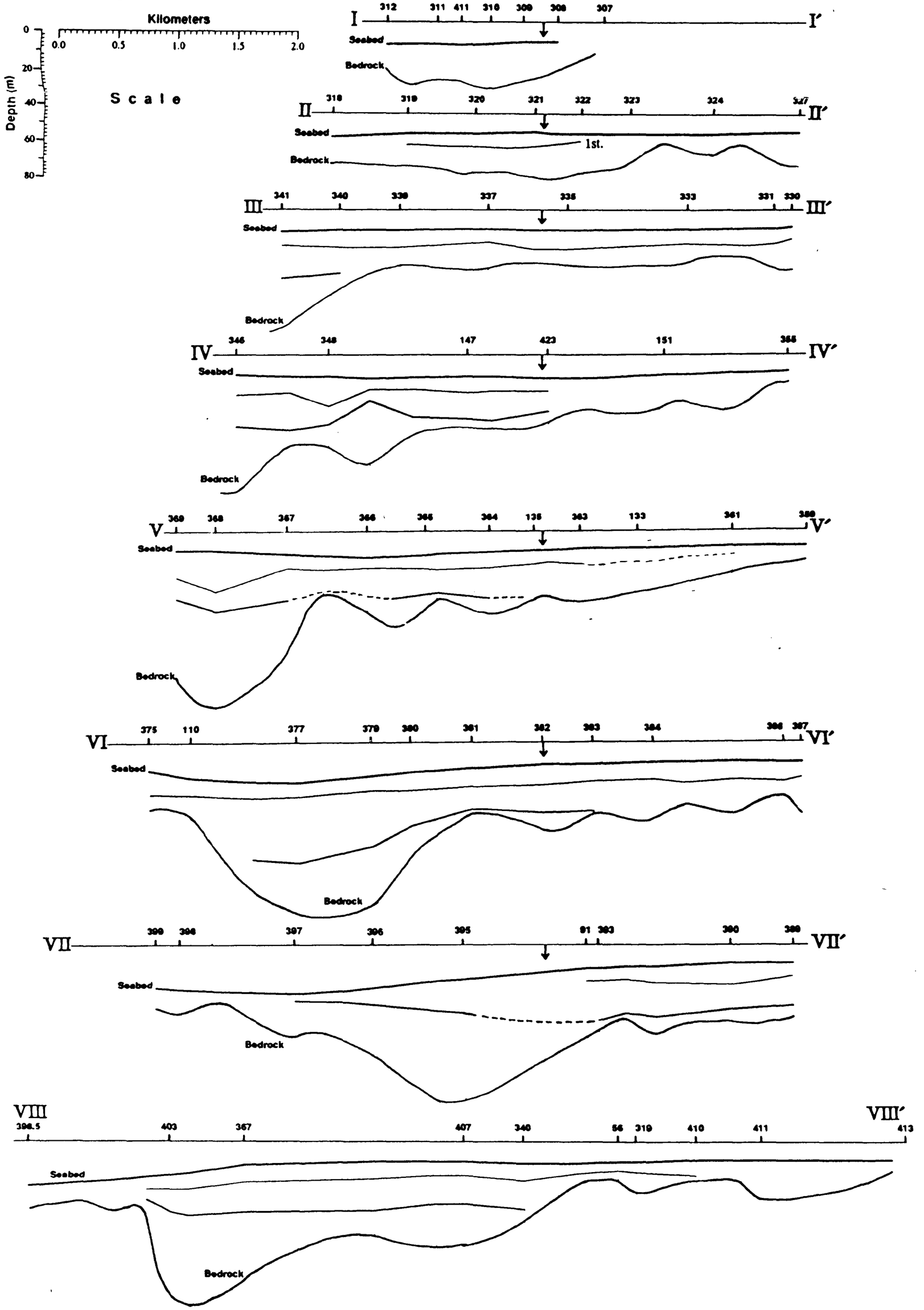

The bedrock reflector shows a channel near Puffin Island, which seems to be an extension of the Dinorwic Fault (Fig. 2.1). The maximum depth of this signal is -99m relative to O. D. Newlyn (Fig. 3.23). The depth of bedrock ranges from 3m to 88m below the seabed. All the sections show bedrock dipping off the coast up to the channel-fill structure.

3.5.4.2 Boomer Record Interpretation

This system was used on two surveys in May 1988. On 24 May, the boomer survey was conducted in parallel lines at about one kilometre distance to each other and on the second day lines were run between the previous survey to increase coverage. About 50% and 65% of the boomer surveys on 24th and 25th May 88, respectively provided acoustic signals. The interpretation of boomer records is shown in Fig. 3.25 and Fig. 3.26.

A survey track of 87 km was conducted by this system. Two subbottom sedimentary layers were detected except fixes 2-4. A maximum depth of 38m was recorded below the seabed.

On most of the survey lines a single major reflecting horizon is identified. The general appearance, dip and depth of this reflector is almost identical to the bedrock traced from the sparker system. Above the main reflector another reflector is recorded in places. Because of discontinuity in detection of the intermediate reflector, it is not always clear that whether this reflector is the 1st

Fig: 3.25

Interpretation of subbottom seismic profiles along Boomer survey lines (24th May 1988). Depth below O. D. Newlyn. Labels are position fixes, shown in Fig. 3.19.

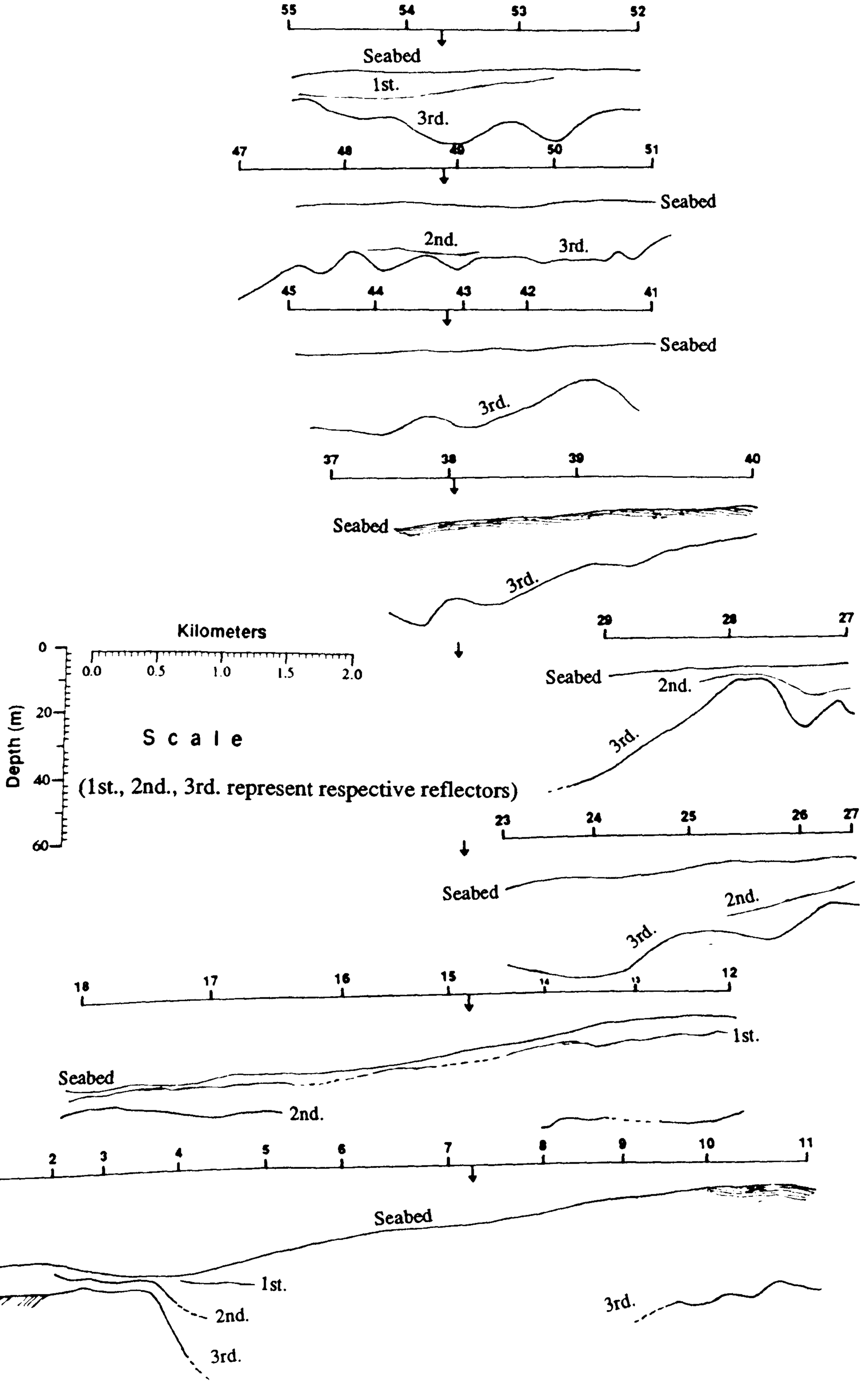

Fig: 3.26

Interpretation of subbottom seismic profiles along Boomer survey lines (25th May 1988). Depth below O. D. Newlyn. Labels are position fixes, shown in Fig. 3.19.

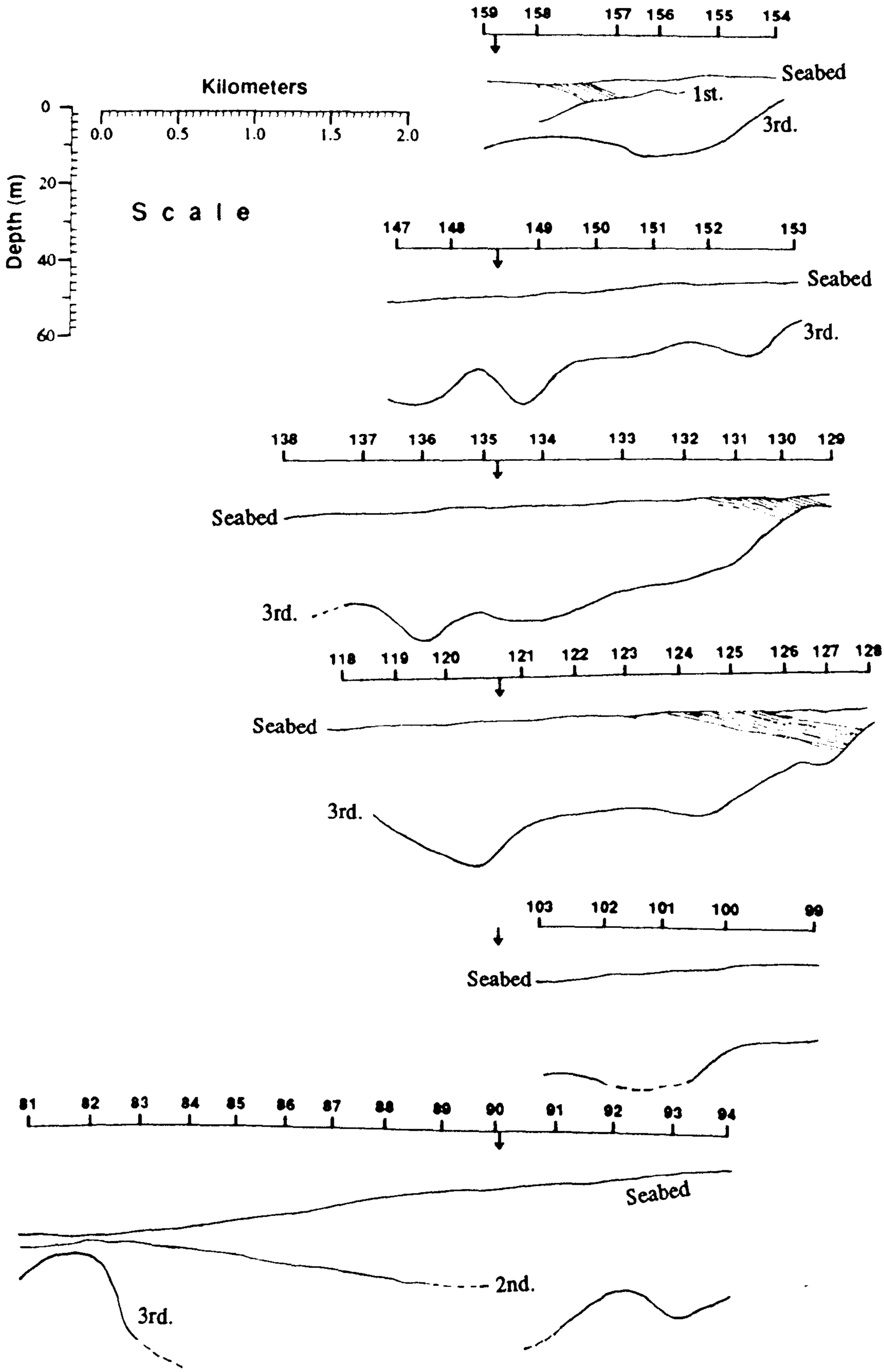

(1st., 2nd., 3rd. represent respective reflectors)

or 2nd (described in the sparker section). The sparker data and pattern of survey lines had made this task easy and increased confidence in these as proper horizons. The reflector that is parallel, straight and closer to the seabed is the 1st. This is further confirmed by comparing their depths with the nearest depth of the 1st reflector found on the sparker record. The intermediate reflector is defined as the 2nd reflector. Again this is confirmed by depth of the 2nd reflector traced during the sparker survey. For an example see seismic boundaries at fix 396 at x-section VII-VII' (Fig. 3.24), fix 4 on survey line 1-11 (Fig. 3.25), and fix 83 on survey line 81-94 (Fig. 3.26). Towards the southeast of these fixes, the sparker continued to record bedrock up to 86m below the seabed but the boomer ceased detecting the deepest reflectors (Fig. 3.27; fixes 4, 83) because of its penetration limit. The general appearance, channel fill structure and dip of acoustic boundaries revealed on the boomer record are almost identical with the boundaries recorded by the sparker. Because of its high frequency compared to the sparker, it has better resolution, which is demonstrated on some survey lines by revealing further thin layers in the top layer of the modern sediments (Fig. 3.28).

The extension of the Dinorwic Fault in Conwy Bay near Puffin Island (Menai Strait main channel) is also observed on the boomer record. But because of the penetration limit, this system could not record bedrock at more than 56m below O. D. (Newlyn).

Fig: 3.27
Maximum bedrock depth recorded by Boomer system on 24th (A) and 25th (B) May 1988 cruises. Locations are shown in Figure 3.19.

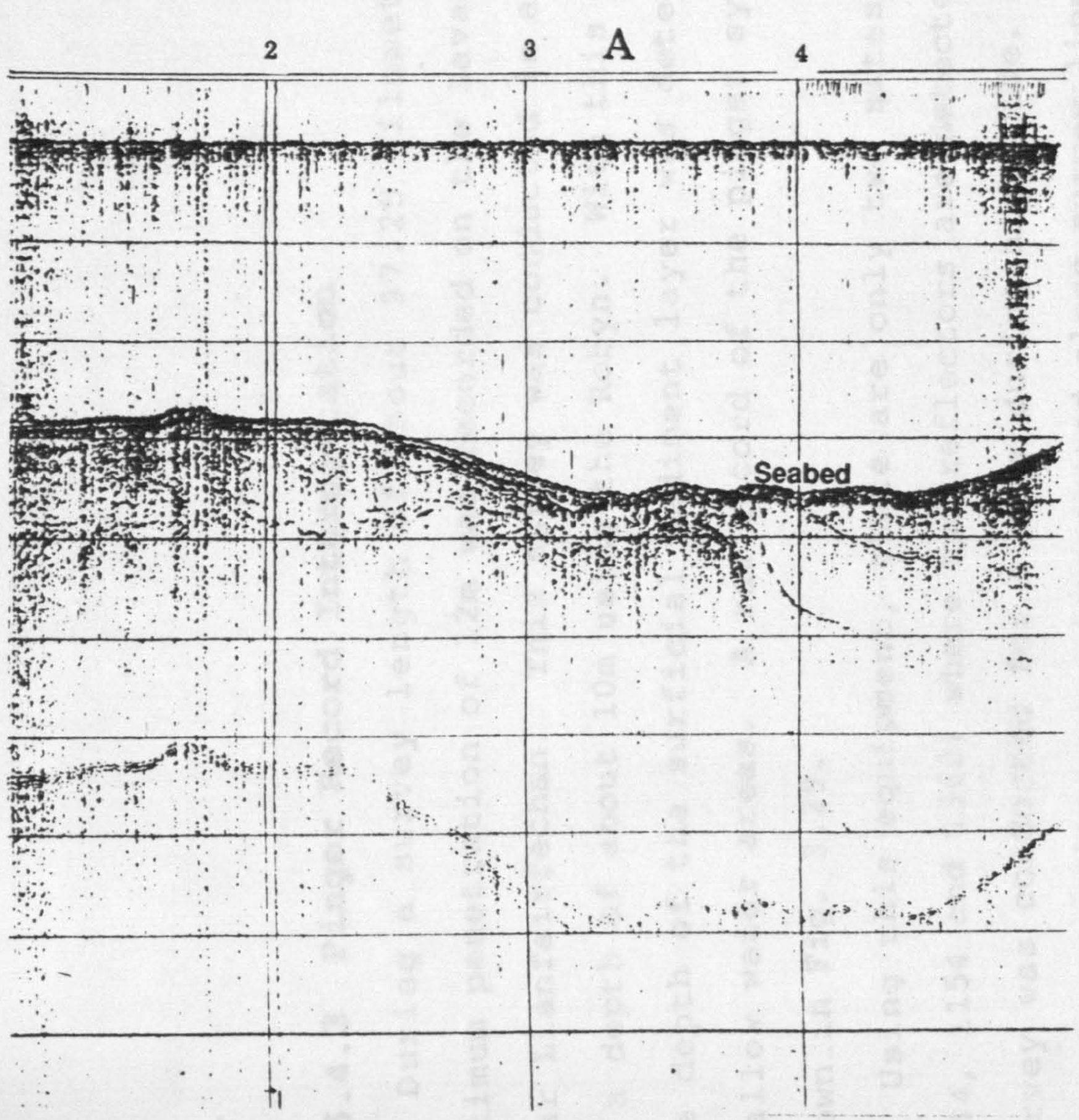

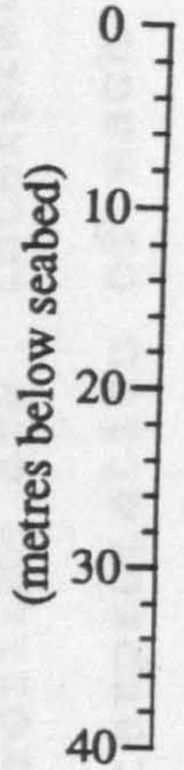

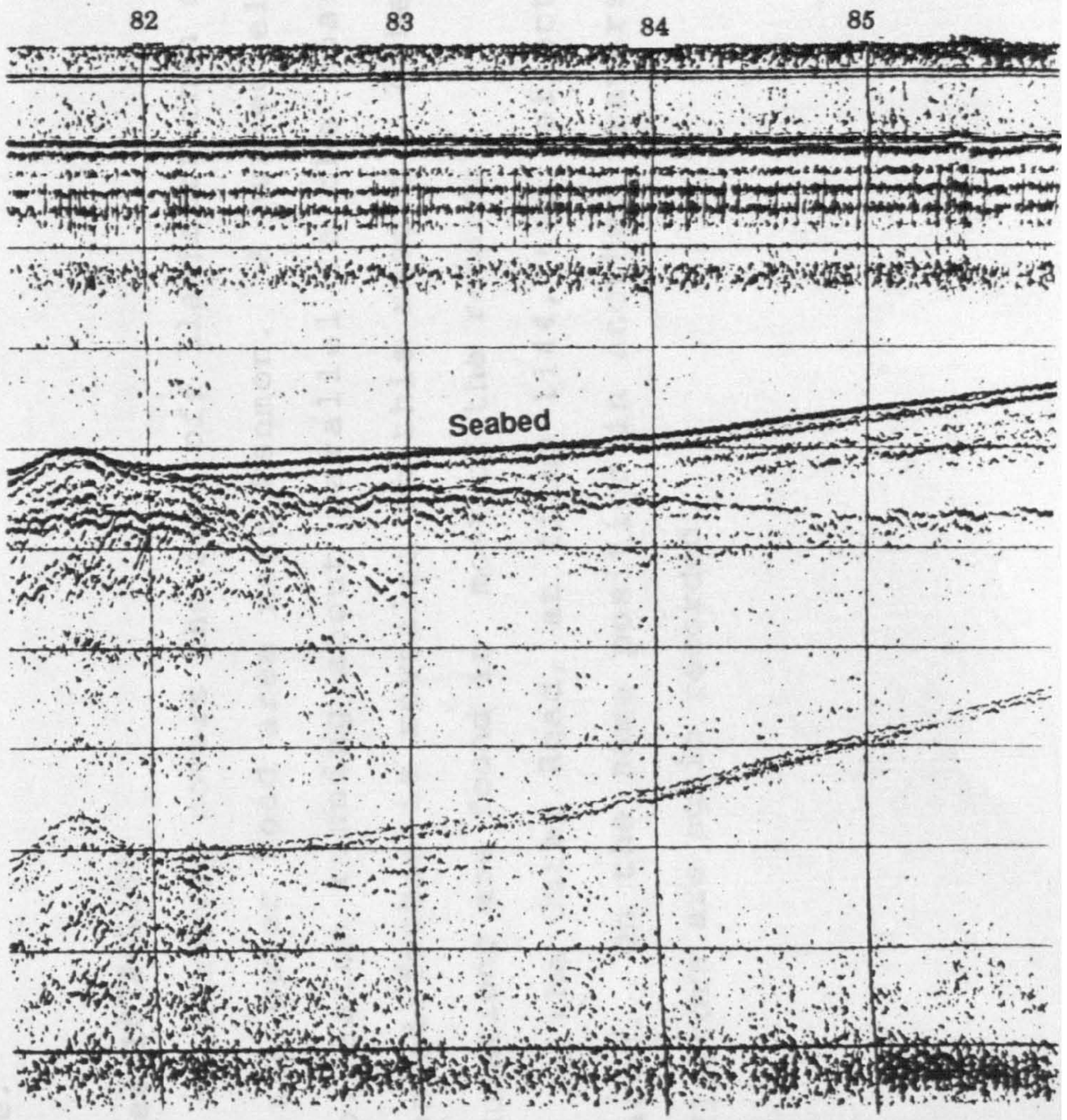

3.5.4.3 Pinger Record Interpretation

During a survey length of about 97.25 kilometres, a maximum penetration of 12m was recorded on the Lavan Sands near Llanfairfechan. This survey was conducted in areas up to a depth of about 10m using the Robyn. With this survey, the depth of the surficial sediment layer was detected in shallow water areas. A raw record of the pinger system is shown in Fig. 3.29.

Using this equipment, there are only two sites (fixes 1144, 1154 and 1360) where two reflectors are detected. The survey was conducted for 4 days during high tide. Pinger subbottom profiles are interpreted along survey lines (Fig. 3.30). Interpretation of each date's record is discussed here.

Fixes 1072-1156

This survey covers the area off Llanfairfechan and some of the Outer Road area near Penmon. A buried elongated depression running about parallel to the coast near Llanfairfechan is revealed on this record. Other minor undulations are found in most of the records.

In the Outer Road, at fixes 1144, two reflectors are traced. On the same position in another traverse these reflectors are again recorded.

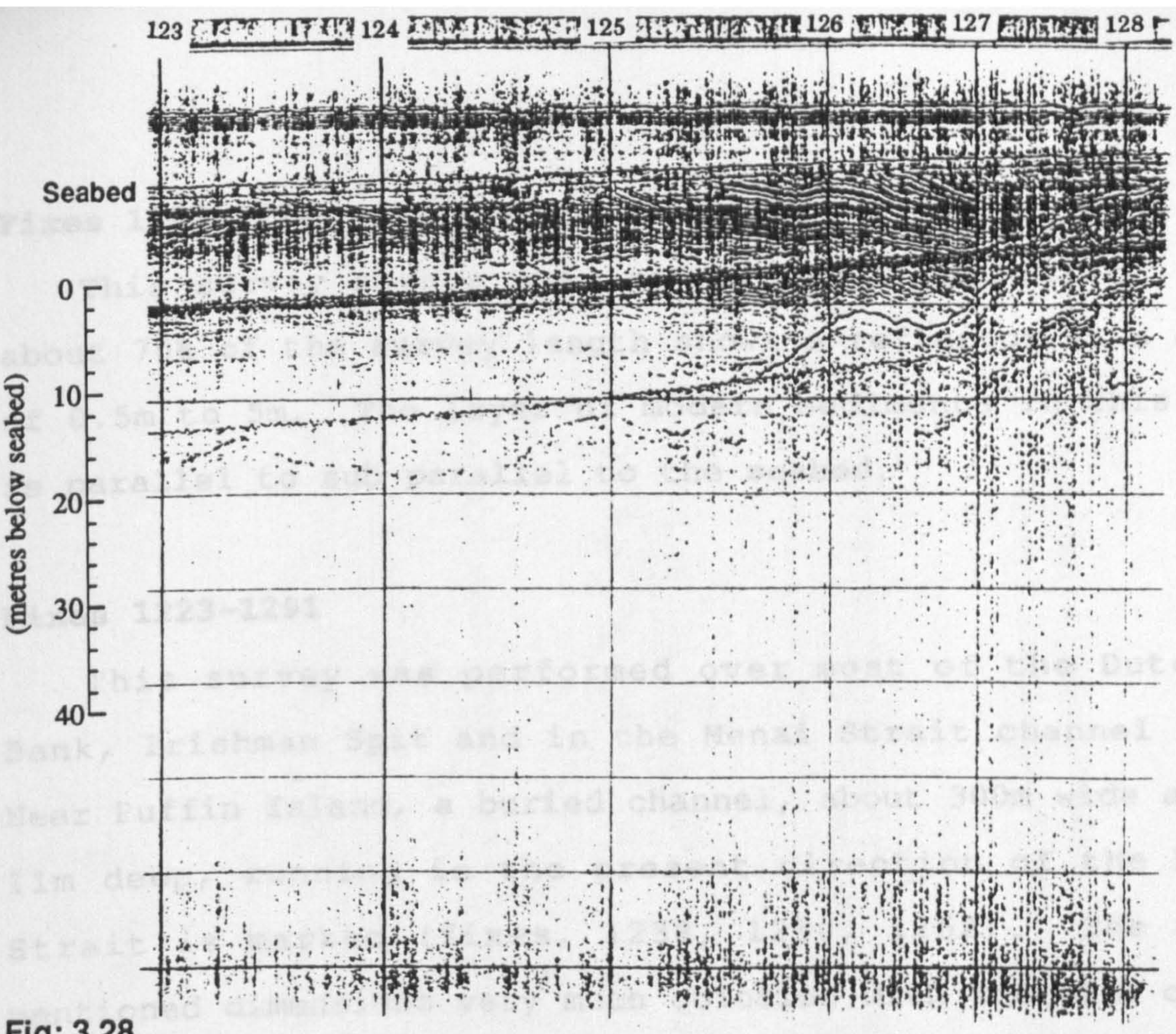

Fig: 3.28
Thin layers within recently deposited sediments on subbottom seismic profile recorded by Boomer. Position fixes are shown in Figure 3.19.

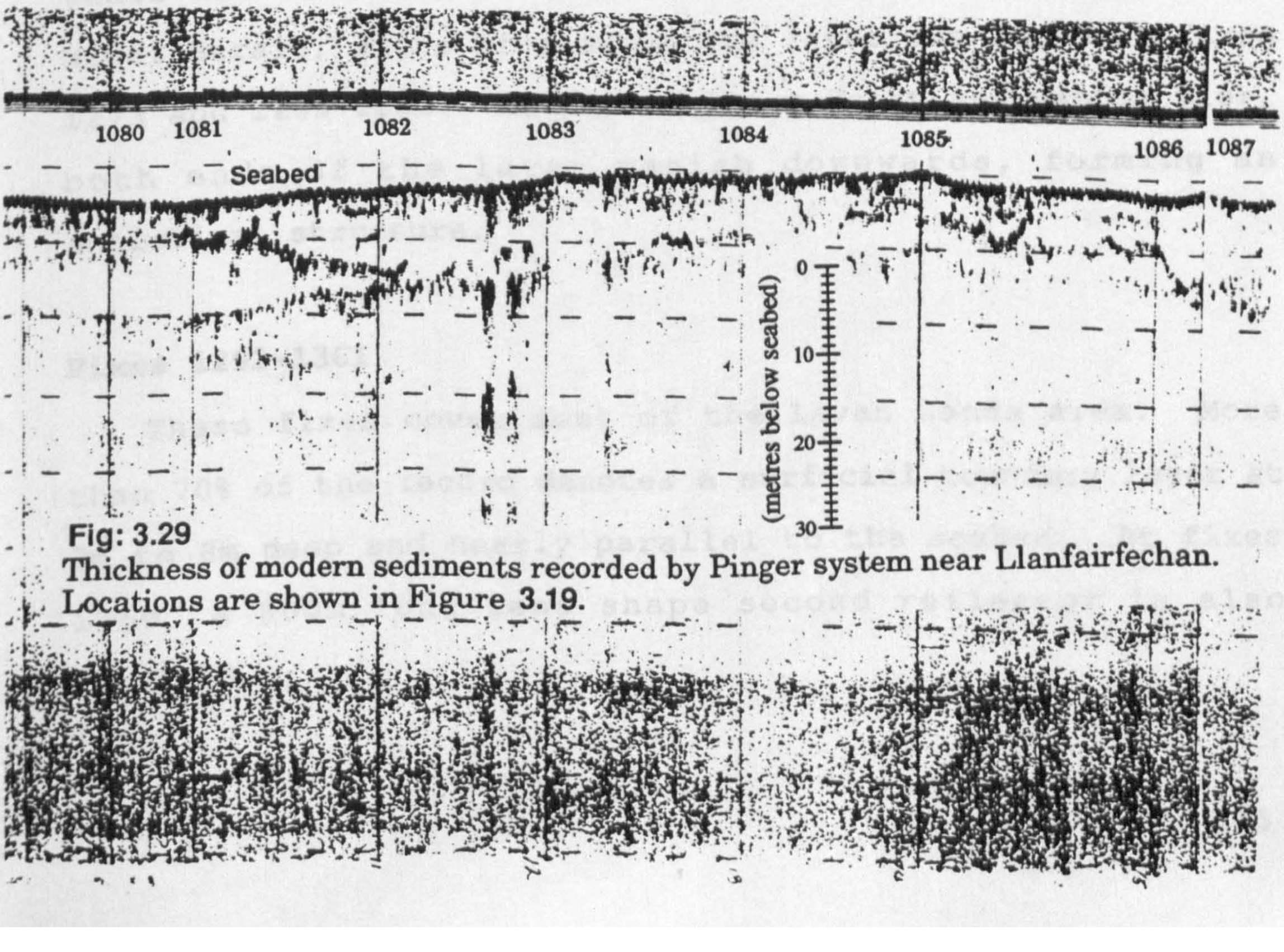

Fig: 3.29
Thickness of modern sediments recorded by Pinger system near Llanfairfechan. Locations are shown in Figure 3.19.

Fixes 1157-1222

This survey covers the area around Penmaenmawr. Here about 70% of the survey length shows a reflector at a depth of 0.5m to 5m. The layer of modern sediments in this area is parallel to sub parallel to the seabed.

Fixes 1223-1291

This survey was performed over most of the Dutchman Bank, Irishman Spit and in the Menai Strait channel area. Near Puffin Island, a buried channel, about 300m wide and 7-11m deep, running in the present direction of the Menai Strait is marked (fixes, 1238, 1250, 1252). The above mentioned dimensions very much coincide with the size of the present course at many places. This probably indicates the path of the Strait at its time of formation (6,000-7,000 years B.P.), i.e., to the east of Puffin Island. In the Menai Strait, signs of a subbottom layer are found at fixes 1273 and 1285-1288. Between Gallows Point and Bangor pier, both ends of the layer vanish downwards, forming an anticlinal structure.

Fixes 1292-1361

These fixes cover most of the Lavan Sands area. More than 70% of the record denotes a surficial boundary layer at 2m to 8m deep and nearly parallel to the seabed. At fixes 1360, a 800m long lens shape second reflector is also detected.

Fig: 3.30
Interpretation of Pinger subbottom profiles along survey lines. Depth below O. D. Newlyn. Labelled position fixes are shown in Fig. 3.19.

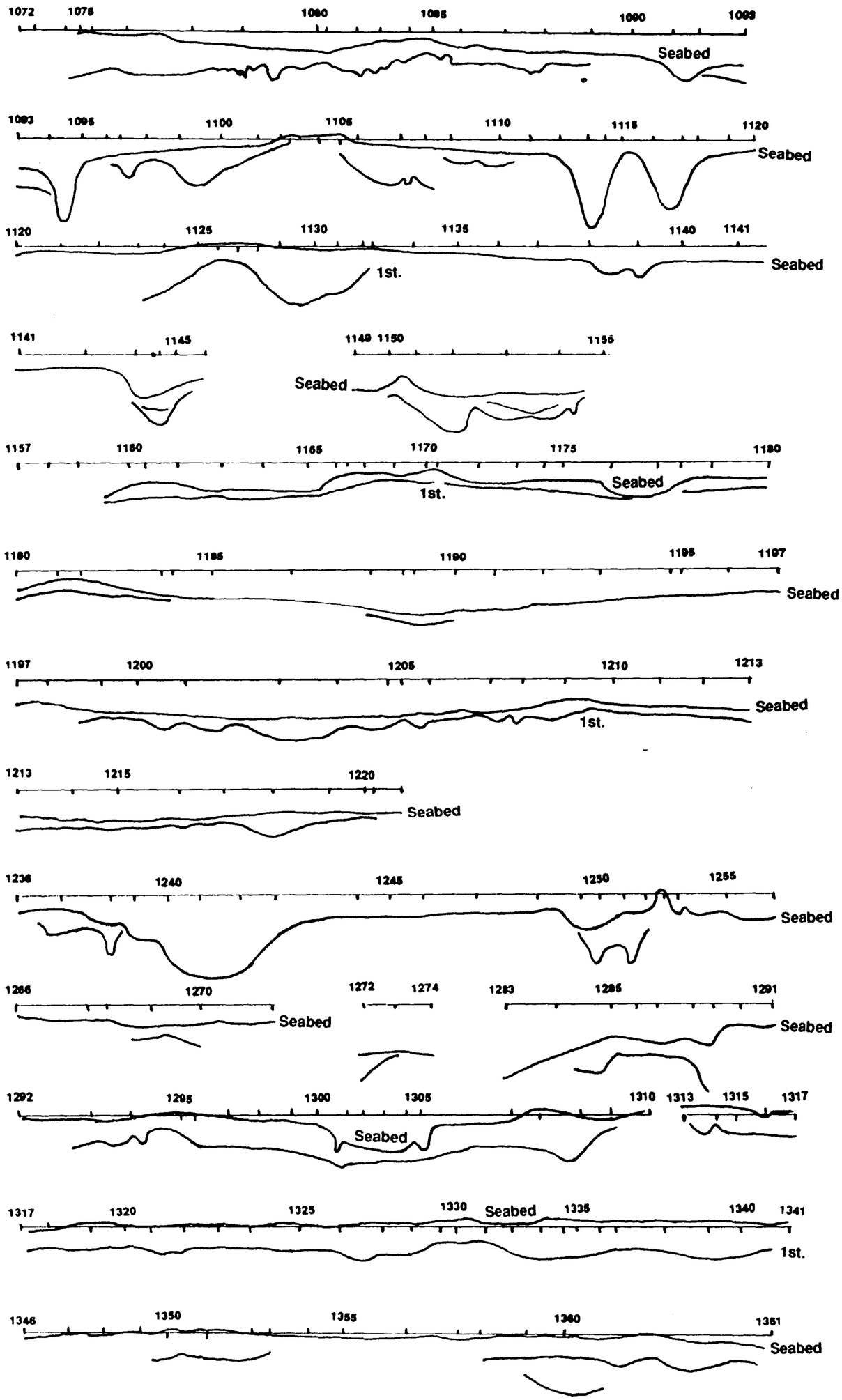

3.5.5 Seismic Stratigraphic Analysis

Vail, Mitchum & Thompson [1977] state that "seismic stratigraphy provides a practical geological/stratigraphical interpretation tool for seismic records". They further describe how the study of the unique patterns of seismic reflection allows the direct application of geologic concepts based on physical stratigraphy, leading to a possible interpretation of depositional environment, geological time correlations, and post depositional structure deformation, etc. One of the main objects of seismic stratigraphy is to work out the geological history of an area [Sheriff, 1980].

From the present seismic records, the main acoustic boundaries have been interpreted from surveys with different cruises and equipment. In the following sections the reflection/structural layers will be further studied for stratigraphic significance, which will help to interpret the Quaternary sedimentary depositional environments in the area.

Seismic stratigraphic analysis is based on the following basic steps.

a- seismic sequence analysis.

b- seismic facies analysis

c- sea level changes

The third step (c) is an inference from the first two, [Vail, Todd & Sangree, 1977].

3.5.5.1 Seismic Sequence Analysis

The main difference between the seismic sequence and the depositional sequence, is that the former is identified by using seismic evidence. Both are used for the description of sedimentary deposits [Mitchum & Vail, 1977]. A seismic sequence is a time-stratigraphical unit, consisting of a set of genetically related facies, which are bounded at top and base by unconformities.

Mitchum & Vail [1977] state that a depositional sequence is defined by the physical relations of the strata at the upper and lower unconformities and their correlative conformities. The concordant sedimentary layers above and below a surface show no physical evidence of the unconformity. If the stratum are discordant (terminate on the surface) then there is physical verification for unconformity. Both concordance and discordance may exist at the upper and lower boundaries of a depositional sequence. Lapout and truncation are two types of discordance. Lapout is the lateral termination of a stratum at its original depositional limit. Truncation is the lateral termination of a stratum as a result of being cut off from its original deposition limits. Figure 3.31 shows the various type of configuration along the boundaries of a depositional sequence. Lapout may occur at both the upper (toplap) and lower (baselap) boundary, while truncation only occurs at the upper boundary.

From the above discussion it is concluded that three seismic reflectors traced in the present study represent the

boundaries of three seismic sequences. These are named A, B and C seismic sequences. Sequence A is the oldest Quaternary depositional sequence bounded by the 3rd reflector (base) and 2nd reflector (top). Sequence B is a post glacial deposit lying between the 2nd and 1st reflectors. Seismic sequence C comprises a recent sediment separated by the 1st reflector from the underlying sequence.

3.5.5.2 Seismic Facies Analysis

Mitchum & Vail [1977] defined seismic facies on the basis of characteristic configuration and continuity of seismic reflections within a given seismic sequence. Figure 3.32 shows the major groups of geometrical configuration including parallel, sub parallel, divergent, prograding and chaotic patterns. Parallel and sub parallel patterns suggest uniform rates of deposition on a uniformly subsiding shelf or stable basin setting. Divergent patterns indicate lateral variation in deposition rate or progressive tilting of the depositional surface. Prograding patterns are generally the results of progressive lateral development of gently sloping depositional surfaces.

Deposition in a variable, relatively high energy environment forms a chaotic pattern. The other reason for this pattern may be post-depositional deformation of initially continuous layers. Reflection-free areas suggest homogeneous, non stratified or steep dipping strata. The other types of progradational facies (Fig. 3.32) that can be

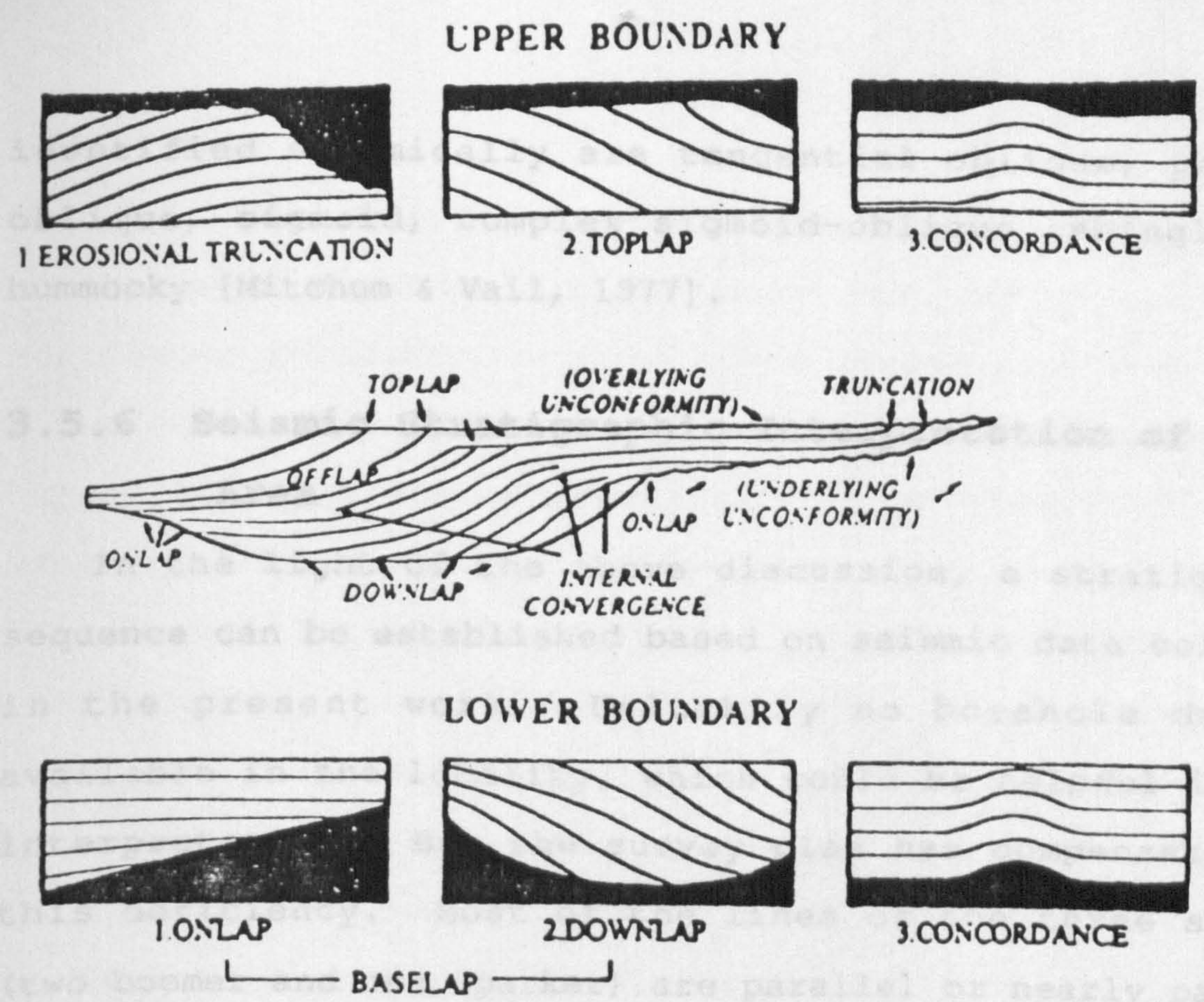

Fig: 3.31 Relationships of strata to boundaries of depositional sequences (after Mitchum et. al., 1977).

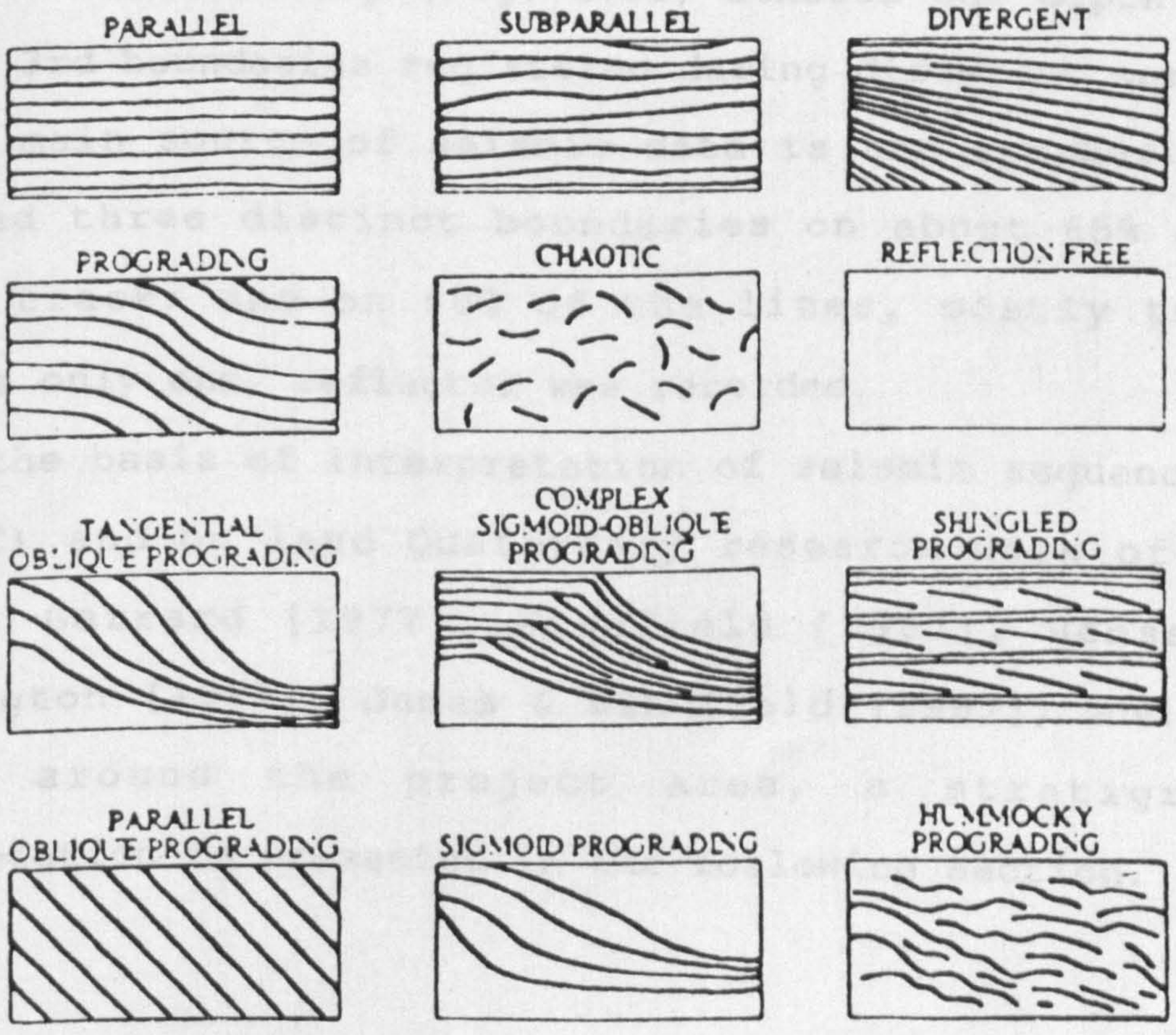

Fig: 3.32 Different types of reflection configurations (after Mitchum et. al., 1977).

identified seismically are tangential oblique, parallel oblique, sigmoid, complex sigmoid-oblique, shingled and hummocky [Mitchum & Vail, 1977].

3.5.6 Seismic Stratigraphic Interpretation of the Area

In the light of the above discussion, a stratigraphic sequence can be established based on seismic data collected in the present work. Unluckily no borehole data is available in the locality, which could be helpful in this interpretation. But the survey plan has compensated for this deficiency. Most of the lines of the three surveys (two boomer and one sparker) are parallel or nearly parallel to each other, and show the reflector depths well matched. The depth recorded from one survey is confirmed by the other surveys. The spot map (Fig. 3.22) denotes the depth of the 2nd and 3rd boundaries registered during different surveys.

The main source of seismic data is the sparker, which provided three distinct boundaries on about 65% of the survey track; and on 80% of the lines, mostly two but sometime only one, reflector was recorded.

On the basis of interpretation of seismic sequences (A, B and C) and on land Quaternary research work of Jasin [1976], Garrard [1977], Wingfield [1987], Henssion & Whittington [1987], James & Wingfield [1987], and Hart, [1990] around the project area, a stratigraphic interpretation is presented in the following section.

3.5.6.1 Acoustic Basement: Glacial Sediments

The signals of the 3rd reflector are sharper, darker and continuous throughout most of the surveyed area and exhibit a more rigid boundary. These acoustic signals are interpreted as bedrock signals. Pre Quaternary bedrock is exposed in the Menai Strait channel area and around Anglesey [Henssion & Whittington, 1987]. In the seismic record a discordance between the bedrock reflector and overlying sequence indicates an unconformity between Pre-Quaternary bedrock and Quaternary glacial deposits. The irregularity in relief and uneven surface of the basal sequence boundary probably represents the result of differential erosion.

The depths of bedrock below the seabed (Fig. 3.33A) and relative to O. D. (Fig. 3.33C) are shown as contour maps. These maps very clearly indicate the extension of the Menai Strait (mentioned earlier). Both sides are dipping toward this channel-like structure. On the northeast flank of this structure, the contour trend is about NE-SW and its closer spacing shows a steeper slope compared to the opposite bank. This structure is most probably the Dinorwic Fault, which runs through the Menai Strait channel area. A maximum depth of 99m below O. D. (Fig. 3.23) at position fix no 368 was recorded in this buried channel. Using comparable seismic surveys, maximum depths of bedrock in various parts of the Irish Sea have been recorded (Table 3.4) by different researchers.

Table: 3.4 Maximum recorded bedrock depth in some parts of Irish Sea during seismic surveys.

Researcher	Locality	Below O.D. (m)
Blundell, Griffiths & King [1969]	Dyfi Estuary	91
Fenemore [1976]	Tremadog Bay	80
Larcombe [1989]	Mawddach Estuary	75
Solangi [1992]	Caernarfon Bay	98
Present Study	Conwy Bay	99

Pleistocene sea level was lowered 110-130m as significant volumes of water were removed as continental glaciers from the ocean basins. Geological evidence on land shows that the Pleistocene epoch was characterised by alternate advances and retreats of ice of the continental glaciers [Anikouchine & Sternberg, 1973]. Milliman & Emery [1968] estimated by radiocarbon that in 13,000-15,000 years B.P. (Late Devensian), sea level was 110-130 metres below present level. Sea level determined by Shepard & Curray [1967] was -120m between 10,000-20,000 years ago. In this way, maximum bedrock depth in Conwy Bay is not inconsistent with Pleistocene sea level. The recorded buried channel is probably the result of erosion during that period when the surface was exposed to atmospheric processes.

The depositional seismic sequence which is bounded by the 3rd and mainly the 2nd reflector on the upper side is defined as seismic sequence A. On its upper surface it is sometimes covered by the 1st reflection. The configuration of seismic boundaries above and below this sequence are such

that it may be differentiated as a separate stratigraphic unit. Figure 3.34A shows the isopach map of this seismic sequence.

3.5.6.2 Glacial-Postglacial Seismic Boundary: Postglacial Sediments

Figures 3.33B & 3.33D are contour maps of the 2nd unfolded seismic layer mapped during the survey. This map is based on the data of the boomer and sparker surveys. Relief of this boundary in the area is 1m to 56m below O. D. (Fig. 3.22B). The general trend of contours below the seabed follow the bedrock configuration. It is generally recorded where the bedrock shows an erosional channel or depression.

The sedimentary layer which is bounded by the 2nd seismic reflector from the bottom and 1st seismic reflector, with sometimes seabed, on the top is defined as seismic sequence "B", which represent sediments deposited during postglacial times. According to Jelgersma [1979], in the early stages of the Holocene, when the eustatic sea level was 60-70m below the present sea level, about half of the ice was melted. As such, in that time Conwy Bay must have been above sea level. So this area was therefore subjected to subaerial erosion and may have constituted a favourable outlet for the glacial rivers (i.e., Cadnant in this area) discussed by Greenly [1919] and Embleton [1964]. The pattern of isopach (Fig. 3.34B) more or less follows the configuration of the channel filled structure during the

Fig: 3.33 Distribution of depth of 3rd reflector (A, C) and 2nd reflector (B, D).

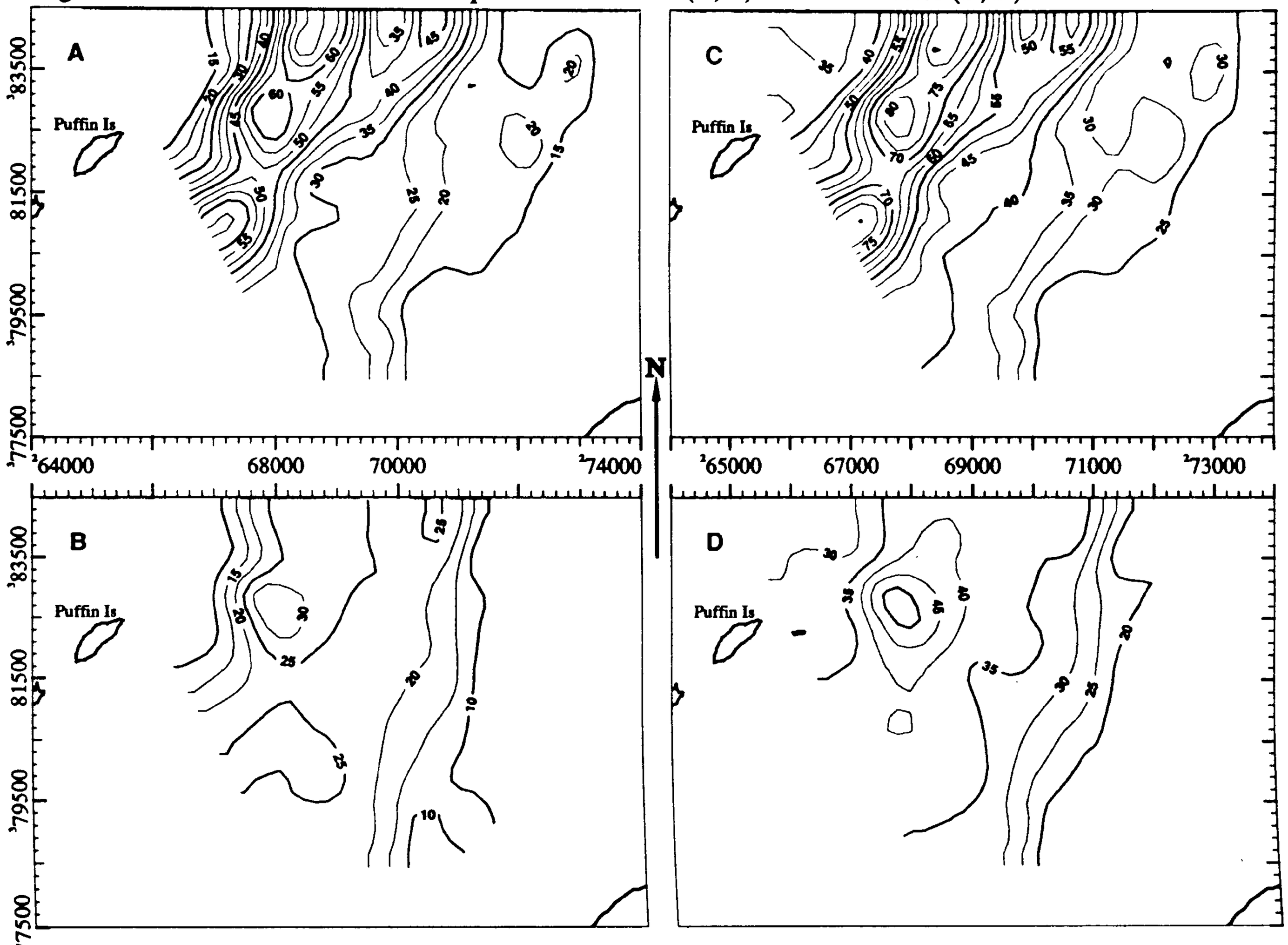

Sparker & Boomer data by R V Prince Madog cruises
Depth below Seabed (A, B) and O D Newlyn (C, D)
Contours interval 5m vertical
Scale 1:100,000
(for data points see Fig. 3.22)

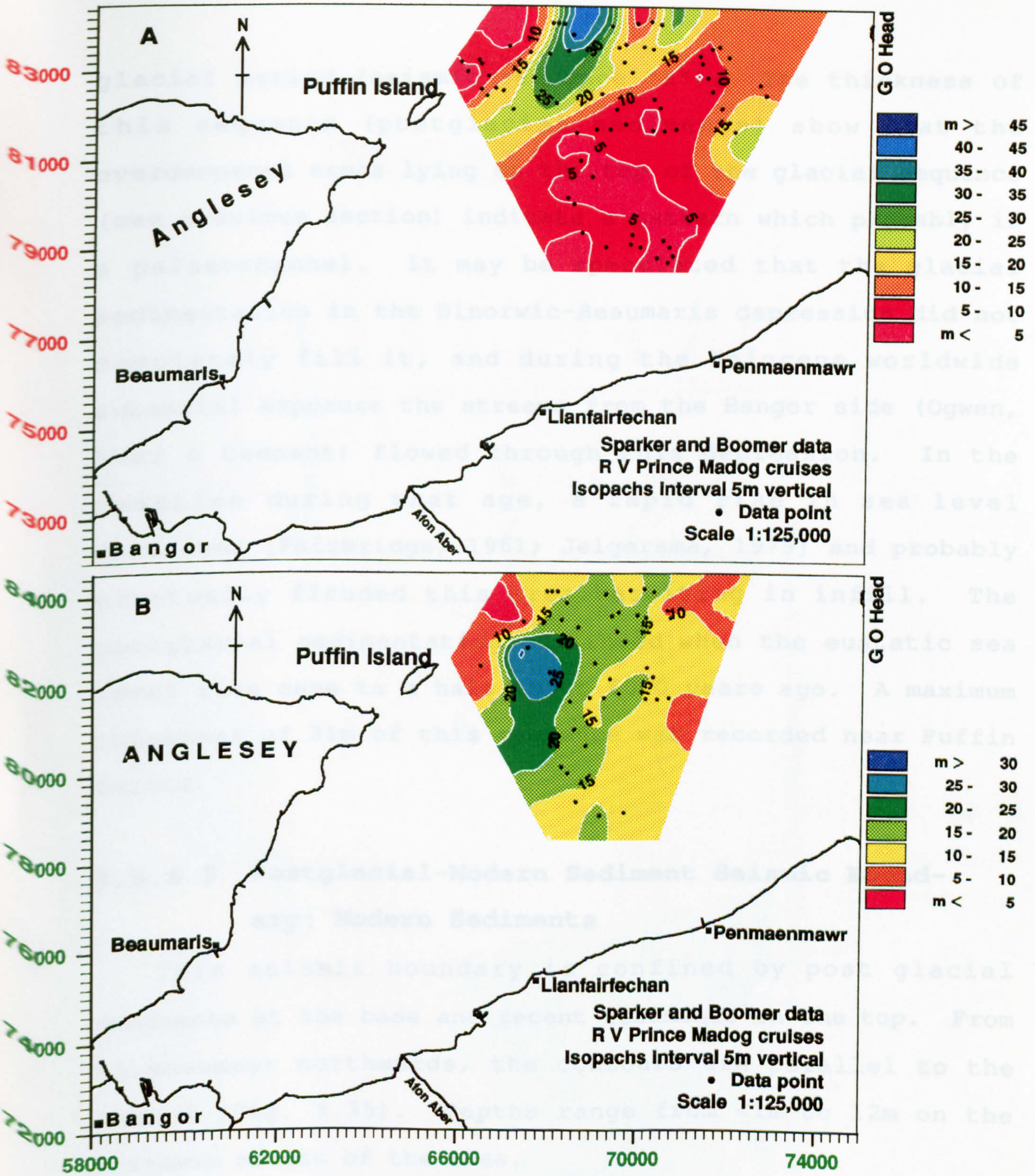

Fig: 3.34

Isopachs of "A" seismic sequence (A) and "B" seismic sequence (B).

glacial period (seismic sequence "A"). The thickness of this sequence (postglacial sediments) show that the overdeepened areas lying on the top of the glacial sequence (see previous section) indicate a pattern which probably is a palaeochannel. It may be speculated that the glacial sedimentation in the Dinorwic-Beaumaris depression did not completely fill it, and during the Holocene worldwide subaerial exposure the streams from the Bangor side (Ogwen, Aber & Cadnant) flowed through this depression. In the meantime during that age, a rapid rise in sea level continued [Fairbridge, 1961; Jelgersma, 1979] and probably eventually flooded this area resulting in infill. The postglacial sedimentation continued when the eustatic sea level rise came to a halt about 6000 years ago. A maximum thickness of 31m of this sequence was recorded near Puffin Island.

3.5.6.3 Postglacial-Modern Sediment Seismic Boundary: Modern Sediments

This seismic boundary is confined by post glacial sediments at the base and recent sediments on the top. From Penmaenmawr northwards, the contours are parallel to the seabed (Fig. 3.35). Depths range from <1m to 12m on the northern margin of the area.

The sediments lying over the 3rd reflector represent a layer of the youngest sediments in the research area. These are unconsolidated sediments, deposited while sea level has

Fig: 3.35 **Isopachs of modern sedimentary deposits (1st reflector).**

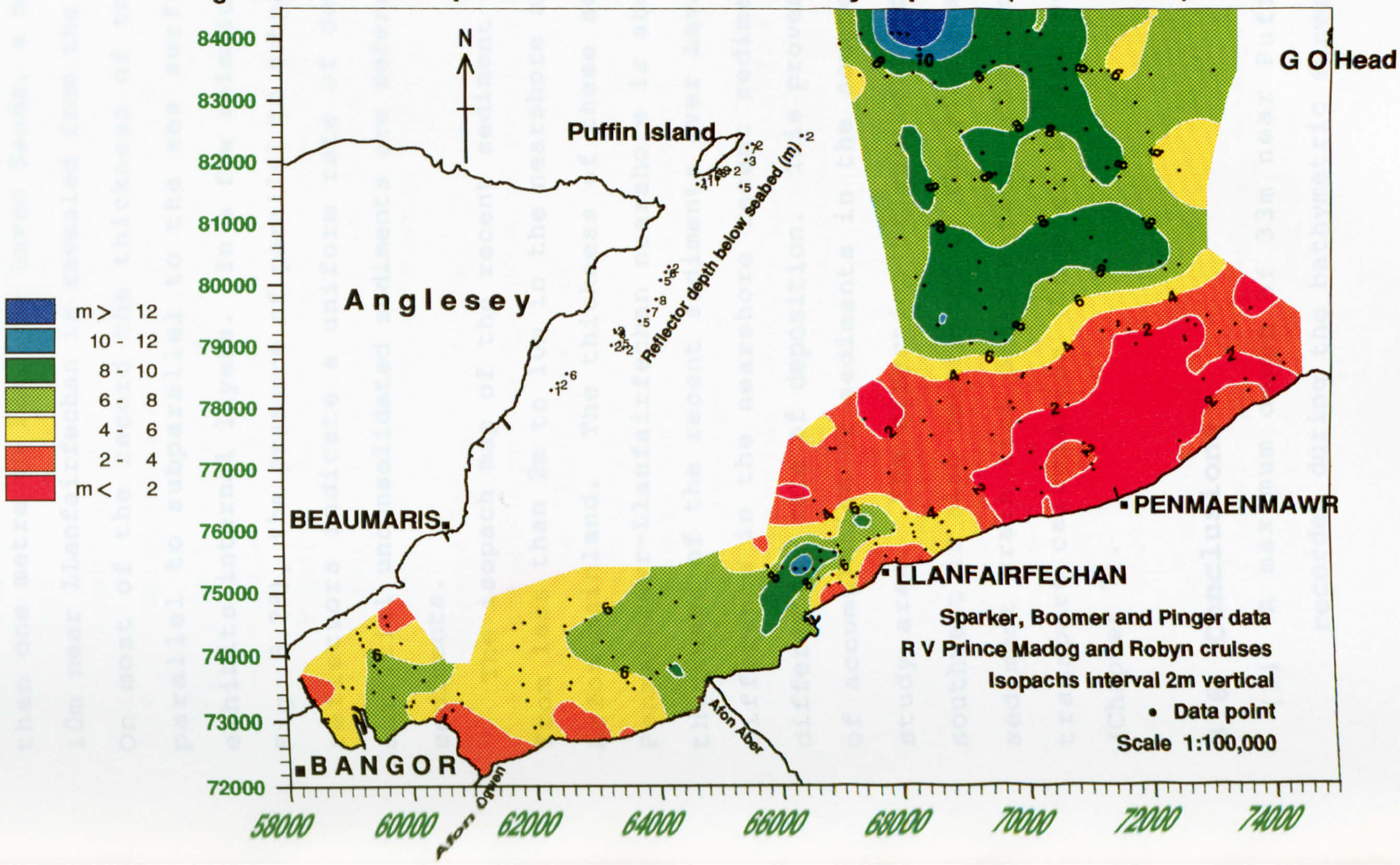

been almost constant since 6000 years B.P., [Jelgersma, 1979]. The depth of the modern sediments ranges from less than one metre to 12m. On Lavan Sands, a maximum depth of 10m near LLanfairfechan is revealed from the seismic record. On most of the record the thickness of this sequence is parallel to subparallel to the sea surface and rarely exhibits internal layers. In a few seismic records (e.g., Fig. 3.28), the presence of parallel to subparallel internal reflectors indicate a uniform rate of deposition. The surficial unconsolidated sediments are referred to as recent sediments.

The isopach map of the recent sediment shows thickness from less than 2m to 10m in the nearshore areas, along the Arfon mainland. The thickness of these sediments in the Penmaenmawr-Llanfairfechan nearshore is about half of the thickness of the recent sediments over Lavan Sands. This difference in the nearshore recent sediments indicate a differential rate of deposition. This proves a greater rate of accumulation of sediments in the southern part of the study area. The direction of sediment transport to the southwest is also determined by the side scan sonar record, sediment grain size distribution (Chapter 5), sediment transport calculation (Chapter 6) and bedform studies (Chapter 7).

3.6 Conclusions

(1) A maximum depth of 33m near Puffin Island was recorded during the bathymetric survey. Most of the

Lavan Sands and Dutchman Bank dry up at low water.

(2) Due to the morphology of the Dutchman and Lavan Sands near Llanfairfechan, flood water is temporally channelled through the Penmaen Swatch and so has overdeepened it to a depth of 17m.

(3) The transverse bedforms found in the area range from ripples to sandwaves of more than 40m in wavelength.

(4) Ripples and megaripples predominately occur over the Lavan Sands and near Great Ormes Head, respectively.

(5) Most of the areas between Puffin Island and Great Ormes Head, and near the Lifeboat Station, are occupied by small sandwaves which indicate asymmetry in the flood direction.

(6) Large sandwaves occupy most of the Dutchman Bank and Irishman Spit and their asymmetry is dominant in the flood direction (SW).

(7) A subbottom seismic survey shows three distinct reflections, indicating three main depositional boundaries.

(8) The bedrock reflector (maximum depth 99m) i.e., the boundary between the Quaternary deposits and ~~Mesozoic~~ bedrock, is successfully mapped by the sparker seismic profiles. In areas where the depth of this boundary is less than 50m, boomer seismic records confirm the depth of this reflection.

(9) A channel filled structure revealed on the seismic records at the NE end of the Menai Strait (near

Puffin Island) most probably indicates an overdeepened extension of the Dinorwic Fault, which lies approximately beneath the Menai Strait.

(10) The thickness of the glacial deposits in the area ranges between 3m and 55m. Deposition of the glacial sediments was largely controlled by the prevailing bedrock topography. Maximum thickness of the glacial deposits occur in the overdeepened depression and decreases towards the coast.

(11) During the postglacial period, the area was subjected to subaerial erosion. Glacial meltwater flowed over this area, mainly as the Cadnant river and its tributaries (discussed by Greenly [1919] and Embleton [1964]). As a result, a channel was incised into the glacial sediments and was later filled with postglacial sediments.

(12) A layer of 4m to 12m thick of recent sediments is deposited in the area. The differential thickness in the deposition of these sediments indicates the active nature of the sediments in the area.

(13) Edge, Hart & Pointon [1990] studied the Quaternary stratigraphic sequence at Aber Ogwen (NGR 61200 72300). In the south west part of the study area at Lleiniog (NGR 62200 79100), Hart [1990] studied the Quaternary sequence and proposed a new revised local stratigraphic sequence of Northern Llyn, South-east Anglesey and Arfon. Coastal sections between Bangor and Conwy, and on the south east of Anglesey, provide

much evidence that Irish Sea ice was in close proximity to, and in intermittent contact with, Welsh Ice [Whittow & Ball, 1970]. Strata estimated by acoustic reflectors are correlated with some of the available onland Quaternary Sequence in Table 3.5.

The seismic sequences A, B and C described in this study seems equivalent to Formations C (till), D (sands, gravels and mud) and E (sands and gravel), respectively of Henssion & Whittington [1987].

It should be emphasised that the area of N Wales has extreme geologic and sedimentologic diversity, so it is not easy to correlate accurately different sites with full confidence.

Table: 3.5 Correlation of Quaternary units in South-east Anglesey, Arfon, (after Hart [1990]) and seismic sequences in Conwy Bay (present study).

New Local Stratigra.	Lleiniog	Aber Ogwen	Glan-y-mor-isaf	Conwy Bay
	Llandona Sand			Sequence C
Irish Sea Diamictons (Upper Till)*	Iwerddon Diamicton	Iwerddon Diamicton	Iwerddon Diamicton	-1st Reflector- Sequence B
Lleiniog Unit (Intermediate Beds)*	Lleiniog Sands and Gravels			-2nd Reflector-
Welsh Diamictons (Lower Till)*	Llwyd Diamicton	Llwyd Diamicton	Llwyd Diamicton	Sequence A
				-3rd Reflector-

* Greenly [1919].

Lleiniog Unit is glacial lake deposit.

Llandona sand is equivalent to Supra-glacial sediments at Dinas Dinlle (NGR 43600 56300), on South east coast of Caernarfon Bay.

CHAPTER FOUR

HYDROGRAPHIC STUDIES OF THE AREA

4.1 Introduction

Water circulation and mixing processes in coastal areas are related to physical factors, such as fresh water input, tidal range and currents, wave activity, coastal morphology, bed topography and bed friction. Hydrodynamics in marine environments are therefore complex and vary both temporally and spatially. Sediment characteristics are directly related to a number of processes and these can be physical, chemical or biological; but the most important are those which produce water movement and turbulence such as tides, waves and wind. Sediment transport and changes in morphology are a direct response to changing flow dynamics. The parameters involved in sediment transport such as flow speed and direction may be measured for short periods at different locations in a study area, though a short term variation due to a semidiurnal tidal cycle may mask a longer term variation due to seasonal or annually varying processes. However, the spatial and temporal variability of controlling parameters will be reflected in the resulting patterns of sedimentary deposits.

Some examples from the literature which deal with near-shore hydrodynamics and sedimentation are given here. Abbe [1895], was one of the pioneers who explained that different shapes of bedforms on the Carolina coast are due to the variable water flows. Klein [1970] showed that the asymmetrical intertidal sand bars of the Minas Basin, Bay of

Fundy are formed and reworked by tidal currents which are characterised by an asymmetric time-velocity profile. Carling [1981] investigated the intertidal water circulation and sediment transport in the Burry Inlet to understand the processes of sedimentation and successfully constructed a stratigraphic model. Pattiaratchi & Collins [1987], observed tidal currents at 11 stations in the Bristol Channel and inferred bedload transport paths from near-bed current meter observations combined with empirically-derived formulae.

4.2 Aims of the Oceanographic Survey

Knowledge of the tidal currents in the area may be used to aid interpretation of:

(1) Geophysical data (Chapter 3), and is particularly relevant for full understanding of the side scan sonar results. Surface topography and the thickness of the subbottom sedimentary layers may then be better described.

(2) Distribution of the surficial sediment grain size (Chapter 5).

(3) Sediment transport rates in the area using empirical equations (Chapter 6).

(4) Bedform asymmetry and orientation and the internal structures of bedforms (Chapter 7).

Although waves undoubtedly influence sediment transport,

especially in the shallower parts of the area, they have not been considered in this study.

4.3 Methods

Measurements of current speed and direction were taken at one metre above the seabed using Aanderaa Recording Current Meter Model 4 (RCM4) and Braystoke BFM008 MK3 current recording meters. The current metre stations were positioned to provide a representative coverage of the whole area. The current meter rig was not set up over the Lavan Sands intertidal area because of difficulties of deployment in shallow water. The Stations were fixed with a Decca Navigation System, mounted on the 14m Lewis Morris or the 8m Sand Pebbler boat. The summer season was chosen for these deployments, so as to minimise contamination of data by waves (since the current meters used are unable to measure wave-induced currents). At each station, a complete lunar cycle (spring/neap) was planned but unfortunately this target was not achieved. On each station after some days, weeds stuck in the rotor and effectively terminated the time series.

Tidal flows at different stations were recorded using a Aanderaa RCM4 for a longer time series and a Braystoke BFM008 MK3 for one tidal cycle. Some additional data were obtained from Admiralty Hydrographic charts. Details of these stations are shown in Fig. 4.1 and Table 4.1.

Table: 4.1 Details of Fixed Current Recording Stations.

St.	Easting	Northing	Instrument	Date	Recording Period
1	65412.1	80833.6	RCM4	10/6/90	10/6-22/6/90
2	67529.5	80092.7	RCM4	22/6/90	22/6-10/7/90
3	69948.7	79029.2	RCM4	10/7/90	10/7-27/7/90
4	67420.5	80000.7	RCM4	27/7/90	27/7-10/8/90
5	65359.2	80927.4	Braystoke	30/7/91	12 hours
6	69983.9	79102.5	Braystoke	1/8/91	11 hours
7*	66832.7	82594.9	Braystoke	25/6/79	12 hours
8*	70498.7	83056.2	Braystoke	27/6/79	12 hours
9*	73947.9	83708.2	Braystoke	10/7/79	12 hours
10+	68583.2	81807.9	Chart 1978		13 hours
11+	64343.1	80620.3	Chart 1464		13 hours
12+	60774.6	75707.4	Chart 1464		13 hours

* Data from Unit for Coastal and Estuarine Studies.
+ Data from the Tidal Diamonds of Admiralty Hydrographic Charts, [1986].

From June 10th to August, 10th 1990, the RCM4 was deployed at Stations 1 to 4, for about two weeks on each station. A sampling rate of 5 minutes was set for all measurements. The RCM4 is a self recording current meter for recording temperature, speed and direction of currents. As an option it can be furnished with sensors for recording conductivity and water pressure. It is intended to be anchored in the sea below the wave zone. Although two typical ways of anchoring this instrument are 'U-anchoring' and 'I-anchoring', neither could be used in this area because of shallow water and much traffic. The method adopted for anchoring of the RCM4 is shown in Fig. 4.2. The instrument was fixed in the centre of a scaffolding frame (1.5m*1.5m*1.5m) so that it could swing completely free around the spindle. Two heavy anchor chains on opposite

Fig: 4.1 Current Recording Meter Stations.

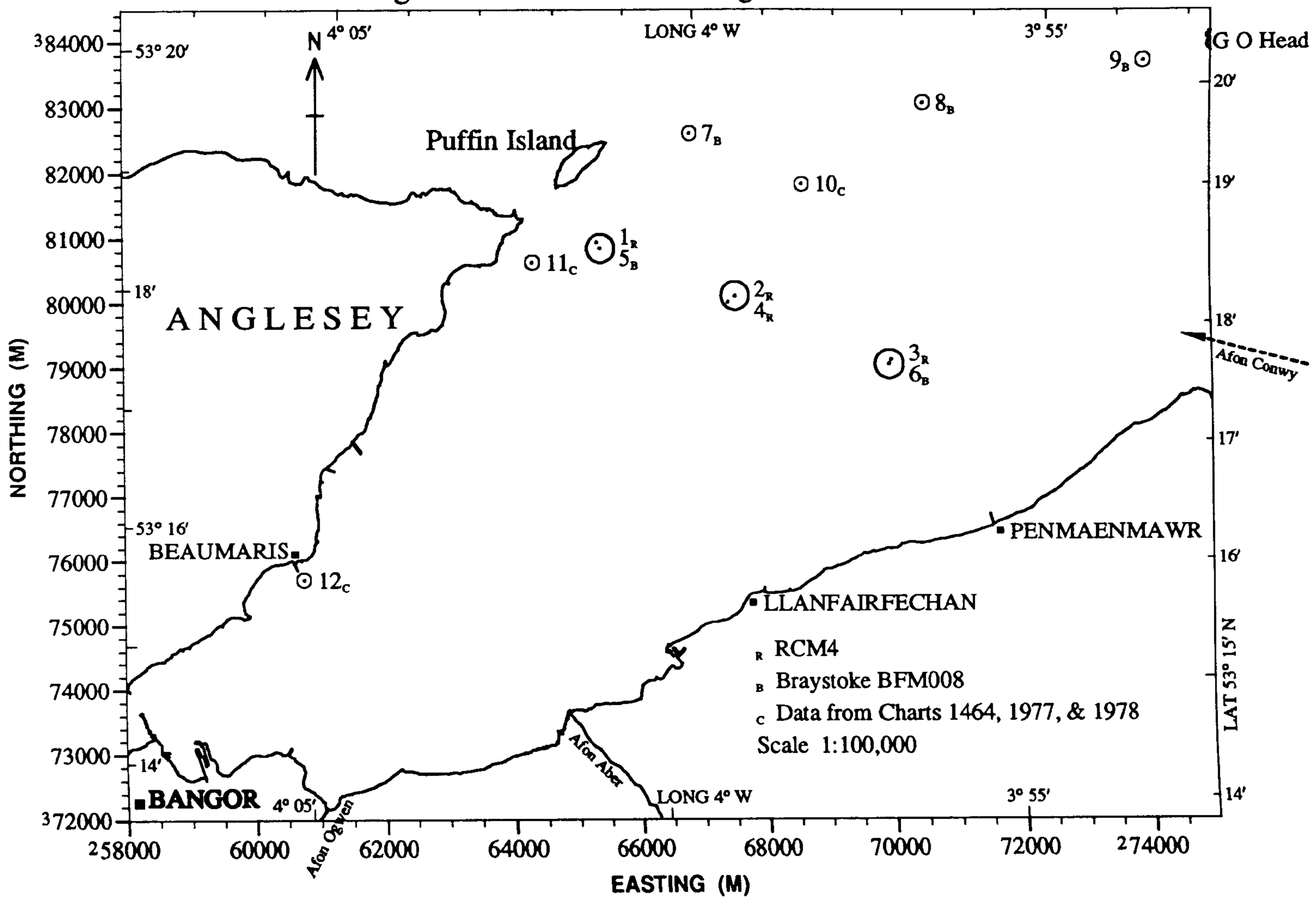

Fig: 4.2
Anchoring of Aanderaa Recording Current Meter model-4 deployed in Conwy Bay (Lewis Morris cruise).

sides of the frame were used to prevent any dragging.

A 1/4 inch reel-to-reel magnetic tape internally records the data at fixed regular intervals, triggered by a built-in quartz clock. The data from the magnetic tape were transferred to the University College North Wales (UCNW) Main Frame (VAX) through the Tape Reader 2650, Serial No. 92 (Aanderaa Instruments, Bergen Norway). The mathematical calibrations and data processing were done in the MINITAB package on VAX. Three consecutive readings of 5 minutes were averaged to obtain a sampling rate of 15 minutes, which is used in all the calibrations. The times of first measurement on stations 1, 2, and 3 were adjusted according to the onset of the tide [Menai Strait Tide Tables, 1990].

During analysis of the data at Station 1, the recorded velocity was found to be zero for most of the time after about 24 tidal cycles. The same situation occurred at Station 2 and Station 3 after about 6 and 8 tidal cycles, respectively. At Station 2 the RCM4 was redeployed as Station 4, but after analysis, it was found that the data return was again unsatisfactory due to fouling of the rotor.

A Braystoke BFM008 MK3 directional recording current meter and Valeport Series 600 CTDS System (Valeport Development Ltd.) were deployed on Station 5 and Station 6. A period of one tidal cycle was recorded on each site. The purpose of this survey was to check the current directions previously measured by the RCM4 on these sites (Station 1 and Station 3, respectively).

The Braystoke Directional Reading Current Flow Meter BFM008 MK3 and CTDS were used all together as one unit at Stations 5 and 6. The current and CTDS meters were attached to a stainless steel tackle and weighted with a sinker weight (streamlined-mass) of 15 kilos, to reduce the swinging and to keep the assembly in a horizontal position. A hand-winch attached to the boat's derrick was used to raise and lower the assembly.

The measurements were begun at low water before the onset of the flood tide and continued for about 12 hours. At one meter from the sea bottom, depth, temperature, salinity, conductivity, current speed and current direction were taken. The measurements were repeated at a depth interval of 2 meters between the bottom and surface. The readings at the maximum height from the seabed were taken 0.5m below the water surface. At each height, measurements of every parameter (mentioned above) were taken at an interval of 15 minutes. Two control units were on the deck, one for measuring current speed and current direction, and other for depth, temperature, salinity and conductivity. All the read-outs were noted manually.

Data at Stations 7, 8 and 9 (Appendix-I) are used with the courtesy of the Unit for Coastal and Estuarine Studies (UCES), Menai Bridge. Hunter & Sherwin [1979] surveyed each site for one tidal cycle by using a Braystoke BFM008 MK1 current meter.

At Stations 10, 11 and 12, current speed and direction have been obtained from Admiralty Chart nos., 1464, 1977 and

1978; observations are hourly recorded for six hours after and before high water. Note that at these locations, currents were measured near the water surface.

For each reading at Stations 1 - 6, direction was subsequently adjusted from the magnetic to the true compass. High water in the study area is -28 minute from high water at Liverpool (High Water reference).

4.4 Results

After current data analysis, the results (tidal range, current direction and speed) of longer recorded time series (Stations 1 - 3) are discussed in separate sections but these parameters measured for one tidal cycle (Stations 5 - 12) are discussed in the same section for each station.

4.4.1 Tidal Range

The morphology of coastal sand bodies is controlled by the interaction of numerous hydrographic processes/parameters, including tidal range, tidal currents, wave conditions and wind speed. The dominant physical processes (tide, wave) play a key role in the geometry and types of sediment bodies of a coastal zone and produce a recognisable stratigraphic sequence [Heward, 1981]. Wind speeds are generally not considered because of their lesser significance and because of difficulties in data collection.

On the basis of tidal range, Davies [1964] proposed this classification.

Tides	Coasts	Tidal Range
Microtidal	Microtidal Coast	< 2 m
Mesotidal	Mesotidal Coast	2 - 4 m
Macrotidal	Macrotidal Coast	> 4 m

A further subdivision of the Davies' coastal classification, was done by Hayes [1979].

Microtidal Coast	< 1 m tidal range
Low-mesotidal Coast	1 - 2 m
High-mesotidal Coast	2 - 3.5 m
Low-macrotidal Coast	3.5 - 5 m
Macrotidal Coast	> 5 m

The mean tidal height in the study area is 5.25m relative to Ordnance Datum (Newlyn), so on the basis of Davies [1964], Hayes [1979], and Davies & Hayes [1984] the coasts of the study area are macrotidal. The most important feature of this types of coast is the overwhelming dominance of tidal currents [Hayes, 1975]. The evenness/smoothness in the continuity of tidal currents and directions at all current recording stations (discussed later) may indicate the ineffectiveness of waves, i.e., dominance of tides. Although, of course, care was taken to avoid periods of prolonged wave action when deploying the current meters.

From the onset of the tide, it took 6.25 hours for the

flood tide to reach its maximum height and about the same time for the ebb tide to fall to its minimum height. The average recorded tidal heights relative to Ordnance Datum (Newlyn) at Station 1 during spring tides (tides 2-5 & 20-24) and neap tides (tides 6-19) were 7.5m and 6.25m, respectively. The variation in depth with time in a tidal cycle at stations 1, 2 and 3 are shown in Fig. 4.3. Tidal range at Station 1 varied from approximately 4m to 5.3m during the sampling period. At Station 2 maximum recorded tidal range was 5.75m (ST+2). On Station 3 all the measured tides had almost the same tidal range (5.5m).

4.4.2 Tidal Direction

Tides at all stations were essentially rotary rather than rectilinear, but all showed marked time-direction asymmetry.

Station 1

The variation in the tidal flow direction for each recorded tide is shown in Fig. 4.4A & C. In a typical tide (e.g., tide 4), as the flood commences, the direction of flow changes from 80° to 96° in the first 15 minutes and then rotates progressively towards the south. After 1.5 hours the flow direction is to the southeast, and after 2.0 hours it is to the south. In 3.5 hours the current direction then gradually changes from southerly to westerly. For the next 2.0 hours it is in a northward direction and

Fig: 4.3 Variation in water depth during a recorded tide at Stations 1, 2 and 3.

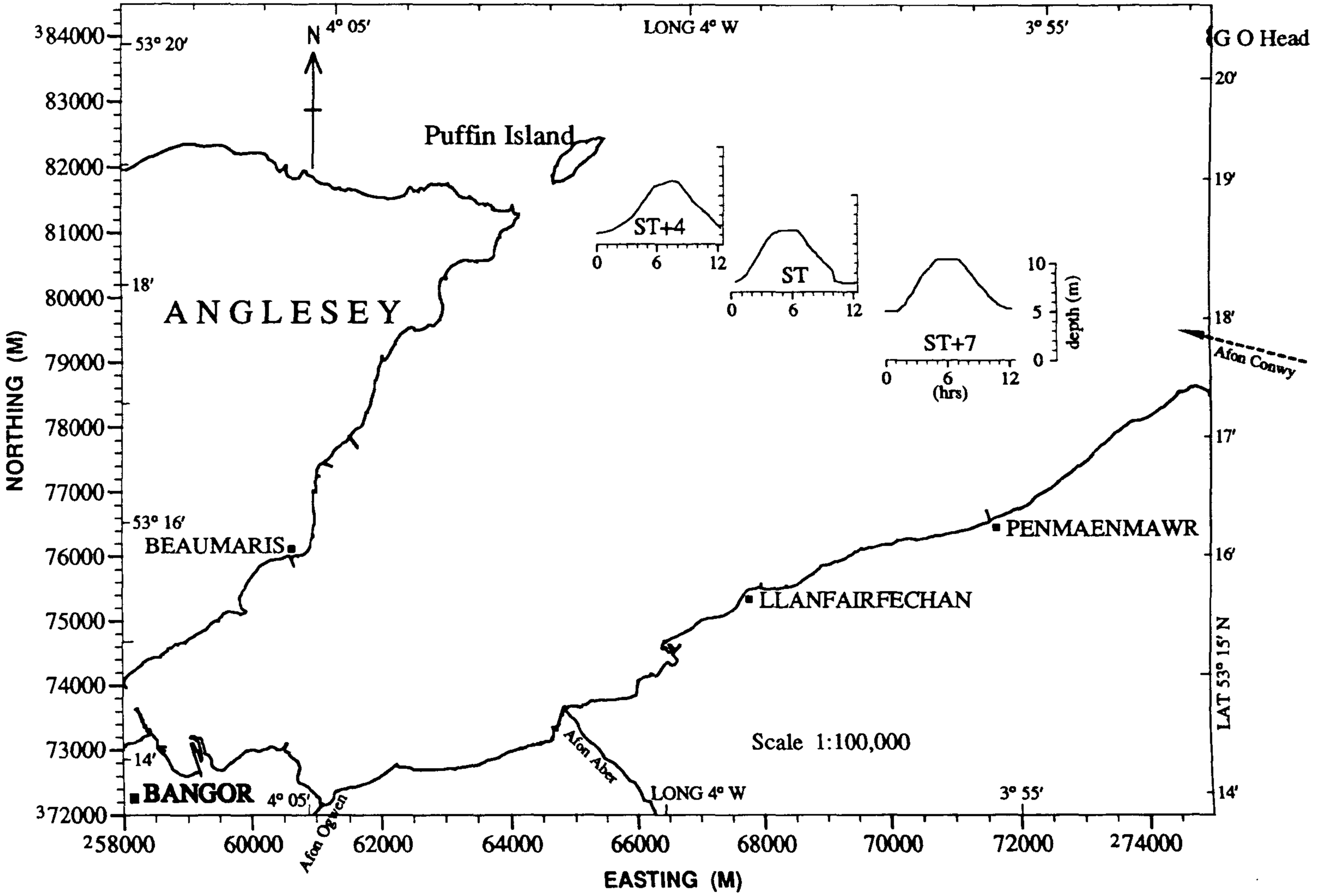

for the rest of the cycle (5 hours) it changes progressively from a northerly to an easterly direction. So in this tidal cycle, the northerly and southerly components of direction are 7.0 and 5.5 hours, respectively. Table 4.2 shows the average flow time in the different directional components for 23 measured tidal cycles.

Station 2

The relationship of the measured flow directions with time at this station is shown in Fig. 4.5A & C.

The direction of a typical spring tide (tide 4) on the onset of the flood is 126°. After 0.5 hours it starts flowing towards the southwest quadrant and remains there for 5.5 hours. After high water, the direction changes more rapidly from west to north and most of the ebb flow is in the northeast quadrant. In the final 1.5 hours the flow direction is about 100°. Average flow time in each quadrant is shown in Table 4.2.

Station 3

The flow direction on the onset of a typical flood tide (e.g., tide 4) is 86°. After 15 minutes and for the next 6.0 hours, current flows towards the northeast quadrant. At the onset of the ebb the flow direction changes to southwest and within half an hour it becomes northwest and remains there for 4.5 hours. In the last 0.5 hour, the water flows in the northeast quadrant. Table 4.2 gives the average of the recorded flow time in each direction. The direction of

Fig: 4.5 Time series of direction (A) and velocity (B), a nd vector diagram (C) at Station 2.

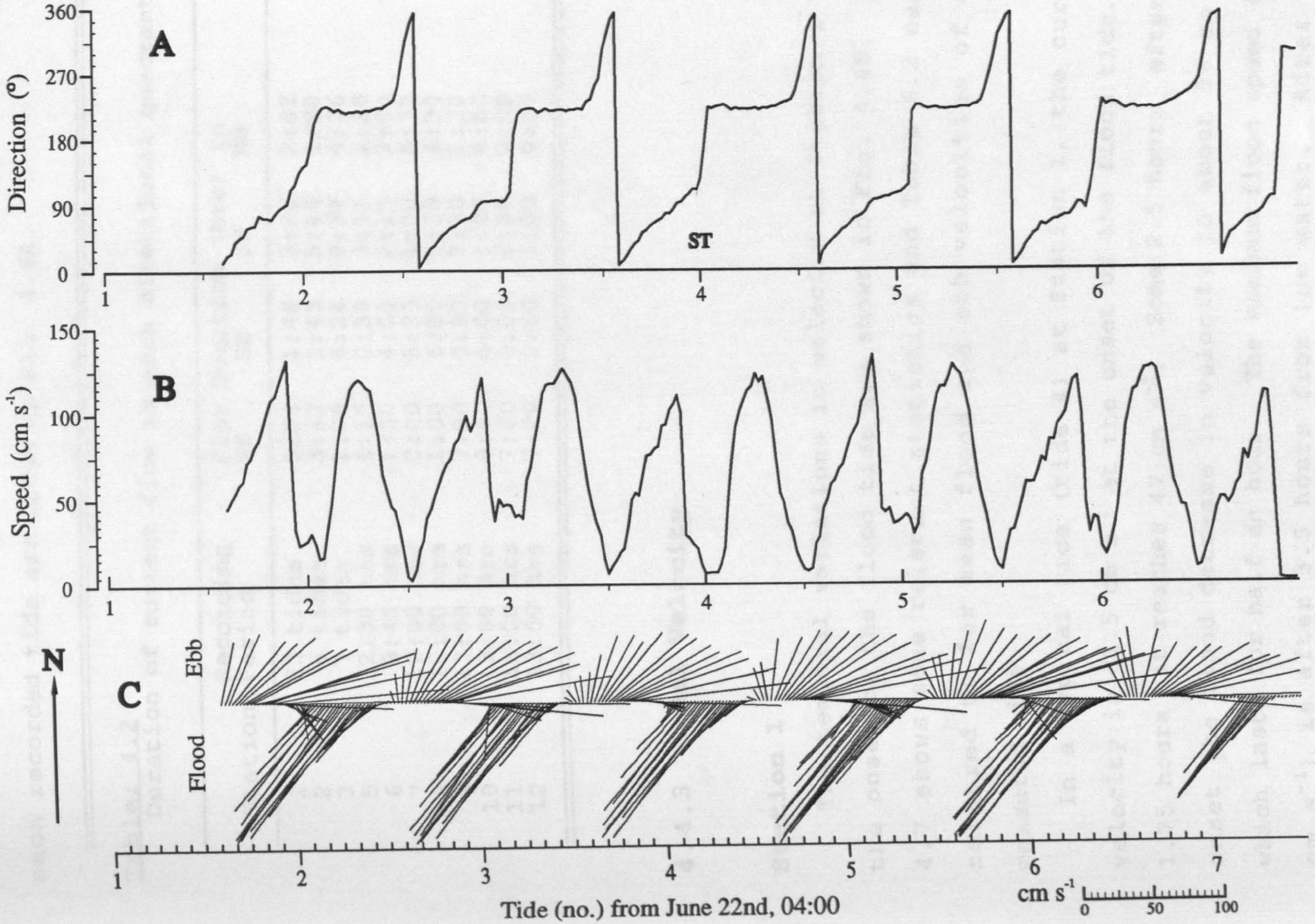

each recorded tide are shown in Fig. 4.6A.

Table: 4.2
Duration of current flow in each directional quadrant.

Station	Recording Period	Flow Duration (hrs) in NE	SE	SW	NW
1	23 tides	5:20	1:48	3:20	2:02
2	6 tides	3:42	1:43	5:45	1:20
3	7 tides	1:08	6:24	0:32	4:26
5	12:30 hrs	6:15	0:30	3:15	2:30
6	9:45 hrs	1:30	4:00	2:15	2:00
7	12:00 hrs	0:00	5:30	1:00	5:30
8	12:00 hrs	1:00	6:00	0:30	4:30
9	12:00 hrs	7:30	0:30	2:30	1:30
10	13:00 hrs	0:00	6:00	1:00	6:00
11	13:00 hrs	7:00	0:00	6:00	0:00
12	13:00 hrs	7:00	0:00	6:00	0:00

4.4.3 Tidal Velocity

Station 1

The temporal variations in velocity at Station 1 from the onset of the flood tide are shown in Fig. 4.4B. Fig. 4.7 shows some relevant statistics and Table 6.2 can be referred to for mean flood and ebb velocities of each measured tide.

In a typical tide (tide 4) at Station 1, the current velocity is 31.5 cm s^{-1} at the onset of the flood tide. In 1.75 hours it reaches 47 cm s^{-1}. Some 2.5 hours after its onset the flood decrease in velocity to about 16 cm s^{-1}, which lasts for half an hour. The maximum flood speed (61.4 cm s^{-1}) is after 3.5 hours from low water. After high

Fig: 4.6 Time series of direction (A) and velocity (B), and vector diagram (C) at Station 3.

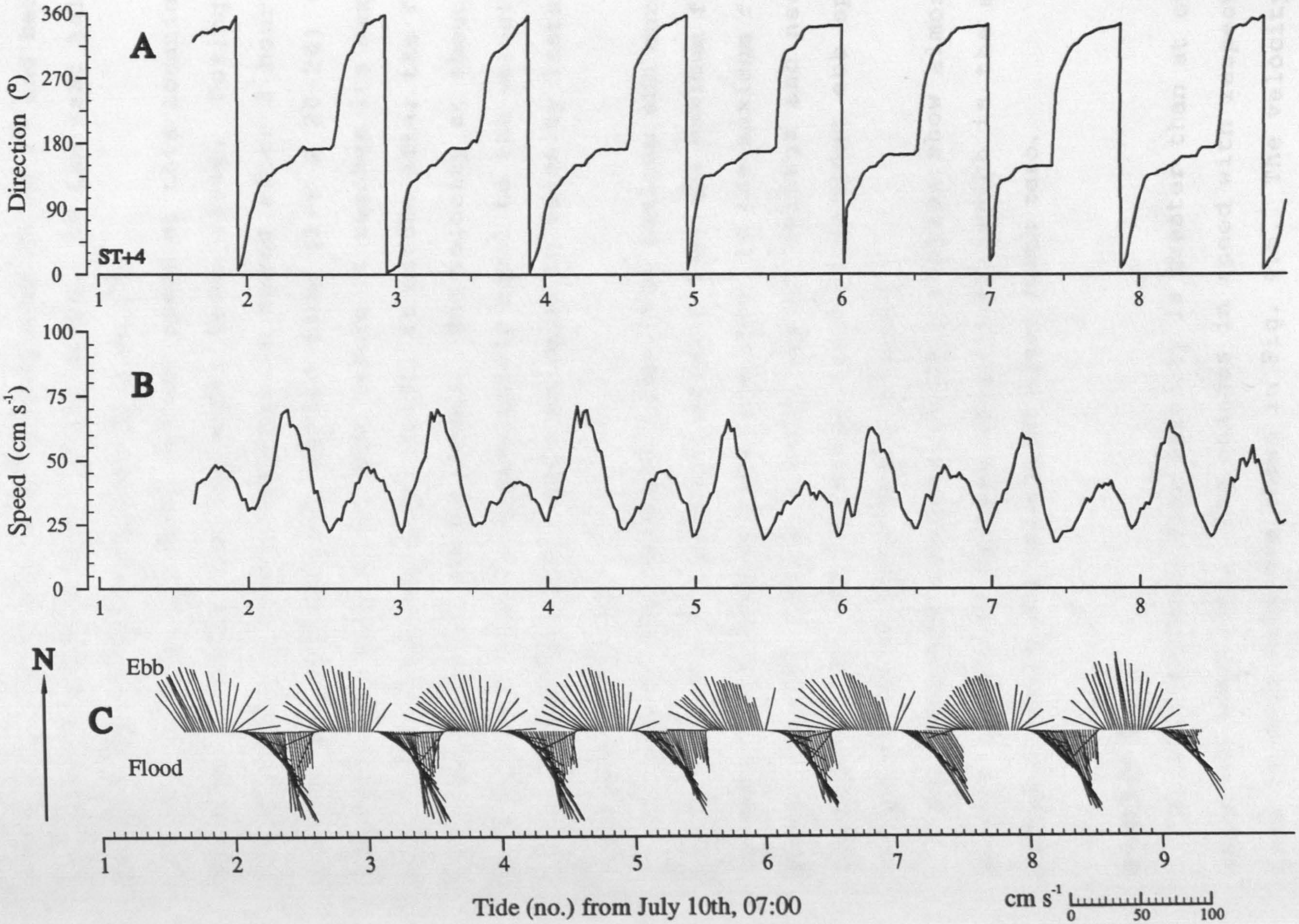

water, velocity starts increasing from 25 cm s^{-1} and becomes 74 cm s^{-1} (maximum ebb) in 3.5 hours. In the last half an hour, the velocity drops to 30.3 cm s^{-1}.

The general trend of current speed at this location is that it increases as the water level rises. During the flood tide, a sharp decrease in speed after 3 hours is recorded. Around the spring tide (1-6 & 20-24) this decrease in velocity is just before it reaches its maximum but around the neap tide (7-19), it occurs after the flood tide attains its maximum speed. The velocity at about mid of the flood tide is approximately equal to the velocities at high and low tide. This decrease in velocity lasts for less than one hour.

In 82% of the recorded tides, the maximum ebb current speed is 10 cm s^{-1} (average) greater than the maximum flood current. The average time from onset to the maximum flood speed is 3.25 and 2.5 hours during springs and neaps, respectively. The average time of maximum ebb speed occurrence is 10 hours from the onset.

The recorded currents at this station show almost a rotary clockwise ellipse (Fig. 4.4C) which is the most probable reason why velocities never reach zero.

Station 2

At this station, flow velocity is greater than at other recorded locations. The changes in speed with respect to time in each tide are shown in Fig. 4.5. The velocity at

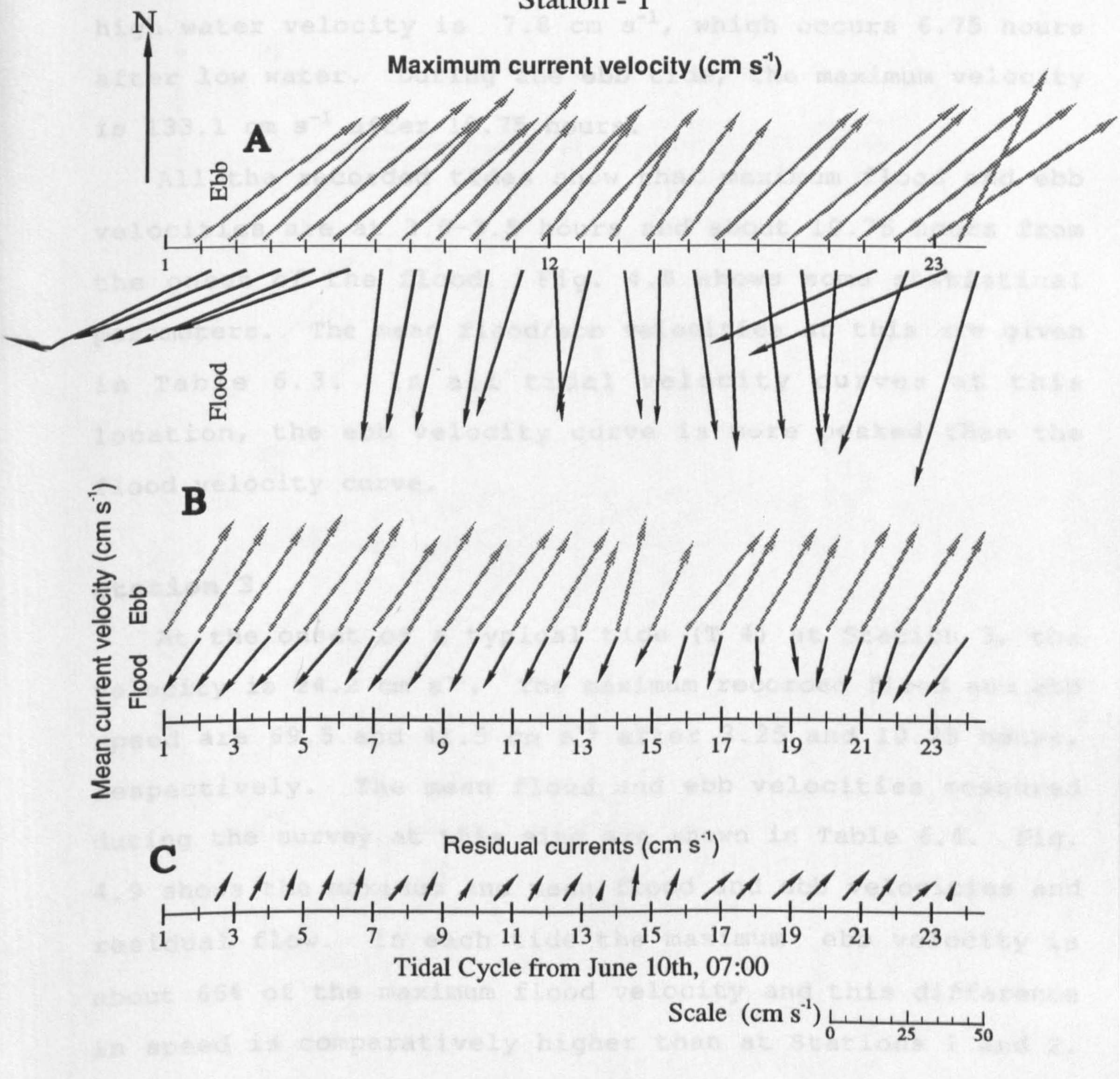

Fig: 4.7

Maximum (A) and mean (B) flood-ebb velocities, and residual tidal currents (C) during the recorded period at Station 1.

the beginning of tide (tide 4) is 6 cm s^{-1}. Flood water attains maximum speed of 122.5 cm s^{-1} after 3.25 hours. At high water velocity is 7.8 cm s^{-1}, which occurs 6.75 hours after low water. During the ebb tide, the maximum velocity is 133.1 cm s^{-1} after 10.75 hours.

All the recorded tides show that maximum flood and ebb velocities are at 3.0-3.5 hours and about 10.75 hours from the onset of the flood. Fig. 4.8 shows some statistical parameters. The mean flood/ebb velocities at this are given in Table 6.3. In all tidal velocity curves at this location, the ebb velocity curve is more peaked than the flood velocity curve.

Station 3

At the onset of a typical tide (T 4) at Station 3, the velocity is 24.2 cm s^{-1}. The maximum recorded flood and ebb speed are 69.5 and 41.5 cm s^{-1} after 3.25 and 10.25 hours, respectively. The mean flood and ebb velocities measured during the survey at this site are shown in Table 6.4. Fig. 4.9 shows the maximum and mean flood and ebb velocities and residual flow. In each tide the maximum ebb velocity is about 66% of the maximum flood velocity and this difference in speed is comparatively higher than at Stations 1 and 2. The average time after low water to attain maximum velocity on the flood tide is 2.66 hours and 9.75 hours for the ebb tide. There was no slackening of water recorded at this station. The currents show rotation in the NW and SE quadrant during flooding and ebbing, respectively.

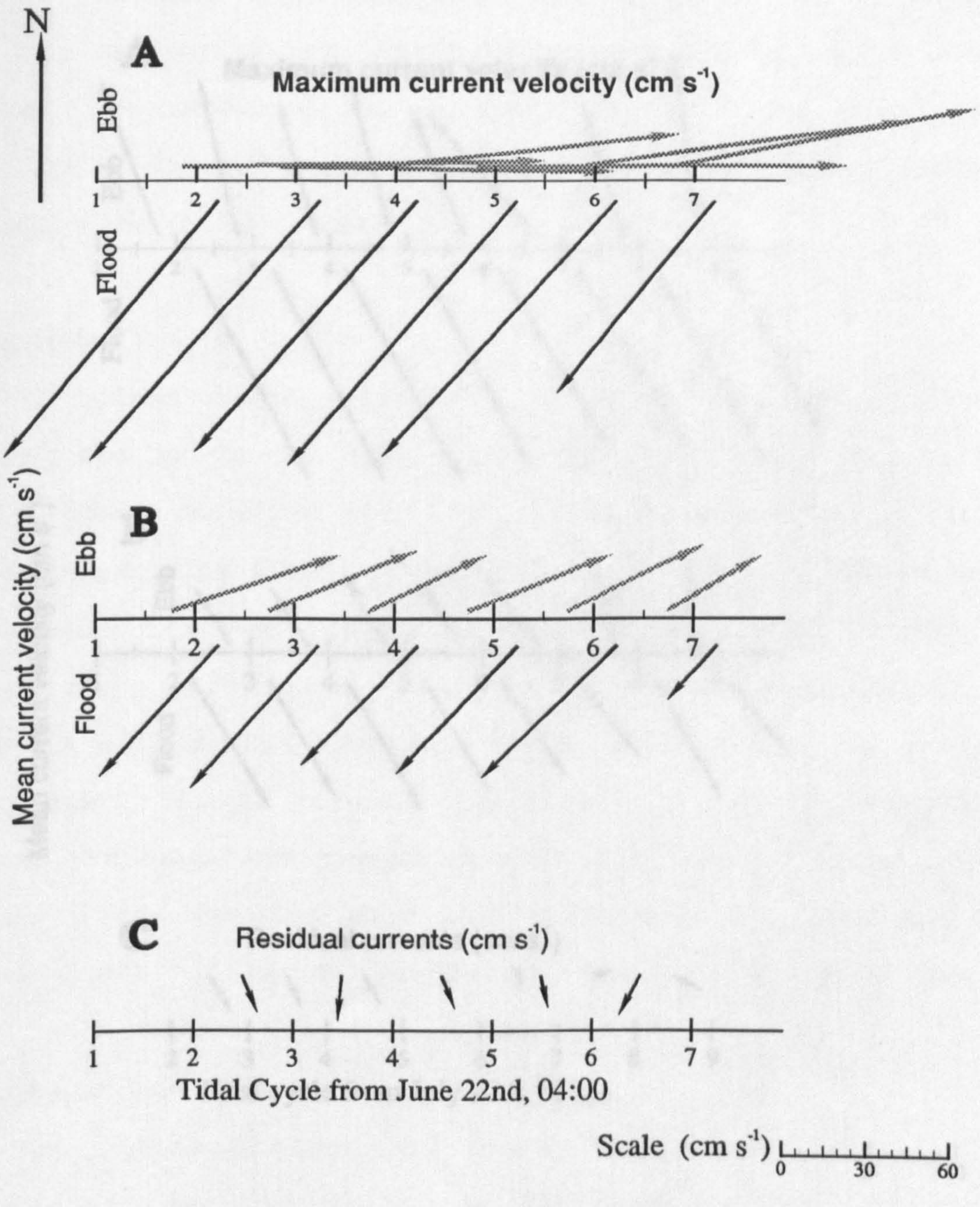

Fig: 4.8

Maximum (A) and mean (B) flood-ebb velocities, and residual tidal currents (C) during the recorded period at Station 2.

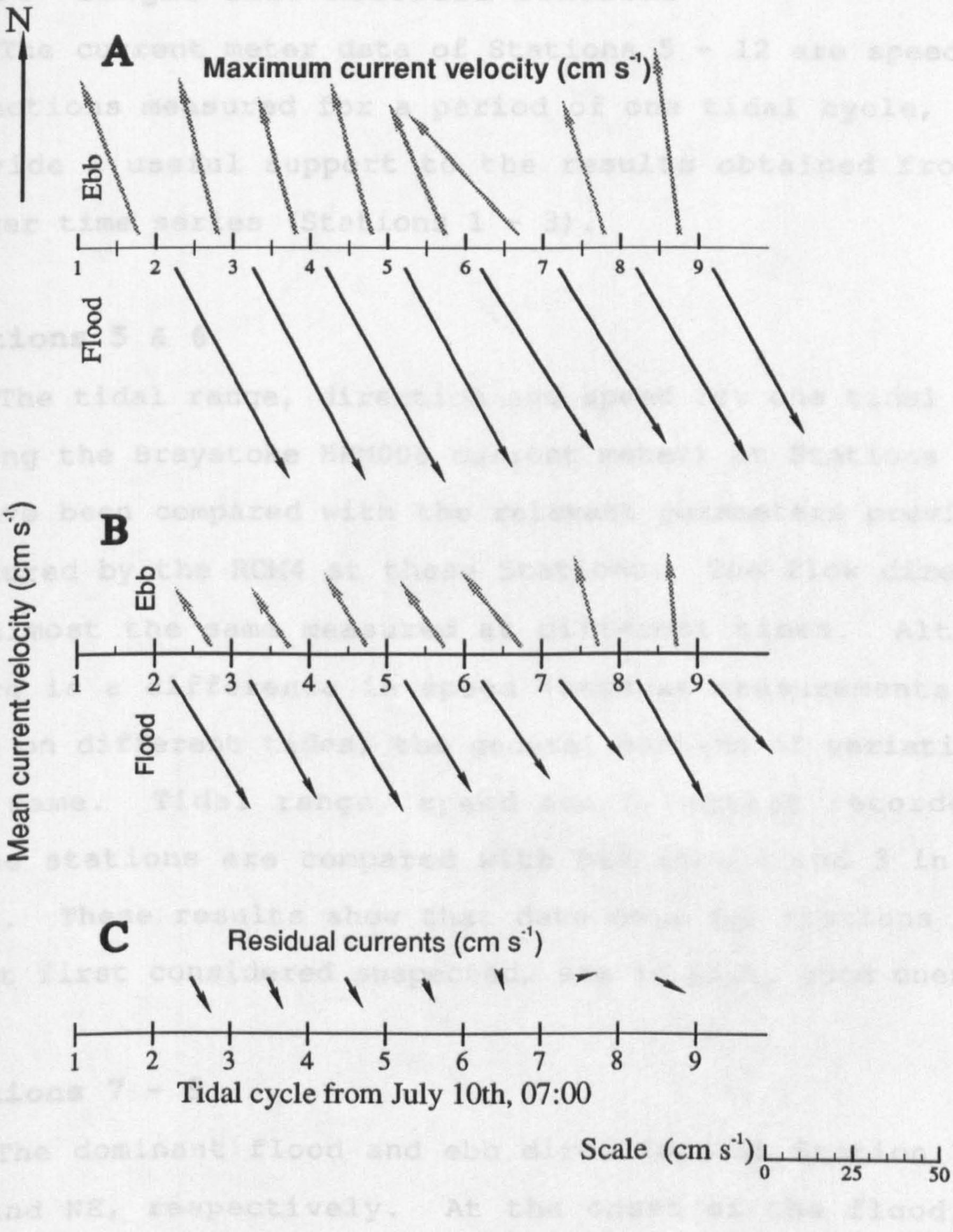

Fig: 4.9

The observed maximum (A) and mean (B) flood-ebb velocities, and residual tidal currents (C) at Station 3.

4.4.4 Single Tide Recorded Stations

The current meter data of Stations 5 - 12 are speeds and directions measured for a period of one tidal cycle, which provide a useful support to the results obtained from the longer time series (Stations 1 - 3).

Stations 5 & 6

' The tidal range, direction and speed for one tidal cycle (using the Braystoke BFM008 current meter) at Stations 5 and 6 have been compared with the relevant parameters previously measured by the RCM4 at these Stations. The flow direction is almost the same measured at different times. Although there is a difference in speed (because measurements were made on different tides) the general pattern of variation is the same. Tidal range, speed and direction recorded at these stations are compared with Stations 1 and 3 in Fig. 4.10. These results show that data sets for Stations 1 and 3, at first considered suspected, are in fact, good ones.

Stations 7 - 9

The dominant flood and ebb directions at Station 7 are SE and NE, respectively. At the onset of the flood, the recorded direction is 11°, which changes to SW in half an hour and flows between 121° and 134° up to -1 hour high. At high water the direction is to the south and in the next reading changes to SW and continuously keep rotating to the

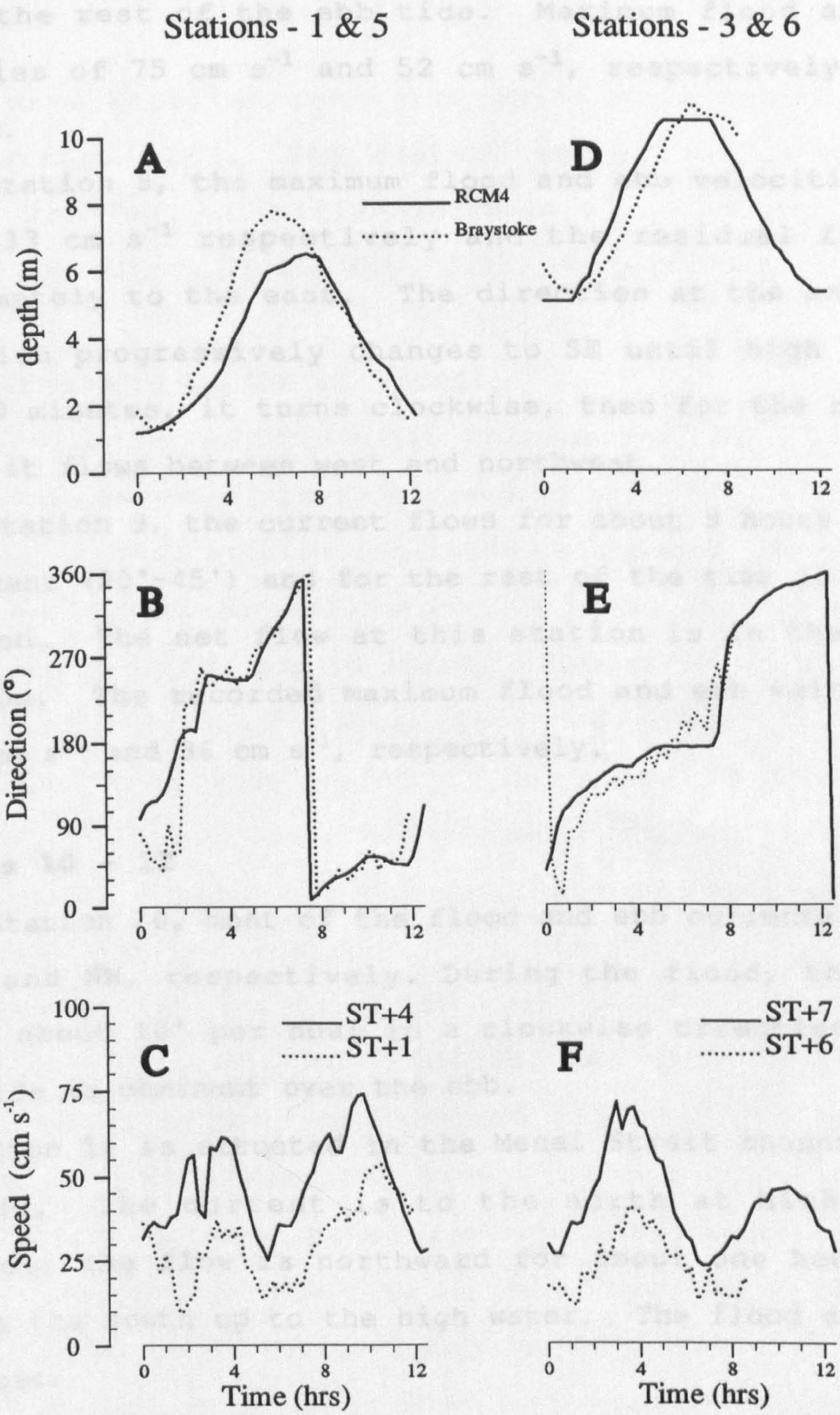

Fig: 4.10
Tidal parameters recorded in summer 1990 by RCM4 at Stations 1 & 3 and in summer 1991 by Braystoke BFM008 at same positions as Stations 5 & 6.

NW for the rest of the ebb tide. Maximum flood and ebb velocities of 75 cm s^{-1} and 52 cm s^{-1}, respectively, were recorded.

At Station 8, the maximum flood and ebb velocities are 39 and 33 cm s^{-1} respectively and the residual flow is approximately to the east. The direction at the onset is 70°, which progressively changes to SE until high water. After 30 minutes, it turns clockwise, then for the rest of the ebb it flows between west and northwest.

At Station 9, the current flows for about 9 hours in the NE quadrant (20°-45°) and for the rest of the time in the SW direction. The net flow at this station is in the flood direction. The recorded maximum flood and ebb velocities are 56 cm s^{-1} and 36 cm s^{-1}, respectively.

Stations 10 - 12

At Station 10, most of the flood and ebb currents are to the SE and NW, respectively. During the flood, the tide rotates about 10° per hour in a clockwise direction. The flood tide is dominant over the ebb.

Station 11 is situated in the Menai Strait channel near Trwyn-du. The current is to the north at high water Liverpool; the flow is northward for about one hour then turns to the south up to the high water. The flood duration is 4 hours.

At Station 12 the water flows to the south west at high water Liverpool. The dominant flow direction at this station is to the south west during a tidal cycle.

The mean tidal current vectors on each position are shown in Fig. 4.11. The spatial variations of average maximum flood/ebb velocities and mean flood/ebb velocities are shown in Fig. 4.12 and Fig. 4.13, respectively.

4.4.5 Currents in Menai Strait

The following hydrographic information for the Menai Strait have been obtained from previous studies.

In April 1961, British Insulated Callenders Construction Co Ltd. deployed a current meter 1.2m above the bottom near the Britannia Bridge for 25 hours. They recorded a maximum velocity of 120 cm s^{-1} to the SW and 80 cm s^{-1} to the NE during this spring tide period. Jones & Haq [1963] observed a residual flow from Conwy Bay to Caernarfon Bay through the Menai Strait during a biological investigation of the distribution of Phaeocystis.

Harvey [1968] investigated the residual flow in the Menai Strait by using Woodhead sea-bed drifters, direct current measurements from anchored vessels, and salinity observation. He measured a flow of about 30 millions m^3 during a semi diurnal tidal period, corresponding to an average residual velocity of 15 cm s^{-1} to the southwest. Simpson, Forbes & Gould [1971] estimated a residual flow of ~600 m^3 s^{-1} in the absence of wind to the SW through the Menai Strait using electromagnetic observations.

Fig: 4.11 Mean tidal range current vectors in Conwy Bay & NE Menai Strait.

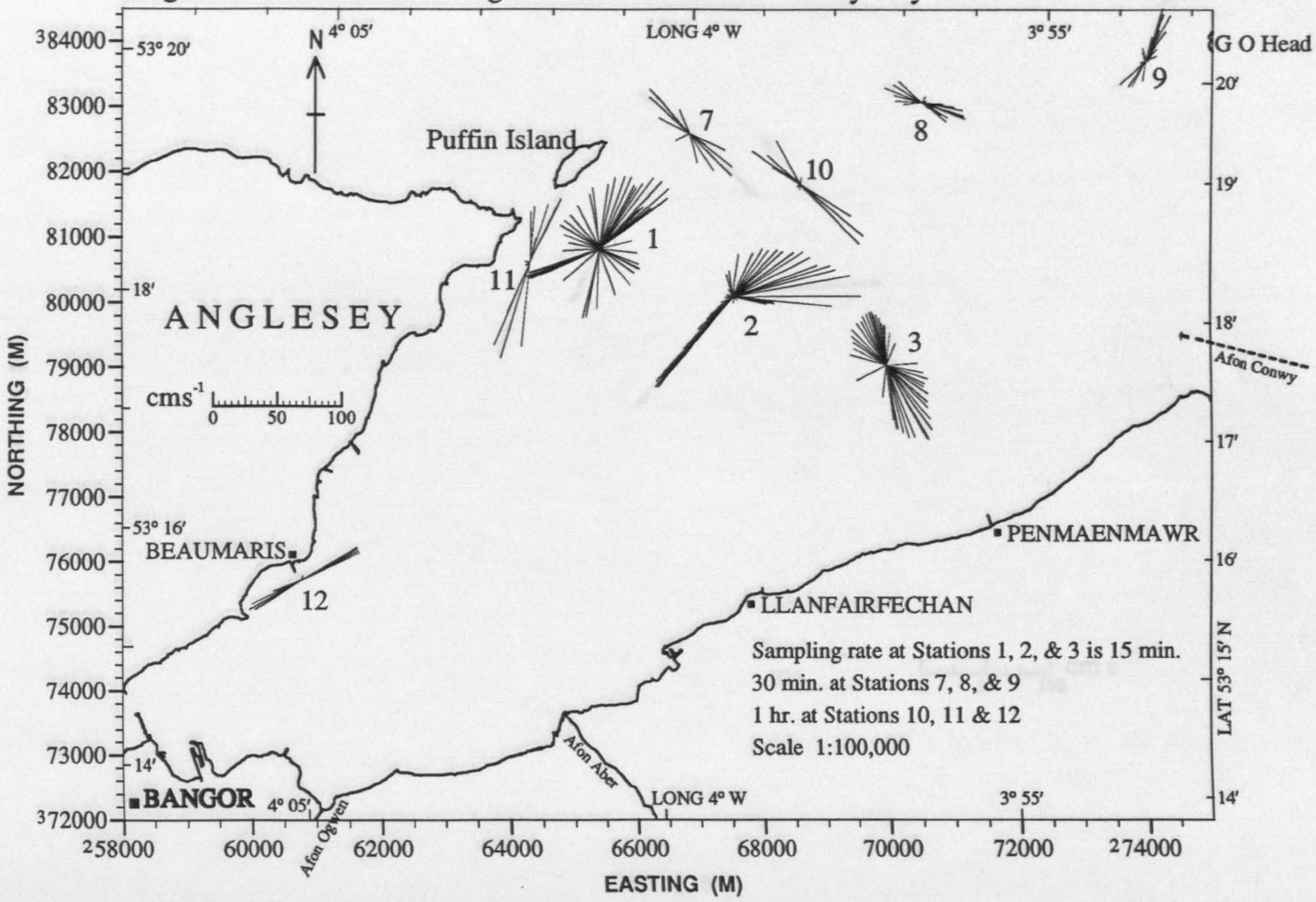

Fig: 4.12 Average recorded maximum flood and ebb velocities.

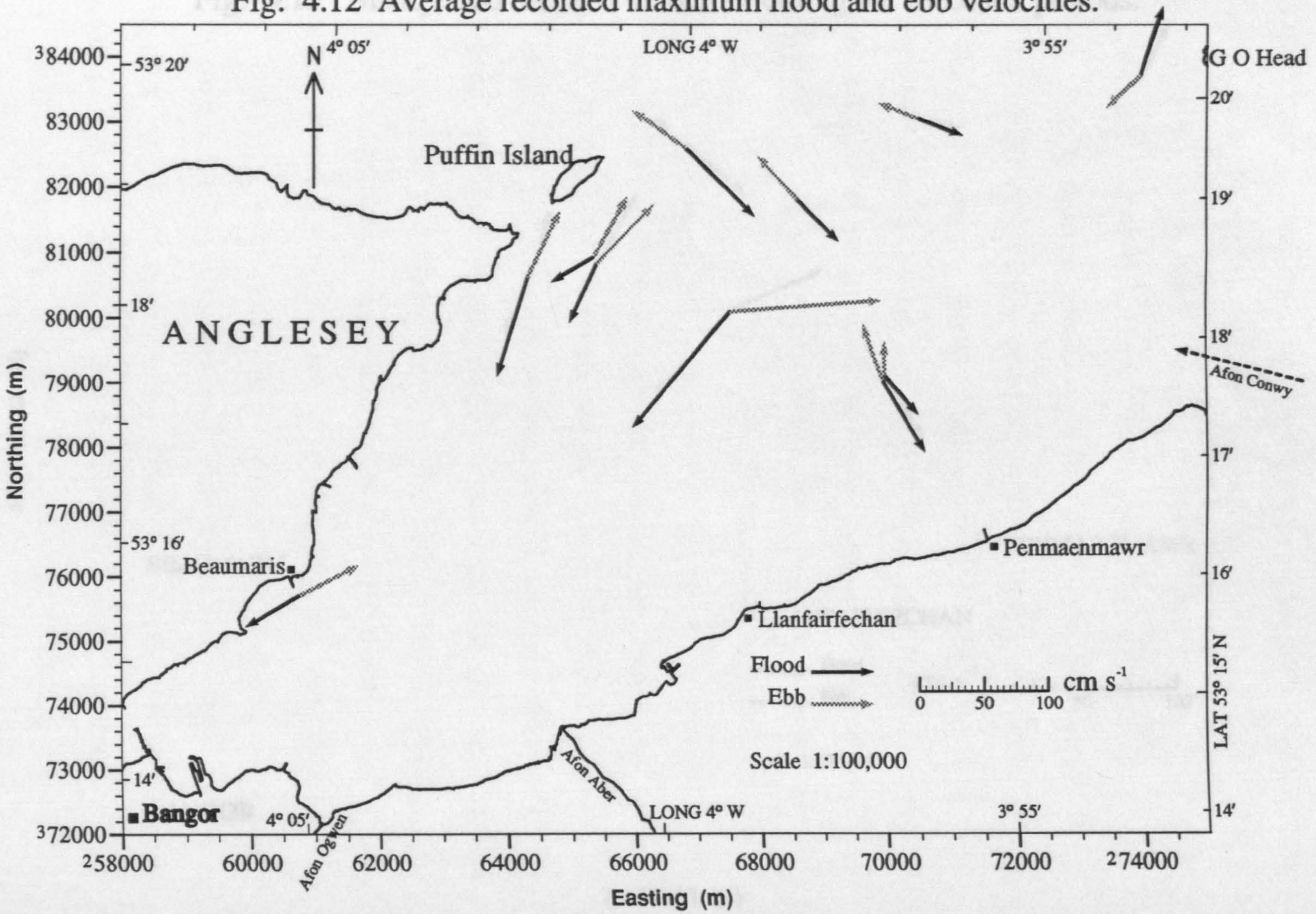

Fig: 4.13 Mean flood and ebb velocities during the recorded periods.

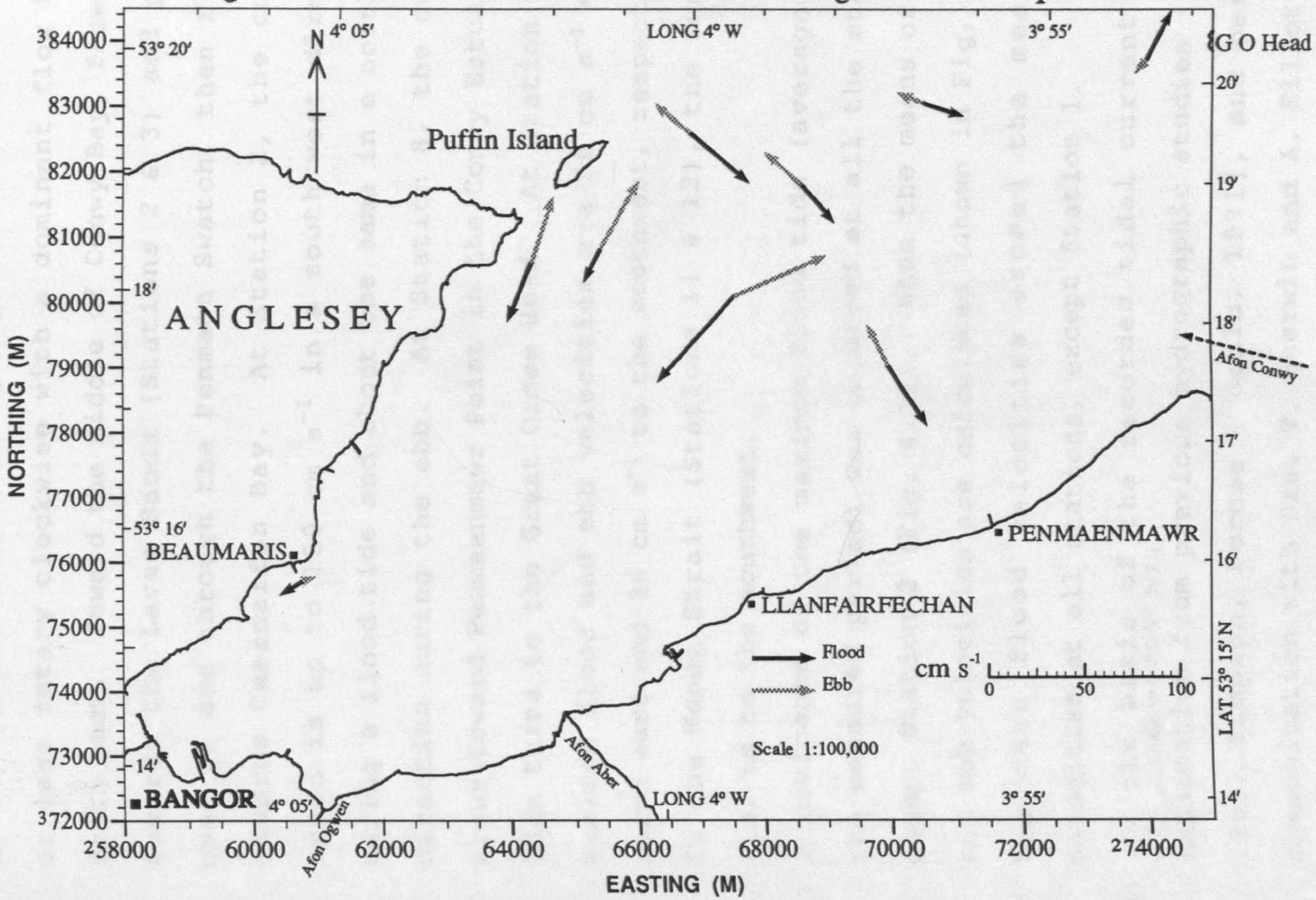

4.5 Conclusions

(1) The current patterns at Stations 1, 7 and 10, show that on the western side of Conwy Bay, the currents are more or less rotary clockwise with a dominant flow to the south east. Toward the middle of Conwy Bay, flow turns towards the Lavan Sands (Stations 2 & 3) and passes over it and through the Penmaen Swatch, then flowing towards Caernarfon Bay. At Station 2, the current speed is up to 150 cm s^{-1} in a south west direction during a flood tide and about the same in a north east direction during the ebb. At Station 8, the current flows toward Penmaenmawr Point in the Conwy Estuary and then turns to the Great Ormes Head. At Station 9, the maximum flood and ebb velocities are 56 cm s^{-1} to the north east and 36 cm s^{-1} to the southwest, respectively. In the Menai Strait (Stations 11 & 12), the residual flow is to the southwest.

(2) A dominance of the maximum flood tide (averaged over the measured period) was observed at all the stations except Station 2 (Fig. 4.12). When the means of flood and ebb velocities are calculated (shown in Fig. 4.13), the mean flood velocities exceed the mean ebb velocities at all stations, except Station 1.

(3) On the basis of the recorded tidal current data, sandwave bedforms (Chapter 3.7), information from previous hydrographic studies [Harvey 1968, Simpson, Forbes & Gould, 1971], and personal communication with Drs. T. Sherwin and A. Elliott from UCES, a residual tidal current model of the area is presented in Fig. 4.14.

Fig: 4.14

Residual currents in Conwy Bay & NE Menai Strait.

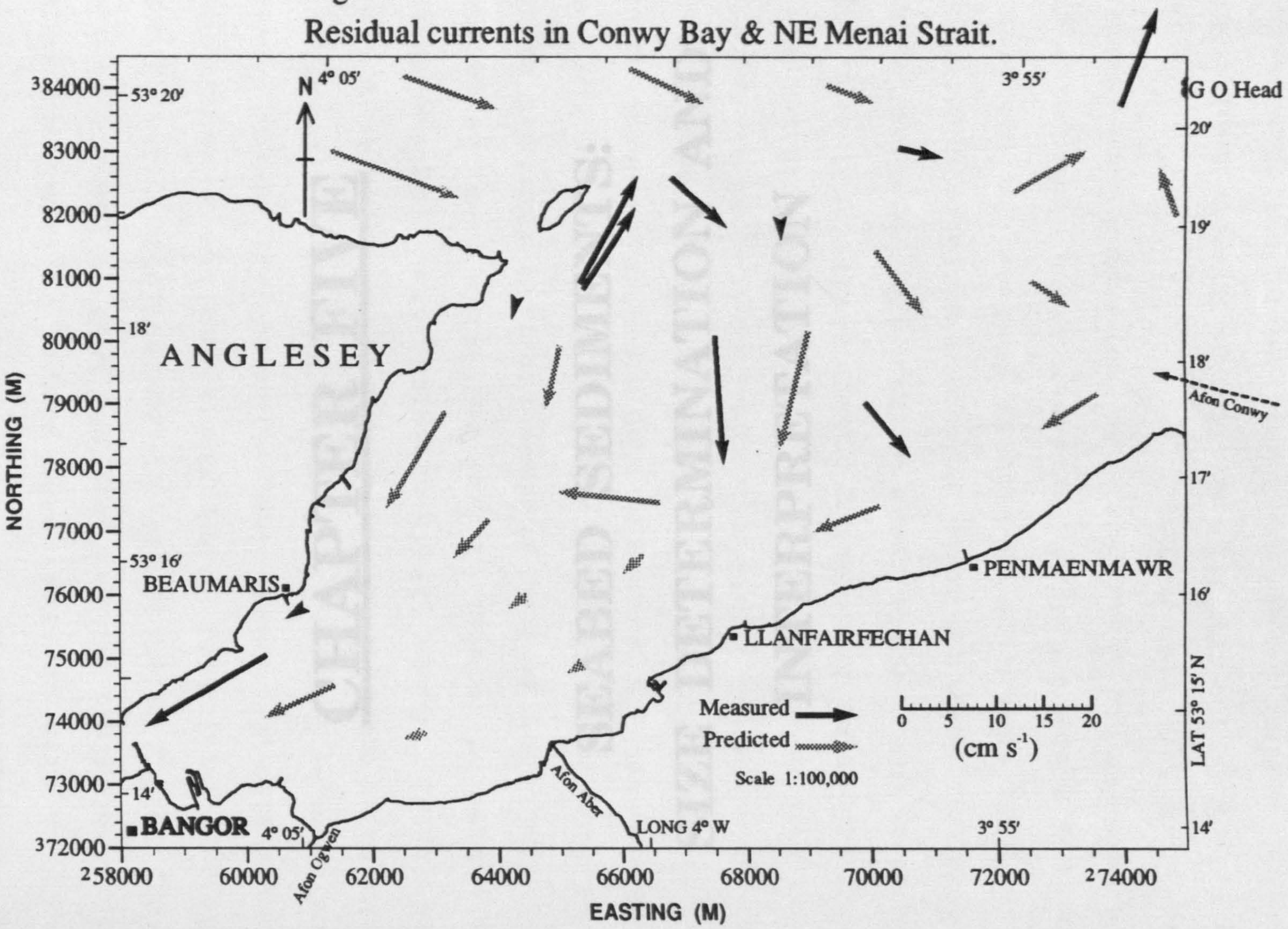

CHAPTER FIVE

SEABED SEDIMENTS: SIZE DETERMINATION AND INTERPRETATION

5.1 Introduction

Grain size analyses have played an important part in sedimentological studies over the last 70 years. Wentworth [1922, 1929], Trask [1932], Krumbein [1932, 1934], Krumbein & Pettijohn [1938] first described the size frequency distribution by various statistical coefficients. Advances were made by Inman [1952] who suggested new formulae for grain size statistics; those were later modified by Folk & Ward [1957]. Duane [1964] suggested that negative skewness was caused by removal of fine particles from the sediments by a winnowing action, whereas positive skewness resulted from the accumulation of fine grains in sheltered environments. He concluded that negative skewness occurred in areas of demonstrable erosion or non-deposition and positive skewness indicated deposition. Areas characterised by no particular dominance of negative or positive skewness were regions of fluctuating energy level. Friedman [1961] suggested that, on the basis of mean grain size and skewness parameters, dune and beach sediments could be separated, as dune sands were more positively skewed. In addition, by plotting sorting against skewness, river and beach sands could be distinguished, with the river sand more positively skewed and less well sorted.

Friedman [1967] stated that no single approach can uniquely define depositional environment but size frequency studies, if properly applied and their limitations realised,

can help the environmental interpretation. Textural parameters are environmentally sensitive and combinations of these parameters may permit separation of, for example, beach sands from river sands.

Taira [1973] and Taira & Scholle [1974, 1979a], through multivariate discriminate function analysis, found river, beach and dune sediments can be well discriminated and the variables that are most effective for environmental discrimination are those mainly related to the tails of the distribution, i.e., skewness and kurtosis.

McLaren [1981] studied spatial trends in grain size measures. He suggested that these trends could be used to identify both the probable source and the probable deposit, and hence help to identify net sediment transport paths. He argued that if a source sediment undergoes erosion, and the resultant sediment in transport is deposited completely, the deposit must be finer, better sorted, and more negatively skewed than the source. The lag remaining must therefore be coarser, better sorted and positively skewed. If the sediment in transport undergoes selective deposition, the resultant deposit may either be finer or coarser than the source, sorting will be better and skewness more positive.

Sly, Thomas & Pelletier [1983] studied the significance of sorting, skewness and kurtosis in different parts of the particle size distribution using approximately 670 sediment samples from Liverpool Bay and its beaches and River Mersey (U.K.), and about 800 sediment samples from the Lake Ontario

(Great Lakes, Canada/USA). They demonstrated that skewness vs kurtosis plots could define separate fields for sediments apparently close to hydrodynamic equilibrium but in separate hydraulic environments.

The aim of the present grain size distribution study is, first, to identify the textural characteristics of sediments in different parts of the study area and their relationship to the prevailing hydrodynamic conditions. Second, to identify any grain size trends occurring in the area which could be used, together with other results (Chapters 3, 4, 6, 7), to identify possible sediment transport pathways in the area.

5.2 Methods

A total of 235 seabed sediment samples (Fig. 5.1) were collected from the NE of Menai Strait and Conwy Bay at various times as shown in Table 5.1.

Fig: 5.1 Surficial Sediment Sampling Positions in Conwy Bay & NE Menai Strait.

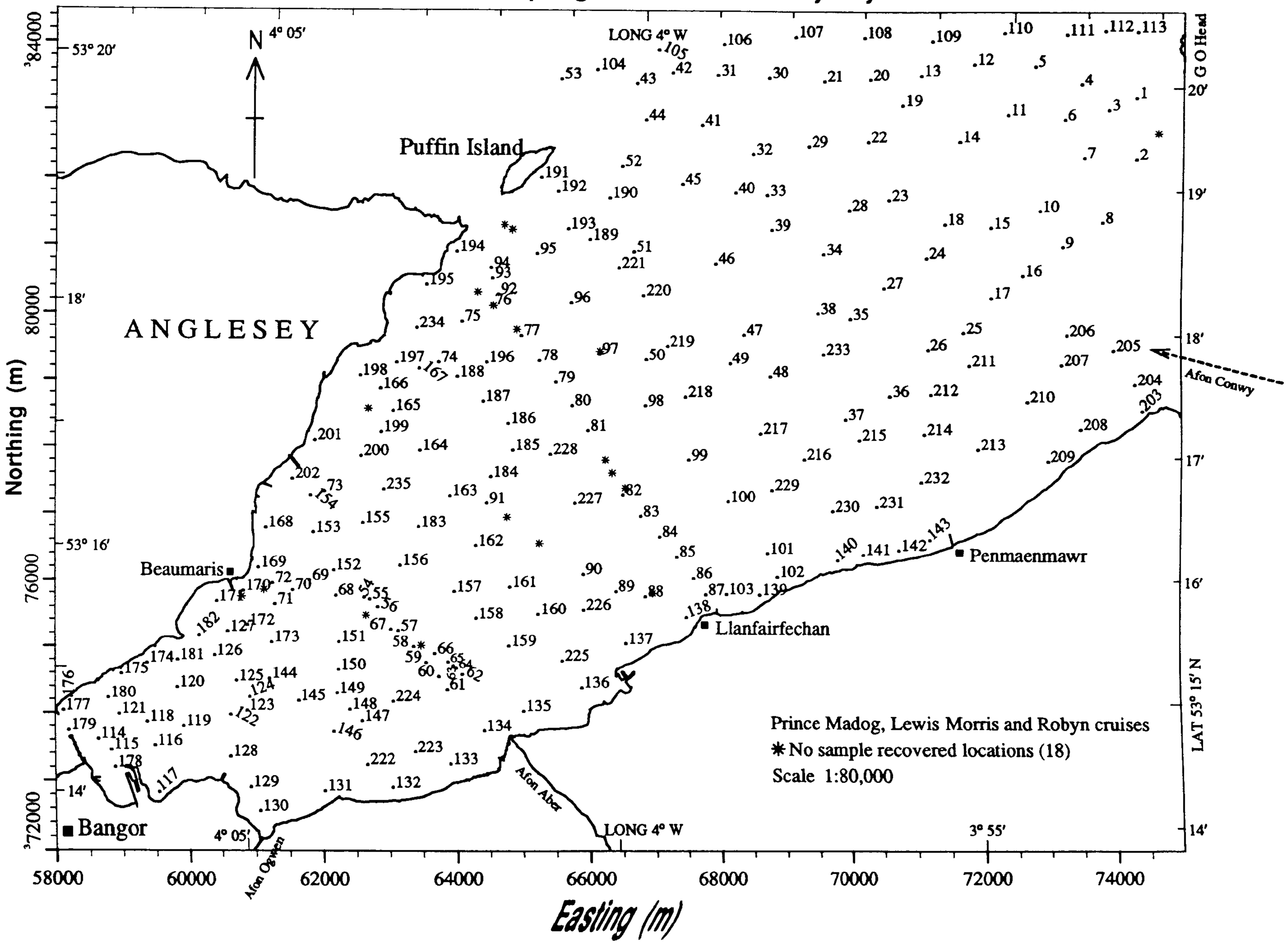

Table: 5.1 Field Cruises for Sediment Sampling.

No.	Date	Cruise	Sample Nos.
1	23 May 1988	Prince Madog	1-53
2	5 July 1988	Lewis Morris	54-71
3	6 July 1988	Lewis Morris	72-91
4	7 July 1988	Lewis Morris	92-103
5	20 July 1988	Prince Madog	104-113
6	3 July 1989	Robyn	114-127
7	4 July 1989	Robyn	128-143
8	5 July 1989	Robyn	144-171
9	6 July 1989	Robyn	172-182
10	7 July 1989	Robyn	183-202
11	12 July 1989	Robyn	203-221
12	14 July 1989	Robyn	222-235

On the research vessel Prince Madog, 66 samples were taken by Shipek (Fig. 3.1-a) grab, on the Lewis Morris the Shipek and modified Van Veen grabs were used for 30 samples, and all other samples were taken on Robyn Cruises with the modified Van Veen grab. The positions of samples were located by using a Trisponder system except samples no 65 to 80 and 121 to 131, where positions were fixed by the Decca Navigation system. All sediment samples were separated by sieving into gravel, sand and mud fractions based on the Wentworth Size Classification [Wentworth, 1922]. The percentage of each fraction was calculated by washing 200-300 gm of sample through a 63 micron sieve. The sediment retained was oven dried at 105°C for 24 hours and separated into gravel and sand by passing through a 2 mm sieve. From the sediment passed by wet sieving, a known volume was dried to calculate the total weight of mud in the sample and

rest was analysed down to 0.25 micron by Sedigraph 5000ET. Grain size frequency distributions of gravel, sand and mud may be obtained by many methods, reviewed by Krumbein [1932], Krumbein & Pettijohn [1938], Irani & Callis [1963] and McManus [1988]. Each technique (sieving, settling tube, sedigraph, pipette analysis, hydrometer) defines the "size" of a particle in a somewhat different way. Samples having 5% or more by weight of gravel, sand and mud were analysed for grain size distribution by sieving, fall tower and Micromeritics Sedigraph 5000ET, respectively.

In the present study, the phi (Ø) scale was used as a grade scale. The geometric grain size scale of Udden [1914], modified by Wentworth [1922], was introduced by Krumbein [1938] as a log-transformation of grain diameter in mm.

$$\emptyset = -\log_2 d$$

d = grain size in mm

After phi transformation, the geometric scale converts into an arithmetic scale of positive and negative integers. The larger the phi values, the finer the particle size. The grain size results plotted on the phi scale give a visual equality to the scale divisions. The statistical advantages of the phi scale have made it a standard grade in sedimentological studies.

Textural parameters of each sediment sample were calculated by a Fortran grain-size analysis package [Jones, 1990], by which the raw data from sieves, fall tower and Sedigraph were combined to generate a grain diameter curve.

Sengupta & Veenstra [1968] and Sanford & Swift [1971], comparing grain sizes determined by sieving and settling tube techniques, found that the results from both techniques are generally very similar to each other. Komar & Cui [1984], in an analysis of Oregon beach samples, used sieving, settling and microscopic techniques. They concluded (their Fig. 6, Fig. 7) that grain size distributions determined by sieving and settling tube show close similarities to each other.

5.2.1 Sieving - Gravel Fraction

Grain size determinations of samples containing more than 5% by weight of gravel (Appendix-II) were performed by conventional sieving methods, at 0.25Ø class intervals using mechanical sieve shaker (Pascall Inclyno) for 15 minutes (recommended by Folk [1974], Buller & McManus [1979], Friedman & Johnson [1982], and Lewis [1984] as standard duration) and each fraction was weighed to 0.001 gm [Folk & Ward, 1957; Mason & Folk, 1958; Buller & McManus, 1979; and Chauhan & Chaubey, 1989]. A total of 38 samples was analysed by this method.

5.2.2 Fall Tower - Sand Fraction

A fall tower (also known as a sedimentation tube, sedimentation column, water column, settling tube) was used to measure the distribution of settling velocity of particles in a column of water. The fall tower is a very

useful technique for the rapid determination of sand grain sizes. Like hydrometer and pipette analyses, it is based on Stoke's Law, which states that the force exerted on a sphere falling at low velocity is directly proportional to the product of the fluid viscosity, particle velocity and particle diameter.

A plastic tube, 2m long with 28.5cm internal diameter, an Oertling balance (0.001g resolution), a sample releasing system at the top and an interfaced micro-computer are the main components of this fall tower. Details of the fall tower at UCNW, School of Ocean Sciences are given by Larcombe [1989].

A moisture-free sample was carefully split into sub samples weighing 4 to 6 gm [Rigler, Collins & Williams, 1981; Slot & Geldof, 1986; and standard procedure adopted at UCNW], using a mechanical rotary sample splitter. A total of 324 samples, including 46 samples (Appendix-IV) with three replicates, was analysed.

5.2.3 Sedigraph 5000ET - Mud Fraction

The Micromeritics Sedigraph 5000ET is a particle size analyser for the fine grade (from 100 to 0.1 micron). The mechanism of this analyser is that a beam of x-radiation passes through a solution of sample; it detects relative particle concentration because the magnitude of x-rays absorbed by a particle is directly proportional to its mass. In this way the x-ray beam measures the suspended sediment concentration and hence sedimentation rate of a sample

suspended in water in a sample cell, and internally converts this into equivalent spherical diameter using Stoke's Law.

Sediment samples containing 5% or more by weight of mud (Appendix-II) were analysed by this technique. Including the replicates of 4 samples, a total of 59 samples were analysed down to 0.25 microns. The sediment finer than 63 micron was separated by wet sieving and then centrifuged with distilled water. The sample was then treated with 10% hydrogen peroxide to remove organic matter and then again washed with distilled water by centrifuge. Stein [1985] suggested that a fairly good dispersion of the sample could be achieved by a 15 minute ultrasonic treatment. Calgon was used to deflocculate the sample and then dispersed in an ultrasonic bath for 15 minutes. A magnetic stirrer was used to aid the dispersing process between the ultrasonic bath and sedigraphic analysis. Samples were analysed between 70 micron and 0.25 micron. It was insured that the temperature of the sample was (~32 °C) in accord with the working temperature of the sedigraph, because the selected program converts the values at this temperature. All the samples were prepared to be 3 to 5% by concentration. After loading the suspended sample in the sample cell, the intensity of x-rays passing through the sample was adjusted at 700 (best rate; Micromeritics 5000ET Instruction Manual) before starting analysis. The cumulative percentage data was stored in the attached computer and a cumulative weight frequency plot was obtained.

5.2.4 Organic Matter and Carbonate Determinations

The *Loss-on-ignition* technique was used to determinate organic matter and carbonate contents [Kolthoff & Sandell, 1952; Galle & Runnels, 1960; Carver, 1971; Allen, Grimshaw, Parkinson & Quarmby, 1974; Dean Jr., 1974; Engstrom & Wright, 1984; and Bengtsson & Enell, 1986] of 64 sediment samples (Appendix-III). This procedure is based on the weight loss principle. When the samples containing organic matter and calcium carbonate are heated in a muffle furnace, the organic matter begins to ignite at about 200°C and completely ignites when temperature is about 550°C, and CO_2 evolves from dolomite and calcite at 700-750°C and 800 to 850°C respectively [Dean Jr., 1974].

The percentages of organic matter and carbonate in the sediments were analysed by this *loss-on-ignition* technique. Positions of sediment samples (Fig. 5.12, Fig. 5.13) for this purpose were carefully chosen, so that the results were representative of the whole of the area. About 40 gm of evenly mixed sediment sample were dried at room temperature in an evaporating dish and powdered in a pestle and mortar. Porcelain crucibles were washed with distilled water, dried at 100-115°C for one hour in the oven and cooled in a dessicator. Samples were weighed to four decimals of a gram. About 5 gm of sediment sample were weighed in a pre-weighed crucible and put into the oven at 105°C for 12 hours, cooled in a dessicator and re-weighed. Then sample and crucible were heated in a muffle furnace for one hour at

550°C, cooled and again weighed. The weight loss at this temperature was equal to the weight of organic matter. The crucible and sample were returned to the muffle furnace and heated to 1000°C for one hour. The weight loss between 550-1000°C due to CO_2 evolved from carbonate minerals. As carbonate compounds become volatile at different temperatures [Dean Jr., 1974], this carbonate estimation is only a rough determination. An estimate of carbonate content was determined by multiplying the weight loss obtained between 550-1000°C by 1.3636 [Bengtsson & Enell, 1986].

Most clays contain five percent or less lattice OH water, which is not removed until temperature reach 550 to 1000°C [Grim, 1953]. Sediments containing 100 percent clay would presumably yield up to 5% weight loss between 500-1000°C [Dean Jr., 1974]. Among the sediment samples analysed, 7 samples were of medium sand size; 47, fine sand; 9, very fine sand and one sample (no. 114) medium silt size, according to the Wentworth size classification. So the loss on ignition due to lattice water was probably negligible. Three replicates of 9 samples (Appendix-III) were analysed for an estimation of error within the samples. The mean coefficient of variation between 105-550°C and 550-1000°C was 4.954% and 4.510%, respectively.

5.3 Grain Size Textural Parameters

In sediment grain size analysis, there are two common

ways of obtaining the statistical information. The first is by *graphical* method, in which values derived directly from plotted cumulative curves are entered into established formulae. The second is the method of *moments* in which every grain in the size population of an analysed sample is accounted for in the computation of grain size parameters.

A major controversy is whether one should use graphical or moment statistics. Each method has its advantages and drawbacks in determining mean, sorting, skewness and kurtosis, and each is equally valid for comparing a suite of samples. Folk [1966] mentioned that " presumably the same geologic conclusion would be reached no matter which method is used because of sample-to-sample variation in most geologic suites is so large as to outweigh hair-splitting over details of statistical orthodoxy".

Koldijk [1968], and Dyer [1986], for example, preferred the moment measures over percentile measurements. Folk [1966] on the other hand advocates the use of graphical techniques for a visual appreciation of the distribution.

McCammon [1962] criticised both graphic and moments methods and prepared a rectangular distribution and triangular distribution.

The statistical parameters used in this study are calculated by the graphical method using the formulae of Folk & Ward [1957]. According to Buller & McManus [1979], this graphical method is the most popular method for the computation of statistical parameters from sedimentary data.

5.3.1 Modal Grain Diameter

The modal size is the maximum percentage occurring at an equal size interval within a sample. Folk [1966] stated it as the most frequently-occurring grain diameter. On grain frequency histograms, the highest bar provides the modal class. On a graphical plot of grain size and weight percentage frequency, it is the value of grain size at the peak point of the curve. When the frequency curve exhibits several peaks, the sample is said to be polymodal. A polymodal distribution shows the presence of more than one grain size population. In a log-normal distribution the mode is identical to the mean grain diameter. In areas where there are several sources of sediments, modal analysis is especially useful and the modes may have greater genetic significant than the mean grain size.

5.3.2 Mean Grain Size

This is an expression of the average size of a sediment. This parameter was calculated by the formula given by Folk & Ward [1957],

$$M_z = \frac{\emptyset_{16} + \emptyset_{50} + \emptyset_{84}}{3}$$

The mean grain size gives a simple indication of the magnitude of the energy applied by the transporting agent. A spatial decrease in mean size value indicates the direction of transport; the value of phi units would

increase in the direction of transport due to progressive sorting (i.e. small grains out running larger grains).

5.3.3 Standard Deviation

The standard deviation of a sample is a measure of its degree of sorting (spread, dispersion, scatter, deviation), and provides values which indicate the spread of data about the average grain size of the sample. In the direction of transport, the sediments gradually become better sorted; the more sorted the material the less would be the value of the standard deviation [Chakrabarti, 1971]. Inman [1949] suggested that once the sediment attains a minimum phi value (best sorting: approximately a single size), if it continues to get finer, it will "round the turn" on the curve and sorting will worsen with further transport. After Krumbein [1938] and Otto [1939], Inman [1952] suggested the phi standard deviation as,

$$\sigma = \frac{\phi_{84} - \phi_{16}}{2}$$

Because this formula is based only on the central part of the distribution and ignores about one-third of the sample, Folk & Ward [1957], calculated the standard deviation of grains by,

$$\sigma = \frac{\phi_{84} - \phi_{16}}{4} + \frac{\phi_{95} - \phi_{5}}{6.6}$$

and named it as inclusive graphic standard deviation. This formula is used in the present study.

According to Steidtmann [1982], some of the important variables which together or independently are involved in the sediment sorting are:

(a) sediments accumulation rate (slow, rapid, none)

(b) nature of the sediment surface (size distribution, packing and arrangement of grains)

(c) style of grain motion (traction, saltation, suspension)

(d) fluid characteristics (velocity, turbulence, depth)

(e) grain characteristics (size, shape, density)

Generally sorting indicates the range of fluid velocities i.e., hydraulic energy.

5.3.4 Skewness

Skewness is determined by the Inclusive Graphic Skewness formula of Folk & Ward [1957] as,

$$S_k = \frac{\phi_{16} + \phi_{84} - 2\phi_{50}}{2(\phi_{84} - \phi_{16})} + \frac{\phi_5 + \phi_{95} - 2\phi_{50}}{2(\phi_{95} - \phi_5)}$$

which is a combination of Inman [1952]'s two measures of skewness (one for the central and another for the tail of the distribution). This measures the *swing* of the particle size curve on one side or other of the median. Positive values in phi indicate that the *tail* of the sample has fine grains and negative values show a tail of coarser grains on the frequency distribution curve. Skewness is a positive or negative dimensionless number and has a range of -1 to 1.

The environmental significance of skewness suggested by Duane [1964], that the negative skewness (shows demonstrable erosion or non-deposition areas) results when the fine particles from the sediments are removed by a winnowing action whereas positive skewness (indicates deposition) is normally due to accumulation of fine grains in low energy environments. Areas showing no particular dominance of negative or positive skewness are normally regions of fluctuating energy levels.

5.3.5 Kurtosis

Kurtosis is a measure of the peakedness of a frequency curve. The graphic kurtosis (K_g) used here is given by the formula,

$$K_g = \frac{\phi_{95} - \phi_5}{2.44(\phi_{75} - \phi_{25})}$$

It is a sensitive and valuable test of the normality of a distribution and is used to measure the ratio of the sorting of the tails and centre of the distribution. A normally distributed Gaussian curve has a kurtosis value of one. Platykurtic values (Kg <0.90), show the distribution curve less peaked than the normal curve, and leptokurtic values (Kg >1.11) show a distribution curve more peaked than a normal curve. Kurtosis is also a dimensionless parameter.

5.4 Presentation of Sediment Grain Size Data

After analysis and calculation of statistical parameters, the distribution size data are presented in different forms. Contour maps of grain parameters are used to show their spatial variations. Tables are used to compare the statistical parameters of grain size data from different geographical subareas. Bivariate scattergrams are used to distinguish fields of sediments having similar characteristics and to identify different subenvironments. In these plots, parameters of 235 sediment samples are compared with each other. The grain size distributions of individual sediment samples are presented as: (i) histograms of weight percentage frequency, (ii) distribution curves of frequency percentage by weight, (iii) cumulative weight percentage frequency on an arithmetic scale, and (iv) cumulative weight frequency percentage on a probability scale. Weight percentage frequency plots of grain size are further compared with each other by plotting them at their collected positions (Fig. 5.18, Fig. 5.19) on index maps. This provides a better comparison of size frequency data of different areas.

5.5 Analytical and Expressional Errors

Krumbein [1934] discussed in detail the probable sources of errors in sediment sampling and grain size determination. All errors up to the process of splitting for size determination are considered constant for each sample. Among analytical errors, sample splitting and instrument

errors have been calculated by analysing three replicates each of 44 samples and 2 replicates each of 2 samples (Appendix-IV).

The mean coefficient of variation (CV) for the mode is 1.127%. Samples 114 and 216 have relatively higher CVs of 6.24% and 3.46%, respectively. The average CV, excluding these two samples, reduces to 0.958%, a variation of $\pm$0.024Ø for the average mode 2.526Ø.

The average of mean grain size of 46 samples is 2.698Ø and the CV is 0.81%. The percentage of variation is comparatively high in the coarse sands. Three samples (Appendix-IV) in this size category have a CV of 7.25, 3.93 and 1.18%. The mean CV of the other replicate samples is 0.58% i.e., an error of $\pm$0.0156Ø.

The calculated error for standard deviation is 2.669%; an average error of $\pm$0.0236Ø for 0.886Ø sorting. Two samples (nos. 18, 112) have 11.55% and 20.87% CV. By excluding these, the variation is $\pm$0.019Ø for the average 0.915Ø sorting.

The variation in skewness is comparatively higher than other textural parameters, and each descriptive class [Folk & Ward 1957] has a markedly different values of coefficient of variation. These errors probably represent splitting errors.

Descriptive Class	Samples	CV (%)
Very negative skewed	4	2.79
Nearly symmetrical	13	85.60
Positive skewed	12	23.36
Very Positive skewed	17	4.47

For the kurtosis the mean CV calculated from 42 samples is 4.16%. Sample nos. 13, 112, 115 and 172 has a CV of 10.15, 12.53, 14.56 and 49.72% respectively, so the mean CV for 46 samples is 5.70%.

These grain size parameter errors are compared (Table 5.2) with a similar replicate analysis using the same apparatus (UCNW fall tower) by Larcombe [1989] and Shaghude [1990]. Larcombe calculated the replicate error of four sediment samples from Barmouth Bay and one from the Mawddach Estuary. Shaghude analysed the sand fraction of 10 sediment samples (3 replicates of each) taken from a dynamic shelf environment in the Christchurch Bay (English Channel).

Table: 5.2 Average textural parameters and error calculated from replicate analysis using UCNW fall tower.

Mode (Ø)	Mean (Ø)	Sorting (Ø)	Skewness	Kurtosis
Larcombe [1989], 5 samples, 23 replicates, confidence limits 95%.				
2.080±0.133	2.057±0.045	0.504±0.052	-0.199±0.113	1.144±0.143
Shaghude [1990], 10 samples and 30 replicates				
	2.360±0.101	0.430±0.025	-0.830±0.390	2.870±1.252
This Study, 44; 3 replicates and 2; 2 replicates of each sample				
2.530±0.029	2.698±0.022	0.886±0.023	0.197±0.063	2.172±0.124

The statistical parameters are expressed here as tables, scatter diagrams, histograms and contour maps. The error in presenting data in tables and comparing various parameters to each other as scatter diagrams, involves the conversion of 3 decimal data values to 2 decimal data values i.e., ±0.005. Contour maps have been plotted by UNIRAS Graphic Programme. The error in contours depends on the number of grid cells selected for the calculation in the programme. An area of 50m by 50m was selected for calculation of the data points. By the proper selection of the contour limits, error in the contour map can be minimised. So in the contour diagrams an error of less than ±50m in contour positions may be expected. In the interpretation of grain size distributions of each sediment sample, the weight percentage frequencies are plotted as histograms and line

graphs at 0.5Ø and 0.25Ø intervals, respectively. In plotting the cumulative weight percentages on arithmetic and probability scales, each measured phi interval (which is less than 0.04Ø) is used.

5.6 Regional Distribution of Gravel, Sand and Mud

The percentage of each main grain size class (gravel, sand, and mud) was determined and after plotting these percentages as contour plots, regional variations are found. Most of the area is dominant by sand (Fig. 5.3). Mud occupies some of the coastal area (e.g., near Bangor Pier and near Great Ormes Head, Fig. 5.4), and gravels are observed generally in areas deeper than 14m near Puffin Island and in some parts of the Menai Strait channel which are probably high energy areas (Fig. 5.2). Details of the percentages of gravel, sand and mud size are given in Appendix-II.

5.6.1 Gravel Size

The regional distribution of gravel is shown in Fig. 5.2. 83.4% of the total samples (235) contain less than 5% of gravel and only two samples have more than 90%.

Near the Arfon mainland coastline, sample nos. 117, 130 and 204 have 14.2% and 8.1% and 42.3% of this size respectively. On the Lavan Sands and Dutchman areas almost all the samples have less than 5% gravel. To the north east

of Puffin Island, gravel ranges between 10% and 30% in most of the sediment samples. From sample positions 46, 40 and 41 towards Great Ormes Head, all the samples have less than 5% gravel.

In the Menai Strait channel, this fraction was found more than 10% in 55% of the collected samples. Near Beaumaris two samples (169 and 170) show maximum gravel percentage (>90%) among the collected samples. The majority of sediments with high values of the gravel fraction are located in areas of comparatively high flow velocity and deep water. Most of the gravel is adjacent to the rocky coast of Anglesey and to the main channel.

5.6.2 Sand Size

This is the most abundant size fraction in the NE Menai Strait and Conwy Bay area. Only one sample was less than 5% sand by weight. In 38.7% and 60.4% of the collected sediment samples, the sand fraction is 5-95% and >95%, respectively. Fig. 5.3 shows the regional variations in the percentage of sand in the area. Apart from the area close to Bangor Pier, almost all of the intertidal area comprises more than 90% sand. Near Great Ormes Head, sand is locally <5% and this is the only area where sand is not abundant. In the Menai Strait main channel area, sand frequency is very variable. Between Puffin Island and Great Ormes Head, about 2km offshore of both coastlines all the samples have more than 95% sand.

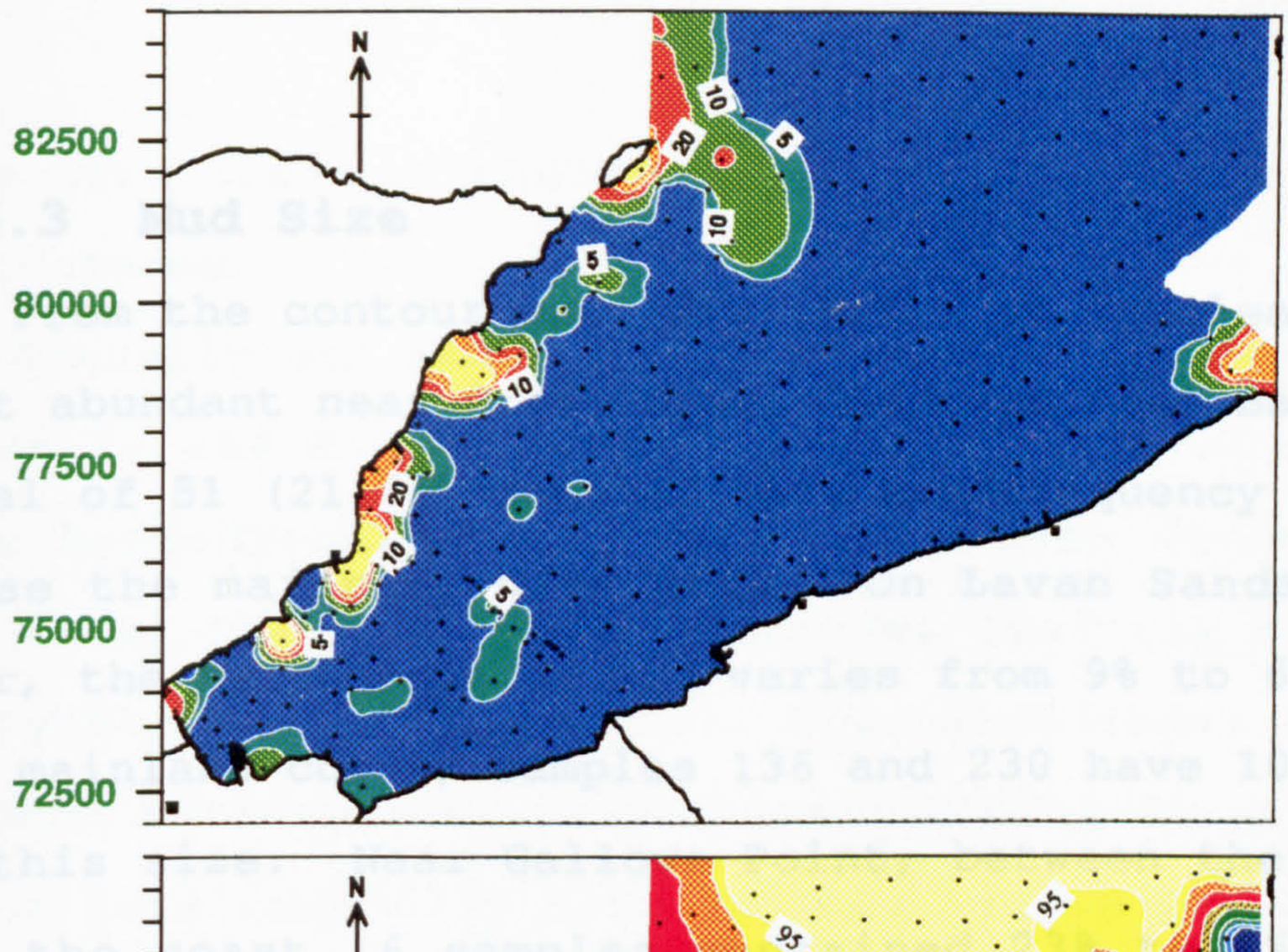

Fig: 5.2

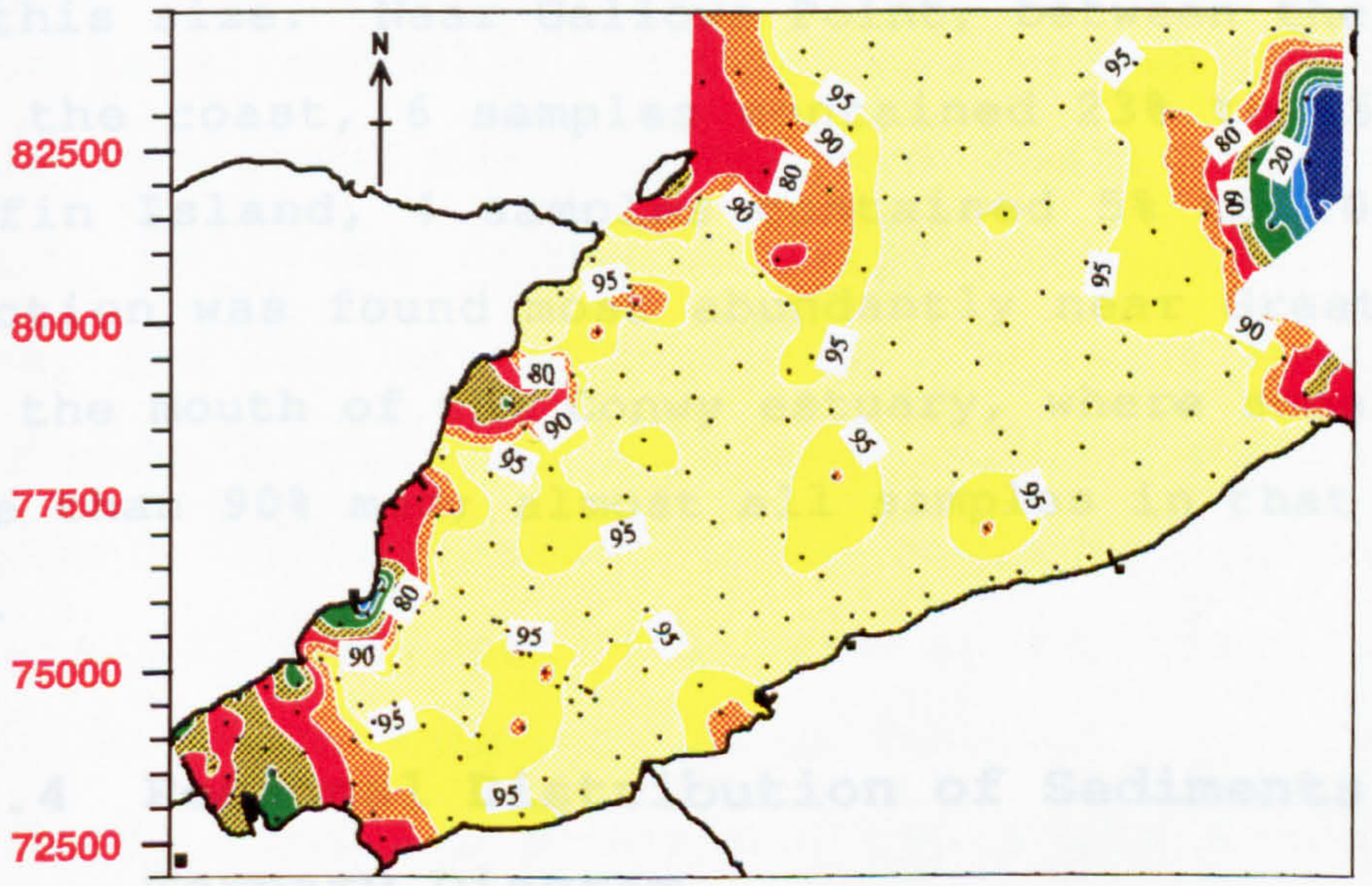

Fig: 5.3

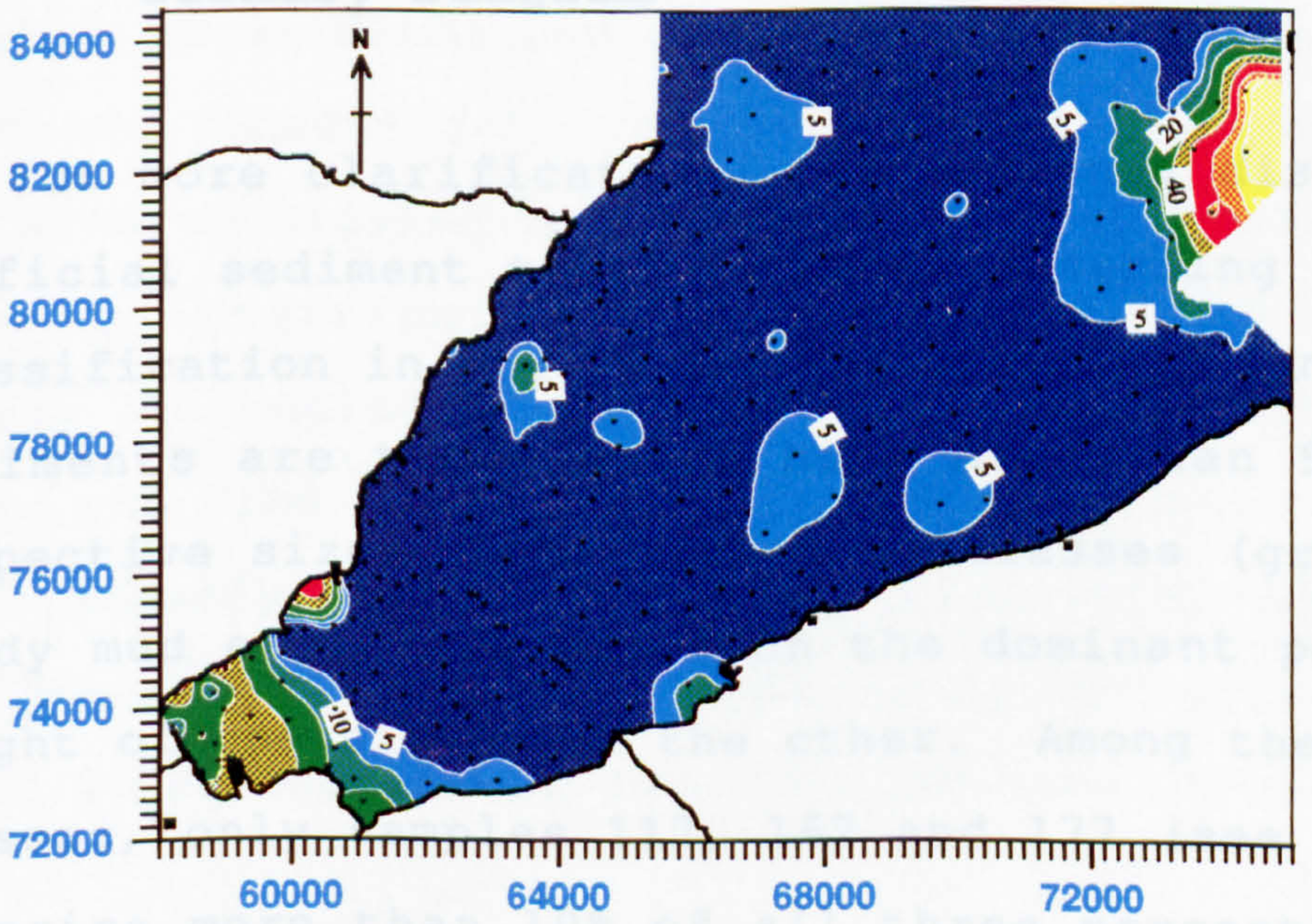

Fig: 5.4

5.6.3 Mud Size

From the contour map (Fig. 5.4), it is clear that mud is most abundant near Great Ormes Head and near Bangor Pier. A total of 51 (21.7%) samples have mud frequency >5% and among these the majority have <15%. On Lavan Sands near Bangor Pier, the percentage of mud varies from 9% to 65%. Close to the mainland coast, samples 136 and 230 have 10.9% and 11.5% of this size. Near Gallows Point, between the main channel and the coast, 6 samples contained 23% to 65% mud. Near Puffin Island, 4 samples contained 5% to 10% mud. This fraction was found most abundantly near Great Ormes Head, off the mouth of the Conwy estuary, where some samples have more than 90% mud; almost all samples in that area had >5% mud.

5.6.4 Regional Distribution of Sediments based on Ternary Diagram

For more clarification, the regional distribution of surficial sediment types is shown according to a ternary classification in Fig. 5.5. The gravelly, sandy and muddy sediments are those which have more than 90% of those respective sizes. The composite classes (gravelly sand, sandy mud etc.) are based on the dominant percentage by weight of one size over the other. Among these composite classes, only samples 117, 167 and 177 (see Appendix-II) comprise more than 10% of all three percentages and the

composite class of these samples is based on the two higher percentages.

Gravelly and sandy gravel sediments are found in limited areas in the Menai Strait channel, which is comparatively more hydrodynamically active. The area deeper than about 15m (near Puffin Island) comprises gravelly sands. On the bathymetric map (Chapter 3), this area shows a narrow deep channel with current velocities (Chapter 4) up to 100 cm/s. Other local gravelly sand patches are in the middle of the Lavan Sands and near Penmaenbach Point. Near Penmaenbach Point, only one sediment sample (no. 204) falls in this class, and lies at the border of the study area.

Sandy sediments are the most abundant surficial sediments in the area. These sediments cover most of the intertidal and subtidal area up to depth of about 14m relative to the Ordnance Datum (Newlyn).

Muddy sand and sandy mud types are found near Bangor Pier on Lavan Sands and near Great Ormes Head. Some local patches of muddy sand are found along the mainland coast. The area comprising muddy sands and sandy muds near Bangor Pier is intertidal and the pattern of the coastline is nearly semienclosed. So it can be deduced that during high water the flow in this area is a minimum and fine particles most probably transported by the flood water can settle out.

The only area which contains muddy sediments is near Great Ormes Head at the mouth of the Afon Conwy.

Fig: 5.5 **Surficial sediments based on ternary diagram - distribution.**

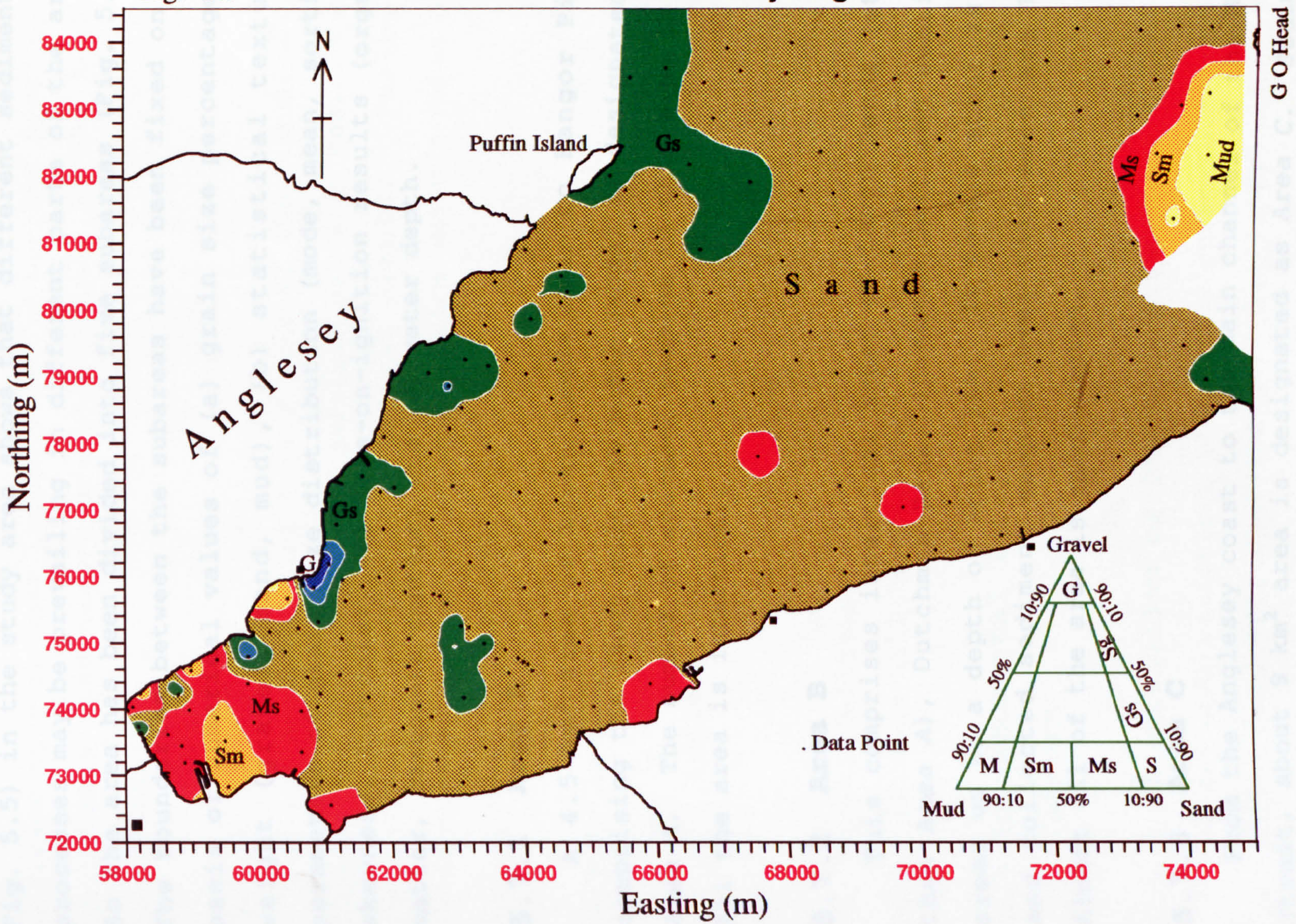

5.7 Subdivision of the Area

The distribution of surficial sediments (Fig. 5.2 to Fig. 5.5) in the study area shows that different sedimentary processes may be prevailing in different parts of the area. So the area has been divided into five subareas (Fig. 5.6). The boundaries between the subareas have been fixed on the basis of numerical values of (a) grain size percentage by weight (gravel, sand, mud), (b) statistical textural parameters of grain size distribution (mode, mean, sorting, skewness, kurtosis), (c) loss-on-ignition results (organic matter, carbonate content) and (d) water depth.

5.7.1 Area A

A 4.5 km^2 area of Lavan Sands near to Bangor Pier, comprising the sandy muds and muddy sands, is designated as *Area A*. The number of sediment samples in this area is 13. All the area is intertidal.

5.7.2 Area B

This comprises intertidal areas of Lavan Sands (other than *Area A*), Dutchman Bank, Irishman Spit and subtidal areas up to a depth of about 14m. It covers about 78 km^2 and collected sediment samples over this area are 158. Almost all of the area is sand covered.

5.7.3 Area C

From the Anglesey coast to the main channel of the Menai Strait, about 9 km^2 area is designated as *Area C*. Sediment

samples (total 29) in this area show a variation from gravelly sediments to sandy muds. This spatial variation in sediment type is most probably due to varying hydrodynamic conditions, and nature and orientation of the Anglesey coastline.

5.7.4 Area D

To the north east of Puffin Island, about 9.5 km^2 area deeper than about 14m, with gravelly sands is designated as *Area D*. It comprises 20 sediment samples. During the fathometer survey of the study area, the maximum water depth was recorded in this subarea.

5.7.5 Area E

This is covered by muds and sandy muds. *Area E* is about 13 km^2, adjacent to Great Ormes Head, and comprises 15 samples.

In the following sections, the grain size results of these subareas will be compared to each other.

5.8 Environmental Interpretation from Sediment Texture

5.8.1 Distribution of Textural Parameters

The regional variations of textural parameters are shown as contour maps cf., Chakrabarti, [1971]; Cronan, [1972];

Fig: 5.6

Subarea division based on the surficial sediment types.

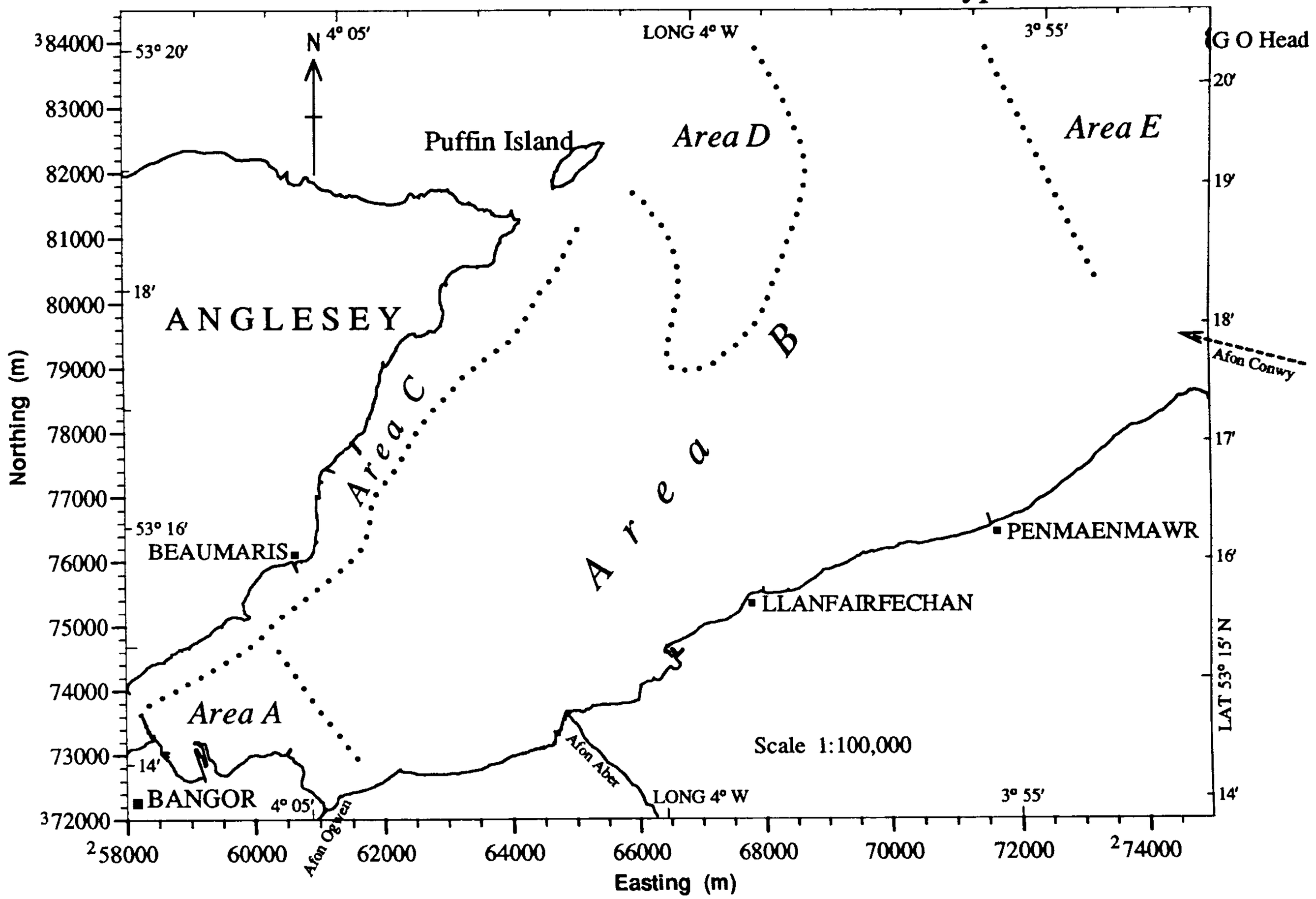

Sha, [1990].

5.8.1.1 Modal Grain Diameter

From the contour map (Fig. 5.7), it is clear that there is a general trend of increasing phi value from the north (open sea) toward the south and south-west, i.e., the phi value increases from *Area D* towards *Area A* via *Area B*. Another trend in increasing modal phi values is from the areas north east of Puffin Island (*Area D*) towards the Great Ormes Head. Thus a general modal gradient from north to south and then to the south west occurs in the area. Schlee [1973] states that a pronounced modal gradient up to a limited distance is an indicator of sediment transport direction.

In *Area A*, only one sample (no. 122, at the boundary with *Area B*) has a mode less than 3.0Ø; all other sediment samples have mode grain size >3.0Ø and so the general values of contours are higher in this area The average mode grain diameter in this area (*Area A*) is 3.15Ø. In *Area B* only one sample (no. 163) has a medium sand mode. The location of this sample is Penmaen Swatch which has a comparatively higher water depth than other samples around this locality. All the samples in the subtidal area and in the northern parts of the Lavan Sands consist of a fine sand modes. In the southern parts of the Lavan Sands, some of the samples (10.8%) have a very fine sand mode. In *Area C*, no clear trend in the contours is observed. The modal grain diameter in phi decreases as the distance increases from the coast

toward the channel between Beaumaris and Gallows Point i.e., the mode, in mm become coarser towards the main channel. In all other parts, the trend is opposite. Four samples in this area have modal values less than zero phi, 6 have medium sand modes, 14 samples lie in fine sand mode and the other 5 are more than 3.0Ø.

All the sediment samples in *Area D* have modal grain diameter ranging between 2.08 and 2.72Ø.

In *Area E*, 12 samples have modal diameter between 2.16-2.52Ø, 3 samples (nos. 1, 2, 8) have high modal values (11.3, 11.2, 11.3Ø) and these are the only samples that have more than 90% mud.

5.8.1.2 Mean Grain Size of Sediments

The regional distribution of mean grain size diameter (Fig. 5.8) similarly shows a very clear trend of fining from north towards the south and southwest of the study area. The same trend was observed in the residual currents in the area (Chapter 4). So it may be concluded that as coarse sediments are transported from the open sea to Conwy Bay and Lavan Sands areas, the size of sediments decreases due to hydraulic sorting. Details of grain sizes in each subarea are given in Table 5.3.

Table: 5.3 Percentage of sediment samples according to the Wentworth Size Classification in A-E subareas.

Areas:	***A***	***B***	***C***	***D***	***E***
	%	%	%	%	%
Gravel	-	-	13.79	-	-
Coarse sand	-	-	13.79	15.00	-
Medium sand	-	1.90	31.03	10.00	-
Fine sand	-	69.62	27.59	75.00	66.67
Very fine sand	30.77	27.85	-	-	-
Coarse silt	15.38	-	3.45	-	6.67
Medium silt	46.16	-	-	-	-
Fine silt	7.69	-	10.35	-	-
Very fine silt	-	-	-	-	6.67
Clay	-	-	-	-	20.01

In the north of the area (*Area D*) sediment mean grain size is coarse sand to fine sand; as the sediments move towards *Area B* they become medium sands to very fine sands, until in *Area A* all means are very fine sands and silts. From the mean grain size trend it can be concluded that the direction of sediment transport in the area is from north to south and south-west parallel to the coast line.

5.8.1.3 Standard Deviation

Fig. 5.9 is the regional distribution of standard deviation and contour intervals are according to the descriptive scale of Folk & Ward [1957]; the percentages of samples according to this scale are given in Table 5.4.

Table: 5.4 Percentage of sediment samples showing different classes of Sorting according to the Descriptive Scale of Folk & Ward [1957] in different subarea.

Areas:	***A***	***B***	***C***	***D***	***E***	***Total***
	%	%	%	%	%	%
Very Well Sorted (< 0.35Ø)	-	72.15	13.79	-	26.67	54.04
Well Sorted (0.35 - 0.5Ø)	-	16.46	6.90	10.00	6.67	13.19
Moderately Well " (0.5 - 0.7Ø)	-	5.06	6.90	15.00	-	5.11
Moderately Sorted (0.7 - 1.0Ø)	-	1.27	6.90	10.00	6.67	3.40
Poorly Sorted (1.0 - 2.0Ø)	30.77	5.06	20.69	25.00	26.67	11.49
Very Poorly Sorted (2.0 - 4.0Ø)	61.54	-	37.93	15.00	33.33	11.49
Extremely Poorly " (> 4.0Ø)	7.69	-	6.90	-	-	1.28

Sediment samples in *Area A* are poorly to very poorly sorted (1.11-4.27Ø). Most of the samples in *Area B* are very well to well sorted. Regional distribution of sorting shows an overall improvement from northern parts of the area towards the south western up to the boundary between *Area A* and *Area B*. Another trend is observed from *Area D* towards *Area E*. The very poor sorting in areas *A* and *B* is due to dominance of fine grain sizes. These trends most probably indicate sediment transport from north western part of the study area toward *Area A* and *Area E* via the *Area B*.

5.8.1.4 Skewness

This parameter ranges from very negative-skewed to very positive-skewed. Table 5.5 shows the percentage of samples

in the subareas on the basis of Folk & Ward's [1957] descriptive scale.

Table: 5.5 Percentage of sediment samples showing different classes of Skewness according to the Descriptive Scale of Folk & Ward [1957] in different subarea.

Areas:	***A***	***B***	***C***	***D***	***E***	***Total***
	%	%	%	%	%	%
Very negative-skewed (-1.0 - -0.3)	-	1.90	37.93	25.00	6.67	8.51
Negative-skewed (-0.3 - -0.1)	-	13.29	17.24	35.00	13.33	9.36
Nearly symmetrical (-0.1 - 0.1)	7.69	14.54	17.24	10.00	26.67	20.43
Positive-skewed (0.1 - 0.3)	7.69	53.16	3.45	10.00	13.33	38.30
Very positive-skewed (0.3 - 1.0)	84.62	17.09	24.14	20.00	40.00	23.40

The regional distribution of skewness of the sediments examined in this work is presented in Fig. 5.10. In *Area A* most of the samples are very positive-skewed, which shows this area is associated with a lower energy environment. The samples in *Area B* have -0.1 to 0.3 skewness. In *Area C* and *D*, more than 2/3 of the samples have negative values, indicating areas with higher energy environments.

5.8.1.5 Kurtosis

Spatial distribution is shown in Fig. 5.11. Table 5.6 denotes the percentage of samples on the basis of the descriptive classification of Folk & Ward [1957] in the total area and Areas A-E.

Modal grain diameter (ϕ) - regional distribution.

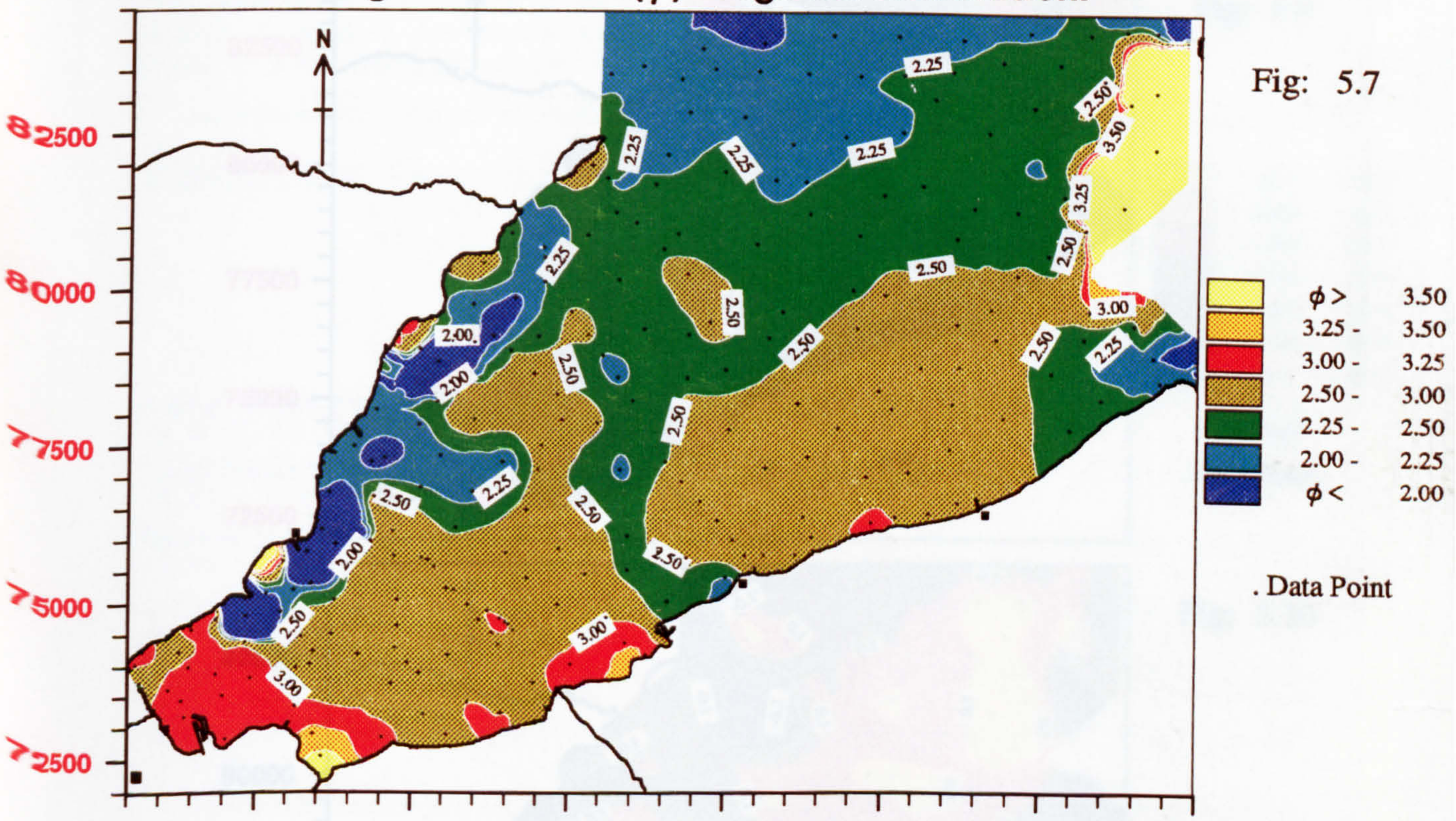

Fig: 5.7

Sediment mean grain size (ϕ) - regional distribution.

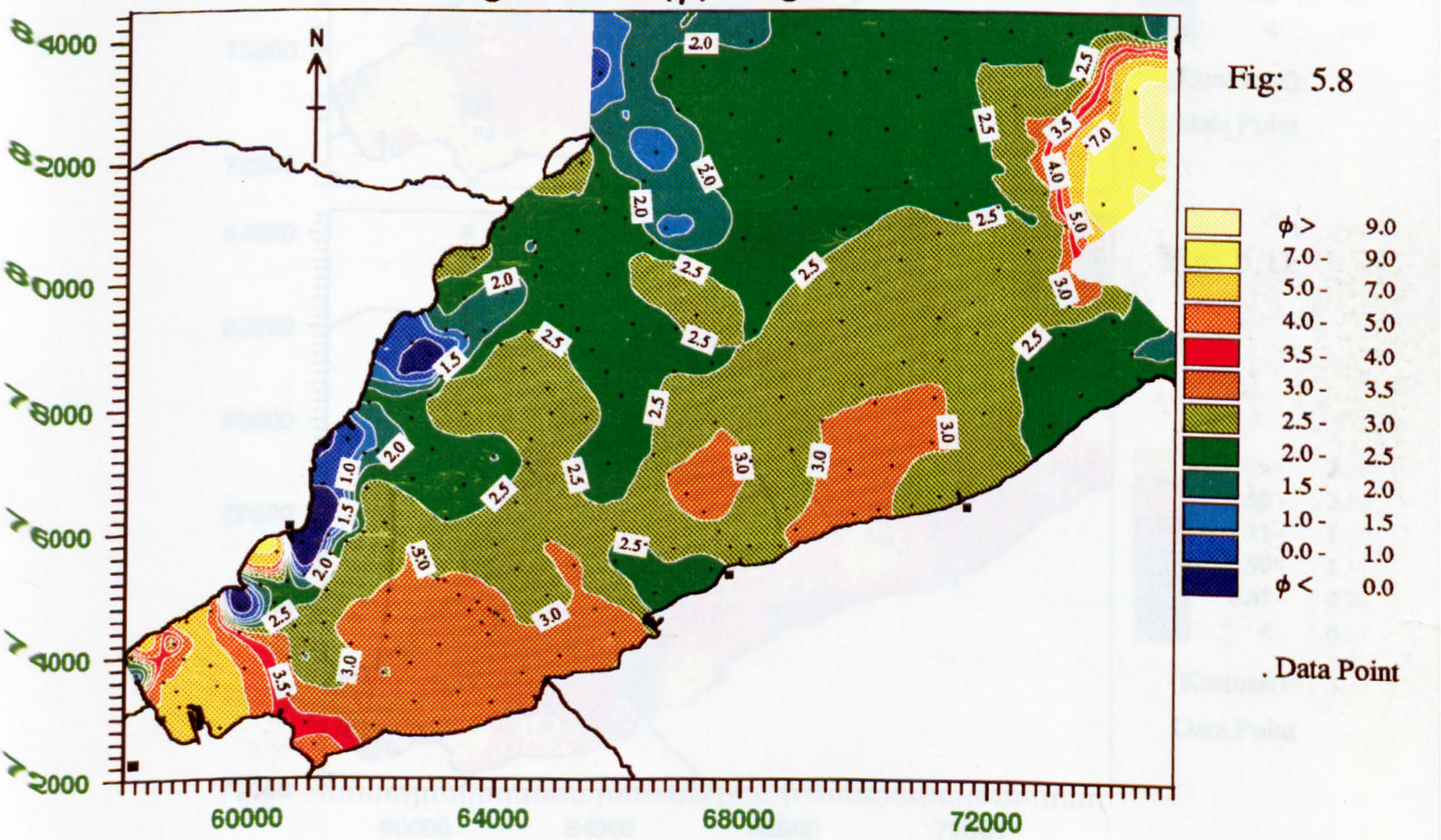

Fig: 5.8

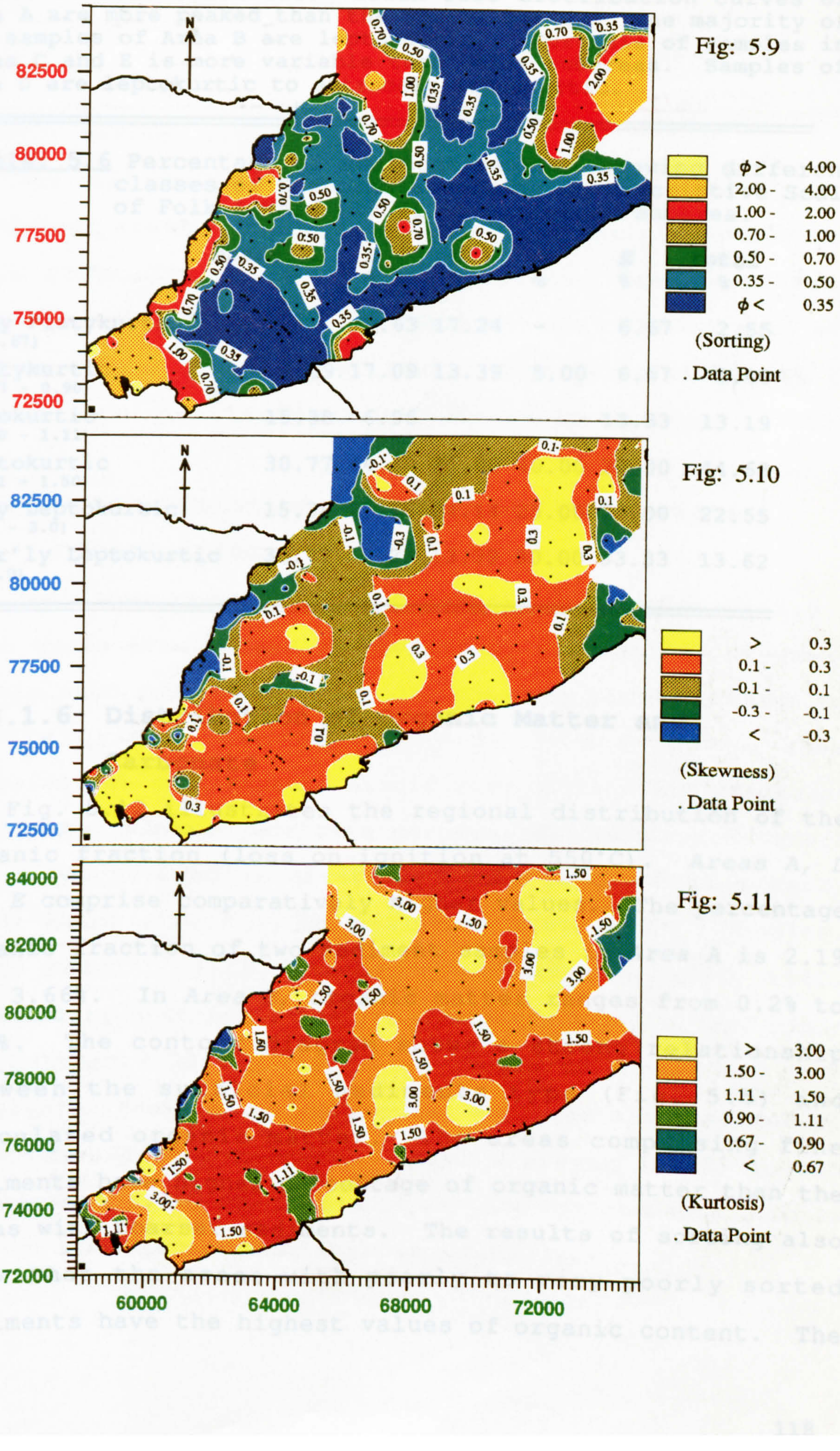
N
82500
80000
77500
75000
72500
0.70
0.50
1.00
0.35
2.00
Fig: 5.9
φ > 4.00
2.00 - 4.00
1.00 - 2.00
0.70 - 1.00
0.50 - 0.70
0.35 - 0.50
φ < 0.35
(Sorting)
. Data Point
Fig: 5.10
> 0.3
0.1 - 0.3
-0.1 - 0.1
-0.3 - -0.1
< -0.3
(Skewness)
. Data Point
Fig: 5.11
84000
82000
80000
78000
76000
74000
72000
60000
64000
68000
72000
3.00
1.50
1.11
> 3.00
1.50 - 3.00
1.11 - 1.50
0.90 - 1.11
0.67 - 0.90
< 0.67
(Kurtosis)
. Data Point

Regional distribution of kurtosis shows a trend of decreasing values towards southwest. Grain size distribution curves of Area A are more peaked than the normal curves. The majority of the samples of Area B are leptokurtic. Kurtosis of samples in Areas C and E is more variable than other subareas. Samples of Area D are leptokurtic to extremely leptokurtic.

Table: 5.6 Percentage of sediment samples showing different classes of Kurtosis according to Descriptive Scale of Folk & Ward [1957] in different subarea.

Areas:	***A***	***B***	***C***	***D***	***E***	***Total***
	%	%	%	%	%	%
Very Platykurtic (< 0.67)	-	0.63	17.24	-	6.67	2.55
Platykurtic (0.67 - 0.90)	7.69	17.09	13.39	5.00	6.67	3.40
Mesokurtic (0.90 - 1.11)	15.38	6.96	-	-	13.33	13.19
Leptokurtic (1.11 - 1.50)	30.77	44.30	31.09	40.00	20.00	44.68
Very Leptokurtic (1.5 - 3.0)	15.38	22.78	24.14	25.00	20.00	22.55
Extr'ly Leptokurtic (> 3.0)	30.77	8.23	13.39	30.00	33.33	13.62

5.8.1.6 Distribution of Organic Matter and Carbonate

Fig. 5.12 illustrates the regional distribution of the organic fraction (loss on ignition at 550°C). *Areas A, D* and *E* comprise comparatively higher values. The percentage organic fraction of two sediment samples in *Area A* is 2.19 and 3.66%. In *Area B*, organic matter ranges from 0.2% to 1.8%. The contour diagram shows a strong relationship between the surficial sediments type (Fig. 5.5) and calculated organic matter. The areas comprising fine sediments have higher percentage of organic matter than the areas with coarser sediments. The results of sorting also show that the areas with poorly to very poorly sorted sediments have the highest values of organic content. The

regional variations in organic matter percentage therefore closely reflect sediment type.

Regional variation of carbonate (Fig. 5.13) shows three different areas. Near Puffin Island and near Bangor Pier, high carbonate areas are pronounced. The third area comprises the Lavan Sands and most of the subtidal area off Puffin Island towards Great Ormes Head where carbonate is rather low. However, these differences are not very great.

5.8.2 Discrimination of Subareas by Bivariate Scattergrams

The inter relationship of numerical descriptors i.e., mean grain size, standard deviation, sorting and skewness within each subarea may be highlighted by plotting these as scattergrams. Generally the sediments of the same depositional environments should make similar fields/groups on scatter plots. For this purpose, different parameters are often plotted as bivariate plots [e.g., Folk & Ward, 1957; Mason & Folk 1958; Friedman, 1961, 1967; Doeglas, 1968; Koldijk, 1968; Cronan, 1972; McLaren, 1981, 1982; Sedimentation Seminar, 1981; Sly, Thomas & Pelletier, 1983; and Forrest & Clark, 1989]. It should be emphasised that samples on the boundaries between subareas are expected to show transitional results. Viard & Breyer [1979] quoted this method as useful in discriminating environments locally but not successful where applied generally.

Organic matter percentage by weight - spatial distribution.

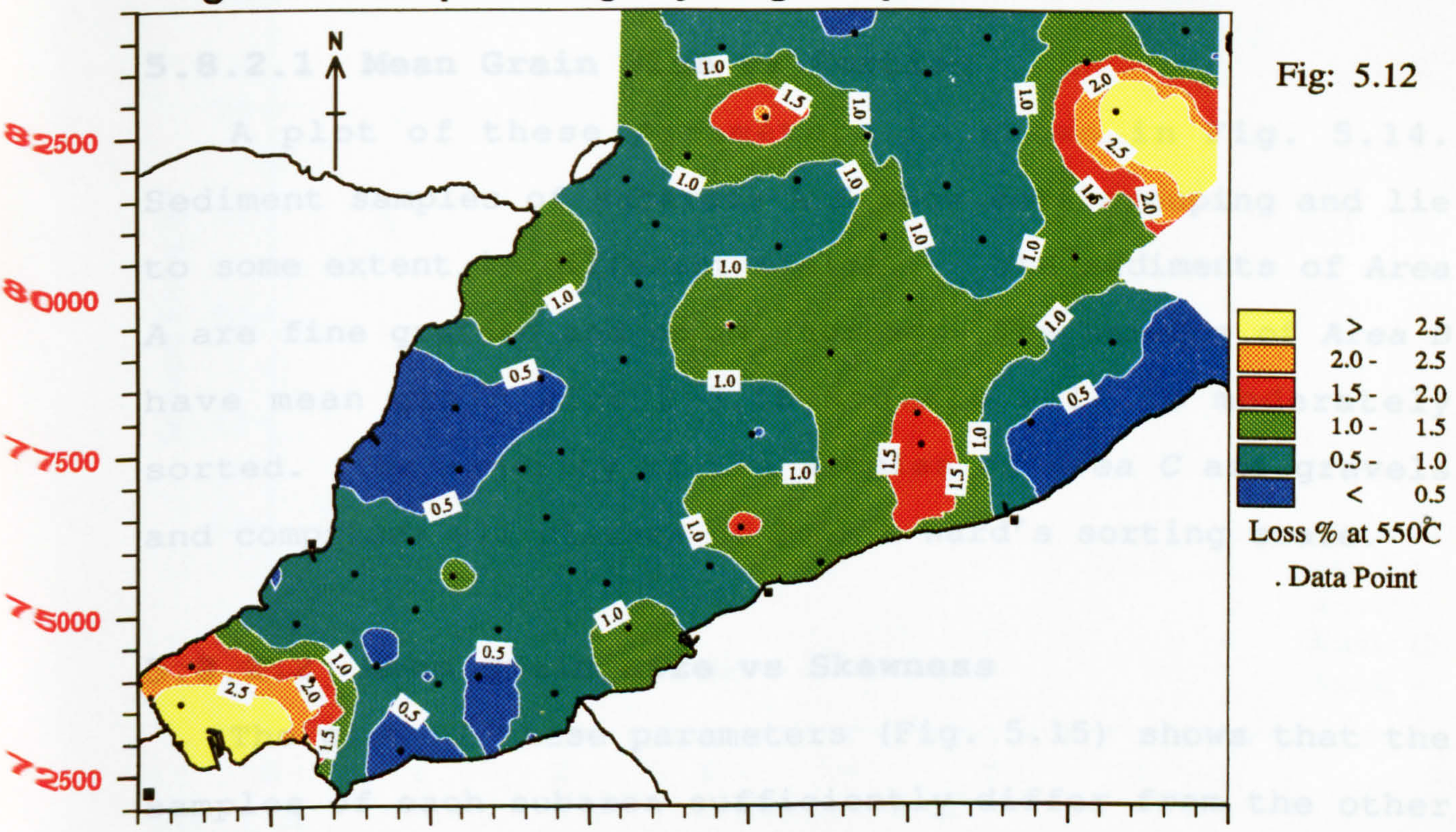

Fig: 5.12

Carbonates percentage by weight - spatial distribution.

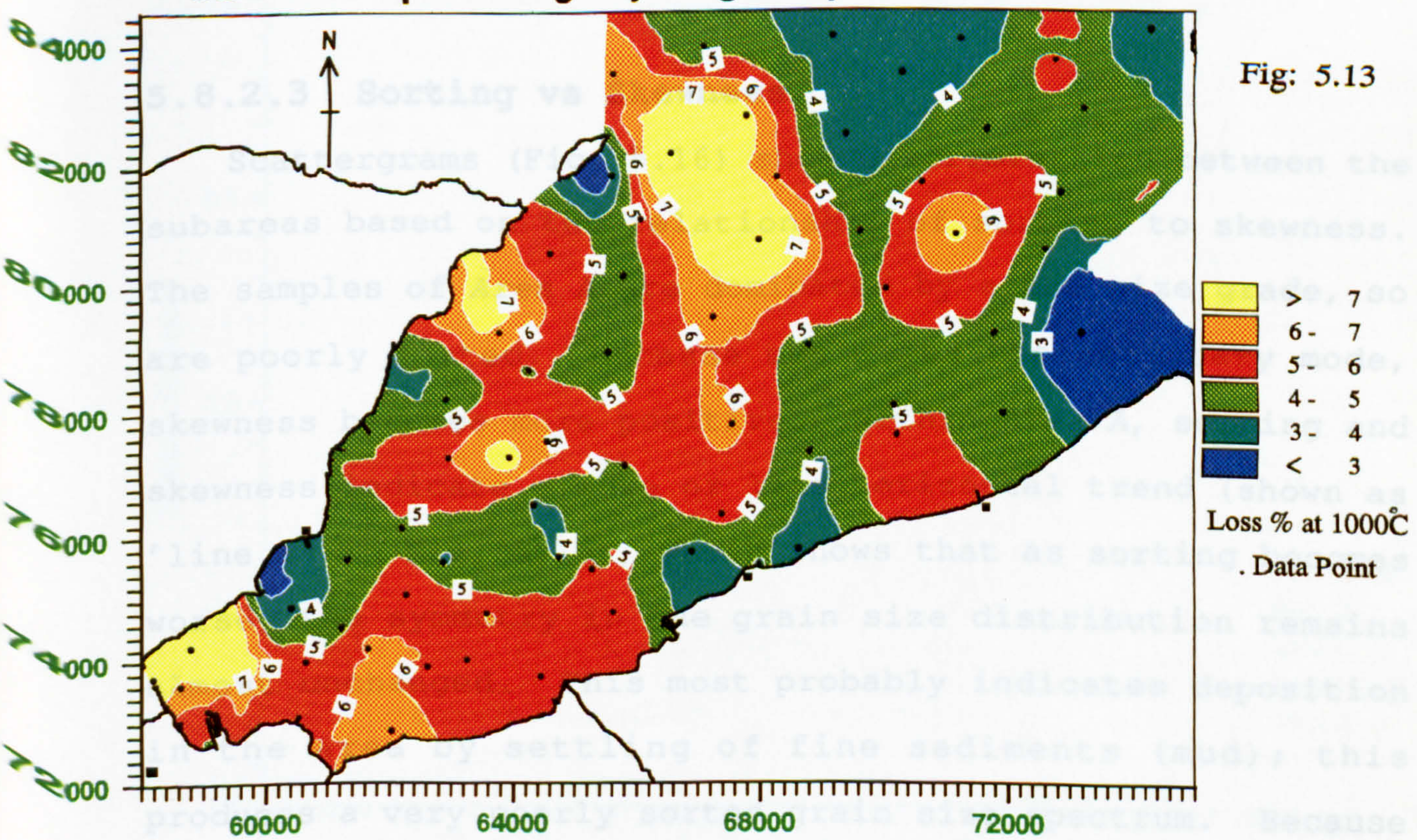

Fig: 5.13

5.8.2.1 Mean Grain Size vs Sorting

A plot of these parameters is shown in Fig. 5.14. Sediment samples of subareas A-E show some grouping and lie to some extent in different fields. The sediments of *Area A* are fine grained and poorly sorted. The samples of *Area B* have mean grain size 2-3.5Ø and are well to moderately sorted. The majority of the samples of *Area C* are gravels and comprises all classes of Folk & Ward's sorting scale.

5.8.2.2 Mean grain size vs Skewness

The plot of these parameters (Fig. 5.15) shows that the samples of each subarea sufficiently differ from the other subareas. Samples of the same subarea have a common trend. The fields of 5 subareas are clearly discriminated.

5.8.2.3 Sorting vs Skewness

Scattergrams (Fig. 5.16) show discrimination between the subareas based on the relationship of sorting to skewness. The samples of *Area A* are dominated by a mud size grade, so are poorly sorted. Because mud makes the secondary mode, skewness becomes more positive. Within *Area A*, sorting and skewness indicate a more or less horizontal trend (shown as 'line A' in Fig. 5.16), which shows that as sorting becomes worse, the symmetry in the grain size distribution remains almost unchanged. This most probably indicates deposition in the area by settling of fine sediments (mud); this produces a very poorly sorted grain size spectrum. Because the fine grains are uniform in size, the symmetry of the

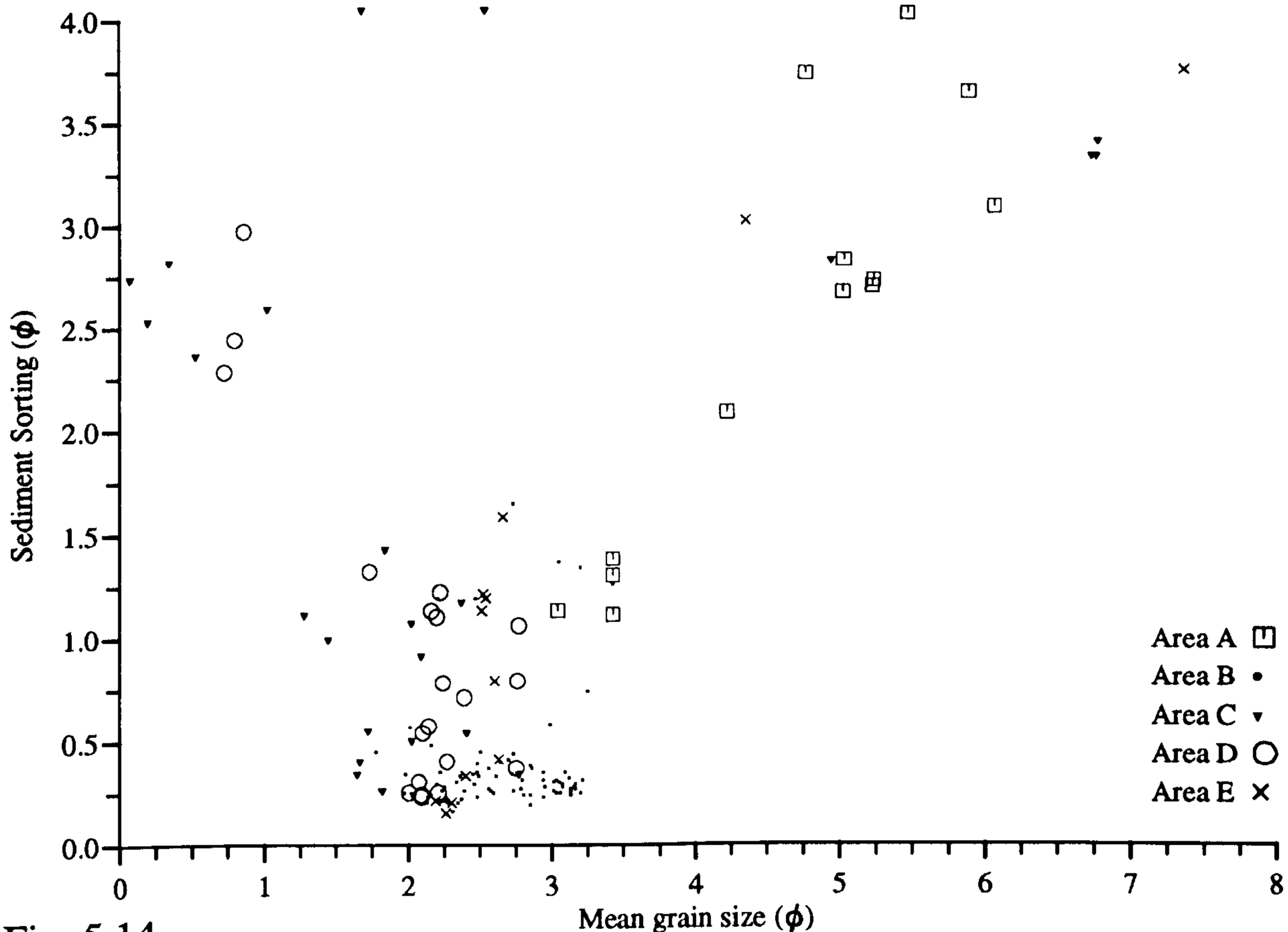

Fig: 5.14

Comparison between mean grain size and sorting of sediments in Areas A-E.

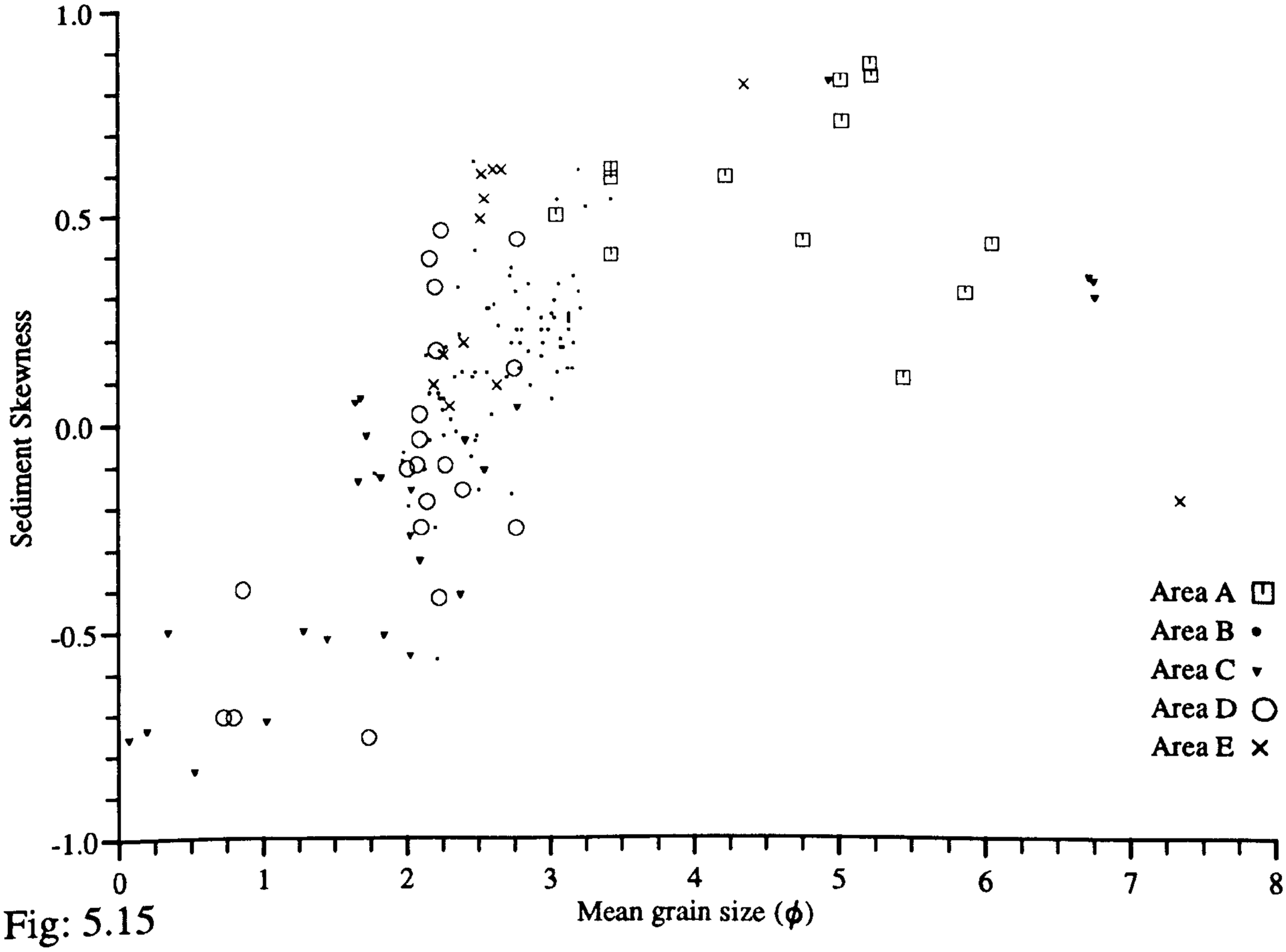

Fig: 5.15

Scattergrams of mean grain size and skewness of sediments in Areas A-E.

distribution is not generally changed.

The samples of *Area B* are very well sorted and have a variable skewness from negative to very positive (but the majority of samples show positive skewness). The sands of *Area B* therefore are well sorted sediments, skewed to the left or right depending on the preponderance of coarse or fine particles. Within the samples of this area, the trend of these parameters is almost vertical compared to the trend of *Area A* (marked by 'line B' in Fig. 5.16). Almost all the samples are very well sorted but display different symmetries. This shows that in different parts of *Area B* coarse grains or finer grains skew the distribution curves in different directions. The sediment transport explanation from this relationship may be that as sediments enter from deeper parts (the northern part of the area) from the Irish Sea by bedload transport, they are already well sorted though comparatively coarse. As they further progress towards Lavan Sands (the southern part of the study area) they become very well sorted but now show a dominance of fine particles. Thus sorting changes very little, while skewness changes more. This would be expected as skewness is more sensitive to the tails of the grain size distribution.

Samples of *Area C* do not show any particular trend, which indicates variations in sedimentary processes within the area due to rapid changes related to the main channel. The samples of *Area D* show comparatively wider ranges of

both sorting and skewness. The trend within this area is shown as 'line D' in Fig. 5.16, which probably indicates that as the sediments enter this area from the open sea under the influence of the flood tide (dominant tide recorded there), the sediments are comparatively coarse, poorly sorted and negatively skewed. As they further approach near the boundary of *Area B*, due to progressive sorting they become less coarse, well sorted and symmetrical to positive skewed. *Area E* shows a relationship of sorting and skewness that is opposite to that of *Area D*. As some of the sediment from *Area D* is also transported to *Area E* (see Chapter 4, Chapter 6) through the northern parts of *Area B*, grain size distributions becomes finer in mean grain size, sorting decreases, and skewness becomes very positive.

5.8.2.4 Mean Grain Size vs Water Depth

The relationship of water depth and mean grain size (Fig. 5.17) indicates the existence of different energy areas. Though overall, there is a trend of increasing phi diameter (therefore finer sediment) with decreasing depth. However, the water depths of many sediment samples of *Area B* are the same as in *Area A* but the grain size of both areas are markedly different. This is most probably due to comparatively more dynamic tidal (and wave) conditions in *Area B* and decline in energy in *Area A* because of configuration and orientation of adjacent coastline. A similar disparity exists between the samples of *Area B* and *C*. The majority of samples deeper than 14m (*Area D*) show a

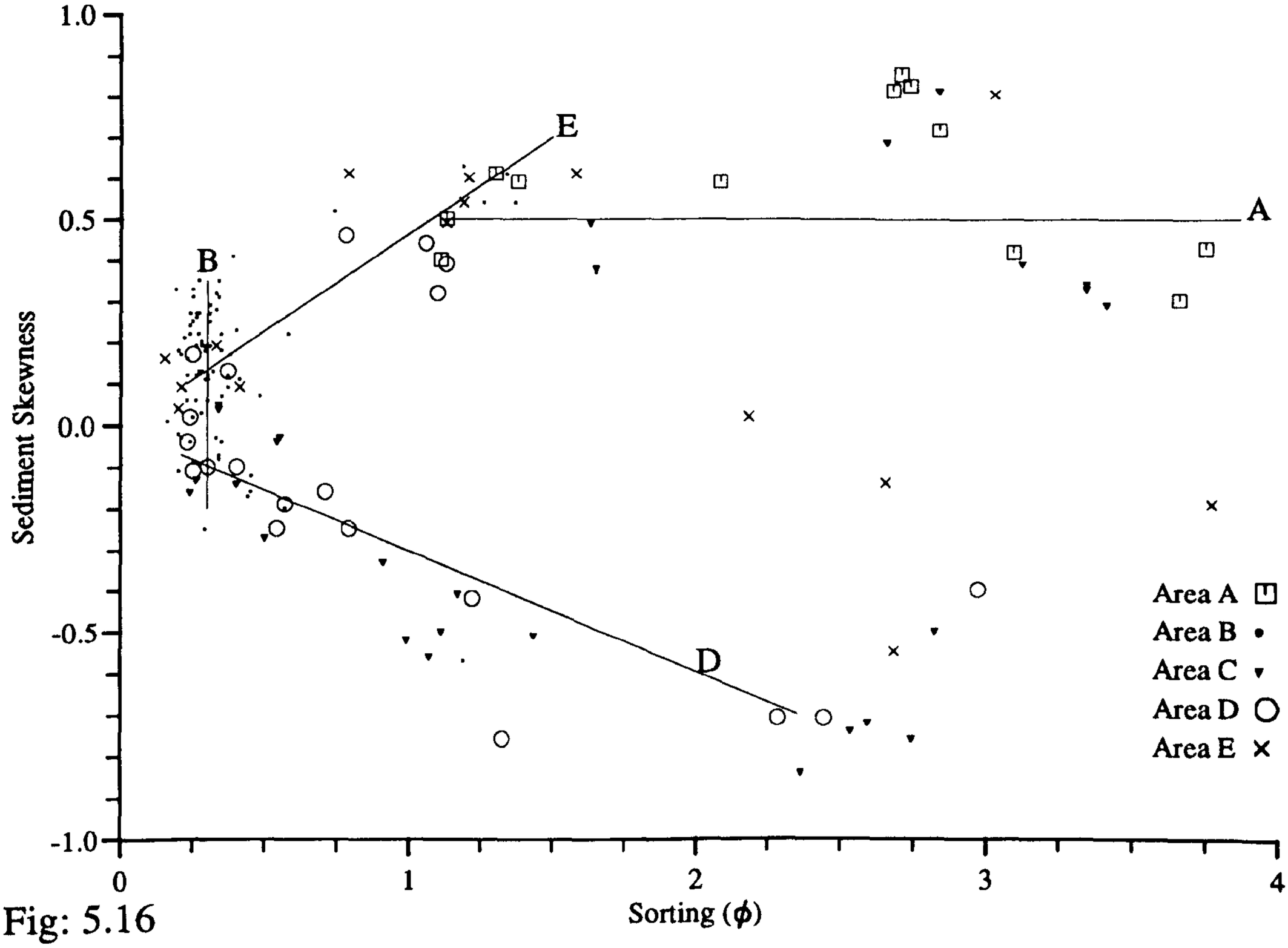

Fig: 5.16

Scattergrams of Sorting and Skewness of sediment samples in Areas A-E.

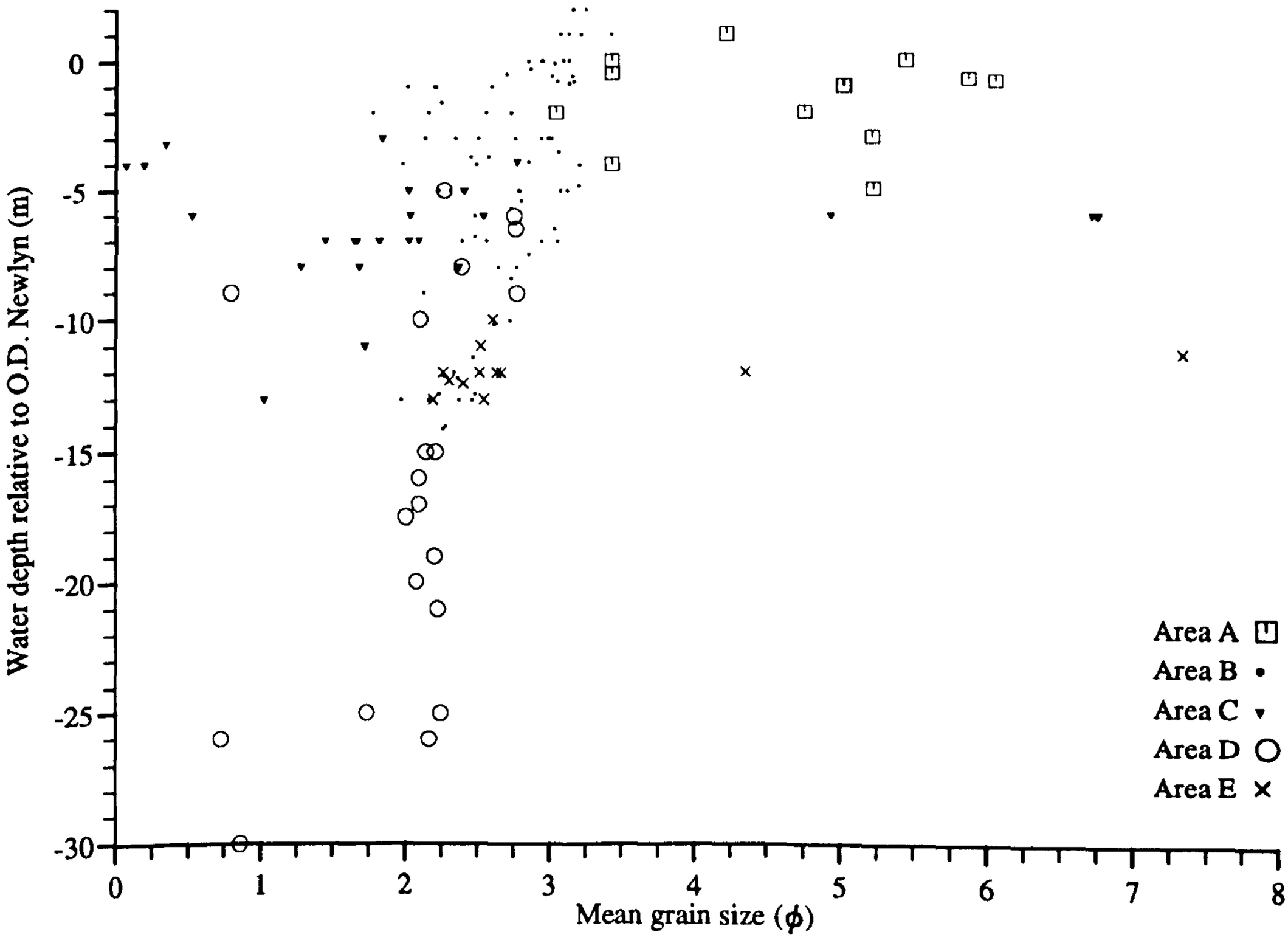

Fig: 5.17

Comparison between mean grain size and water depth of A-E subarea samples.

quite narrow range (~0.25Ø) in mean grain size.

5.8.3 Sediment Grain Size Distribution

The study of sediment grain-size distributions is commonly used to investigate the mechanisms of sediment transport and deposition, and to determine aspects of hydrodynamics conditions associated with deposition [Visher, 1969; Middleton, 1976; Taira & Scholle, 1979a, 1979b; and Viard & Breyer, 1979].

The graphical presentation of grain size data is very important for the interpretation of sedimentary environments form grain size characteristics. In the present work, the grain size distribution is presented in the form of bar graphs and frequency curves, and as cumulative weight percentage frequency curves on arithmetic and probability scales.

5.8.3.1 Histograms

This is the simplest type of graph for the presentation of grain size data in graphical form. Grain size and weight percentage are the independent and dependent variables, respectively, and therefore are used as horizontal axis and vertical axis, respectively. Other than the pictorial importance of the histograms [e.g., Udden, 1898, 1914; Krumbein, 1938; McLaren, 1981; Mahamod, 1989; Forrest & Clark, 1989], data at a small quantitative interval can be read from them and are easy to understand.

Grain size histograms of some samples are shown in Fig. 5.18 at an interval of 0.5Ø. Among statistical parameters, histograms are good indicators of the mode especially in unimodal sediments. In the Menai Strait channel, the modal size is 2.0Ø. The general trend in increasing modal values is from the NE to the SW in the area. For example, the modal size of samples 14, 20, 22, 232 & 34 is 2.5Ø whereas the samples to the SW on Lavan Sands (nos. 55, 62, 160) have a modal size of 3.0Ø. Further to the SW near Bangor Pier (samples 116, 121), this size is 3.5Ø.

5.8.3.2 Weight Percentage Frequency Curves

The weight frequency curve of a normally distributed sample on an arithmetic scale is symmetrical and bell shaped. However natural sediments rarely follow this pattern and deviations from the standard shape provides clues for interpretation of depositional environment. In these graphs, a much smaller class interval can be used than with the histograms. The frequency curves are much clearer in showing pictorial values of statistical parameters such as sorting, skewness and kurtosis. This type of presentation is very useful for polymodal sediments.

From Fig. 5.19 it clear that almost all the samples in the area are essentially unimodal. Only samples 1 and 2 in *Area E* show more than one mode. The weight frequency plots show that the curves of samples in *Area A* are comparatively less peaked, show large dispersion and major portions of the curve lies around higher phi values of the grain size. In

Fig: 5.18 Histograms showing sediment grain size distribution in Conwy Bay & NE Menai Strait.

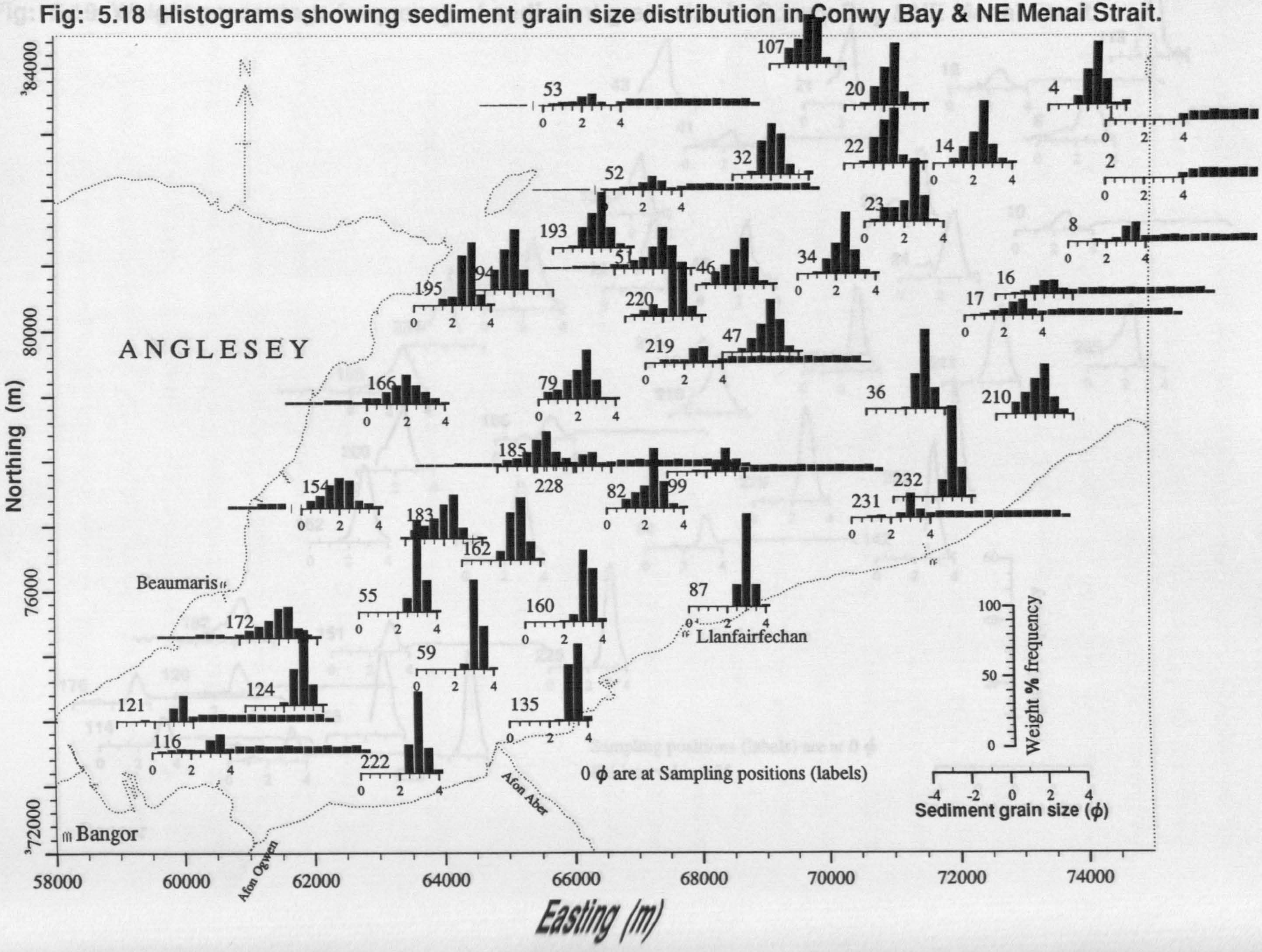

Fig: 5.19 Weight percentage frequency of sediment grain size in Conwy Bay &NE Menai Strait.

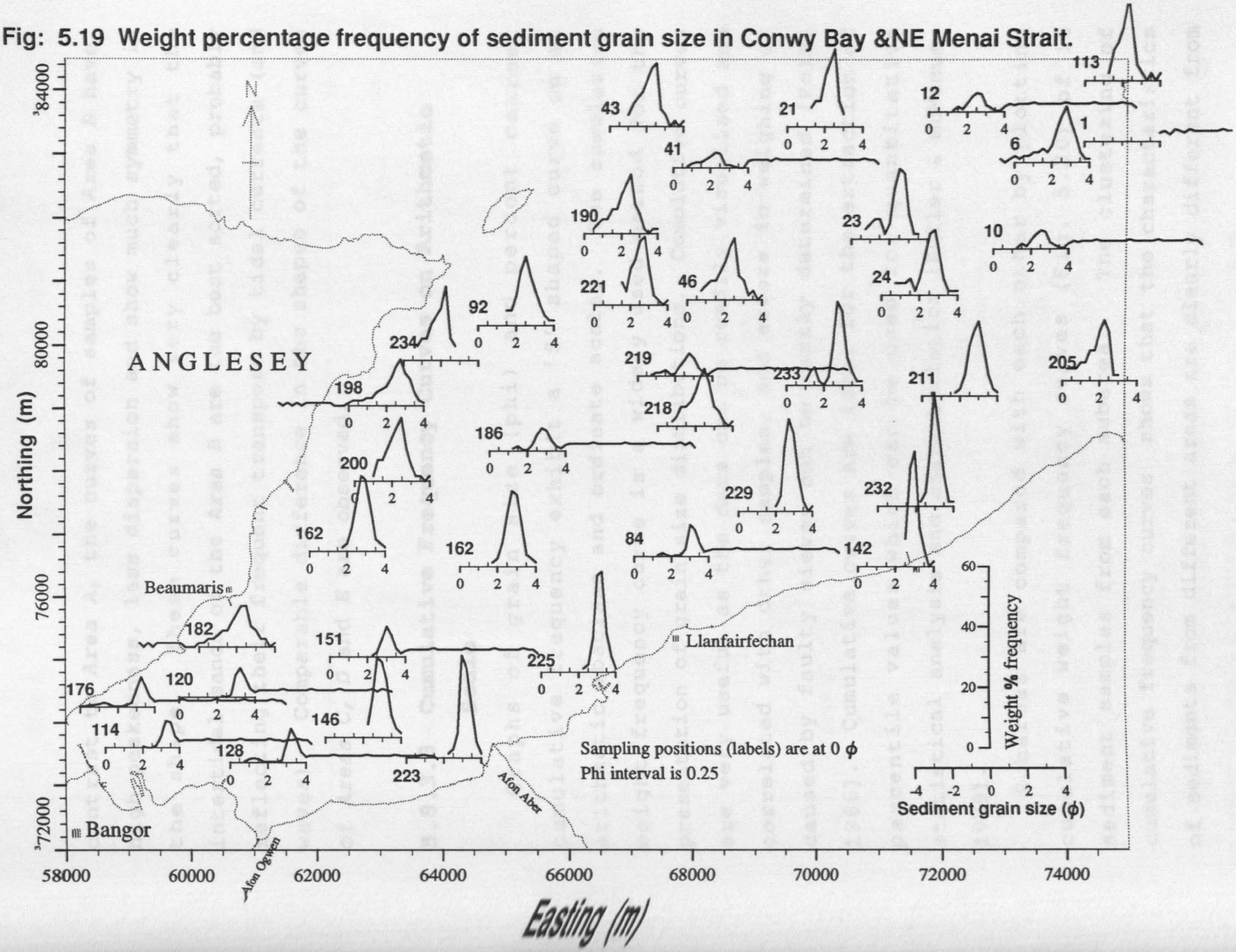

contrast to *Area A*, the curves of samples of *Area B* have, high peakedness, less dispersion and show much symmetry in the shape. These curves show very clearly that the intertidal sands of the *Area B* are the best sorted, probably reflecting their frequent transport by tidal currents (and waves). Comparable difference in the shapes of the curves of *Areas C, D* and *E* are observed.

5.8.3.3 Cumulative Frequency Curves on Arithmetic Scale

Graphs of grain size (phi) and percent coarser cumulative frequency exhibit a 'S' shaped curve on an arithmetic abscissa and ordinate scales. The cumulative weight frequency curve is a widely used method for the presentation of grain size distributions. Cumulative curves are very useful as the data can be readily visualised and correlated with other samples, and errors in weighing or caused by faulty sieves can be easily determined [Folk, 1966]. Cumulative curves are ideal for the extraction of percentile values which can be used for quantitative statistical analysis and characteristics [Buller & McManus, 1979].

Subareas are compared with each other by plotting cumulative weight frequency curves (Fig. 5.20) of 10 sediment samples from each subarea. The clustering of cumulative frequency curves shows that the characteristics of sediments from different areas are clearly different from

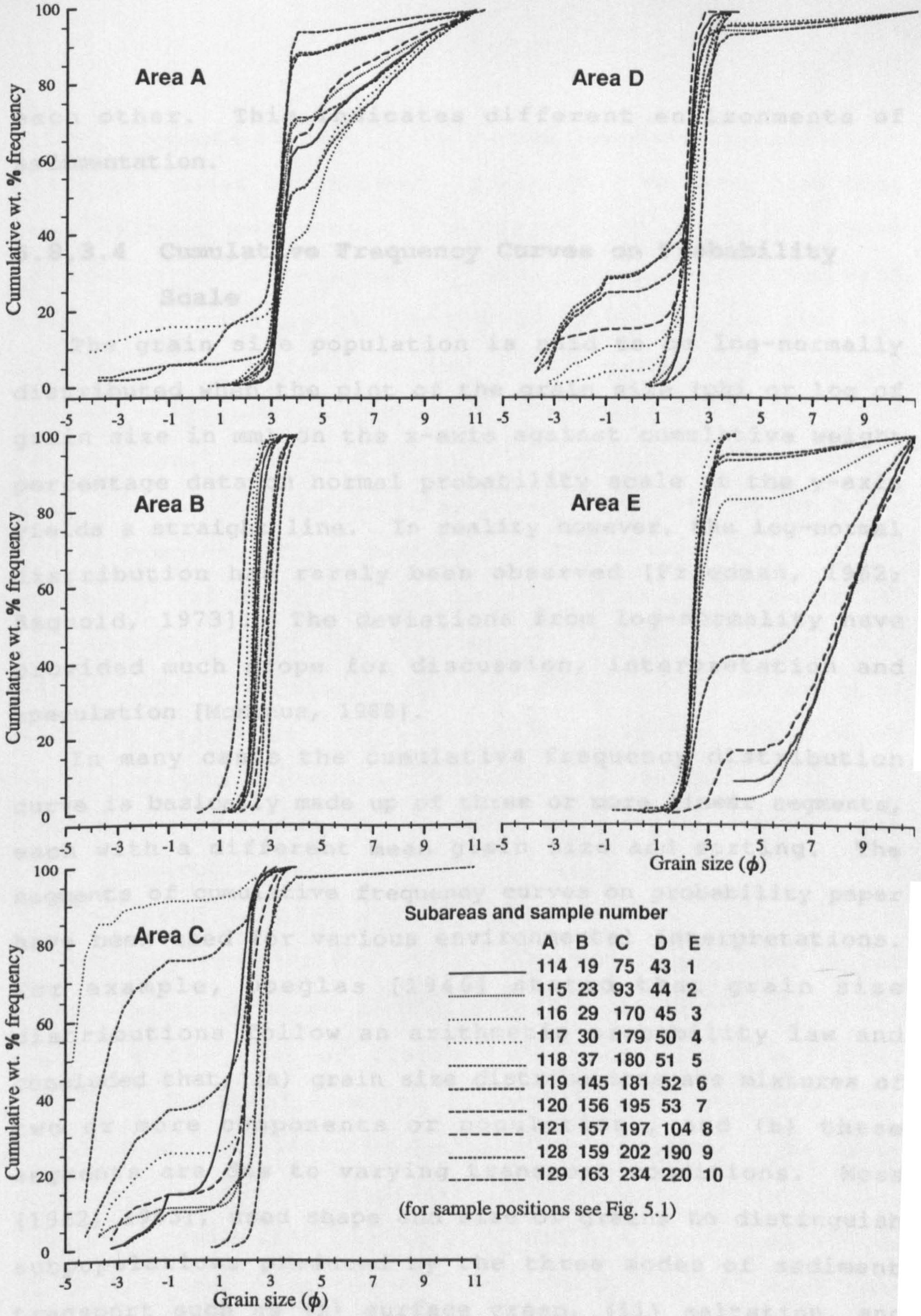

Fig: 5.20 Cumulative weight percentage frequency distribution curves on arithmetic scale of sediment samples from A-E areas.

each other. This indicates different environments of sedimentation.

5.8.3.4 Cumulative Frequency Curves on Probability Scale

The grain size population is said to be log-normally distributed when the plot of the grain size (phi or log of grain size in mm) on the x-axis against cumulative weight percentage data on normal probability scale on the y-axis yields a straight line. In reality however, the log-normal distribution has rarely been observed [Friedman, 1962; Bagnold, 1973]. The deviations from log-normality have provided much scope for discussion, interpretation and speculation [McManus, 1988].

In many cases the cumulative frequency distribution curve is basically made up of three or more linear segments, each with a different mean grain size and sorting. The segments of cumulative frequency curves on probability paper have been used for various environmental interpretations. For example, Doeglas [1946] stated that grain size distributions follow an arithmetic probability law and concluded that, (a) grain size distributions are mixtures of two or more components or populations, and (b) these segments are due to varying transport conditions. Moss [1962, 1963], used shape and size of grains to distinguish subpopulations produced by the three modes of sediment transport such as (i) surface creep, (ii) saltation, and (iii) suspension. Visher [1969] related the shapes of

linear segments of cumulative curves (probability scale) to different modes of sediment transport. He concluded that each segment represents a separate subpopulation whose character is determined by the dynamics of sediment transport such as rolling & sliding, saltation and suspension. Glaister & Nelson [1974] related the segmented shapes of probability plots to various environments of depositions. Sagoe & Visher [1977] explained the presence of inflection points (breaks, irregularities) between the linear segments on log probability grain size distribution plots as; (a) mixing of two or more overlapping lognormal populations, and (b) mixing of truncated lognormal populations corresponding to the subpopulations of modes of sediment transport. They concluded that the presence of three transport populations preserved in deposits permits a correlation of environmental and genetic criteria with grain size distributions.

Thirteen samples from 5 subareas are plotted on a probability scale in Fig. 5.21. The linear segments of the plots are considered as representing modes of transport based on the work of Visher [1969] and Sagoe & Visher [1977]. Sediment samples from different subareas show significant variations in dynamics of transport. The grain size populations of *Area A* are divided into two segments. One from grain size 1.5 to 3.5Ø and a second from 4.0 to 10.5Ø for both presented samples. These segments show that 60% of the size population is transported as intermittent

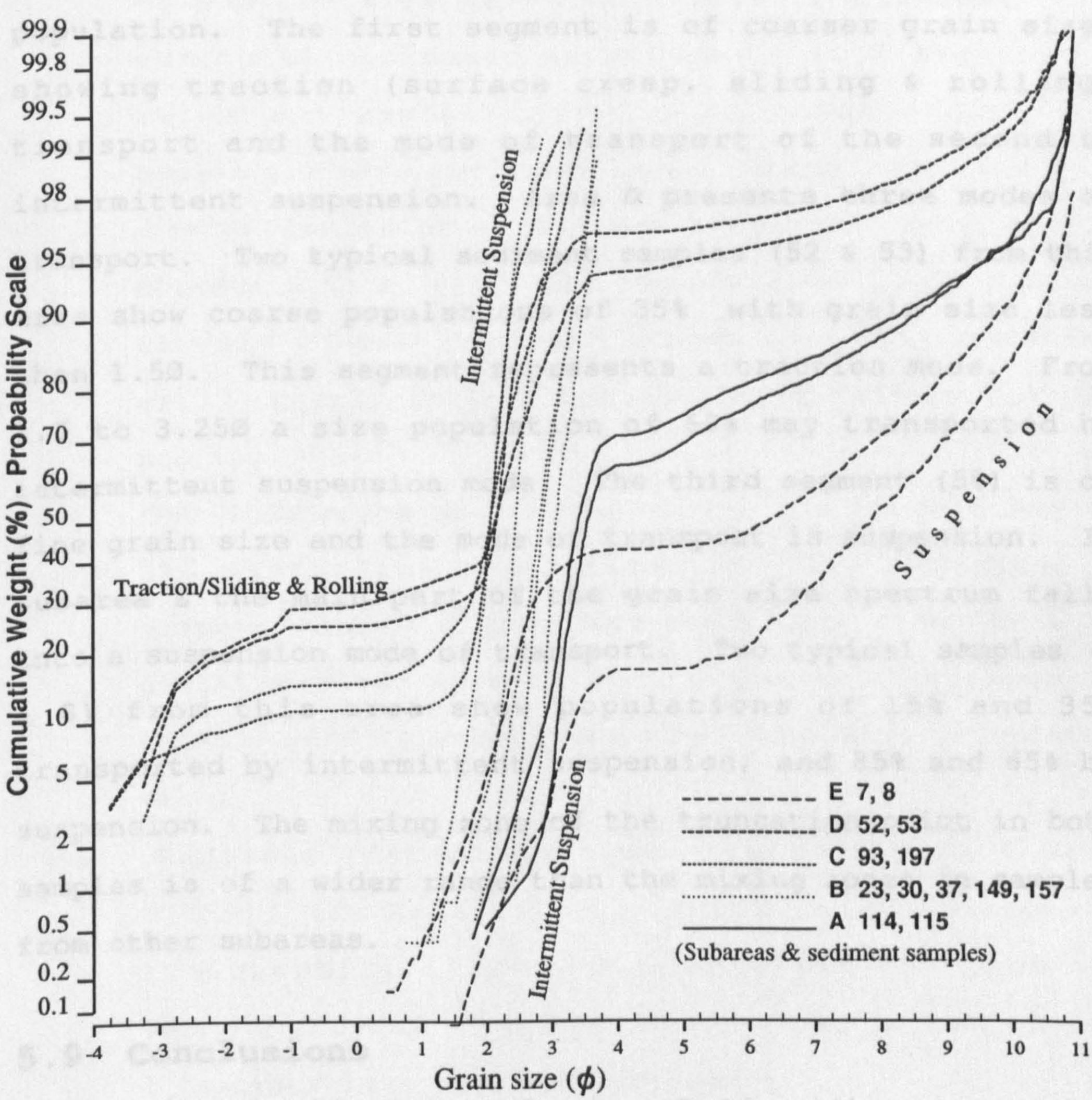

Fig: 5.21

The sub-populations in grain size distributions of typical surficial sediment samples indicating the modes of sediment transport in A-E subareas.

suspension (saltation) mode and 40% as suspension. The grain size distributions of the samples of *Area B* exhibit only one segment which show that the sediment transport mode in this area is predominantly intermittent suspension. In *Area C* two segments comprise 20% and 80% of the grain size population. The first segment is of coarser grain size, showing traction (surface creep, sliding & rolling) transport and the mode of transport of the second is intermittent suspension. *Area D* presents three modes of transport. Two typical sediment samples (52 & 53) from this area show coarse populations of 35% with grain size less than 1.5Ø. This segment represents a traction mode. From 1.5 to 3.25Ø a size population of 60% may transported by intermittent suspension mode. The third segment (5%) is of fine grain size and the mode of transport is suspension. In subarea E the main part of the grain size spectrum falls into a suspension mode of transport. Two typical samples (7 & 8) from this area show populations of 15% and 35% transported by intermittent suspension, and 85% and 65% by suspension. The mixing zone of the truncation point in both samples is of a wider range than the mixing zones in samples from other subareas.

5.9 Conclusions

(1) The replicate analysis of 46 sediment samples confirms the high accuracy of the UCNW fall tower for sand size analysis. The calculated errors for average values of mean grain size, sorting, skewness

and kurtosis are ±0.022, ±0.023, ±0.063 and ±0.124Ø, respectively.

(2) On the basis of surficial sediment types, the study area is divided into 5 subareas. The classification of sediments is based on a ternary diagram. The surficial sediments in subarea A to E are; muddy sands and sandy muds; sands; sands - gravels; gravelly sands; and muddy sands - muds, respectively.

(3) The sediments of *Area A* are poorly and very poorly sorted; *Area B*, very well sorted; *Area C*, all classes of Folk & Ward's sorting scale; *Area D*, moderately well - poorly sorted; and in *Area E*, poorly to very poorly.

(4) The 5 subareas show clear variations in skewness of the grain size distributions. The majority of samples of *Area A* show very positively skew; *Area B*, positive skew; *Area C*, very negative skew; *Area D*, negative and very negative skew; *Area E* very positive skew.

(5) Kurtosis according to the scale of Folk & Ward [1957]: In *Area A* it is leptokurtic - extremely leptokurtic; *Area B*, leptokurtic; *Area C*, leptokurtic and very leptokurtic; and in *Areas D* and *E* leptokurtic - extremely leptokurtic.

(6) The percentage of loss-on-ignition at 550°C and 1000°C show different percentages in *Areas A-E*, confirming the presence of different depositional

subenvironments.

(7) Bivariate scattergrams analysis of (a) mean grain size and sorting, (b) mean grain size and skewness, (c) sorting and skewness and (d) mean grain size and water depth show different fields/groups i.e., indicating different subenvironments in the area.

(8) A comparison of grain size frequencies of sediments as histograms and frequency curves exhibit variations between subareas.

(9) Cumulative weight frequency distributions of 10 samples each from the 5 subareas indicate different hydraulic and sedimentary environments in the area.

(10) Interpretation of lognormal cumulative frequency curves based on the work of Visher [1969] and Sagoe & Visher [1977] indicate that different subarea are characterised by different modes of transport. The transport mode in *Area A* is intermittent suspension (60% of the grain size population) and suspension (40%); in *Area B*, most of the grain size population indicates intermittent suspension transport; in *Area C*, traction (20%) and intermittent suspension (80%); in *Area D*, 35%, 60% and 5% of the population show traction, intermittent suspension and suspension modes of transport, respectively; and in *Area E*, 30% of the grain size distribution shows intermittent suspension transport and the rest suspension.

(11) Grain size characteristics, and deduced transport characteristics, of subareas are:

Area D: sediment source, so partly coarse grained, poorly sorting, negative skewness.

Area B: active zone of transport by tidal currents (and waves), fine sand, so well sorted, nearly symmetrical, also variable skewness.

Area A: Temporary sediment sink, so increasingly fine grained, positive skewness, poor sorting.

Area E: Also mostly fine grained; grain size characteristics are close to the characteristics of *Area A*.

Area C: No clear transport trend, variable grain size textural parameters mainly because of the influence of the main channel and the variable Anglesey coastline orientation.

(12) The modal grain size and mean grain size gradients, sorting, skewness and kurtosis characteristics show that sediments are transported from the open sea to the south western parts of the area.

CHAPTER SIX

SEDIMENT TRANSPORT

6.1 Introduction

The mode of sediment transport in coastal areas can be bedload or suspended load, depending upon flow strength and bed roughness. In bedload transport the grains bounce or roll along the bed continuously or intermittently. It is limited to a relatively thin zone immediately above the seabed. Bedload can occur in laminar as well as turbulent fluids [Bagnold, 1955, 1968]. Einstein [1950] suggested that the bedload is two grain diameters thick but most other researchers prefer a somewhat greater thickness. The movement of sediment in bedload is at a slower velocity than the fluid velocity. Suspended load moves approximately with the mean velocity of the current. In suspension, grains move higher up above the bed. Fine material (silts and clays), having low settling velocities, can be mixed high into the water column by turbulence within the flow field and significant transport of such material can occur well away from the bed. For coarser material such as sands, the height of resuspension is less and transport is restricted to the region close to the bed [Vincent, Young & Swift 1982]. The excess weight of the suspended grain is supported wholly by a random succession of upward impulses imparted by the vertical component of turbulence [Bagnold, 1973, 1977].

The sediment transport rate can be measured by means of

sediment traps, radioactive tracers, acoustic techniques, quantification of bedform migration rate and by studying the physical relationship of flow strength and grain size [Ritter, 1972; Finley, 1978; Langhorne, 1981; Heathershaw, 1981; Lees, 1983; Pickrill, 1986; Heathershaw & Thorne, 1985; Thorne, Williams & Heathershaw, 1989].

A sediment trap is a rectangular orifice with several perforated containers mounted on a sledge frame. Errors arise because of local fluid/bed disturbances, uncertainty in the relative levels of orifice and bed, and the likehood of dredging during the course of recovery. Several types of suspended sediment samplers collect suspended sediment in a container by natural settlement. The most effective method is pumping and filtering of water samples. Simultaneous measurements of current velocities are required to interpret the sediment flux. Pickrill [1986], using the sediment-trapping procedure in Rangan-nu Harbour (New Zealand), identified sediment paths, calculated sediment budget and compared measured and predicted sediment transport rates.

Radioactive tracer techniques can be used to predict bedload transport, [Smith & Parsons, 1965; Heathershaw & Hammond, 1979; Heathershaw, 1981]. In this method the radioactive tracer (normally 46Sc, half-life 84 days) is placed on the seabed at known localities. The movement and distribution of the tracer can be surveyed at intervals by means of a Geiger counter. Heathershaw & Carr [1977] used this technique to determine the movement of sand size material in Swansea Bay, and calculated the net sediment

transport rate (q) by $q=p_{sb}$ VE where p_{sb} is the bulk density of sediment, V is sediment drift rate and E is depth of burial. Lees [1981, 1983] estimated bedload transport on the Dunwich Banks, coast of East Anglia, using fluorescent tracers.

During a tidal cycle, the difference in the total range of movement between suspended load and bedload transport may make it difficult to calculate the total transport rate. Suspended load will tend to become widely dispersed while the bedload remains relatively concentrated, with resulting difficulties in designing a scheme for detection of tracers.

Attempts have been made to measure sediment transport by acoustic techniques which measure interparticle collision noise (sediment generated nose, SGN). Bedeus & Ivicsis [1963], Tywonivk & Warnock [1973], and Jonys [1976] applied SGN to monitor bedload transport. Heathershaw & Thorne [1985] used the SGN technique to monitor marine gravel transport and examined the role of turbulence in sediment mobility. Thorne [1986a, b] improved this method by conducting a series of laboratory experiments. Soulsby, Atkins & Salkield [1987] studied the effects of turbulence on the concentration of suspended sand. An acoustic field measurement system was developed to monitor gravel by measuring the SGN root mean square pressure level [Thorne, Williams & Heathershaw, 1989].

In intertidal areas, where large bedforms are present, sediment transport can be estimated by surveying at regular

intervals along the line of bedform movement [Ludwick, 1972; Kelland & Bailey, 1975; McCave & Langhorne, 1982; Langhorne, 1982]. The horizontal migration can be calculated by measuring crest to trough distance throughout a specific period. The measurement can also be done between brink and toe positions of each bedform from one tide to the next. Detailed surveys can easily be carried out during low tide. Such a survey requires a high precision of measurement.

From the physical relationship of sediments and flow strength, a range of equations is available to calculate bedload and suspended load transports [Stelczer, 1981]. In recent years, there has been remarkable progress in the study of boundary layers and sediment transport which provides a good base for transport estimations [Nowell, 1983]. Sleath [1984] suggests that one or more transport rate formulae, which have been used in similar areas and which give good results, should be selected. Most of the formulae in fact are based on empirical relationships between the rate of sediment transport and flow characteristics of the fluid such as mean velocity or bed shear stress.

In the present study, the transport of sediments will be estimated from the physical relationships of sediment grain size and current flow data. For this purpose 235 sediment samples were grabbed; the grain size parameters of those samples are discussed in Chapter 5. The current data were obtained from 12 positions (Fig. 4.1) in the area. Current velocity and direction measured at 1m above the seabed over

tidal cycles will be used to calculate sediment transport rates at those stations.

6.2 Sediment Transport Equations

Several well known equations for the calculation of bedload transport rate are available [Graf, 1971]. According to Stelczer [1981] anyone faced with the problem of estimating bedload transport rate encounters a large choice of theoretical and empirical approaches. Among the most commonly used bedload transport equations, some include a threshold condition below which no sediment transport take place. Examples are Yalin [1963], Sternberg [1972], Gadd, Lavelle & Swift [1978], White [1979], Langhorne [1981], Hardisty [1983], and Mahamod [1989]. On the other hand, Schmidt's [1925] suspension equation, popularly known as the Rouse equation [Rouse, 1938], Einstein's [1950] bedload equation, Ghastlier's [1965] bedload formula, Bagnold's [1956, 1963, 1966] bedload equations, Engelund & Hansen's [1967] total load equation, Ackers & White's [1973] total load formula, van Rijn's [1986] bedload expression, have no critical velocity conditions.

The most commonly used bedload and total load transport formulae are those of Einstein [1950], Bagnold [1956, 1963, 1966], Yalin [1963], Engelund & Hansen [1966, 1967], Ackers & White [1973], Gadd, Lavelle & Swift [1978] and Hardisty [1983]. Some of those equations are discussed after the following section.

6.2.1 Physical Parameters used in Sediment Transport Equations

When the shear stress due to fluid velocity at the sea bed exceeds a critical or threshold value, the sediments begin to move along the bed, and as the magnitude of the shear stress increases it may force the bed material to move in the form of traction and then suspension. The circumstances necessary to initiate sediment motion are a function of the characteristics of the sediment (size, shape, density, packing, sorting, etc.), the fluid (density and viscosity), and the fluid average velocity [Miller, McCave & Komar, 1977]. The sediment grain can be entrained either directly by the water or by being struck by another moving grain.

The threshold or critical flow stress is dependent on the relative density of the grains and their diameter. Several workers [e.g., Gilbert, 1914; Hjulstrom, 1935, 1955; Shields, 1936; Bagnold, 1963; and Postma, 1967] suggested competency curves which define the threshold of grain motion for various values of stream power and grain size. All of them believed that the shear stress on the bed is the most important parameter in initiating grain motion and in sustaining the movement of coarse material along the bed and of suspended material in the flow. As regards bed load, deposition occurs as soon as the flow causes the shear stress at the bed to fall below the critical value because friction at the bed and the viscosity of the water combine

to overcome any inertia that the grains might have. For suspension, grains require greater critical shear stresses to transport grains above 200 micron diameter in suspension than to support them in the bedload. Finer grains lift directly into suspension when the value of the critical stress is reached. The threshold stress seems to be linearly proportional to the grain diameter for coarse size particles.

Sediment entrainment conditions are commonly estimated using empirical correlations based on laboratory experiments. Krenter [1921] suggested that the critical force required to initiate sediment movement is approximately 20% greater than that which is required to maintain transport.

A major breakthrough in the threshold determination was provided by the Shields [1936] diagrams. Based on physical arguments, it may be expected that the beginning of a grain's motion is dependent upon the grain size, its specific weight, the bed shear stress, fluid viscosity and fluid density. The Shields diagrams are based on assumptions of non-cohesive sediment grains, steady and uniform flow, fully developed turbulent boundary layer, a flat bed and sediments of a single grade. It is very unlikely that natural sediments approach such a narrow grain size distribution, and generally beds are not flat. Furthermore, marine currents are not normally steady and uniform, although it does not appear that they are so

variable as to invalidate completely the general predictions that can be made from such curves.

The grain motion curves of Shields [1936], Inman [1949], Lane [1955], Sundborg [1956], and Yalin [1972] were re-examined by Miller, McCave & Komar [1977]. From these curves they selected laboratory flume data sets, in which the walls were parallel, conditions of uniform and steady flow, flattened bed and nearly uniform particle size of spherical or rounded shape. They modified those threshold curves which are now widely used for the calculation of threshold values.

The threshold velocity (U_{100t}) cm s^{-1} of grain motion employed in sediment transport equations to estimate the transport rate in the North Eastern Menai Strait and Conwy Bay is calculated by Eq. 6.1 from Miller, McCave & Komar [1977]. The conditions for this calculation are, p_s 2.65 g cm^{-3}, water flow at 20°C and d < 2.0 mm.

$$U_{100t} = 62.88\ d^{0.29} \qquad (6.1)$$

Commonly the theoretical entrainment formulae start from a consideration of the balance of forces on a sediment grain which is just at the limit of equilibrium. The forces on the grain include drag, gravity, lift forces and cohesion (interparticle forces) between the particles. The drag (fluid) forces tend to drag the grain from the bed, whereas gravity tends to pull it back. The lift force, however, varies in a complicated way with flow and bed conditions and

cannot be straightforwardly predicted. Einstein [1950] indicates the importance of the lift forces in the movement of sediments, and Helley [1969] and Inokuchi & Takayama [1973] explicitly include the lift force in their analysis of threshold conditions.

The value of the *drag coefficient* (C_{100}) in the marine environment varies by about an order of magnitude, between $5*10^{-4}$ and $5*10^{-3}$ e.g., Sternberg [1967, 1968], Channon & Hamilton [1971], McCave [1973], Harvey & Vincent [1977]. Sternberg [1976] reports a mean drag coefficient value of $3*10^{-3}$ for small scale roughness elements (< 20cm) and for hydrodynamically rough flow (U_{100} > 15 cm s^{-1}). A C_{100} value of $3*10^{-3}$ is frequently used in computations, e.g., Sternberg [1972, 1976], Jago [1981], Yang [1986a, b], Mahamod [1989].

The current velocity (U_{100}) cm s^{-1} at 100 cm above the bed (the standard height of current velocity measurement for sediment transport studies [Hardisty, 1983]), was recorded by an RCM4 and Braystoke current meters (Chapter 4).

From the recorded current velocity and assumed drag coefficient, shear velocity and shear stress are calculated to put into the sediment transport equations used in this study, as:

U_{100*} = shear velocity (cm s^{-1}) where U is measured 100 cm above the seabed.

$$= C_{100}^{0.5}\ U_{100} \qquad (6.2)$$

e.g., Sternberg [1972], Gadd, Lavelle & Swift [1978], Hardisty [1983].

τ = shear stress (dyne cm^{-1})

$= C_{100}\ p\ U_{100}^{2}$ (6.3)

e.g., Hardisty [1983], Thorne, Williams & Heathershaw [1989], Williams, Thorne & Heathershaw [1989].

The other used constants are:

g = gravitational acceleration (981 cm s^{-2})

p_s = sediment density (2.65 g cm^{-2})

p = water density (1.025 g cm^{-2})

6.2.2 Yalin's [1963] Bedload Equation

This equation is thought to be one of the simplest to apply [Gadd, Lavelle & Swift, 1978; Heathershaw, 1981]. The average lift force exerted on a sediment particle is concerned in this equation. Yalin assumed that the movement of particles over the bed is by saltation and that transport rate increases with the increase of particle path length. This equation is restricted to situations where the bed is plane, turbulent flow fully developed, and the ratio of flow-depth/particle-diameter is large.

Yalin estimated bedload transport rate (q) by:

$$q = 0.635\ p_s\ d_{50}\ u_*\ s\ [1 - (1/as)\,In\ (1 + as)] \quad (6.4)$$

where,

$$a = 2.45\ (p/p_s)^{0.4}\ \ [\tau_t/\{(p_s - p)\,g d_{50}\}]^{0.5} \quad (6.5)$$

s is dimensionless excess shear stress

Gadd, Lavelle & Swift [1978] found that near the

threshold velocity, the sediment transports calculated by (i) Yalin's equation for a grain size of 0.45 mm, and (ii) Guy, Simmons & Richardson's [1966] flume data for grain sizes of 0.19 mm and 0.45 mm, compare well with each other. But at higher flow velocities, the predicted values from Yalin are less than those estimated from Guy, Simmons & Richardson's flume experiment.

6.2.3 Bagnold's [1963] Bedload Equation

The bedload equation of Bagnold [1963] expresses the bedload transport rate in term of the stream power w and an efficiency factor K. The relation of q with w and K are given as:

$$q = [p_s/\{(p_s - p)g\}]\ wK \qquad (6.6)$$

$w = \tau\ u_*$ or $p\ u_*^3$ since $\tau = p\ u_*^2$

where K depends on sediment characteristics. Kachel & Sternberg [1971] showed that K not only depends on grain size but also on the excess shear stress.

Gadd, Lavelle & Swift [1978], by using the flume data of Guy, Simmons & Richardson [1966] modified the original Bagnold [1963] equation (Eq. 6.6) in terms of the near bed current (U_{100}) and a threshold velocity (U_t). They obtained the value of q as:

$$q = B(U_{100} - U_t)^3 \qquad (6.7)$$

where B is a coefficient of proportionality obtained from the flume data of Guy, Simmons & Richardson [1966].

6.2.4 Engelund & Hansen's [1967] Total Load Equation

Engelund & Hansen [1966, 1967] express the total load transport in terms of a dimensionless sediment discharge Ø, a friction factor C_f, and a non-dimensional bed shear stress, θ. The θ is commonly referred to as the Shields entrainment function.

$$Ø = \frac{0.1\ \theta^{2.5}}{C_f} \qquad (6.8)$$

where

$$C_f = 2\ \frac{U_*^2}{U^2} \qquad (6.9)$$

$$\theta = \frac{\tau}{(p_s - p)\ gd} \qquad (6.10)$$

$$\phi = \frac{q}{p_s}\left[\frac{P}{gd^3(p_s-p)}\right]^{0.5} \qquad (6.11)$$

By combining Equations 6.2, 6.3, 6.8 to 6.11, Eq. 6.12 is obtained:

$$q = \frac{0.05}{C_{100}}\left(\frac{\tau}{(p_s-p)gd}\right)^{2.5} p_s\sqrt{d^3 g\ \frac{p_s}{p}\ -1} \qquad (6.12)$$

Equation 6.12 is rearranged to Eq. 6.13 to calculate total sediment transport load (q)

$$q = 0.05 p_s U^2\left[\frac{\tau}{(p_s-p)gd}\right]^{1.5}\left[\frac{d}{g\left(\frac{p_s-p}{p}\right)}\right]^{0.5} \qquad (6.13)$$

U = time (15 minutes) average velocity at 100 cm

above seabed

d = sediment mean grain size (cm)

This equation is not applicable in plane beds. Other restrictions in applicability of this formula are the boundary Reynolds number > 12 ($R_e = U_* d/\nu$; where R_e is Reynolds number, ν kinematic viscosity of seawater i.e., ~0.013 $cm^2\ s^{-2}$), and grain size diameter > 0.15 mm. The positions at which transport rate has been calculated in this study, comprises a seafloor characterised by bedforms and a sediment mean grain diameter of more than 0.18mm (Chapter 5). The mean R_e values at all stations ranges from 15 to 45. Beside these above mentioned restrictions, Graf [1971] and the American Society of Civil Engineers [1975], recommended its general use in predicting sediment transport.

The above mentioned formula of Engelund & Hansen [1967] is widely found in literature concerning sediment transport and is used/quoted by various research workers. Some of them are Graf [1971], Raudkivi [1976], Heathershaw [1981], Collins, Amos & Evans [1981], Mahamod [1989], Williams, Thorne & Heathershaw [1989], Larcombe [1989], and Solangi [1992]. A misprint of some parameter/parameters in the same formula of some research workers is noticed. The most probable reason seems to be typographic errors. These misprinted equations are written with corrections in

Appendix-V to avoid further confusion.

6.2.5 Hardisty's [1983] Bedload Transport Equation

A number of changes have been introduced in the basic formula of Bagnold [1963, 1966] by, for example, Sternberg [1972], Gadd, Lavelle & Swift [1978], Langhorne [1981]. After a suggestion of Vincent, Young & Swift [1981], Hardisty's bedload equation is based on the formula of Bagnold [1963, 1966] expressing bedload in terms of stream power and an efficiency factor. A defect in Bagnold's original equation, however, is the omission of a threshold term so that sediment transport is possible at any non-zero flow state. Hardisty modified the original concept of Bagnold to include a threshold term in a parameter describing 'excess' bed stress and proposed this formula.

$$q = k\ (U_{100}^2 - U_{100t}^2) U_{100} \qquad (6.14)$$

Where k is an empirical constant and depends on grain diameter.

Hardisty calculated the calibration coefficient (k) from the regression analyses of flume transport data of Guy, Simmons & Richardson [1966] for 0.18mm, 0.27mm and 0.45mm mean sediment diameter and of Williams [1967] for 1.45mm mean sediment diameter. These calculated values of the k are given in Table 6.1 and Fig. 6.1.

Table: 6.1 Values of k (g cm^{-4} s^2) calculated by Hardisty [1983] for 4 sand sizes.

d_{mm}	Correlation Coefficient	Calibration coefficient
0.18	0.97	$0.68 * 10^{-5}$
0.27	0.96	$0.47 * 10^{-5}$
0.45	0.81	$0.21 * 10^{-5}$
1.45	0.96	$0.16 * 10^{-5}$

Hardisty then further regressed these computed values of k on to the appropriate sediment grain size and derived the following best fit equation.

$$k = \frac{1}{6.6\ d^{1.23}} * 10^{-5} \quad g\ cm^{-4}\ s^2 \quad (6.15)$$

d = sediment grain diameter (mm)

So the values of k can be picked from Table 6.1 for appropriate sediment grain sizes, or measured from the calibration diagram (Fig. 6.1), or from Eq. 6.15. The values of k measured from Fig. 6.1 and calculated from Eq. 6.15 for d=0.21mm and 0.18mm are:

	Station 1	Stations 2 & 3
k from Fig. 6.1	$0.6 * 10^{-5}$	$0.68 * 10^{-5}$
k by Eq. 6.15	$1.033 * 10^{-5}$	$1.249 * 10^{-5}$

The values of k calculated from Eq. 6.15 are much higher than the values of k measured from the calibration diagram. The bedload calculated from Eq. 6.14 by putting k values calculated from Eq. 6.15 is 172% at Station 1, and 183% at Stations 2 & 3, of the bedload calculated at the same stations by using k values calculated from the calibration diagram. The most probable reason for the higher values of k from Eq. 6.15 is that it is based on the regression of a limited number of grain sizes (only 4) [Hardisty, 1983] and in this way the values of k in Table 6.1 and Fig. 6.1 are more original and may be more accurate. So values of k used in Hardisty's [1983] bedload formula are measured from Fig. 6.1 and Table 6.1.

For the estimation of sediment transport rates in the NE Menai Strait - Conwy Bay area, the formulae of Engelund & Hansen [1967], and Hardisty [1983] were selected, as they are widely used in sedimentological studies.

As earlier mentioned, Engelund & Hansen 's total load equation does not contain a threshold velocity but Hardisty 's formula does account for it. For this purpose the threshold values calculated at Station 1 and at Stations 2 & 3 are 40 cm s^{-1} and 38 cm s^{-1} respectively. The sediment transport rate calculated for the flood and ebb periods from both formulae are compared cf. Williams, Thorne & Heathershaw [1989], Mahamod [1989]. To better present this comparison, a plot of transport rate at different velocities, by using the appropriate constants for Station 2, is presented in Fig. 6.2.

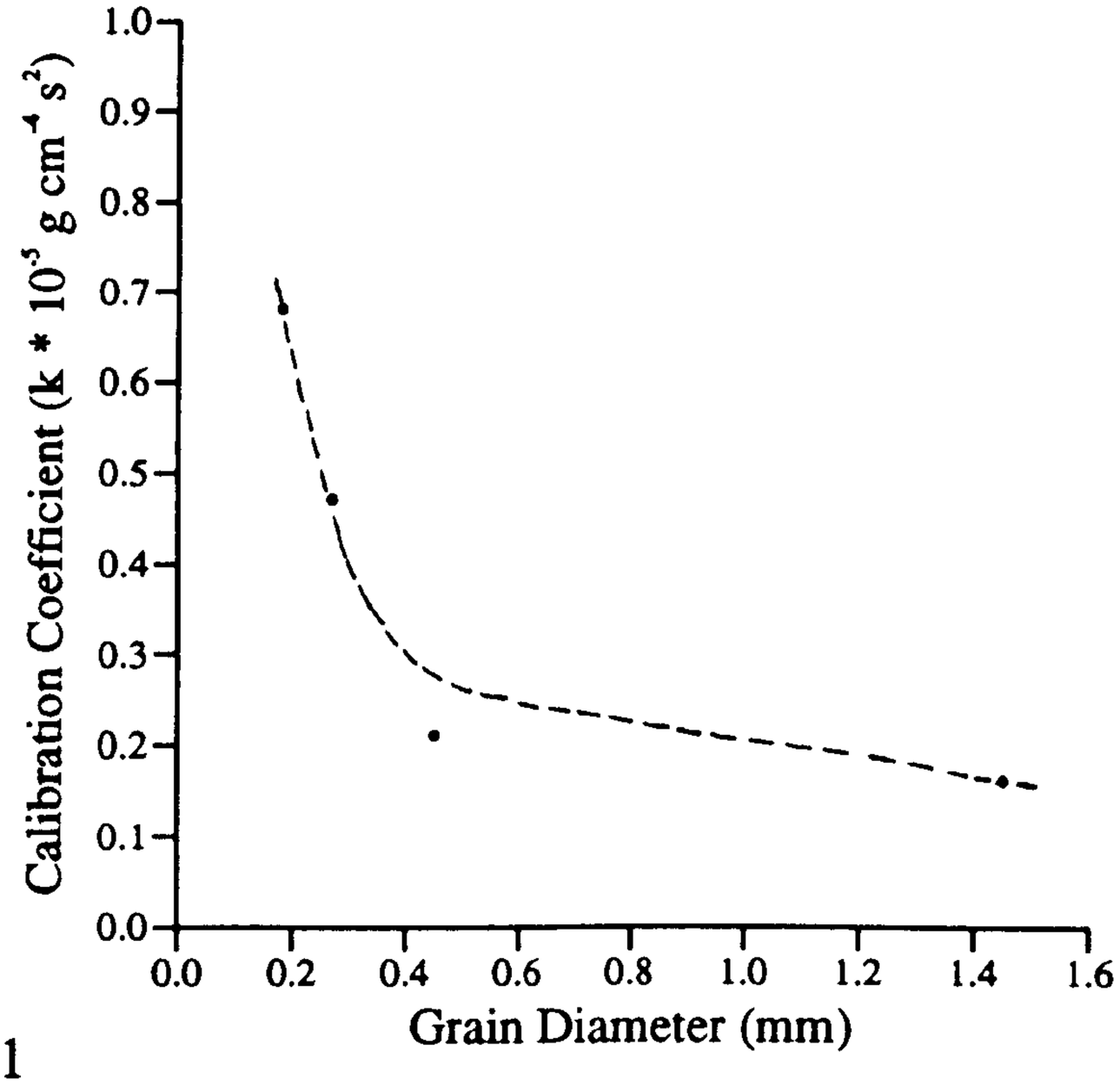

Fig: 6.1

Calibration diagram for k in Equation 6.14 (after Hardisty 1983).

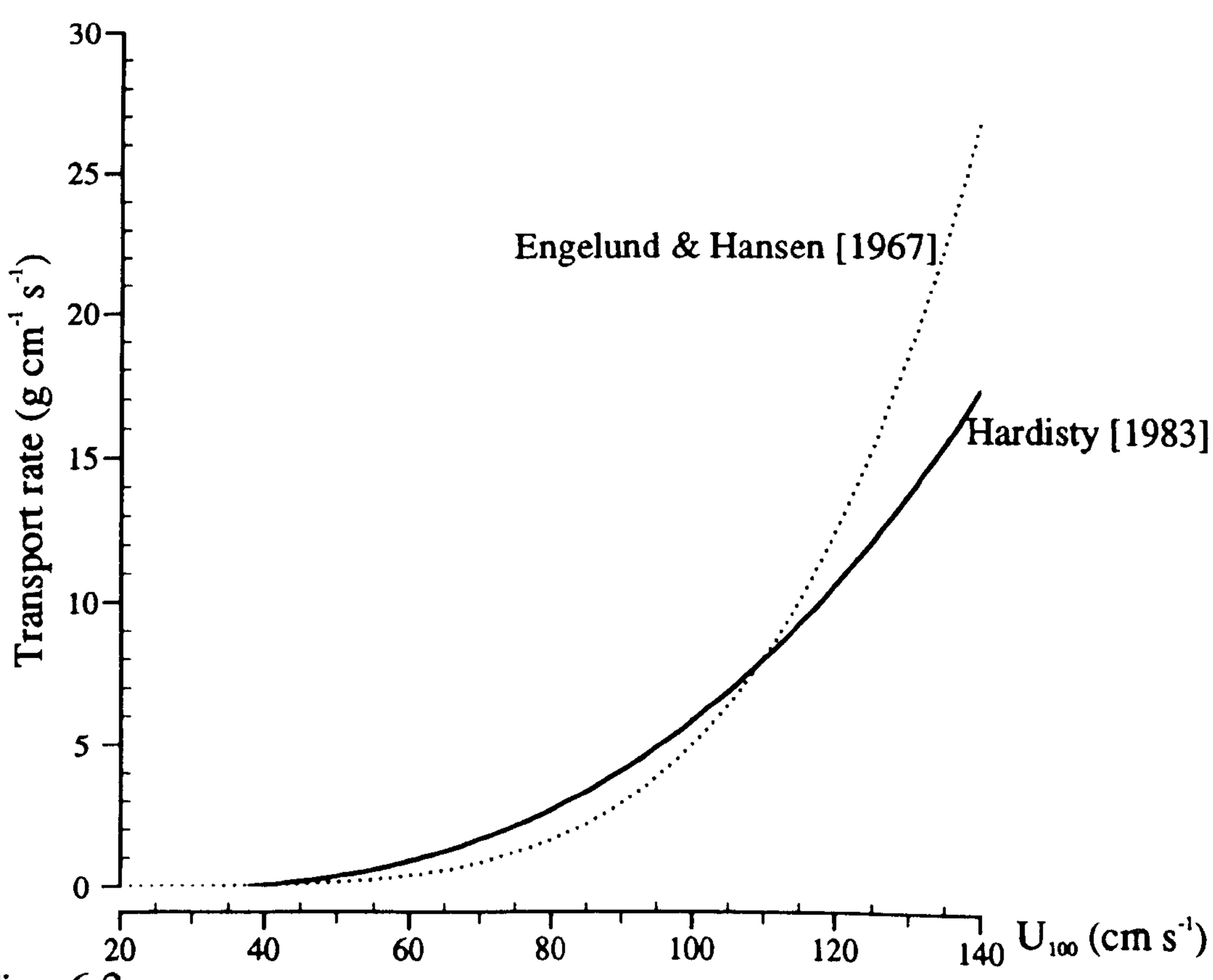

Fig: 6.2

Comparison of transport rates calculated by Hardisty's [1983] and Engelund & Hansen's [1967] formulae at different velocities using parameters of Station 2.

6.3 Sediment Transport Calculated in Study Area

Flow parameters used in the empirical transport formula were velocities at 15 minute intervals recorded by an Aanderaa RCM4 Savonius rotor current meter at Stations 1, 2 and 3. On Stations 5 and 6, Braystoke BFM008 MK3 current meter was used at 15 minute recording interval. Velocity data at Stations 7 to 9 were recorded with a Braystoke BFM008 MK1 current meter at 30 minute measuring intervals. The flow data of Stations 10 to 12 are taken at hourly intervals from the tidal prism given on the Decca Charts 1464, 1977 and 1978. Current velocities above the critical velocity were used in Hardisty's [1983] bed load transport equation for the calculation of bed load transport. The total transport for each flood and ebb cycle was obtained by integration of values of each interval over that portion of the cycle. The residual transport is the vector mean of north and south components of sediment transport.

Station 1

On 10 June 1990, an RCM4 current meter was deployed at Station 1 and currents were recorded for about 22 tidal cycles. The first recorded tide on this station with respect to a spring tide was a spring tide +1 (ST+1). The water depth on this location was 4m with respect to Ordnance Datum (Newlyn). The mean grain diameter was measured as 0.21 mm (2.25Ø) (see Chapter 5).

Details of currents at this station are shown in Chapter 4. As mentioned in Chapter 4, there is an abrupt drop in velocity during a period of the flood tide (see Fig. 4.4B). As a result, on the onset of flow, the transport rates starts increasing but in the early middle of the flood it abruptly decreases. During neap tides, this reduction in transport reaches a minimum almost equal to the transport minima at low and high water. At high water, the transport is at a minimum, then increases to a maximum in mid ebb, then again drops to a minimum at low water. At this station, since the ebb tide is dominant, the net transport rate is in the ebb direction. This is the only station where the net transport is observed in the ebb direction.

The visual expression of sediment movement at this station is shown in Fig. 6.3, Fig. 6.4 and Fig. 6.5. Computed rates of sediment transport at this location are given in Table 6.2. A mean net sediment transport of 5.22 kg cm^{-1} during a tidal cycle averaged over 22 tides has been estimated at this station.

The mean sediment transport of flood tides is greatest around springs and gradually decreases towards neaps. The same trend is observed in the ebb tide transport, but with a marked diurnal inequality.

On spring tides, the transport is dominated by the ebb but on neap tides (e.g., tide no 13), the transport is almost the same in flood and ebb directions. Sediment transports calculated at each interval (Fig. 6.3) using the total load transport equation of Engelund & Hansen [1967]

Fig: 6.3

Sediment transport at each recording interval (15 min.) calculated from Engelund & Hansen's [1967] total load equation.

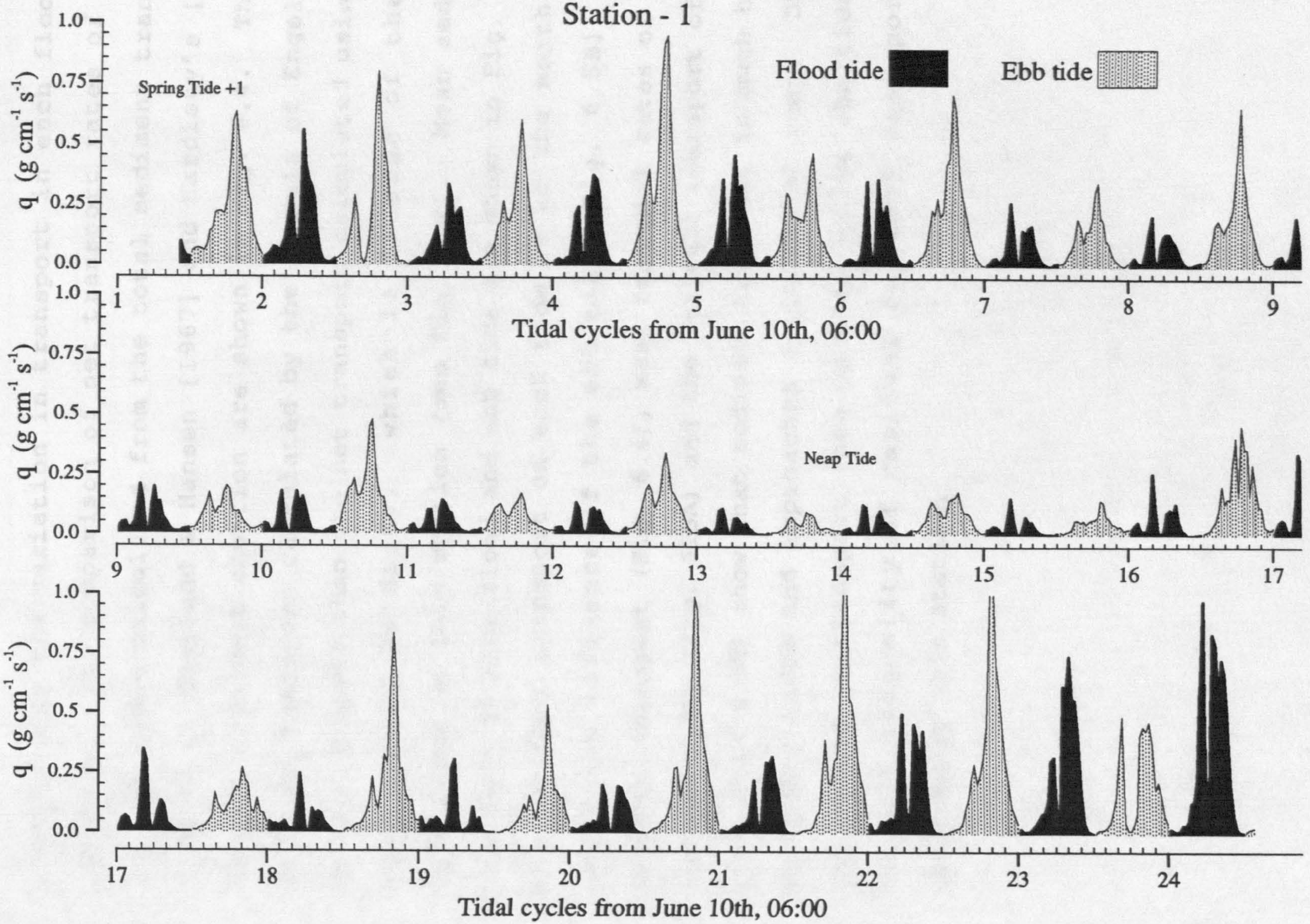

clearly show the variation in transport in each flood and ebb tide. The comparison of net transport rates of flood and ebb tides calculated from the total sediment transport formula of Engelund & Hansen [1967] and Hardisty's [1983] bedload transport equation are shown in Fig. 6.4. The net sediment transport calculated by the formula of Engelund & Hansen is lower than the net transport calculated using the equation of Hardisty, which is because of the low velocities at this station (see Fig. 6.2). Mean sediment transport in each flood and ebb tide are shown in Fig. 6.5A. The residual transport on each tide is to the north east under the influence of the ebb tide (Fig. 6.5B). Net sediment transport (Fig. 6.4), mean transport rates of flood and ebb tides (Fig. 6.5A) and the residual transport of each tide (Fig. 6.5B) show that sediment transport is much higher at spring tides and approaches a minimum at neap. Due to variations in transport rate on alternative ebb tides, a diurnal inequality of residual sediment transport is observed at this station.

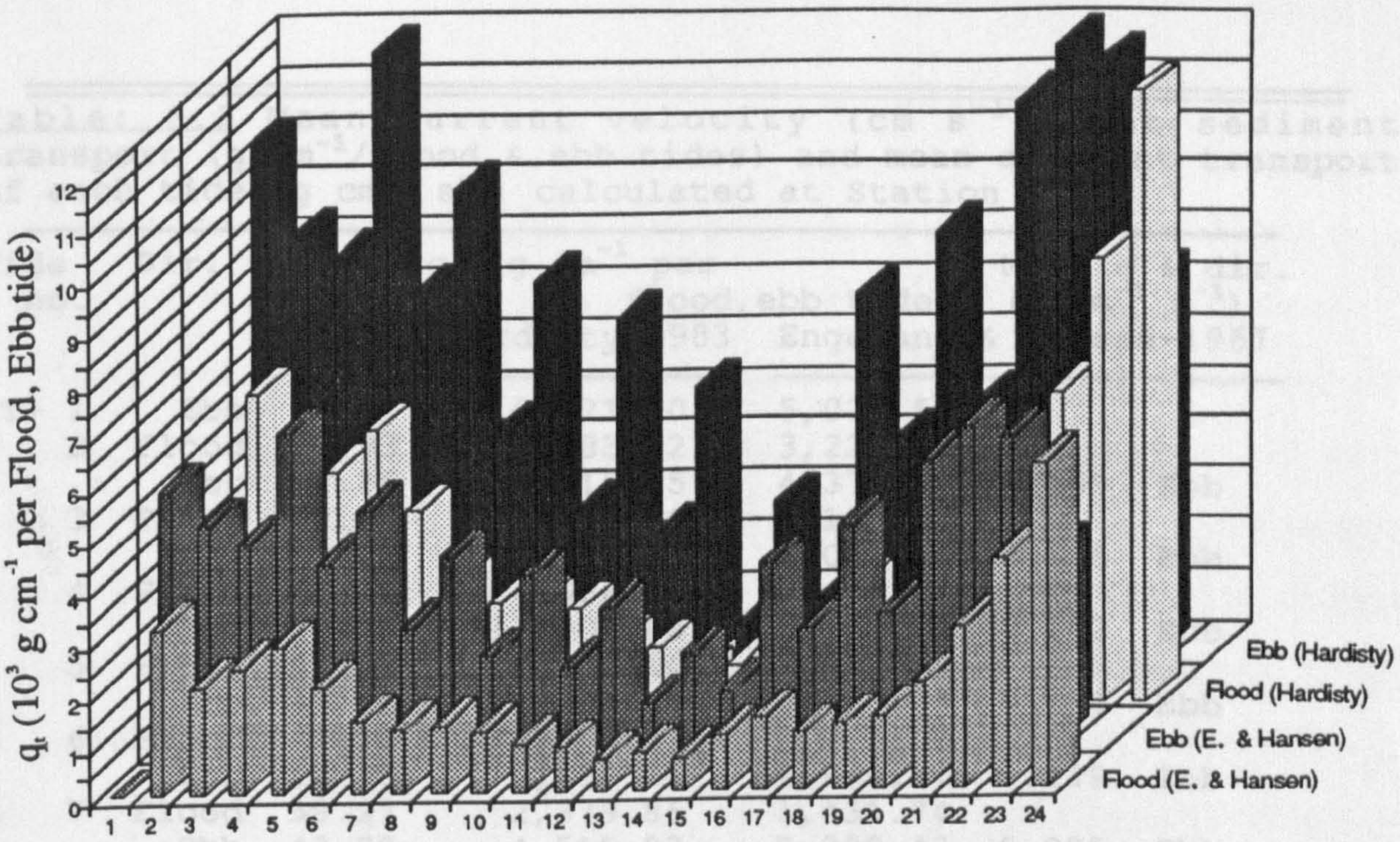

Fig: 6.4

Comparison of net sediment transport calculated by formulae of Engelund & Hansen [1967] and Hardisty [1983] of flood & ebb tides (Station 1).

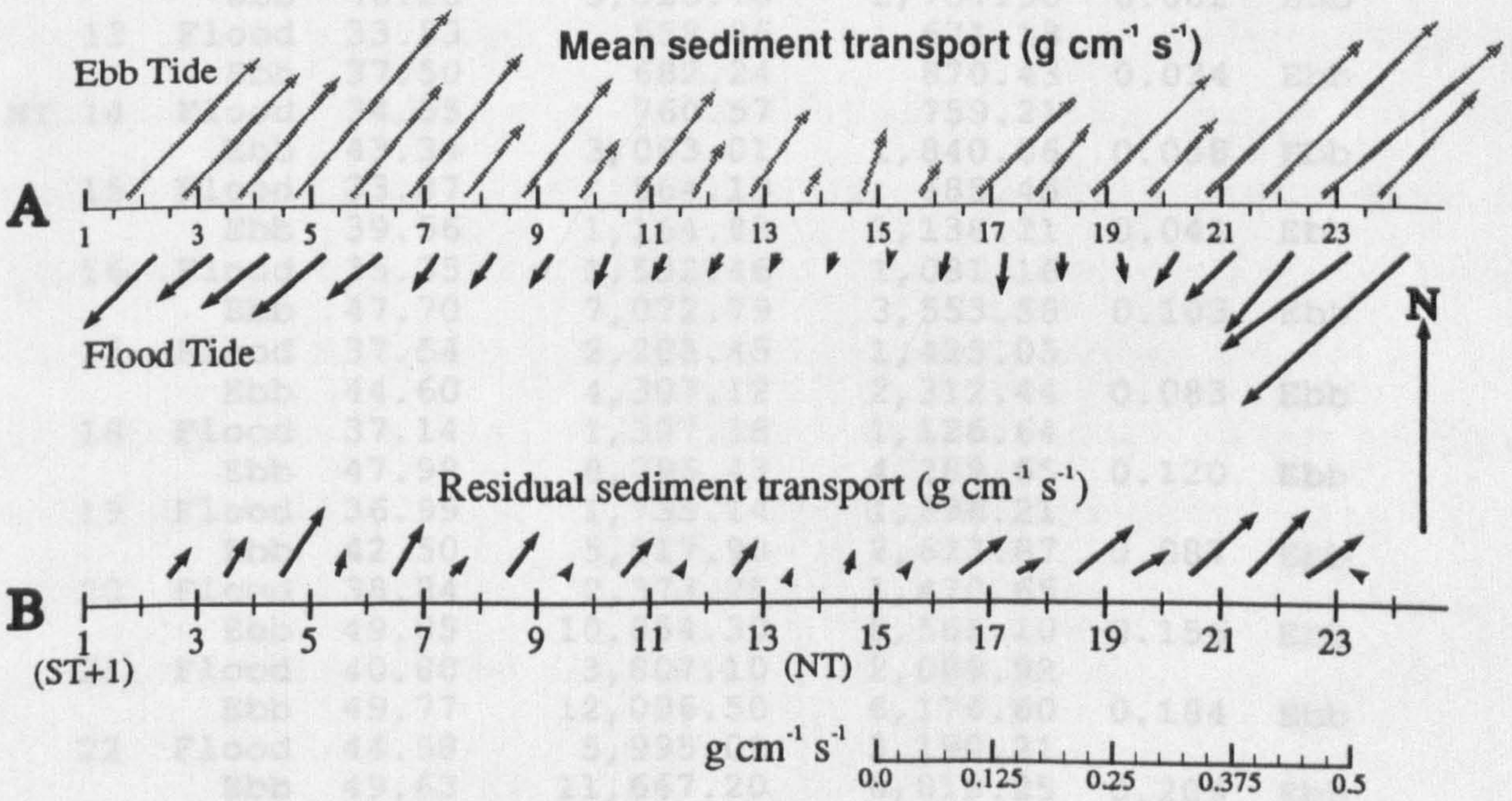

Fig: 6.5

Sediment transport vectors showing mean transport rate of flood & ebb tides (A) and residual transport of each tide (B), using Engelund & Hansen's [1967] equation (Station 1).

Table: 6.2 Mean current velocity (cm s^{-1}), net sediment transport (g cm^{-1}/flood & ebb tides) and mean sediment transport of each tide (g cm^{-1} s^{-1}) calculated at Station 1.

Tide no.		Dir.	$\bar{U}_{100}$ cm s^{-1}	q_t (g cm^{-1} per flood, ebb tide) Hardisty-1983	Engelund & Hansen-1967	Mean q & dir. (g cm^{-1} s^{-1})	
ST+	1	Ebb	52.77	10,121.90	5,071.53		
	2	Flood	46.33	6,083.02	3,224.38		
		Ebb	47.86	8,315.25	4,375.91	0.169	Ebb
	3	Flood	42.08	3,877.86	2,103.92		
		Ebb	49.07	7,912.33	4,016.36	0.136	Ebb
	4	Flood	42.78	4,566.32	2,471.48		
		Ebb	51.83	11,901.00	6,160.01	0.192	Ebb
	5	Flood	44.83	5,392.14	2,862.59		
		Ebb	48.52	7,201.67	3,633.25	0.144	Ebb
	6	Flood	41.16	3,778.21	2,075.92		
		Ebb	49.73	9,190.41	4,638.21	0.149	Ebb
	7	Flood	38.27	2,379.86	1,431.74		
		Ebb	43.79	4,515.87	2,388.43	0.085	Ebb
	8	Flood	38.12	2,015.28	1,289.90		
		Ebb	47.99	7,413.15	3,737.93	0.112	Ebb
	9	Flood	39.19	1,982.06	1,340.18		
		Ebb	43.25	2,967.56	1,819.71	0.070	Ebb
	10	Flood	37.60	1,859.68	1,223.70		
		Ebb	47.61	6,653.13	3,368.24	0.102	Ebb
	11	Flood	36.90	1,195.43	980.01		
		Ebb	42.57	2,479.52	1,637.98	0.058	Ebb
	12	Flood	35.79	1,116.31	909.16		
		Ebb	46.23	5,325.70	2,757.90	0.082	Ebb
	13	Flood	33.53	558.86	671.18		
		Ebb	37.50	682.24	870.43	0.034	Ebb
NT	14	Flood	34.55	760.57	759.21		
		Ebb	43.34	3,063.01	1,840.06	0.058	Ebb
	15	Flood	33.87	564.19	685.45		
		Ebb	39.56	1,164.83	1,138.21	0.041	Ebb
	16	Flood	35.35	1,532.46	1,081.16		
		Ebb	47.70	7,072.79	3,553.58	0.103	Ebb
	17	Flood	37.54	2,205.45	1,425.05		
		Ebb	44.60	4,307.12	2,312.44	0.083	Ebb
	18	Flood	37.14	1,397.18	1,126.64		
		Ebb	47.98	8,296.43	4,289.65	0.120	Ebb
	19	Flood	36.99	1,735.14	1,296.21		
		Ebb	42.50	5,017.98	2,623.87	0.087	Ebb
	20	Flood	38.84	2,373.25	1,470.65		
		Ebb	49.85	10,854.30	5,565.10	0.156	Ebb
	21	Flood	40.80	3,807.10	2,089.92		
		Ebb	49.77	12,096.50	6,176.60	0.184	Ebb
	22	Flood	44.58	5,995.09	3,190.21		
		Ebb	49.63	11,667.20	6,018.25	0.205	Ebb
	23	Flood	46.87	8,580.31	4,505.77		
		Ebb	46.06	7,360.47	3,756.86	0.184	Ebb
	24	Flood	50.48	11,907.80	6,327.05		
Mean		Flood		1,936.59	3,289.72		
		Ebb		3,554.37	6,764.36		

Station 2

Station 2 was occupied from 22 June to 10 July 1990 but after about 8 days, the current meter failed to record current velocities. The most probable reason was fouling by weed, which was found around the rotor on recovery of the instrument. Details of current flow at this site have already been discussed in Chapter 4. At this location sediment transport rates are about twenty times higher than at other stations. Transport during flood tides is dominant over the ebb tide rates. The results at this station show that most of the sediment supply to the Lavan Sands is through this area. Variations in transport rate with respect to time at successive flood and ebb tides are shown in Fig. 6.6.

Because of the comparatively high current velocities at this position, the sediment transports calculated by Engelund & Hansen's [1967] total load equation and Hardisty's [1983] bedload transport formula are almost in the same range (see Fig. 6.2). Net transports calculated from the above mentioned equations are shown in Table 6.3 and compared in Fig. 6.7. Mean and residual rates at this station clearly show the dominance of flood tides (Fig. 6.8) The mean net sediment rate at this location is 136.0 kg cm^{-1} during a tidal cycle (averaged over 8 tides).

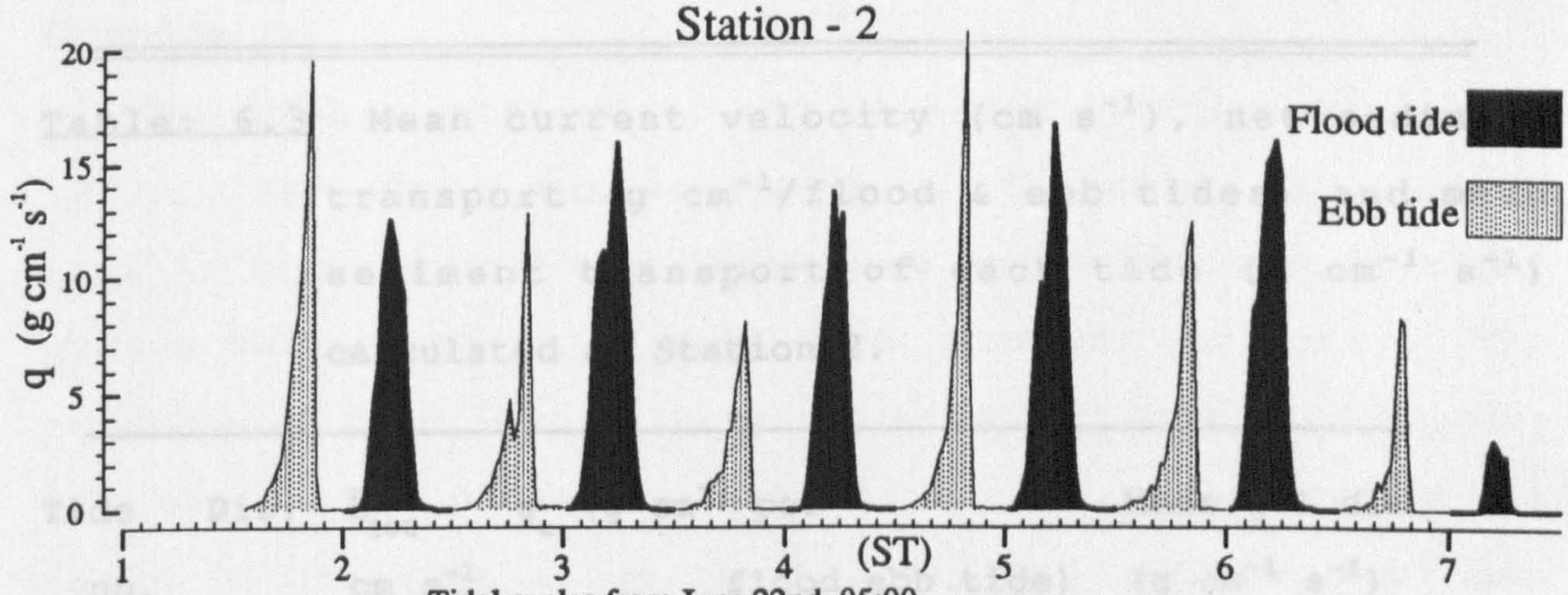

Fig: 6.6

Sediment transport at each 15 minutes recording interval estimated from the total load equation of Engelund & Hansen [1967].

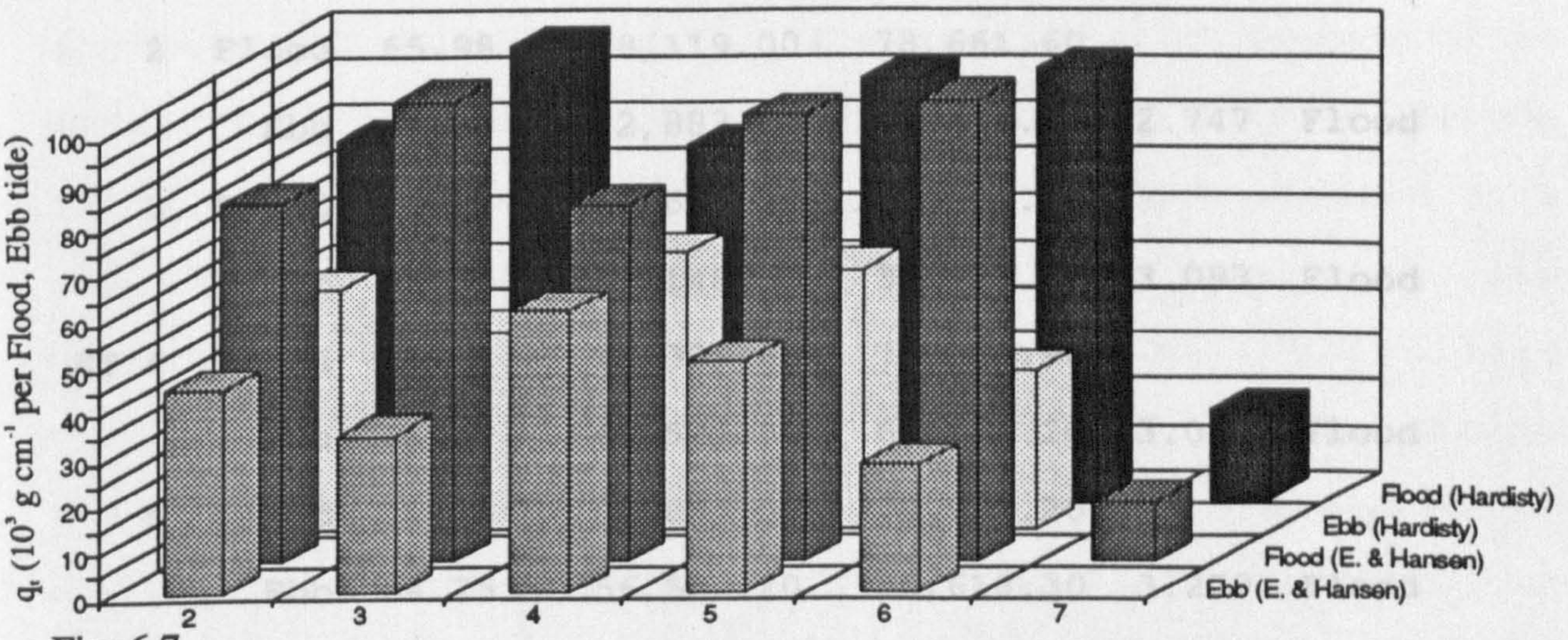

Fig: 6.7

Comparison of net sediment transport calculated by formulae of Engelund & Hansen [1967] and Hardisty [1983] of flood & ebb tides.

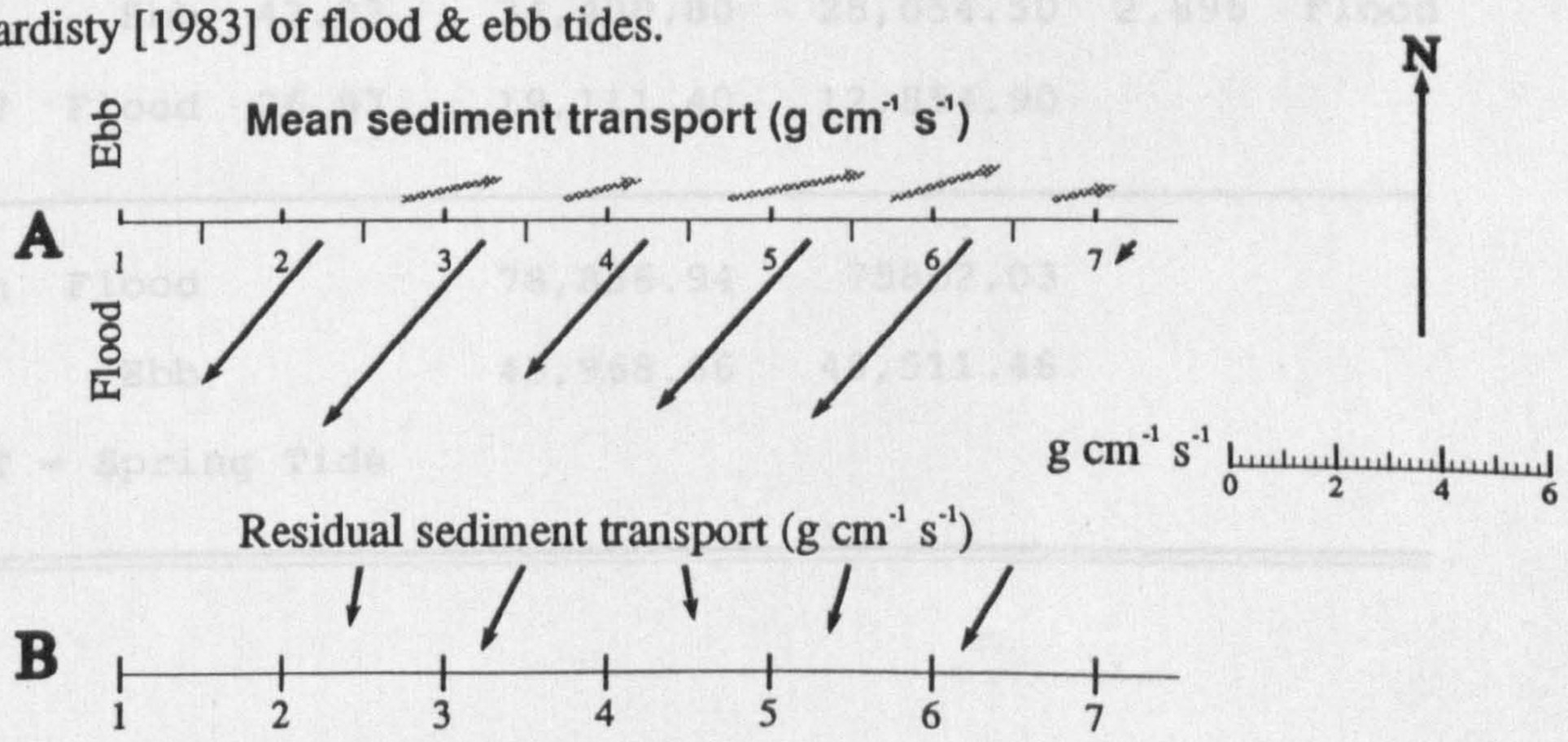

Fig: 6.8

Sediment transport vectors showing mean transport rate of flood & ebb tides (A) and residual transport of each recorded tide (B), using equation of Engelund & Hansen [1967].

Table: 6.3 Mean current velocity (cm s^{-1}), net sediment transport (g cm^{-1}/flood & ebb tides) and mean sediment transport of each tide (g cm^{-1} s^{-1}) calculated at Station 2.

Tide no.	Dir.	$\bar{U}_{100}$ cm s^{-1}	q_t (g cm^{-1} per flood,ebb tide)		Mean q & dir. (g cm^{-1} s^{-1})	
			Hardisty-1983	Engelund & Hansen-1967		
2	Flood	65.98	78,119.00	78,661.60		
	Ebb	64.90	52,883.20	44,972.80	2.747	Flood
3	Flood	74.27	97,622.20	104,446.00		
	Ebb	53.64	43,148.50	34,733.50	3.093	Flood
ST 4	Flood	61.82	76,389.80	77,818.90		
	Ebb	64.02	60,535.70	61,464.20	3.095	Flood
5	Flood	70.60	90,895.00	96,957.20		
	Ebb	64.75	56,589.20	50,618.30	3.279	Flood
6	Flood	70.58	93,034.80	102,283.00		
	Ebb	47.03	34,400.80	28,054.50	2.896	Flood
7	Flood	26.97	19,111.40	12,854.90		
Mean	Flood		78,836.94	75862.03		
	Ebb		43,968.66	49,511.48		

ST = Spring Tide

Station 3

The RCM4 current meter was deployed at this station on 10 July 1990 for a two week period. Unluckily the problem similar to Station 2 was faced here and only about 10 tidal cycles current velocity data were recorded correctly. The currents at this station were explained in detail in Chapter 4. The amount of sediment transport at this location is about in the same range as at Station 1 but the dominant direction is similar to that of Station 2. Variations in sediment transport rates at each velocity recording interval are presented in Fig. 6.9. Transport is estimated to be higher around spring tides than around neap tides. During flood tides, the net sediment transport rate estimated from the equation of Hardisty [1983] is almost double the rate calculated from the Engelund & Hansen [1967] total load equation, because of low current speeds. Mean current velocities of flood tides at this station range from 37.8 cm s^{-1} to 48.8 cm s^{-1}. Net transport during flood and ebb tides calculated from the Engelund & Hansen's [1967] equation and Hardisty's [1983] formula are compared in Fig. 6.10. Statistical parameters of transport rate at Station 3 are given in Table 6.4.

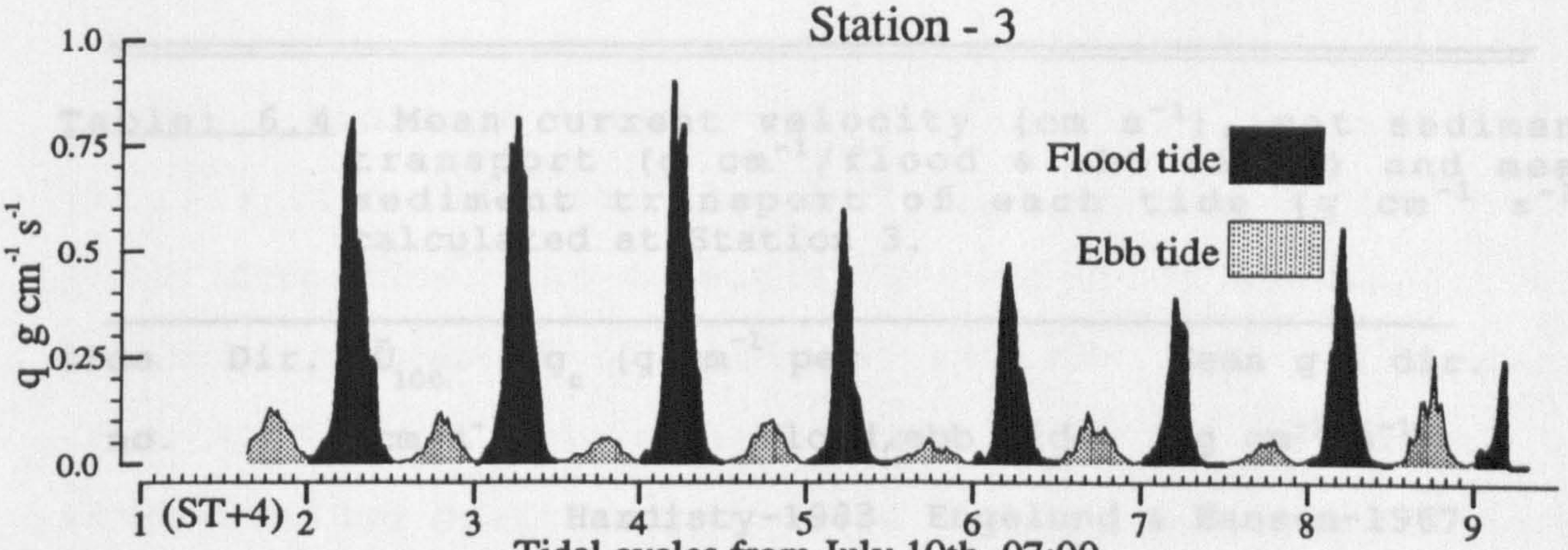

Fig: 6.9

Sediment transport at each 15 minutes recording interval estimated from the total load equation of Engelund & Hansen [1967].

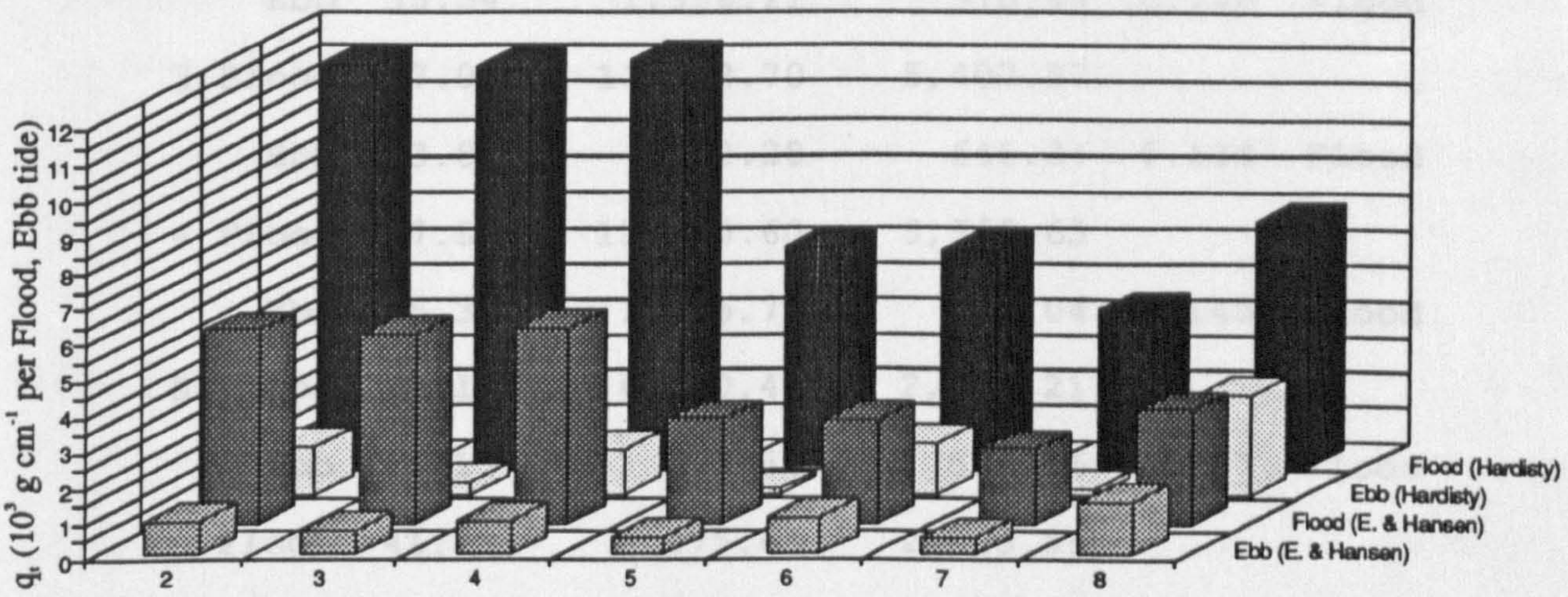

Fig: 5.10

Comparison of net sediment transport calculated by formulae of Engelund & Hansen [1967] and Hardisty [1983] of flood & ebb tides.

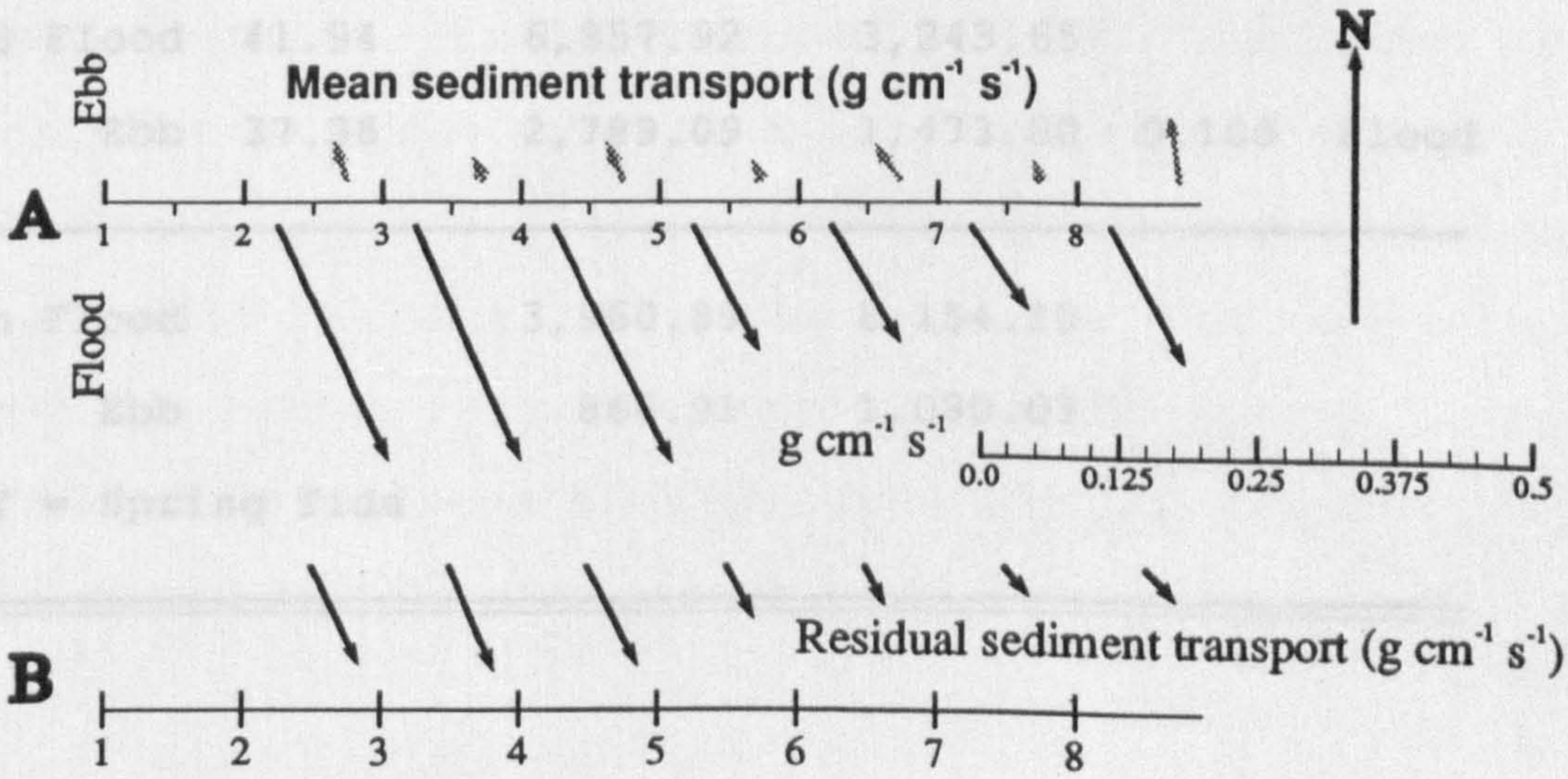

Fig: 6.11

Sediment transport vectors showing mean transport rate of flood & ebb tides (A) and residual transport of each recorded tide (B), using Engelund & Hansen's [1967] equation.

Table: 6.4 Mean current velocity (cm s^{-1}), net sediment transport (g cm^{-1}/flood & ebb tides) and mean sediment transport of each tide (g cm^{-1} s^{-1}) calculated at Station 3.

Tide no.	Dir.	$\bar{U}_{100}$ cm s^{-1}	q_t (g cm^{-1} per flood,ebb tide) Hardisty-1983	Engelund & Hansen-1967	Mean q & dir. (g cm^{-1} s^{-1})	
ST+5	2 Flood	48.79	11,222.00	5,493.34		
	Ebb	35.54	1,356.21	970.49	0.144	Flood
	3 Flood	47.06	11,102.70	5,407.57		
	Ebb	33.89	392.28	646.34	0.134	Flood
	4 Flood	47.54	11,310.60	5,569.63		
	Ebb	35.34	1,276.73	936.04	0.145	Flood
	5 Flood	40.13	6,130.44	2,965.21		
	Ebb	32.15	130.50	510.46	0.077	Flood
	6 Flood	41.24	6,075.65	2,893.99		
	Ebb	36.39	1,430.58	1,032.46	0.087	Flood
	7 Flood	37.81	4,379.39	2,152.82		
	Ebb	31.52	184.81	498.76	0.059	Flood
	8 Flood	41.94	6,857.92	3,243.65		
	Ebb	37.36	2,789.09	1,473.80	0.105	Flood
Mean Flood			3,960.89	8,154.10		
	Ebb		866.91	1,080.03		

ST = Spring Tide

Mean sediment transports during flood and ebb tides (Fig. 6.11A) indicate the dominance of transport in the flood direction. As a result of this flood dominance, the residual transport of sediment at this site is landward (Fig. 6.11B). A mean residual rate of 10.7 * 10^{-3} g cm^{-1} s^{-1} is determined during a period of 7 tidal cycles. Evidence from interpretation of sonograph records (Fig. 3.16) shows that between this station and land the direction of sediment transport is diverted toward the east. Most probably a part of this material goes in to the Menai Strait through the Penmaen Swatch and some sediment deposits over the Lavan Sands during flood tides.

Stations 5 - 12

The locations of these stations in the study area are shown in Fig. 4.1. The currents on Stations 5 - 9 were recorded by the Braystoke Directional Current Flow Recording Meter for one tidal cycle. The current velocities for a spring and a neap tidal cycle were obtained from the Ordnance Datum Charts on Station 10 - 12. For details of current data on these positions see Chapter 4. The results of sediment transport rate on these locations are presented in Table 6.5. Some of these results are inevitably speculative (since they are based on rather sparse velocity data) but nevertheless they provide useful support to the results obtained from the longer time series.

Table: 6.5 Mean current velocity (cm s^{-1}), net sediment transport (g cm^{-1}/ tide) and mean sediment transport (g cm^{-1} s^{-1}) calculated at Stations 5 - 12, using the Engelund & Hansen's [1967] total load equation.

Station no.	$\bar{U}_{100}$ cm s^{-1}	q_t (g cm^{-1} per tide)	Mean q (g cm^{-1} s^{-1})	Dominant Direction	Period (tide)
5	30.51	1655.13	0.037	Ebb	1
6	23.36	411.46	0.009	Flood	1
7	33.25	6768.28	0.157	Flood	1
8	19.72	309.45	0.007	Flood	1
9	22.20	1464.16	0.033	Flood	1
10	32.15	3504.11	0.075	Flood	2
11	43.30	27335.51	0.584	Flood	2
12	37.09	9149.65	0.348	Flood	2

6.4 Conclusions

(1) The net sediment transport direction at all stations follows the respective direction of residual currents (Chapter 4) in the area.

(2) After estimating total sediment transport rates at 12 stations in the area, the spatial distribution of residual transport rates (Fig. 6.12) shows that the

Fig: 6.12

Residual sediment transport (g cm^{-1} s^{-1}) calculated by the formula of Engelund & Hansen [1967].

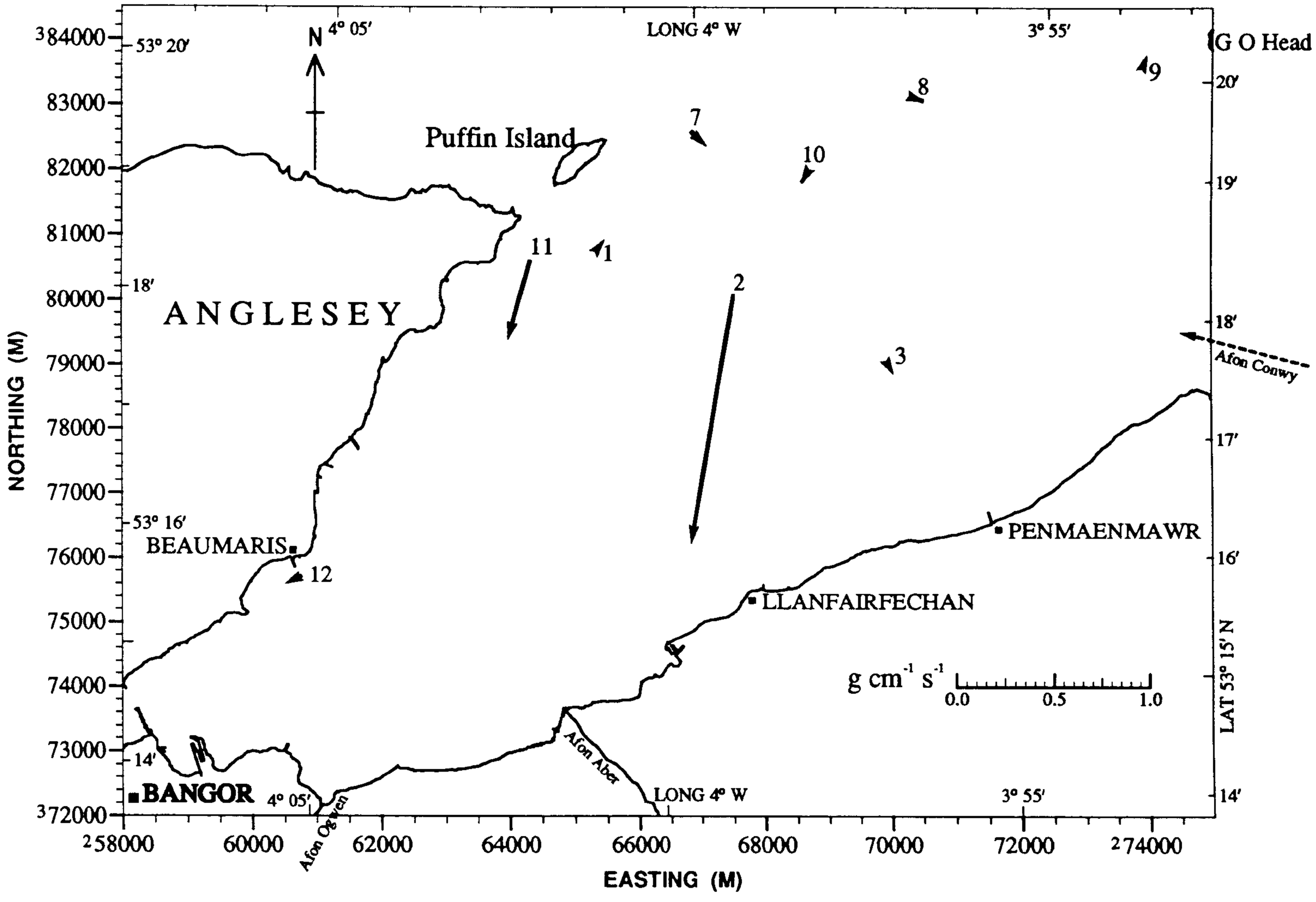

trend in the study area is in the flood direction, except at Station 1. The same trend of transport is also observed in the study of bedforms during the geophysical survey (Chapter 3) and from the study of characteristics of sediment grain size in the area (Chapter 5).

(3) The residual transport vectors show that the sediments in the area enter from the Irish Sea with a dominant transport direction NW to SE. At about the middle of Conwy Bay, near the location of Station 8, the sediment transport direction is approximately eastwards and after some distance changes to northeast (Station 9); but around the locations of Stations 2, 3 & 10, it changes to the southwest.

(4) Sediment transport at Station 2 is much greater and the net transport is to the south and southwest. The high rate of transport at this locality is due to the fast currents and particular topography of the area.

(5) Some of the sediments supplied by the area of Stations 2 & 3 may be deposited over the Lavan Sands and some may be transported to Caernarfon Bay through the Menai Strait (Stations 11 & 12).

(6) A proposed residual transport form Conwy Bay and the NE Menai Strait to Caernarfon Bay is supported by Solangi [1992]. In Caernarfon Bay (at the SW end of the Menai Strait), he concluded that sediments

mainly enter Caernarfon Bay from the north east. Hence sediments are funnelled through the Menai Strait from the Conwy Bay/Lavan Sands area and pass seawards into Caernarfon Bay.

CHAPTER SEVEN

BEDFORM OBSERVATIONS AND SEDIMENTARY STRUCTURES

PART - I

BEDFORM OBSERVATIONS FROM PHOTOGRAPHS AND SURVEYS

PART - II

BEDFORM SEDIMENTARY STRUCTURES FROM BOX CORES

Part - I:

BEDFORM OBSERVATIONS FROM PHOTOGRAPHS AND SURVEYS

7.1 Introduction and Objectives

Large scale bedforms indicate high flow velocities, relatively high rates of bedload sediment transport, and as such can be indicators of the temporal and spatial variations in bedload sediment and water flux. Recently many research workers have used bedforms for this purpose. Klein [1970] found that bedform orientation showed excellent agreement with the dispersal pattern of sand stained with acrylic lacquer. Wright, Coleman & Thomas [1975] used bedform orientation to study sediment transport patterns in the macrotidal Ord River. Boothroyd & Hubbard [1975] used megaripple and sandwave orientation to infer direction and magnitude of sand movement. They directly related the observed bedforms to the tidal currents over intertidal and shallow subtidal deltas in the Gulf of Maine. Langhorne [1982] calibrated a sediment transport equation from the movement of subtidal bedforms. Van den Berg [1987] tested bedload sediment transport equations by comparing results with megaripple migration data. Harris [1988] provided excellent examples of the use of bedforms to indicate mutually evasive sediment transport paths in a wide-mouthed estuary.

In the present section, a reconnaissance of bedforms in

the intertidal area based on observations from photographs is presented. The areas occupied by bedforms were established from the aerial photographs and then a brief ground survey was conducted and photographs taken. The crest trend and the sense of asymmetry of bedforms were observed and wavelength spacing was measured. From these parameters a trend of bedform migration may be deduced.

7.2 Methods

Photographs used for this purposes are:

a- A satellite image (Landsat) taken in 1984. The Landsat image (Fig. 7.1) shows the ridges along the main channel, near the Lifeboat Station and Gallows Point, and runnels over most of the intertidal area. Areas of finer grain size show a darker shade on the image than coarse grained areas.

b- Aerial photographs (1:10,000) obtained from the Committee for Aerial Photography, University of Cambridge. These photographs were taken in August 1982 from a height of about 600m with a RC8 survey camera. Fig. 7.4 shows a mosaic of these photographs.

c- A photographer from the Department of Earth Sciences, Open University took photographs of the study area at low tide especially for this project. These were taken from a height of about 900m. Large bedforms are visible near Llanfairfechan on these photographs (Fig. 7.7).

Fig: 7.1
True Colour LANDSAT Thermatic Mapper Image of the Study Area.

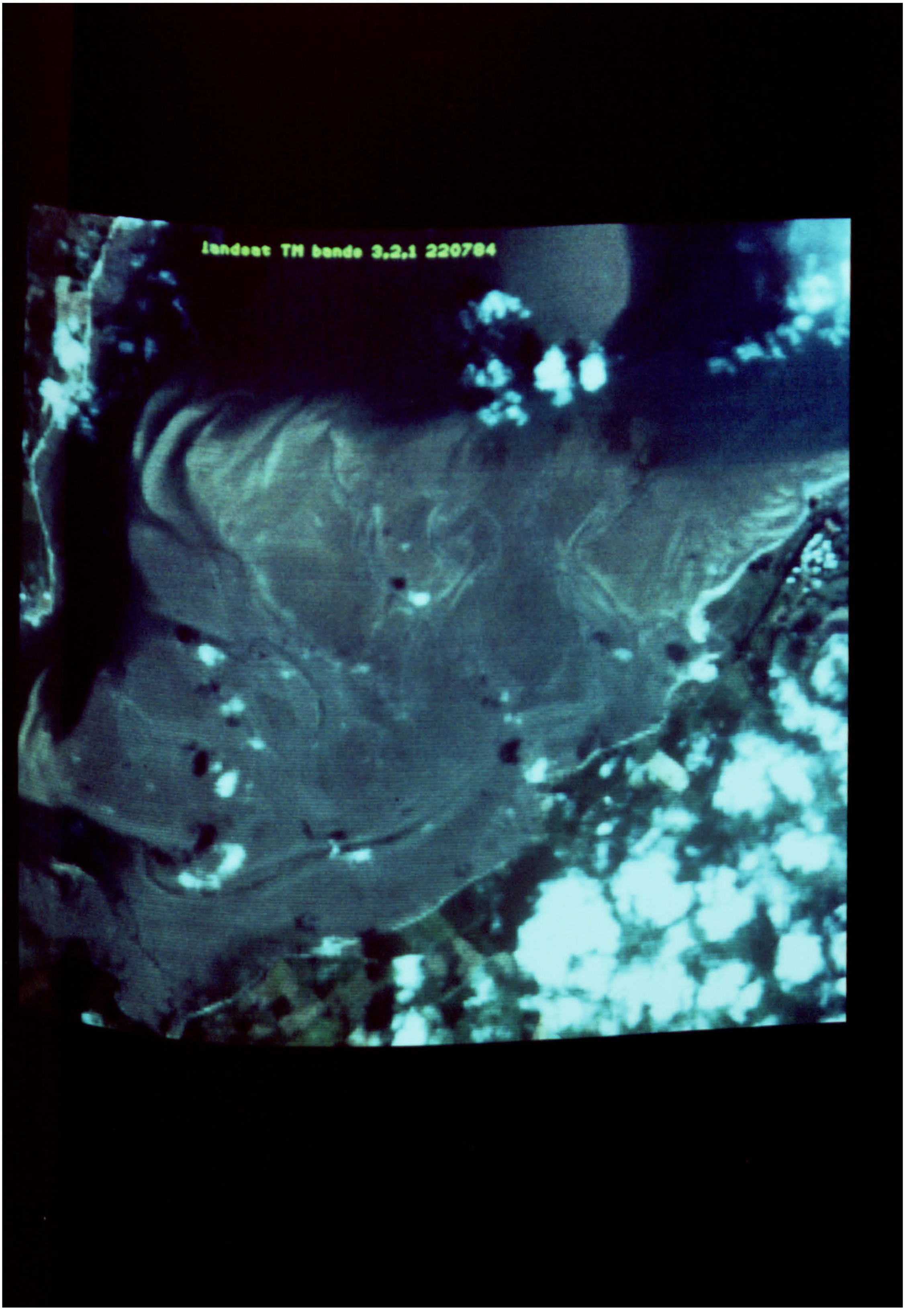
landsat TM bande 3,2,1 220784

d- In intertidal areas, photographs were taken during the box core sampling programme (Figures 7.3, 7.5, & 7.6).

The air photographs obtained from the University of Cambridge most clearly show megaripples (<6m), sandwaves (>6m), ridges and runnels. The asymmetry of the bedforms is seen mainly from the black and white tones [McCave & Geiser, 1978]; lighter tones making the crests and a part of the stoss side and darker ones indicating the troughs. The reason for these different tones is that the higher parts were dryer than the troughs. These tones show an asymmetrical set of light and dark strips. Sets of 10 waves were measured on representative lines at right angles to crestlines in selected areas (where bedforms were continuous up to about 100m).

During visits to these areas, wavelengths and heights of bedforms were measured and asymmetries were noted. The photographs taken during these visits show ripples, megaripples and sandwaves.

The parts of study area covered by aerial photographs and which exhibit bedforms and terrains of bedforms are shown in Fig. 7.2.

7.3 Results

From the air and ground photographs, four bedform terrains were observed in the intertidal area. They are; *Terrain A*, part of Lavan Sands comprising small bedforms; *Terrain B*, off the Gallows Point and off the Lifeboat Station; *Terrain C*, near LLanfairfechan, and *Terrain D*, part

Fig: 7.2

Intertidal areas covered by aerial photographs, shown as Figs. 7.4, & 7.7 - 7.9; and observed A, B, C, & D bedform terrains.

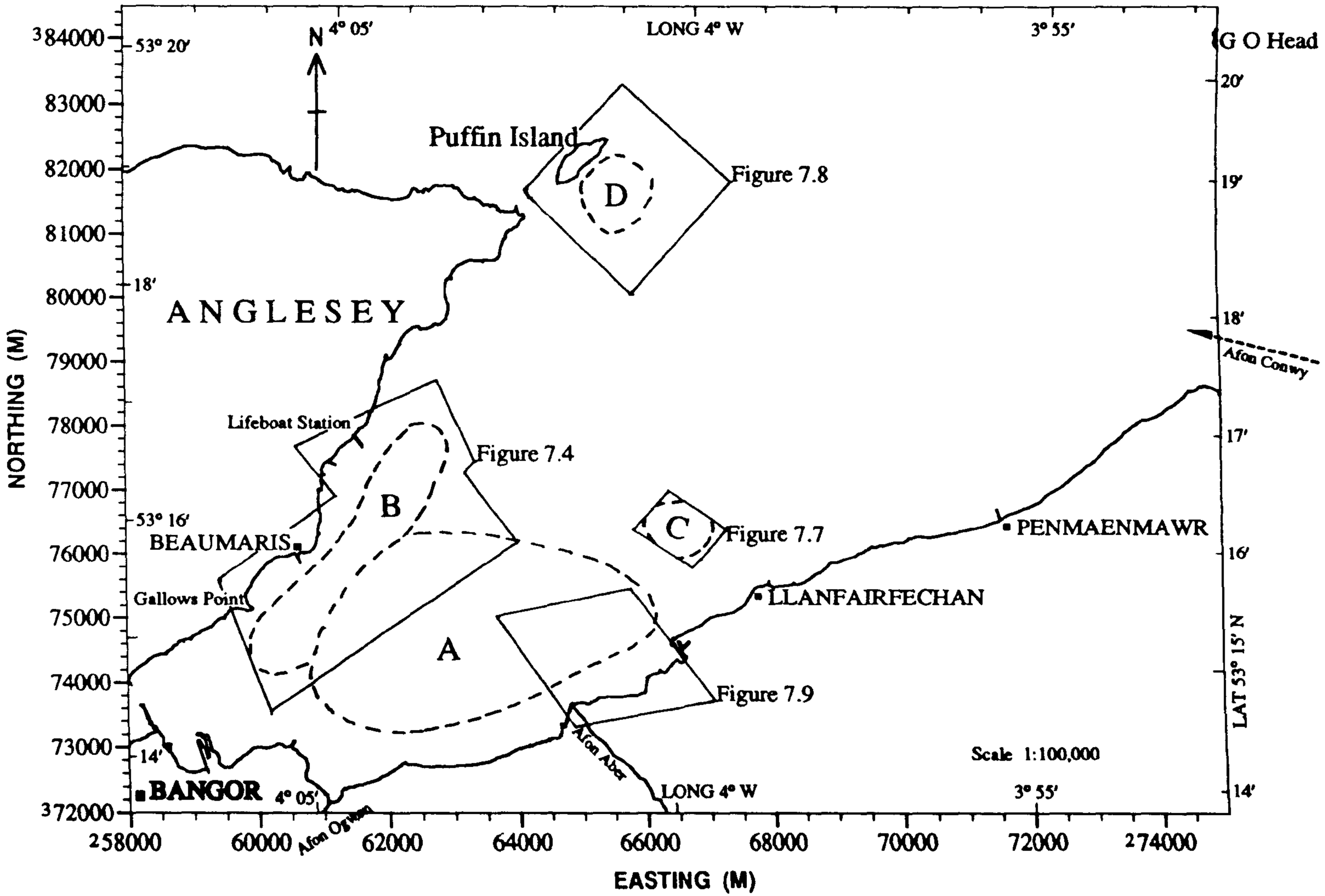

of Irishman Spit near the Puffin Island.

Terrain A:

Terrain A covers most of the Lavan Sands area. The plane surfaces on air photographs are deduced to be rippled but the bedforms are not clear because of their small size (i.e., <2m). Their presence was observed during field visits to the Lavan Sands (Fig. 7.3). The plane surfaces of intertidal areas depicted by Fig. 7.4 & Fig. 7.9, are in fact characterised by small ripples which occur on most parts of the Lavan Sands.

Terrain B:

Near Gallows Point, on the Lavan Sands side of the channel, most of the bedforms have wavelengths of 5m to 12m, and wave heights less than 0.4m. From air photographs, 34 sets of 10 bedforms have been measured. These 34 sets represent a total length of about 2.71km. The ground photographs show the bedforms as 2-D sandwaves with superimposed ebb-oriented ripples and small megaripples (Fig. 7.4, Fig. 7.5A, B).

Near the Lifeboat Station, the bedform population has been measured along sets with a total length of 5.55km. This include 74 sets of 10 transverse bedforms. Wavelengths range between 3m to 20m. During the box coring programme, a slight increase in surficial grain size and asymmetry, in the ebb direction toward the north

A

B

Fig: 7.3
Ripples on Lavan Sands (NGR c. 64100 74600). View of (A) is north and (B) is south.

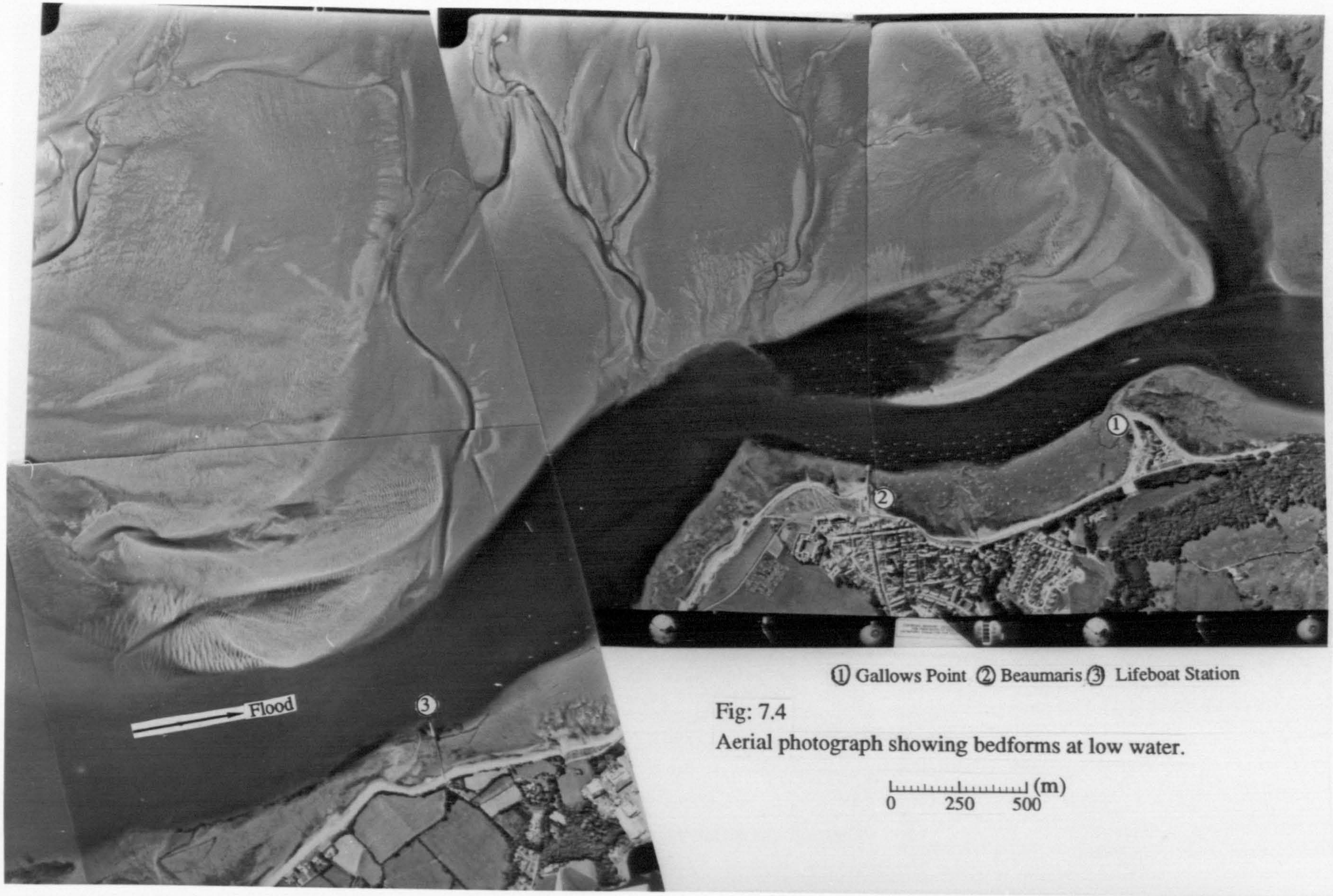

① Gallows Point ② Beaumaris ③ Lifeboat Station

Fig: 7.4

Aerial photograph showing bedforms at low water.

0 250 500 (m)

Fig: 7.5 A: Flood oriented sandwaves near Gallows Point; B,C: Ripples → megaripples → sandwaves terrain (bottom to top; E→W) on Lavan Sands near Gallows Point. Distance between boxes (C) and boat (B) is c. 800m.

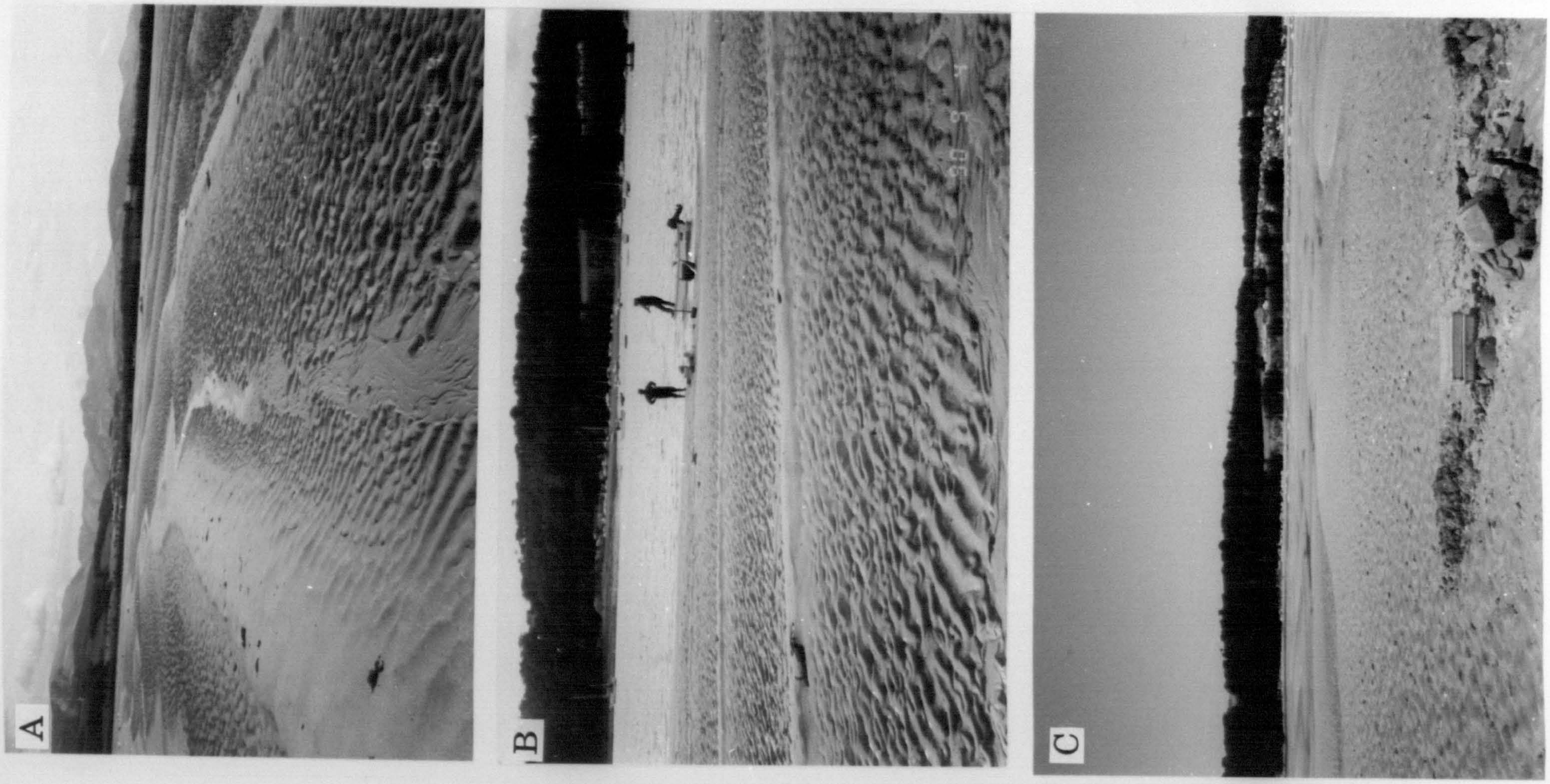

of the area covered by Fig. 7.4, was observed. The large bedforms have superimposed ebb oriented ripples (Fig. 7.4, Fig. 7.6).

Terrain C:

Near Llanfairfechan (Fig. 7.7), sandwaves show asymmetry in the flood direction. The appearance of the crestlines of these bedforms shows that most of the sandwaves in this area are 2-D sandwaves. The locations of these bedforms in Fig. 7.10 may deviate up to about 500m due to lack of geographic features between these photographs and photographs of the mainland (from which this mosaic was formed).

Terrain D:

On Irishman Spit (NGR 66000, 82000), sandwaves occur with wavelengths up to 100m with an asymmetry towards the north (Fig. 7.8).

The bedform types (ripples, megaripples and sandwaves) observed in terrains A to D are shown in Fig. 7.10.

7.4 Discussion and Conclusions

The frequency distribution of bedforms may exhibit modal or polymodal behaviour [Allen, 1978] in terms of their morphometric characteristics. The creation of population modes may be periodic or permanent, depending on the degree of variation in hydraulic conditions [Collinson, 1970;

A

B

Fig: 7.6
Sandwaves superimposed with ripples and megaripples near Lifeboat Station at NGR 61950 77300 on 10/7/91, views E (A); and at NGR 62550 77830, on 26/7/91, views NE (B).

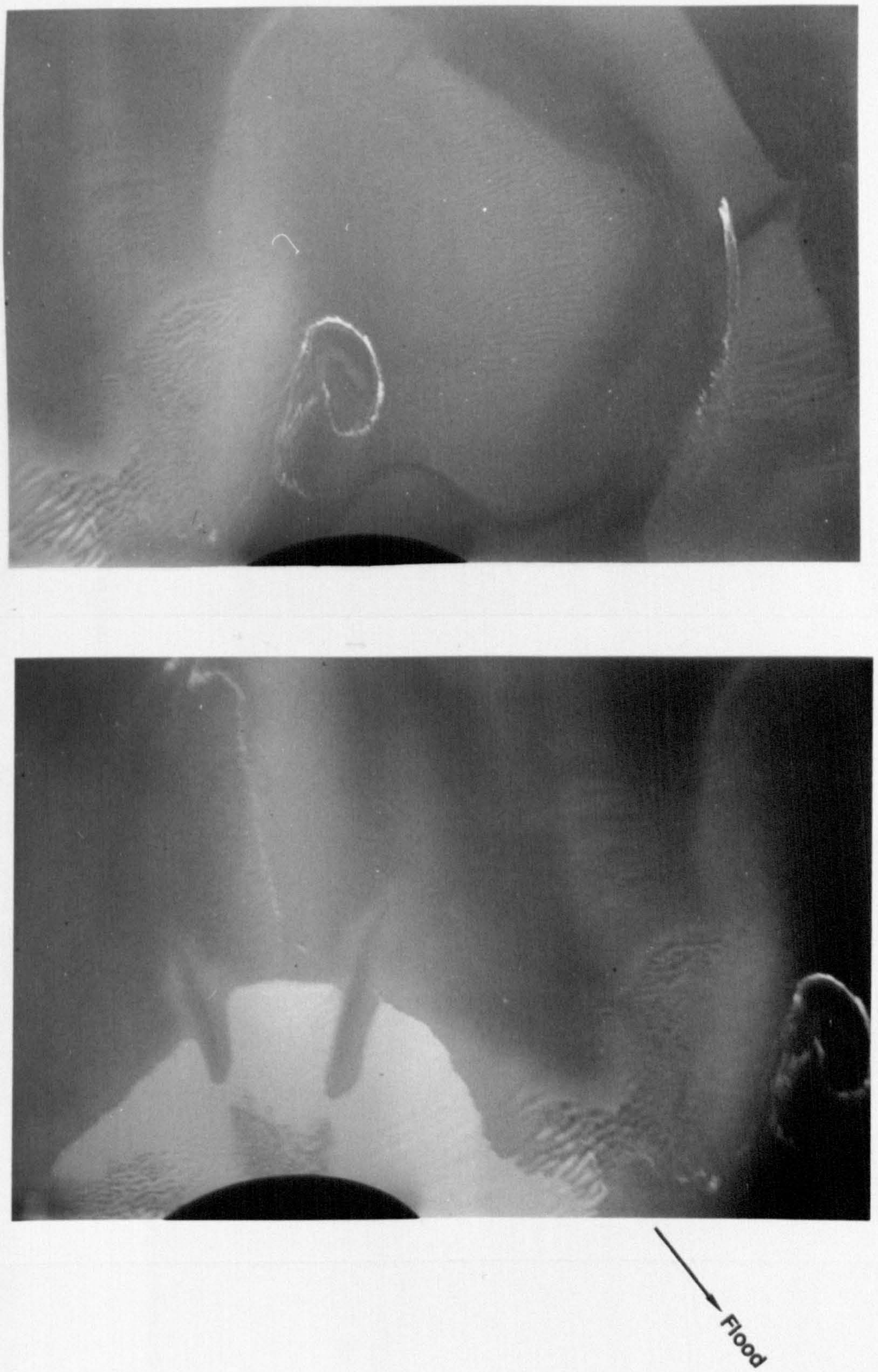

Fig: 7.7
Sandwaves showing asymmetry in flood direction near Llanfairfechan (aerial view).

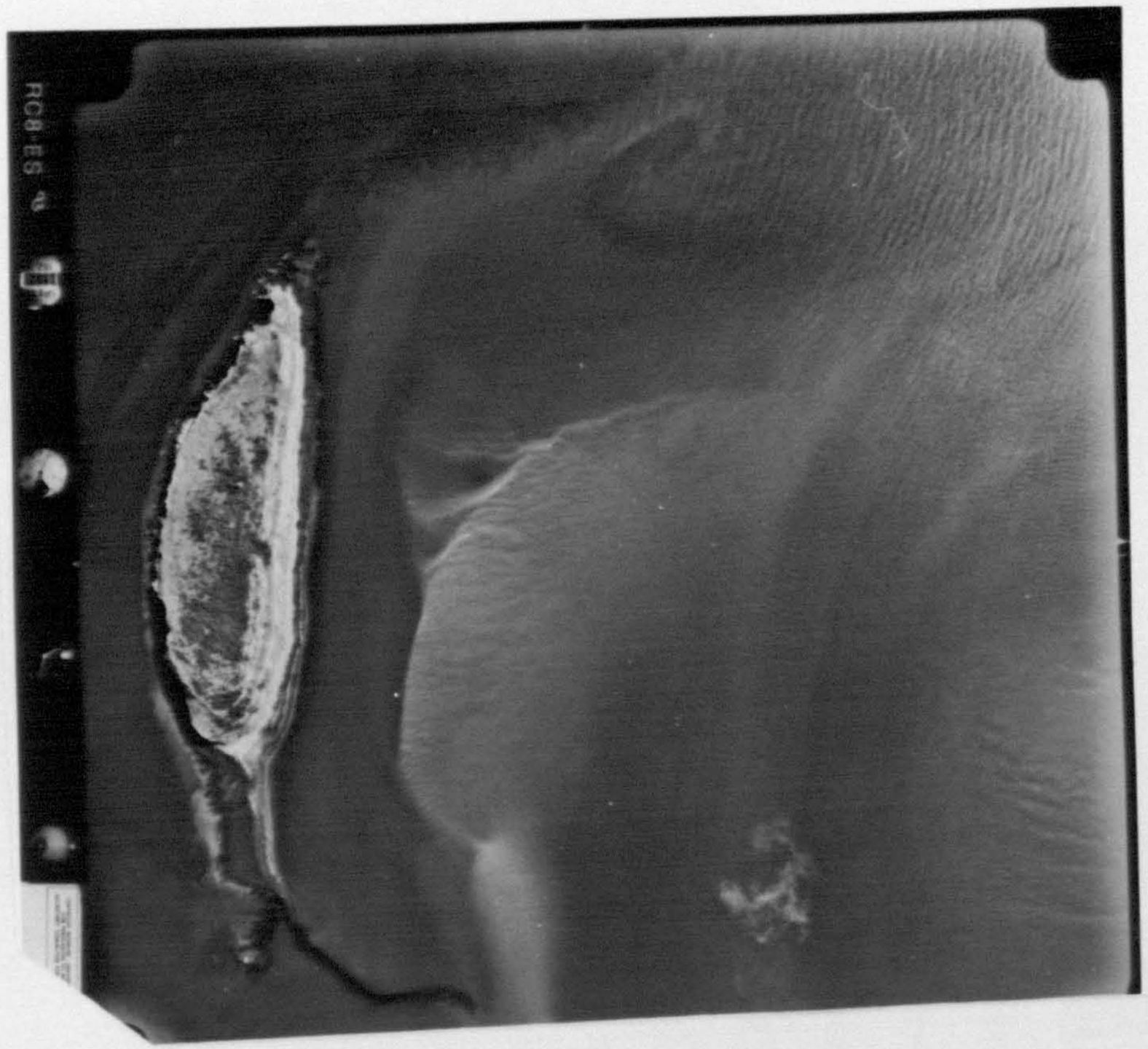

Fig: 7.8
Large sandwaves at Irishman Spit near Puffin Island (aerial view).

Fig: 7.9
Aerial view of parts of Lavan Sands near Arfon coastline; Afon Aber mouth - Llanfairfechan.

Boothroyd & Hubbard, 1974; Allen & Friend, 1976; Zarillo, 1982; Dalrymple, 1984]. Under constant flow, the bedform may adjust until an equilibrium dimension is reached, which implies that both wavelength and wave height become constant. But under changing flow conditions, as in the study area, there is a continuous creation, development and destruction of individual bedforms [Allen, 1982a, b, c; Allen & Friend, 1976; Costello & Southard, 1981; Wijbenga & Klassen, 1983], so equilibrium bedforms cannot be formed.

Most of the central Lavan Sands are in general devoid of any large bedforms, probably due to the fineness of sediment in this area (Chapter 5) and low current speeds compared to the other areas. But the whole area is covered with small ripples with wavelengths and heights less than 30cm and 10cm, respectively. The crests of these ripples are usually sinuous, but sometimes straight. Ripples generally form approximately transverse to the direction of water movement. Small ripples undoubtedly reverse with the changing tide direction, but ripples exposed during low tide are generally ebb-oriented.

Near Gallows Point, the transverse bedforms exhibit polymodal behaviour in terms of wavelength (Fig. 7.11A). The majority of the bedforms have wavelengths 6.0 to 7.5m and a secondary mode occur at a wavelength of about 11.0m. Allen & Friend [1976] recognised morphometric modes on the basis of wavelength within the megaripple populations. They divided the dune (i.e., megaripple) population into

Fig: 7.10

Bedform distributions in intertidal area based on the photographic studies and field surveys.

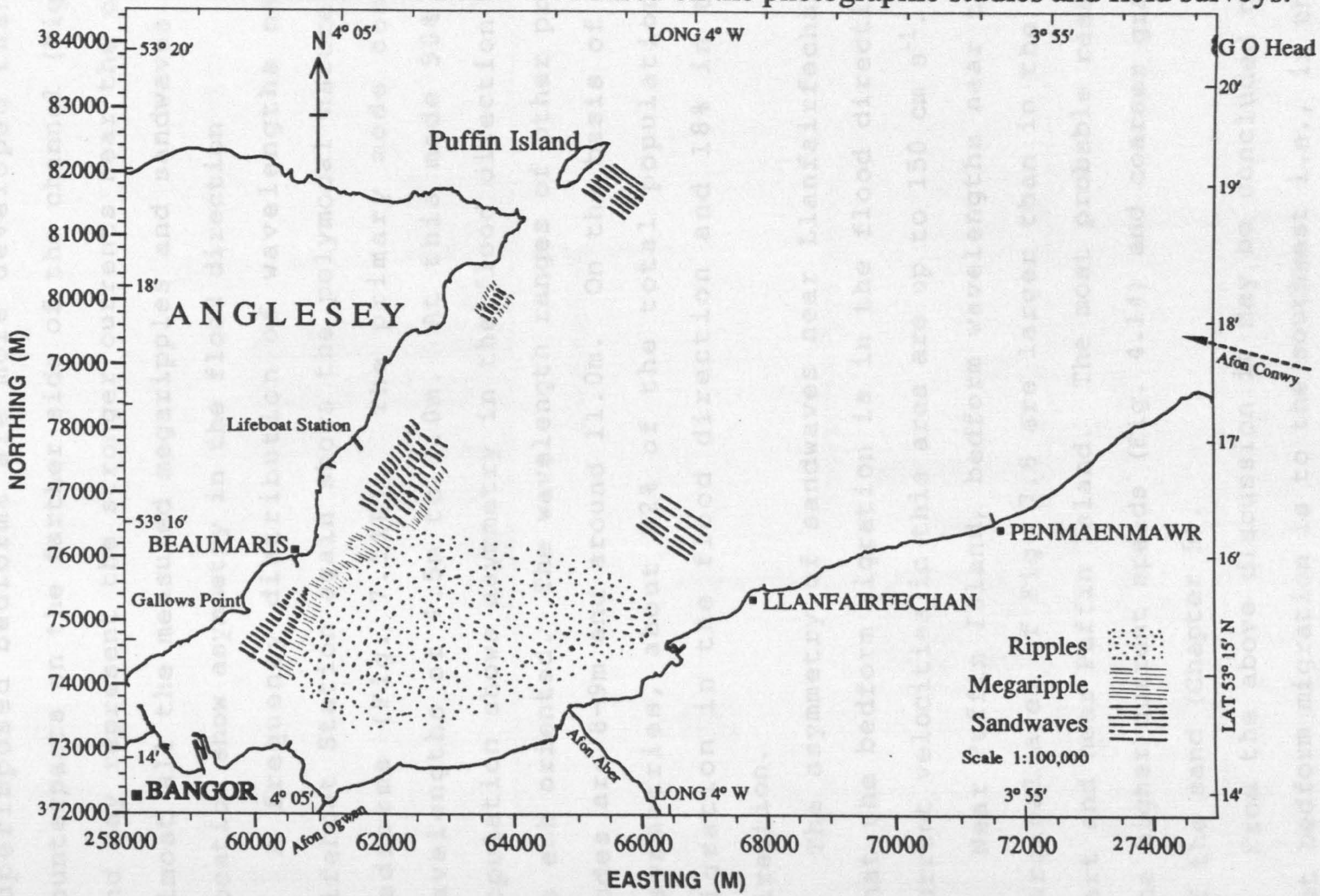

subpopulations of modal wavelength of 1-2, 3.5, 6 and close to 9m. Closer to the channel (Fig. 7.5C), these superimposed bedforms are more developed than their counterparts on the farther side of the channel (Fig. 7.5B) and may represent the stronger currents near the channel. Almost all the measured megaripples and sandwaves in this location show asymmetry in the flood direction

A frequency distribution of wavelengths near the Lifeboat Station again shows the polymodal nature of the bedforms (Fig. 7.11B). The primary mode comprises wavelengths of 4.5m to 7.0m. At this mode 50% of the population shows asymmetry in the flood direction and 11% is ebb oriented. The wavelength ranges of other prominent modes are 8-9m and around 11.0m. On the basis of bedform asymmetries, about 82% of the total population shows migration in the flood direction and 18% in the ebb direction.

The asymmetry of sandwaves near Llanfairfechan shows that the bedform migration is in the flood direction. The current velocities in this area are up to 150 cm s^{-1}.

Near Puffin Island, bedform wavelengths near the east marginal area of Fig. 7.8 are larger than in the central part and near Puffin Island. The most probable reasons are the higher current speeds (Fig. 4.14) and coarser grain size of the sand (Chapter 5).

From the above discussion it may be concluded that the net bedform migration is to the southwest i.e., in the flood direction. Only over Irishman Spit is the asymmetry in the

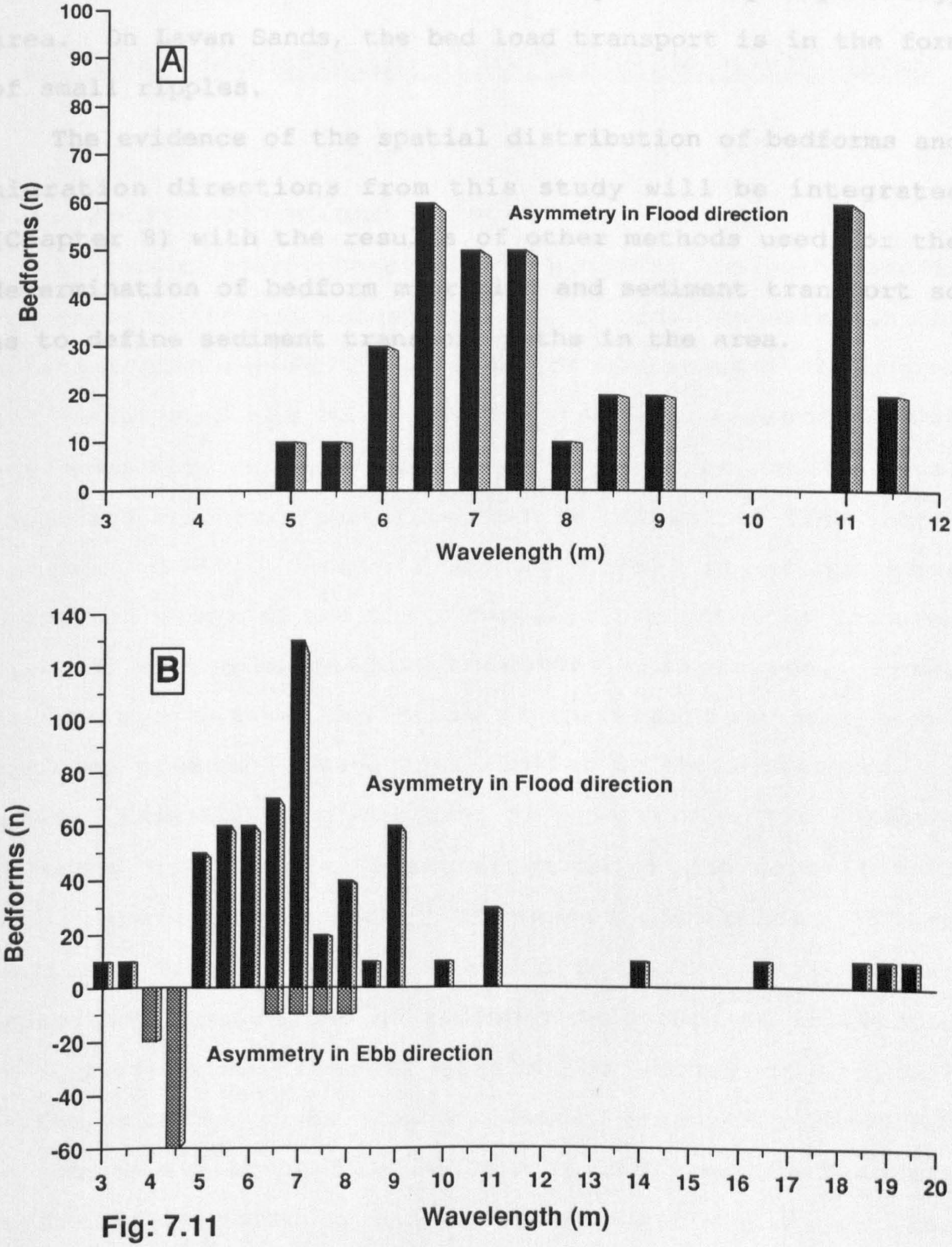

Fig: 7.11

Histogram showing frequency of wavelengths near Gallows Point (A) and near Lifeboat Station (B).

ebb direction. Near the main channel, the presence of large bedforms indicate that this is a comparatively high energy area. On Lavan Sands, the bed load transport is in the form of small ripples.

The evidence of the spatial distribution of bedforms and migration directions from this study will be integrated (Chapter 8) with the results of other methods used for the determination of bedform migration and sediment transport so as to define sediment transport paths in the area.

Part - II:

BEDFORM SEDIMENTARY STRUCTURES FROM BOX CORES

7.5 Introduction and Objectives

In recent years, considerable progress has been made in the recognition and interpretation of tidal deposits in the stratigraphic record. From study of sedimentary structures and textures, the main parameters of the depositional environments, such as flow velocity, water depth, tidal range and sand transport rate, can be determined [Terwindt & Brouwer, 1986]. Rubin & Hunter [1982] point out that migrating bedforms and their deposits are dramatic features rich in geological/sedimentological information. Sorby [1859] was one of the first to realise that migrating bedforms produce cross-strata similar to those preserved in rocks. From the interpretation of such strata, two commonly inferred results are: identification of the depositional environment and sediment transport direction. Where bedforms migrate in the current direction without net deposition, the volume of sediment deposited on lee slopes in a given time interval equals the volume of sediment eroded from the stoss slopes. Hence, except for variation in trough elevation from bedform to bedform, the boundary surfaces generated by all troughs coincide. In an area where net deposition is occurring, however, the volume of

sediment deposited on each lee slope is greater than the volume eroded from the stoss slope up current. The interpretation of the genesis of bedforms from knowledge of internal structures studied from direct observations (e.g., box peels) can eliminate to a great extent the 'matter for speculation' [McCave, 1985] in the dynamic significance of bedform sedimentary structures.

Thus Dalrymple [1984] calculated the migration of asymmetrical sandwaves in the direction of the dominant current in the Bay of Fundy, through study of internal structures of sandwaves examined in a 80 cm deep trench dug at right angles to the sandwave crestlines. He calculated an average rate of 0.11 m/tidal cycle. De Boer, Oost & Visser [1989] studied the diurnal inequality of the tides by measuring thick-thin alternations on a 90 cm high lacquer peel in an excavation pit in the mouth of the Oosterschelde tidal inlet (The Netherlands).

The aims of the box core survey will be to calculate the migration rate of bedforms, and hence to estimate the sediment transport rate and direction of transport. For this purpose 98 box cores were collected from the intertidal area. The results from this survey will be integrated with the previously described methods for the determination of sediment transport i.e., using sediment transport equations, by side scan sonar identification of bedforms, and sediment grain size trends. These results will be used to determine sediment transport paths in the area.

For a description of bedload transport, bedforms can be used in different ways. Various authors have used different terminologies and described them according to related techniques. So a description of the terminology adopted for different parts of the bedform in this study is specified in the following sections.

7.6 General Description of Bedforms

The terminology for the bedforms used in this study are outlined in Table 3.3.

Traditionally, ripple marks are represented and described in terms of vertical profiles parallel to flow and normal to the crestline. A ripple mark is composed of a crest and trough. Some important terms used in this chapter for the description of ripple marks are shown in Fig. 7.12. According to Reineck & Singh [1973] these terms are defined as follows;

Horizontal distance perpendicular to the crest between successive crests (or troughs) is the *ripple length* (L).

The *Ripple height* (H) is the vertical distance between the troughpoint and the summitpoint of a ripple.

The *Summitpoint* is the point of maximum elevation in the vertical plane at right angles to the crest.

The *Toepoint* is that point on the vertical profile of a ripple that separates the slipface from the bottomset.

The *Brinkpoint* is the point on a vertical profile of a ripple that separates the lee side from the stoss side.

The *Troughpoint* is that point of minimum elevation on the vertical profile of a ripple that separates the lee side of the one ripple from the stoss side of the adjacent ripple.
The *Lee side* is the steeply inclined part of a ripple extending downstream from the brinkpoint as far as the troughpoint.
The *Stoss side* is the gently sloping upstream side of a ripple extending from the troughpoint as far as the brinkpoint.
The *Slipface* is the steeply sloping portion of the lee side of a ripple, situated between the brinkpoint and the toepoint.
The *Bottomset* is the gently sloping distal part of a lee side located between the toepoint and the troughpoint.
The *Symmetry index* is defined as the ratio of the horizontal projection of the stoss side and the horizontal projection of the lee side.
(The term ripple represents a general term for ripple marks/transverse bedforms in the above section).

According to Reineck & Singh [1973] the flow pattern on the lee side of the ripple can be divided into three major hydrodynamically different zones (Fig. 7.12D & E). That part of the stream flow which carries sediment in suspension over and beyond the lee slope is the *zone of no diffusion* [Jopling, 1963; Reineck & Singh, 1973]. Beneath this zone is a mixing region which is not stable and which rolls up into the vortices; this is the *zone of mixing*. In this region

Fig: 7.12A & B Various terms used for the description of the bedforms. Profile is parallel to the flow, at right angles to the elongation of the ripple crest.

Fig: 7.12C Internal structures of a well-developed ripple.

Fig: 7.12D Flow pattern over a lee face of a bedform. Velocity distribution, flow separation, and three major zones on the lee side are depicted.

Fig: 7.12E Flow pattern and sedimentation processes on the lee side of a bedform.

Fig: 7.12F Effect of sorting in the foreset laminae. Two sorting processes are active: large particles are concentrated toward the outer side of a lamina under the influence of shear; under the influence of gravity, large particles are concentrated near the base of a lamina (based on Brush, 1965).

(after Reineck & Singh, 1973)

A

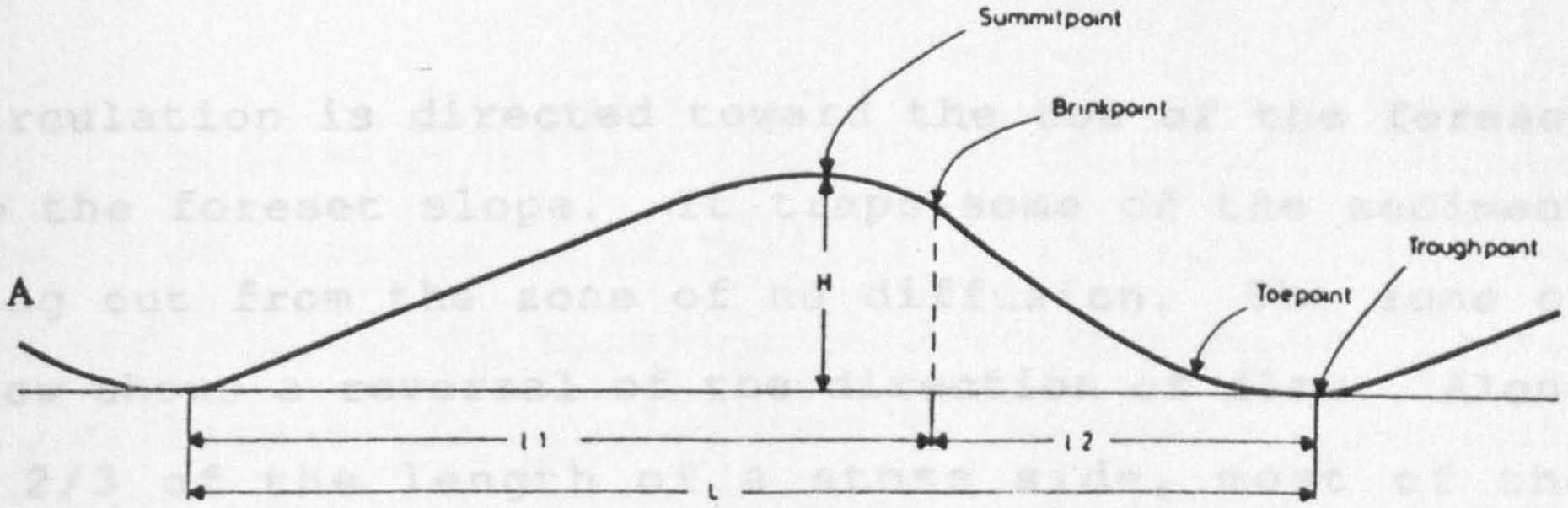
Summitpoint
Brinkpoint
Troughpoint
Toepoint
H
l 1
l 2
L

B

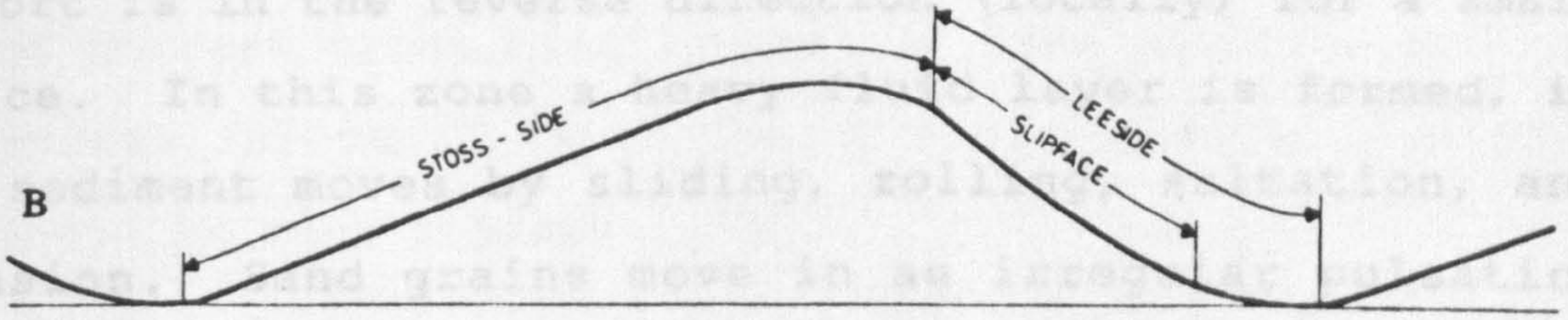
STOSS - SIDE
LEESIDE
SLIPFACE

C

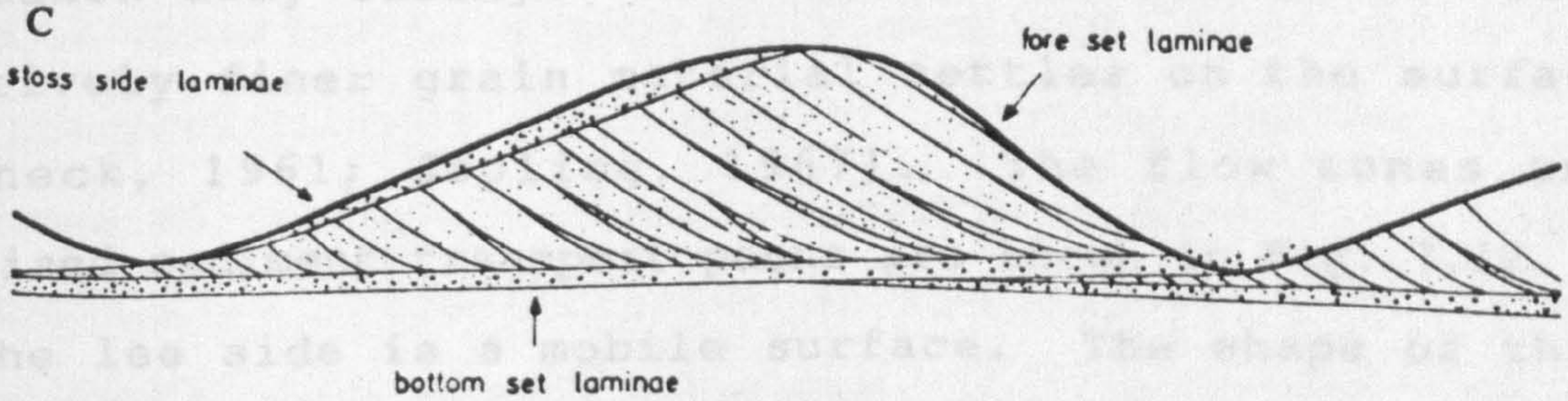
stoss side laminae
fore set laminae
bottom set laminae

D

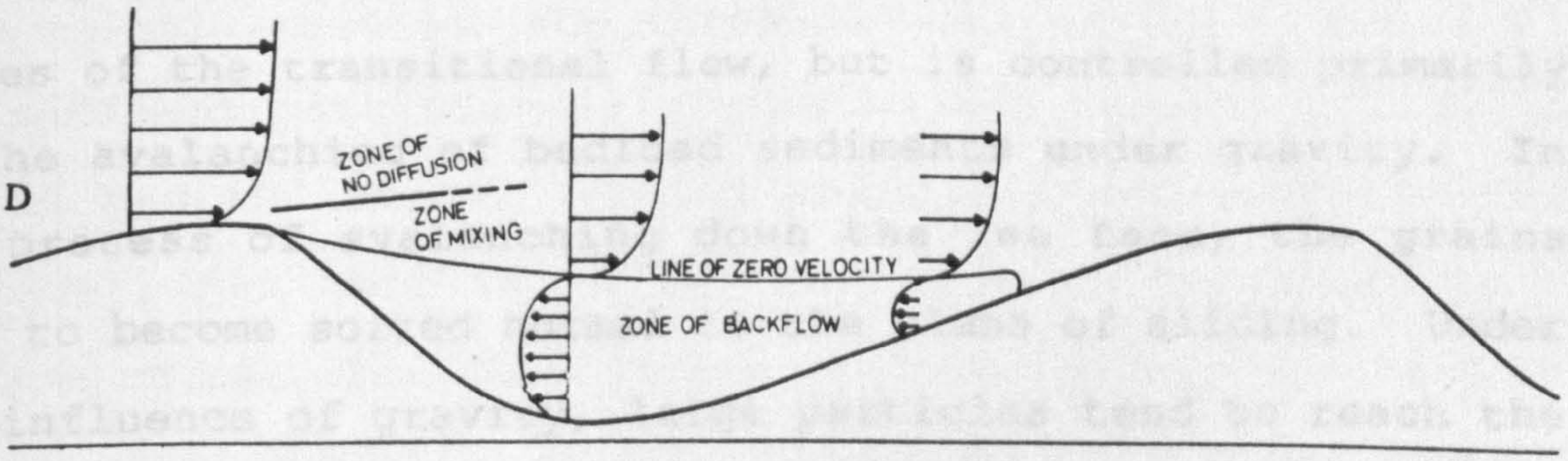
ZONE OF
NO DIFFUSION
ZONE
OF MIXING
LINE OF ZERO VELOCITY
ZONE OF BACKFLOW

E

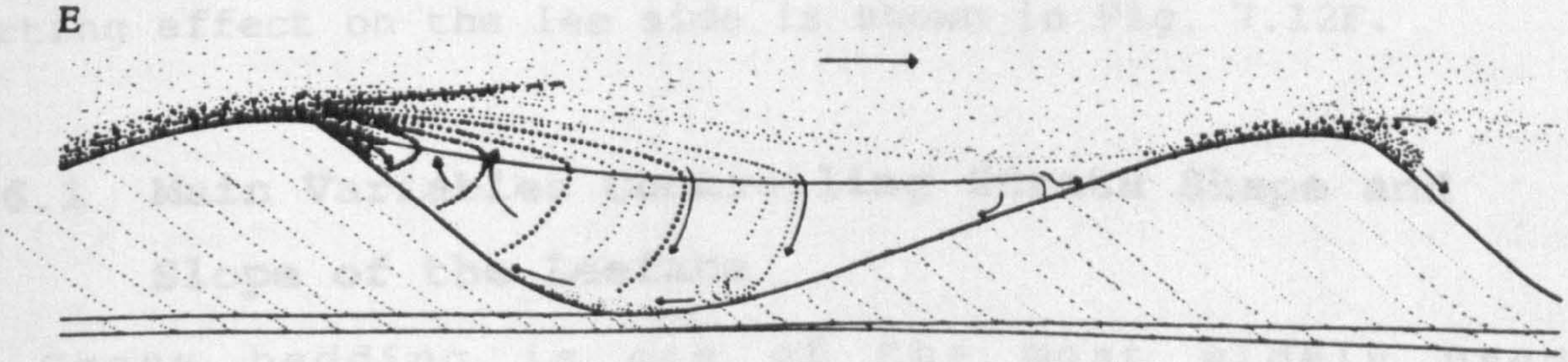

F

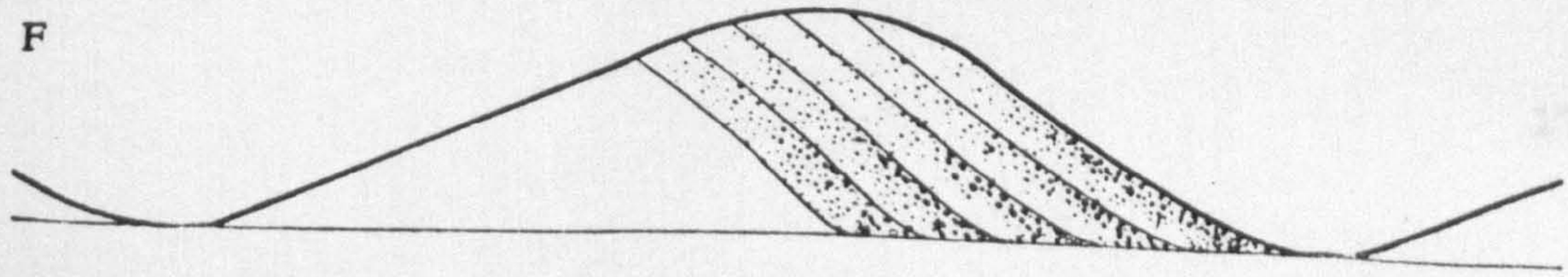

the circulation is directed toward the toe of the foreset and up the foreset slope. It traps some of the sediment settling out from the zone of no diffusion. The *zone of backflow* shows a reversal of the direction of flow. Along about 2/3 of the length of a stoss side, most of the transport is in the reverse direction (locally) for a small distance. In this zone a heavy fluid layer is formed, in which sediment moves by sliding, rolling, saltation, and suspension. Sand grains move in an irregular pulsating movement along the stoss side. At this stage coarse grains are taken away easily. As a result on the stoss side, relatively finer grain material settles on the surface [Reineck, 1961; Jopling, 1967]. The flow zones and idealised sediment transport paths are shown in Fig. 7.12.

The lee side is a mobile surface. The shape of this part of the transverse bedform is partly due to turbulent eddies of the transitional flow, but is controlled primarily by the avalanching of bedload sediments under gravity. In the process of avalanching down the lee face, the grains tend to become sorted normal to the plane of sliding. Under the influence of gravity, large particles tend to reach the bottom of the lee face in larger concentrations. The sorting effect on the lee side is shown in Fig. 7.12F.

7.6.1 Main Variables Controlling Strata Shape and Slope of the Leeface

Cross bedding is one of the most widely used palaeocurrent indicators [Collinson & Thompson, 1982]. So a

general introduction to its formation is required before discussion of results. The leeface is the most important part of the bedform in terms of bedform migration studies and is the main *cross bedding* generating area. Important variables controlling the shape of the leeface, and thus the shape of foreset cross bedding are: a) flow velocity and bed shear stress, b) depth ratio and c) sediment type [Jopling, 1963, 1965; Reineck & Singh 1973].

7.6.1.1 Flow velocity and bed shear stress.

Flow velocity is a specially meaningful parameter for the interpretation of environmental processes, because it is a measure of the dynamics of transport and deposition. From a quantitative hydraulic point of view, however, bed shear stress is the more useful parameter [Jopling, 1965]. As the flow velocity exceeds the threshold for particle movement, the sediment particles on a rippled bed 'creep' along the stream bed and deposit on the upper foreset slope of the bedforms. At this velocity, the rate of transport is a minimum and all transport takes place by bed-load movement. In this case sediments slip downslope from the upper foreset slope under gravity, forming angular cross-bedding. With increasing velocity a greater portion of sediment is taken into suspension and is transported up to the toeset sector at the base of the foreset slope. In this situation the angular contact with the bottomset is replaced by a tangential contact. With a further increase in velocity, a

greater portion of particles is carried in suspension over the front of the bedforms and the toe-set increases in size. The shape of foreset bedding changes with an increase in velocity from angular → tangential → concave. [Jopling, 1965; Reineck & Singh, 1973].

The total shear stress (τ) is equal to the product of the specific weight (δ) of the fluid, the hydraulic radius (R) of the stream, and slope (S) of the energy gradient ($\tau = \delta RS$). When the flow is uniform, it is approximately equal to the product of the specific weight, the stream depth (d) and the slope (s) of the streambed. In sediment transport, it is commonly assumed that the sediment transport rate along the bed is proportional to the shear velocity (u_*) of the sediment. More than the fluid velocity, it will carry particles farther beyond the lee face and therefore enhance the possibility of a tangential contact. The effects of an increasing shear are more or less parallel to those of an increasing velocity. However, direct proportionality between these variables does not exist [Rouse, 1946].

7.6.1.2 Depth Ratio

The depth ratio [Jopling, 1965] is the ratio of the depth of stream flow to the depth of the basin of deposition. Jopling [1965], during the flume experiment concluded that when the water is deep so that the depth ratio is small, the shapes of the laminae on the foreset are angular with steeper angles, whereas in shallow water i.e., high depth ratio, favours the development of tangential

units with gentle dips [Jopling, 1965].

7.6.1.3 Sediment Type

Settling velocity is directly related to size of the sediment particle. According to Jopling [1965], "the ratio of a characteristic flow velocity to the fall velocity (w) of the sediment particles is the fundamental parameter in the study of particle movement. In the hydraulic literature pertaining to sediment transport mechanics, shear velocity is commonly selected as a characteristic velocity because it is directly related to the tractive stress exerted on the streambed. The fall velocity on the other hand, is a measure of the resistance offered by the particle to movement". During flume experiments, he further assumed that the value of shear velocity, basin depth and the thickness of deposit remain constant. Under these restrictions, he studied sediment movement, keeping the sediment type a single independent variable. When the sediments are of coarse grade (high w), there may be little or no suspension transport ($w/u_* > > 1$) [Lane & Kalinske, 1939; Jopling, 1965], and the angular type of basal contact is characteristic for these conditions. However, suspension transport may be important for fine sediments under an identical shear stress, and so provides the possibility of formation of tangential type contact. McKee [1957] found that the foreset slope becomes steeper when the sand grains are coarser and angular, sorting is poor, and clay is

absent.

7.7 Materials and Methods

The study of internal sedimentary structures of unconsolidated sediments in the intertidal part of the study area was carried out by collecting undisturbed sediment samples by means of rectangular metal boxes (Senckenberg boxes). Structures were identified after impregnation with Araldite Resin (Araldite MY753) and Araldite Hardener (Araldite HY951). In this way a sedimentary peel (resin peel, high relief peel of Bouma [1969]) is formed which consists of a layer of about 1-2 cm thick of firmly bounded sediments [see Reineck 1957, 1961, 1967, 1972; Maarse & Terwindt, 1964; McMullen & Allen, 1964; Bouma, 1964, 1969; Reineck & Singh, 1973; Jago, 1974; Visser, 1980; Boersma & Terwindt, 1981a, b; Chakrabarti, 1984; Langhorne & Read, 1986; Terwindt & Brouwer, 1986; Mukherjee, Das, & Chakrabarti, 1987; Imperato, Sexton & Hayes, 1988; Sha, 1989; Frey, Howard & Dorjes, 1989; Jones, 1990]. The impregnation technique makes otherwise undiscernible structures quite visible, and accentuates already distinct structures.

7.7.1 Sample Boxes

The sample box is a rectangular metal (stainless steel) box with two parts, an open ended base and a cover. Any reasonable dimensions and pattern of a sampling box could be adopted [Reineck, 1960]. The size of boxes used in the

present study is 31cm * 21cm * 5.5cm which was found to be convenient for easy use in the field. The boxes were well cleaned to prevent any resistance which can cause sample disturbance.

7.7.2 Field Work

A comprehensive field plan was made to collect boxes from representative intertidal areas. Keeping the prime target of this study (estimation of sediment migration and transport directions) in mind, more attention was given to the sandwave fields because they are the clearest indicators of bedform transport in the area [Dalrymple, 1984; Terwindt & Brouwer, 1986]. The areas for box sample collection were initially determined from aerial photographs and sonograph map (Fig. 3.16). A summary of the field work conducted for this purpose is given in Table 7.1.

Table: 7.1 Summary of fields for box samples collection.

Fields	Date	Positions	Boxes	Tide
1	17 Jul 90	1-13	1-27	NT-4
2	4 Sep 90	14	28-42	ST-5
3	10 Jul 91	15	43-60	NT+6
4	26 Jul 91	16	61-79	St-5
5	7 Nov 91	17-25	80-98	St+3

The positions of samples are plotted in Fig. 7.13. Positions 1 - 14 were fixed by sextant, and all other

Fig: 7.13 Box Core Sampling Positions.

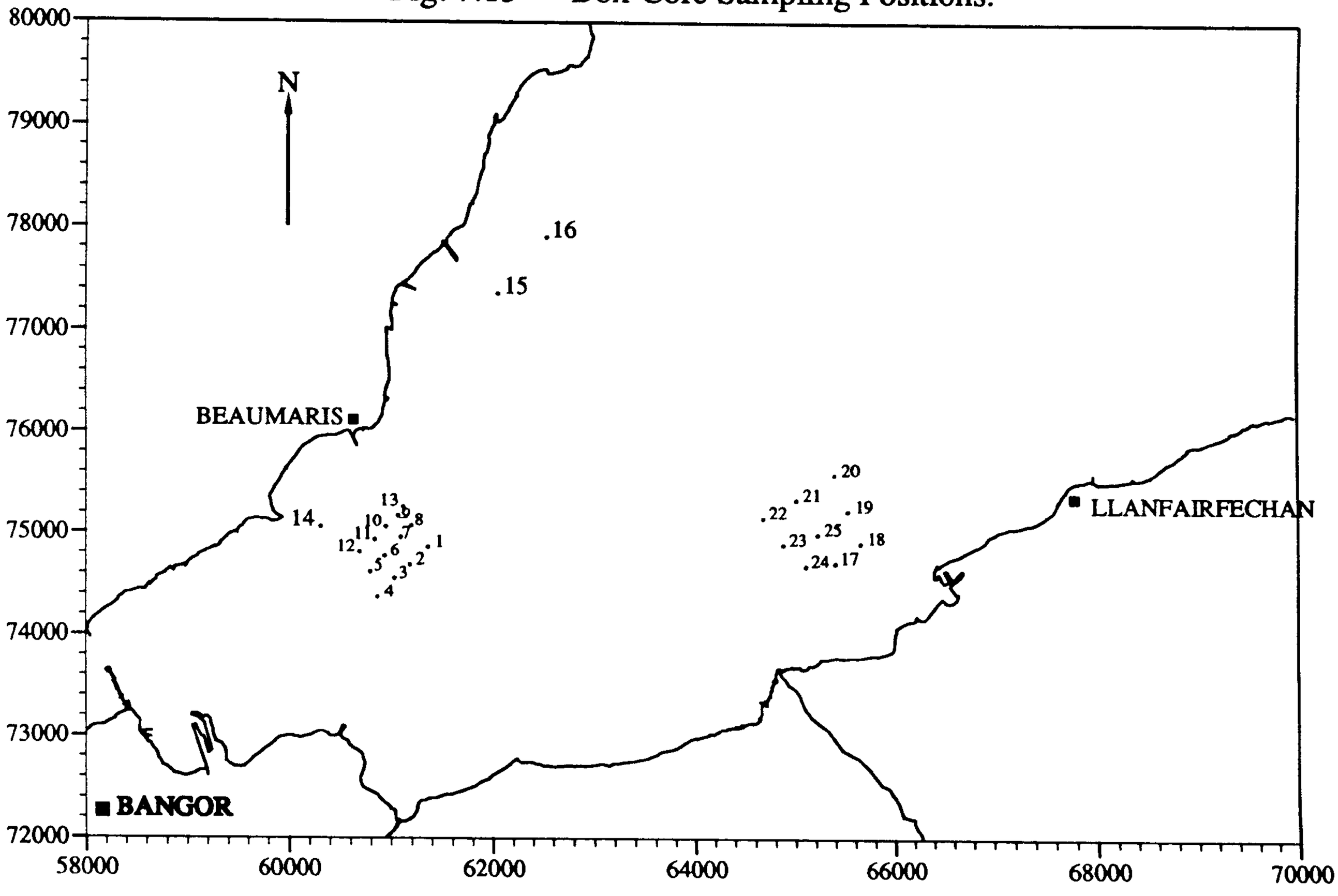

positions were located using a Global Positioning System (Raystar 920 GPS Navigator, Raytheon Marine Company). Bullcok [1988] and Reynolds [1990] forecast the GPS positional accuracies within ±1m, when this system will fully established. At Positions 1 - 12 and 17 - 25, a set of two boxes at right angles to each other was collected. At Position 13, three boxes in a line, parallel to the main channel, were obtained. At Positions 14, 15 and 16, boxes were taken on sandwaves in a straight line normal to the crestline. The boxes at Positions 14 and 15 were taken side by side. At Position 16, a trough to trough transect was covered with a length of 0.5m from the centre of a box to the centre of adjacent box. The layout of the box samples on these sandwaves in shown in Fig. 7.14.

Sampling (15 boxes) at Position 14 was carried out after ST-5. The measured wavelength and height of the sandwaves were 7.42m and 0.34m, respectively; a line of 1.72m on the stoss side and 2.1m on the lee side was covered. One box each at right angles to boxes 30 and 41 were taken to study the structures in three dimensions.

A total of 18 boxes was collected at Position 15. The wavelength and sandwave height at this location were 8.9m and 0.38m, respectively The shape of the sandwave was symmetrical with superimposition of ebb oriented ripples. A line of 1.8m on each side of, and at right angles to, the crest was covered and one box was taken parallel to the crestline at the crest.

Fig: 7.14
Layout of box sampling on sandwaves at Position 14 (A), Position 15 (B) and Position 16 (C).

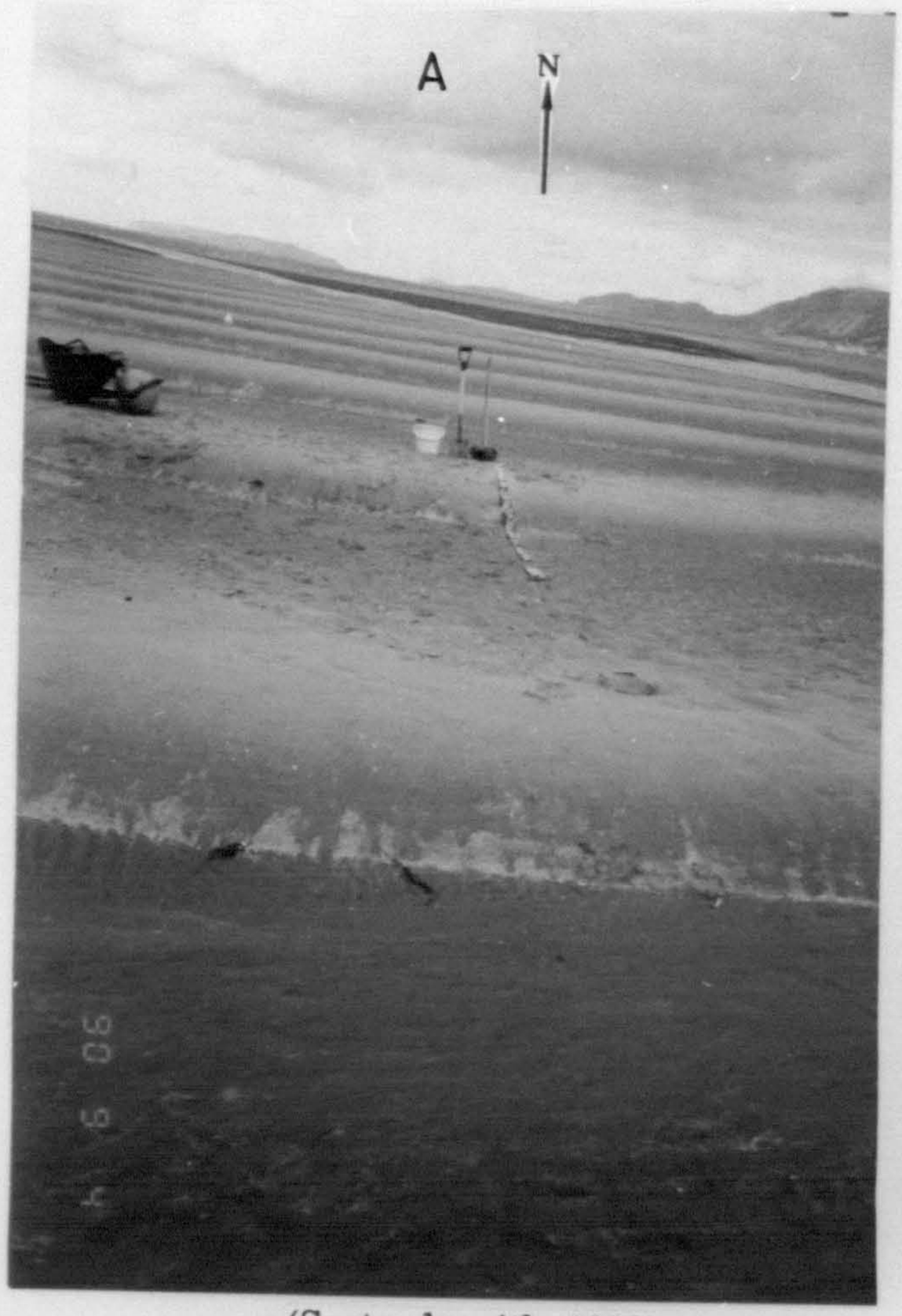

(September 4th, 1990)

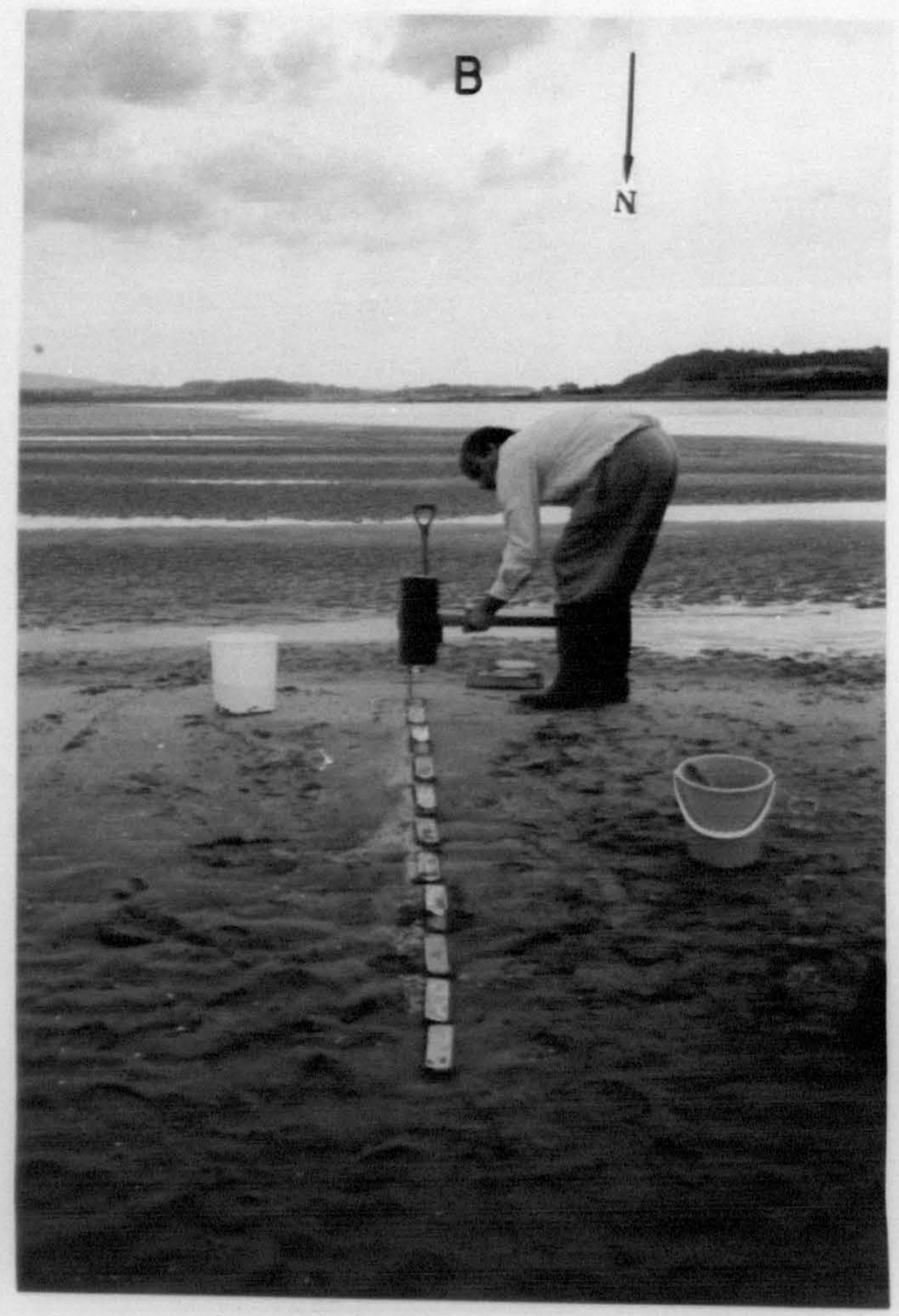

(July 10th, 1991)

(July 26th, 1991)

The sandwaves at Position 16 had 8.5m and 0.40m wavelength and height, respectively. A trough to trough transect was covered by 15 boxes and two further boxes were taken parallel to the crestline at the crest.

7.7.3 Box Sampling Procedure

Box cores were taken with the open ended base in a vertical position with a predetermined orientation. The base is forced carefully, smoothly and vertically, until it is completely inserted in the sediment. At some locations, where there were shells or it was hard to push manually, the box was gently tapped with a rubber tip hammer. The cover was placed over the base and it was pushed down. The box was removed by digging with a spade. The cover was taken off and dry sand packed where required to fill the gaps, and then the cover was replaced in its original position. The positions of boxes with open sides facing towards the south-east and parallel to the coastline were suffixed by "A", and boxes with open sides towards the north-east and perpendicular to the coastline were denoted with suffix "B". Boxes were transported to laboratory with care to avoid any disturbance.

7.7.4 Laboratory Work

In the laboratory after about 24 hours the boxes were opened. The cover was removed by sliding it off the base and putting it under the base, leaving only the upper side of the box exposed. About 1-2 cm of the surface sediment

was scraped off with a sharp knife, leaving about 1/2 cm of sample along the rims to avoid direct contact of adhesive with the box. The surface of the sample was smoothed and levelled. Boxes were then oven dried at 50°C for about 48 hours.

A mixture of about 200 ml of Araldite MY 753 and Araldite HY 951 with a ratio of 5:1 was used to impregnate the sample. This mixture was poured when the sample in the box was still slightly warm. The ratio and volume of the mixture was determined on the basis of best results (visually) after a number of trials. The impregnated samples were stripped off the box about 48 hours after the Araldite pouring. The orientation, position numbers and date of box coring were marked on the sample. The resin peel was then cleaned with a brush; some were washed with water. Finally the peels were photographed to keep a permanent record of sedimentary structures.

Before interpretation and discussion of the internal sedimentary structures of bedforms preserved in the box cores, the following section is devoted to a discussion of the response of internal structures to variations of current speed and direction during a single tidal cycle. In the present study, changes in internal structures under the influence of tidal current are based on the model of Boersma & Terwindt, [1981a, b] and Kohsiek & Terwindt, [1981]. During a dominant tide, reactivation, full vortex and

slackening structures are the most commonly occurring structures in the tidal bundle. But in a subordinate tide, erosional surfaces and ebb caps are the main structures in a tidal bundle.

7.8 Tidal Bundles and Pause Planes

A lateral succession of cross-strata, generated during a single dominant tide is called a *tidal bundle* [Boersma, 1969; Boersma & Terwindt, 1981a]. Allen [1980c] described this as *master bedding*. The characteristic feature of the tidal bundle is that it has laterally enclosed gently sloping erosional or non erosional surfaces, representing the stand-still phases of bedform migration. These pause planes are also called *reactivation surfaces* [Klein, 1970], *bounding surfaces* [Collinson, 1970] and *bed contacts* [Collinson & Thompson, 1982]. In areas such as estuaries, where there are comparatively large amounts of suspended mud, the more appropriate term for this surface may be *mud drape*. Variations in thickness of successive bundles reveal a periodic pattern that follows from periodically varying conditions. The bounding surface [McKee & Weir, 1953] separate the set of strata within the bedform from underlying strata and is the result of movement of the trough.

The two main factors controlling tidal bundles are sediment texture and hydrodynamic conditions [Terwindt, 1981]. Among hydrodynamic conditions, tidal currents are most important in the study area. Generally a change in

magnitude of the tidal currents in any area may be due to: the diurnal inequality of the tide; the neap/spring tidal cycle with high and low tides alternating; extra inflow or outflow due to wind setup or setdown; and configuration of the tidal area [Terwindt, 1981]. These variations in current strength effect the pattern of internal structures.

7.8.1 Structural Response to the Dominant Tide

On the basis of current strength, Boersma & Terwindt [1981a, b] described three structural intervals within tidal bundles arranged in a lateral sequence during a single tidal cycle (Fig. 7.15). Sedimentary structures formed in these intervals by the dominant tide in a cross-stratified bedform are:

1- Reactivation Structures

2- Full Vortex Structures

3- Slackening Structures

7.8.1.1 First Interval: Reactivation Structures

Reactivation structures represent an acceleration of the flow at the onset of the dominant tide. This interval can be divided into three sub intervals.

(i) As the tide turns shortly after slack water, the currents are comparatively weak. When the currents exceed the threshold velocity, ripples migrate along, as well as across, the resident sandwaves. Under these currents indistinct crinkled

lamination, and occasionally small scale cross bedding, form. The typical form of this subinterval is shown as D1 in Fig. 7.15.

(ii) In this subinterval, small ripples start moving first parallel, then perpendicular to the crest of sandwave. The leeface angle is smaller than the angle of repose of the material, which may have been more or less degraded by the previous subordinate tide. Because of this lower lee side angle, ripples reaching the summitpoint will not feed their material to an avalanche and so they retain their identity (Fig. 7.15; D2). High flow strengths at this stage can produce cross bedding.

(iii) At this stage the slipface angle will build up to the angle of repose. Ripples reaching the summitpoint lose their material to avalanches. Cross beds produced at this subinterval are still imperfect as they tend to be suppressed by relatively larger amounts of material falling out from suspension on the slipface. This suspension is due to imperfect flow separation which only gradually develops into a vortex. Grain size grading in foreset bedding is poor at this stage.

The above three events constitute the pre-vortex acceleration stage and a fully developed sandwave is reactivated during this sequence. Reactivation structures are shown in Fig. 7.17.

Fig: 7.15

Succession of events during a single tide: flow pattern and associated structures (after Boersma & Terwindt, 1981a).

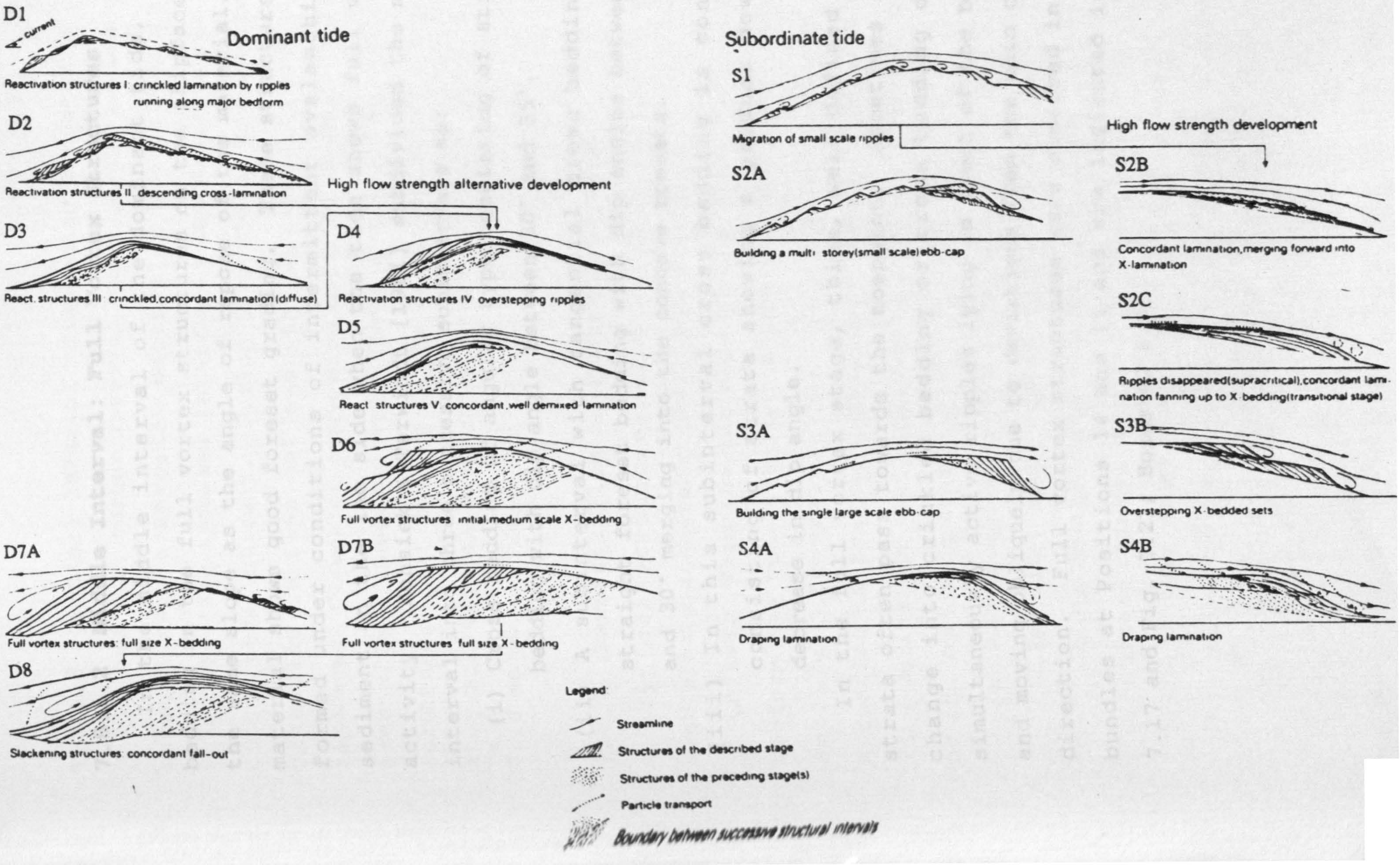

7.8.1.2 Middle Interval: Full Vortex Structures

In the middle interval of the dominant tide, cross bedding in the full vortex structures on the slipface have the same slope as the angle of repose of the material. The material shows good foreset grading. These structures are formed under conditions of intermittent avalanching of sediment on the lee side when the tide shows full vortex activity. Kohsiek & Terwindt [1981] subdivided the middle interval into three successive subintervals as:

(i) Cross bedding of angular type consisting of straight bedding with dip angle between 30° and 35°.

(ii) A subinterval with tangential cross bedding and straight foreset bedding with dip angles between 25° and 30° merging into the concave toesets.

(iii) In this subinterval cross bedding is concave, consisting of strata showing a gradual downward decrease in dip angle.

In the full vortex stage, thick, well defined cross strata often pass towards the toepoint. Sometimes strata change into crinkled bedding or cross bedding due to simultaneously active ripples lying in front of the bedform and moving obliquely due to deviations from the main current direction. Full vortex structures were observed in tidal bundles at Positions 14 and 16 and are indicated in Fig. 7.17 and Fig. 7.21; Boxes 62 & 63.

7.8.1.3 Terminal Interval: Slackening Structures

In the full vortex interval, some of the sediments are brought into suspension because of the higher current velocity. The terminal interval is the deceleration stage of the tidal current. During this stage, suspension load gradually settles out over the lee side trough of the sandwave. Clouds of suspension material deposit in the toe area with a progressively lower angle. The slackening structures start forming in the deceleration to slack water stages. Typical slackening structures are shown in Fig. 7.15 as D8.

7.8.2 Reversal Flow in Subordinate Tide

Typical structures of a bedform produced in the subordinate (generally ebb) tide are shown in Fig. 7.15 as S1 to S4B. When the lee side of the basic flood-oriented bedform has been reworked during the ebb tide, forming a small ebb foreset slope, it is called an 'ebb cap'. According to Boersma & Terwindt [1981a], reversal of the flow during the next subordinate tide may have one or more of the following stages.

(i) Accentuation of the pause plane by erosion at the lee side, as it converts into a stoss side. The dip angle of the pause plane in this erosional stage is lower than the angle of the underlying foresets.

(ii) At this stage, generation of upslope and obliquely climbing ripples on top of the pause planes gives rise to opposite ripple forsetting and crinkly

bedding.

(iii) An ebb cap formed on top of the sandwave, when ripples override each other along horizontal or descending planes, over the crest.

Caps formed in the reversed flow can be in the form of small scale cross bedding, overriding each other (Fig. 7.15; S2A) or large scale cross bedding (Fig. 7.15; S3A). Larger caps are the result of stronger currents and may display a lateral sequence of reactivation and full vortex structures. These structures can be compared with the dominant tide structures, described above.

Among the pause planes, erosional pause planes are easily recognisable because of their erosional nature and because they occur between distinct slackening and reactivation structures. By contrast, non-erosional pause planes are comparatively difficult to identify because they occur in a concordantly deposited succession of slackening and reactivation structures.

7.9 Bioturbation

According to Frey, Howard & Dorjes [1989], physical and biogenic sedimentary structures tend to be distinctive end-members in the continuum of coastal energy levels, especially where rates of sediment accumulation are low [Nittrouer & Sternberg, 1981]. In coastal areas, the water depth at which the boundary between biogenic structures and physical structures generally occur is related to wave

characteristics (i.e., wave height and wave length) [cf. Jago & Barusseau, 1981; Howard & Reineck, 1981]. Most of the box peels at positions 1 - 13 and 17 - 25 in their subsurface parts are bioturbated to a variable degree. Bioturbation in these peels is estimated and presented according to the verbal scale of Frey & Pemberton [1985], as:

Nomenclature	Degree of Bioturbation (%)
Essentially unbioturbated	<1
Very slightly bioturbated	1-5
Slightly bioturbated	5-30
Moderately bioturbated	30-60
Highly bioturbated	60-90
Intensely bioturbated	90-99
Completely bioturbated	100

7.10 Interpretation of Internal Sedimentary Structures

In quantifying sedimentary structures, the percentage distribution of different types of structures in each box core has been calculated [Jago & Hardisty, 1984; Mukherjee, Das, & Chakrabarti, 1987]. The principal types of structures encountered in the cores are cross bedding (small scale, large scale, festoon-shaped, herringbone type) [Reineck & Singh, 1973] and bioturbation [Frey, Howard, Han & Park, 1989]. Random events such as storms or atmospheric pressure changes can disturb the thick-thin alternations of tidal bundles. A thick bundle is defined as one in which

the thickness is more than the mean of the two adjacent bundles, and a thin bundle is one in which the thickness is less than this mean [De Boer, Oost & Visser, 1989]. Large scale cross bedding has been defined as cross sets with thickness more than 2cm and is comparable to the 'downcurrent-dipping cross stratification' of Banks [1973], and the 'inclined cross bedding and large scale foresets of Dalrymple, [1984].

From the physical sedimentary structures studied in the core, the percentage of bedform migration in the flood and ebb directions have been estimated.

Positions 1 - 13

The measured sedimentary structures at these positions are given in Table 7.2. The thickness of laminae increases toward the Menai Strait channel, probably as a consequence of increasing bedload transport. The dominant dip of the cross bedding in this area is in the flood direction. At most of the locations whole shells of intertidal organisms are embedded in the sands. In some of the cores the bedding is slightly modified on the top of shells. The subsurface structures are destroyed because of bioturbation. The percentage of reworked sediments due to bioturbation in each box peel is given in Table 7.2. An estimate of percentage of transport at positions 1 - 13 is made by assuming that the recorded cross beds show a 100% transport. Cross bedding in this area is of the small scale type. Laminae

thickness in the peels of boxes 1 - 14 were measured as 1-3mm. But the laminae nearer to the Menai channel (peels 15 - 27) range from 2mm to 4mm. The dominant direction of migration of the bedforms is to southwest based on the cross bedding directions of the core peels.

Percentages of reworked sediment vary from place to place. On positions 1 - 13, the percentage of bioturbated sediments generally increased to the South-West (see Fig. 7.16 with reference to positions in Fig. 7.13) Bioturbation characteristics were variable and largely related to the types of organisms inhabiting the sediment. The most probable control seems to be grain size, which decreased to the south west, and a slightly increased exposure time at low tide. A similar trend is observed in the cores at positions 21 - 25. Increased peel percentage of bioturbation may also indicate decreased rates of sediment accumulation [Frey, Howard, Han & Park, 1989].

Fig: 7.16
Sedimentary structures preserved in box peels at Positions 1-13 (for detail see text; fig. continue to next page).

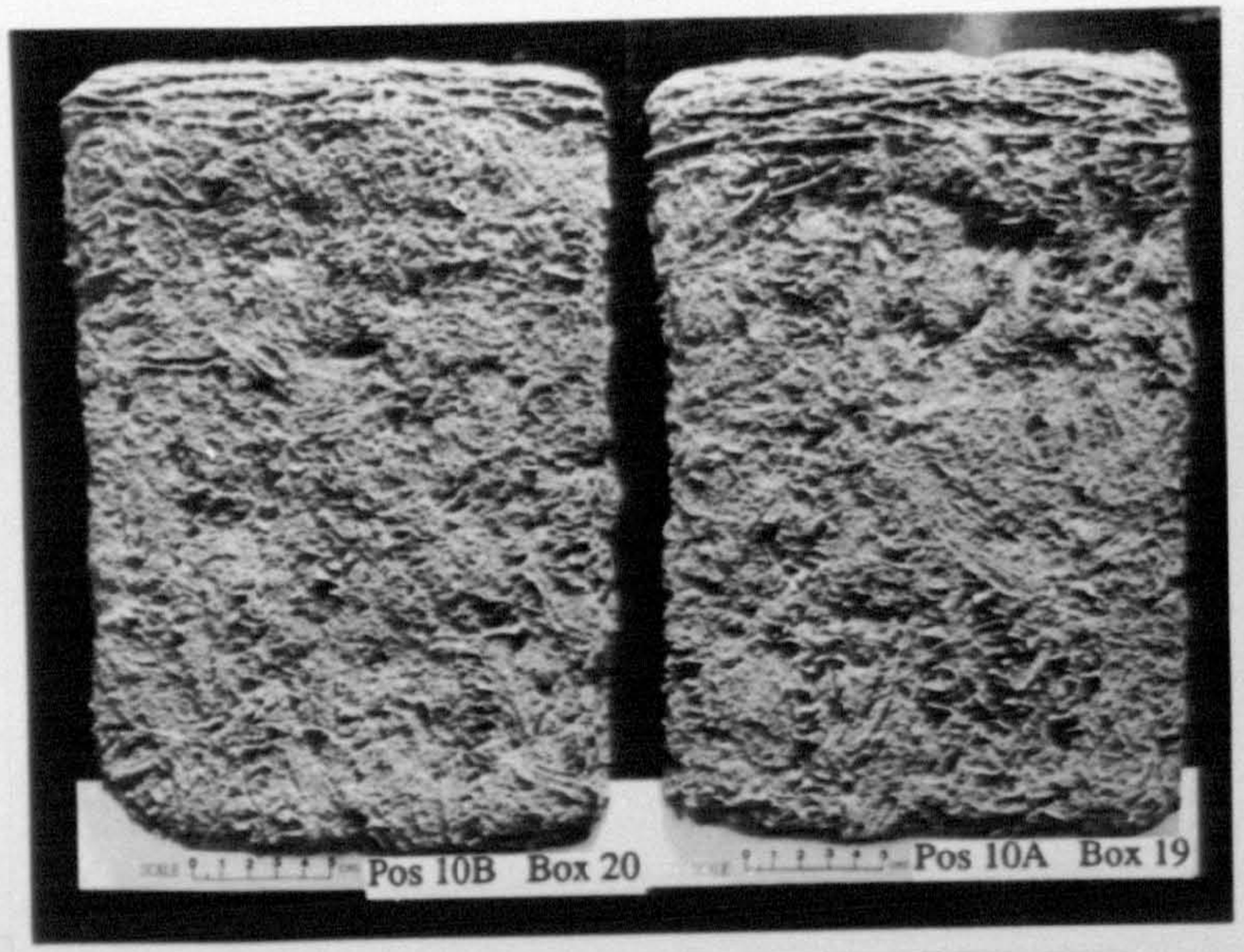
Pos 10B Box 20

Pos 10A Box 19

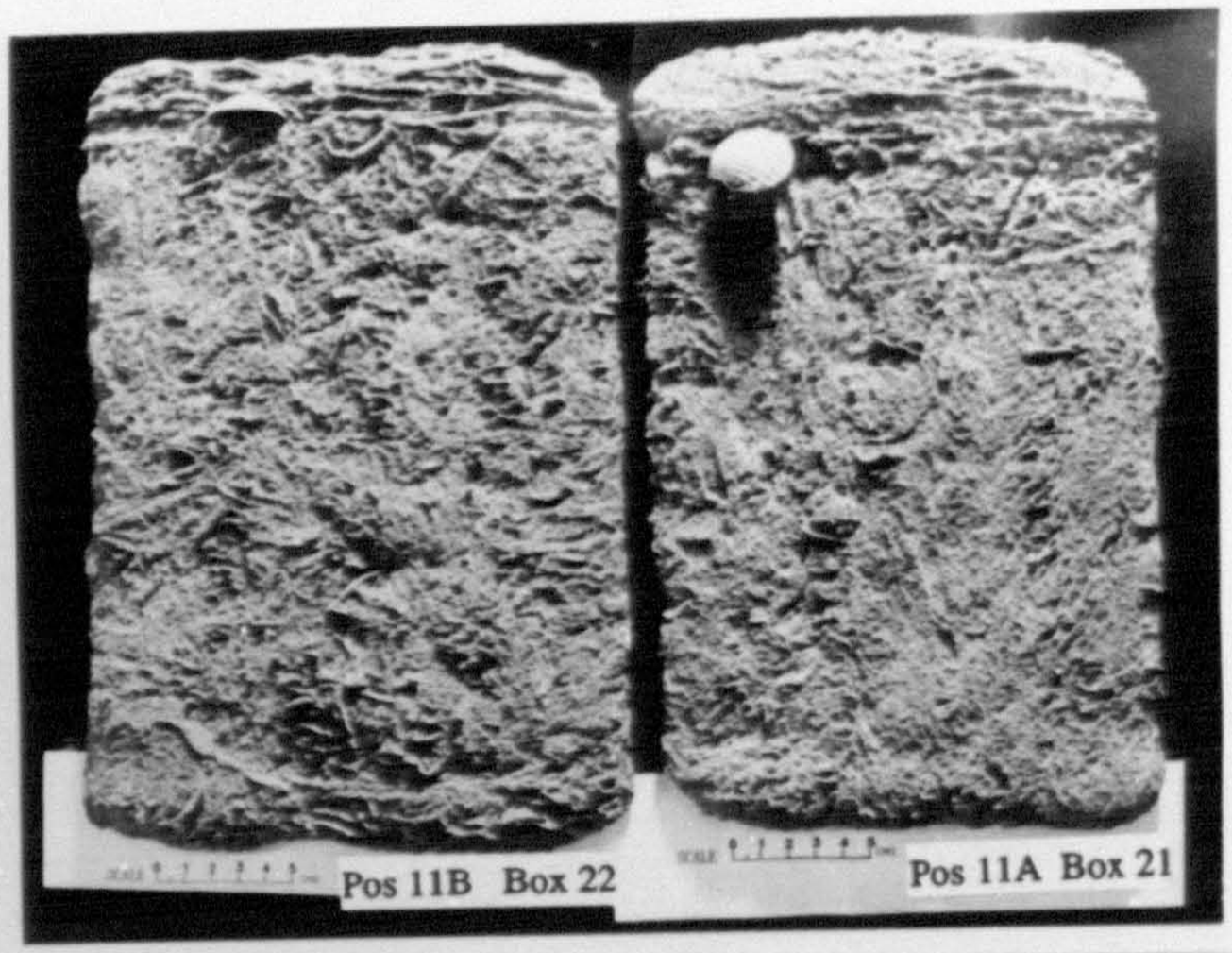
Pos 11B Box 22
Pos 11A Box 21

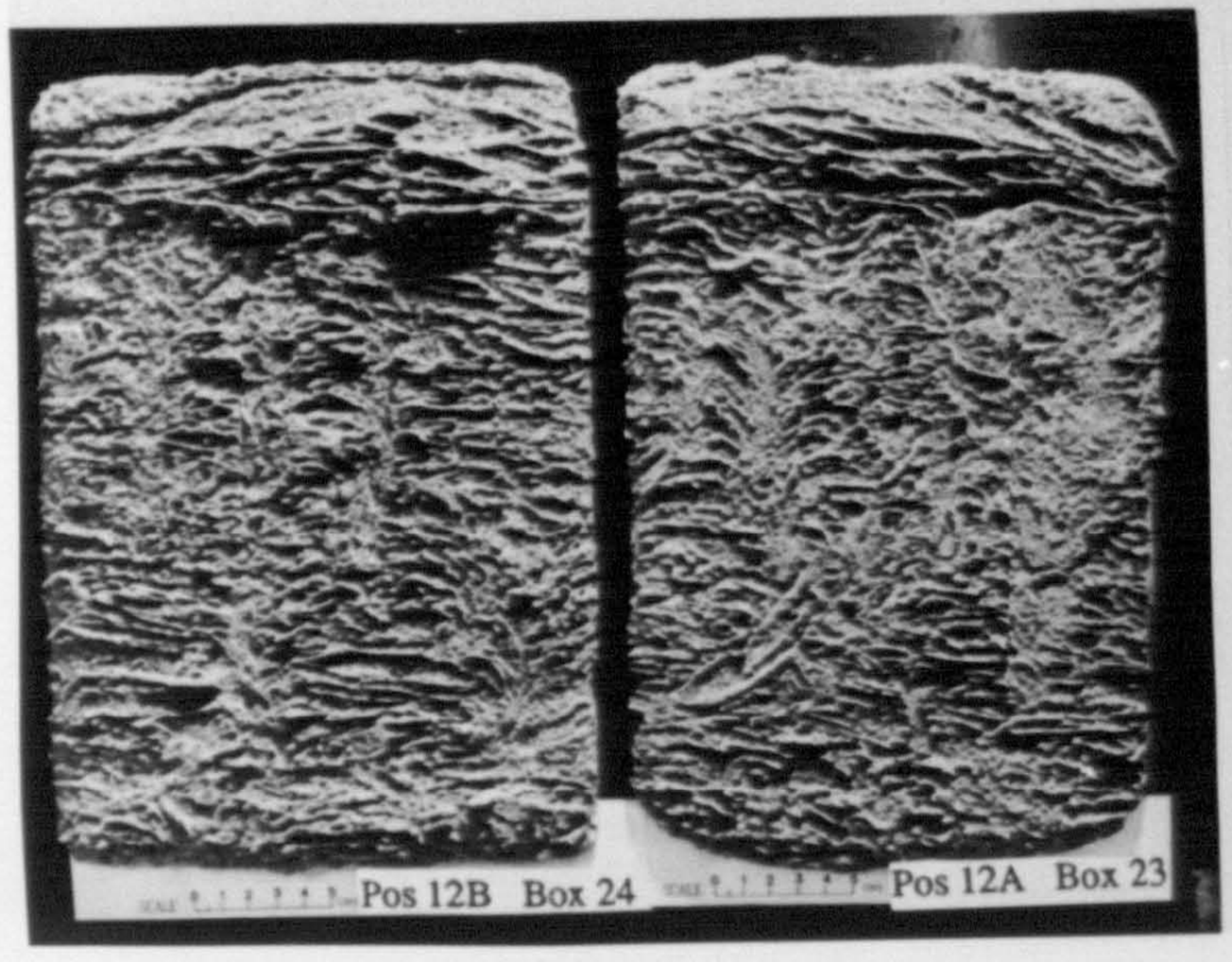
Pos 12B Box 24
Pos 12A Box 23


Pos 13A Box 25
Pos 13A Box 26
Pos 13A Box 27

Table: 7.2 Quantitative analysis of sedimentary structures at positions 1-13 measured from the resin peels.

Pos. No.	Box No.	X-bedding direction (% of core) Flood	Ebb	Other	Bioturbation (% of core)	Degree(%)
1A	1	48	38	-	14	>60
2A	3	12	8	49	31	>95
3A	5	64	11	-	25	>95
4A	7	5	-	13	82	>95
5A	9	17	-	-	83	>95
6A	11	14	-	13	73	>90
7A	13	33	9	7	51	>95
8A	15	19	8	39	34	>90
9A	17	38	-	-	62	>95
10A	19	11	-	-	89	>90
11A	21	15	-	-	85	>90
12A	23	18	-	-	82	60-90
13A	27	-	-	12	88	>90
		59	15	26		

Position 14

The flood lee side was almost unmodified and over this sandwave superimposed ebb-oriented ripples were observed at troughs. The angle between the crestlines of ripples and sandwaves was about 40°. Towards the channel these ripples were well developed. Near the channel, the sandwaves had ebb-oriented leefaces but the flood leeface was still pronounced (Fig. 7.5A). During the flood tide the structural responses of the tidal current in the form of reactivation, full vortex and slackening structures are determined in the lateral sequence. Internal sedimentary structures of this sandwave are shown in Fig. 7.17. The

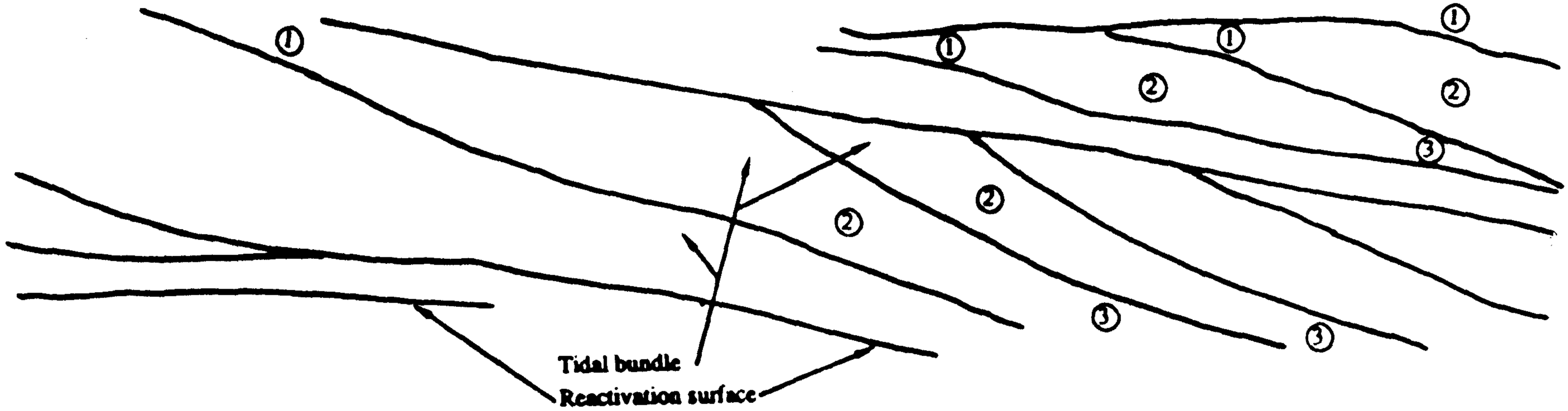

① Acceleration stage
② Full vortex stage
③ Deceleration stage

Fig: 7.17

Section of a sandwave at Position 14 according to box core sampling layout, showing internal structures.

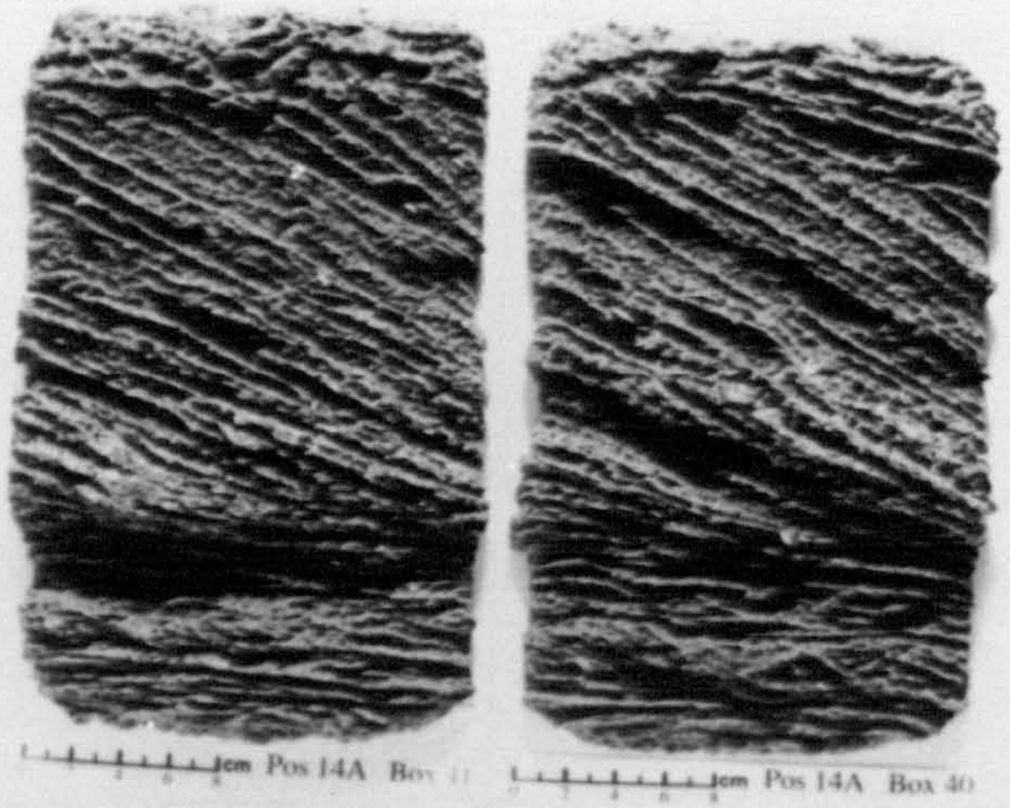

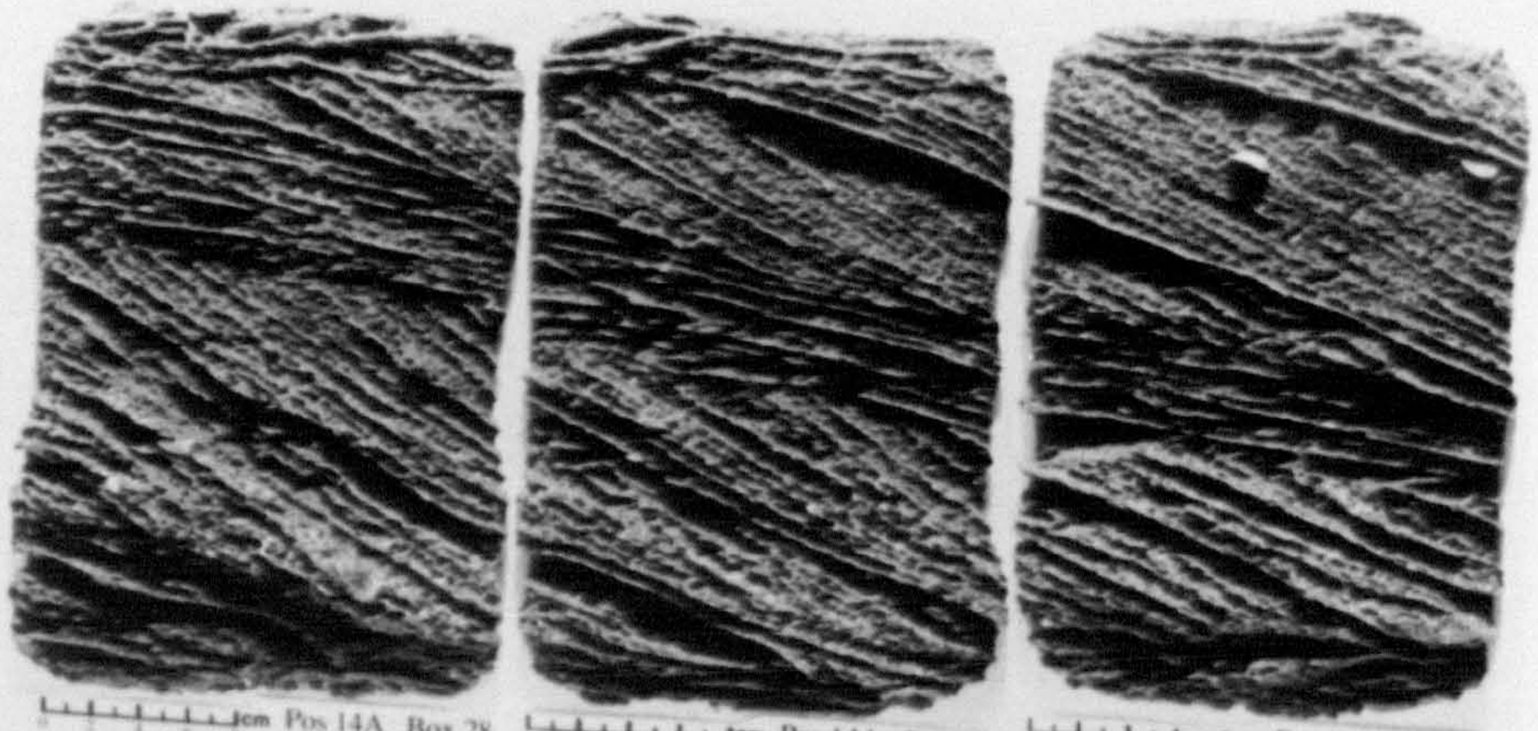

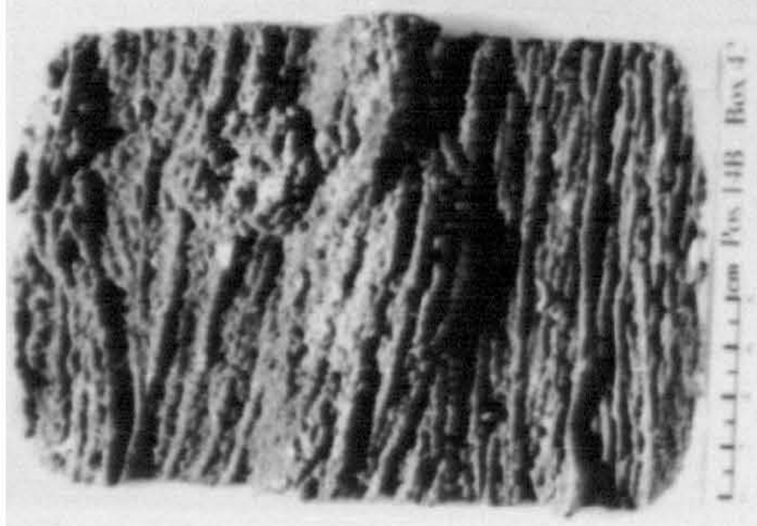

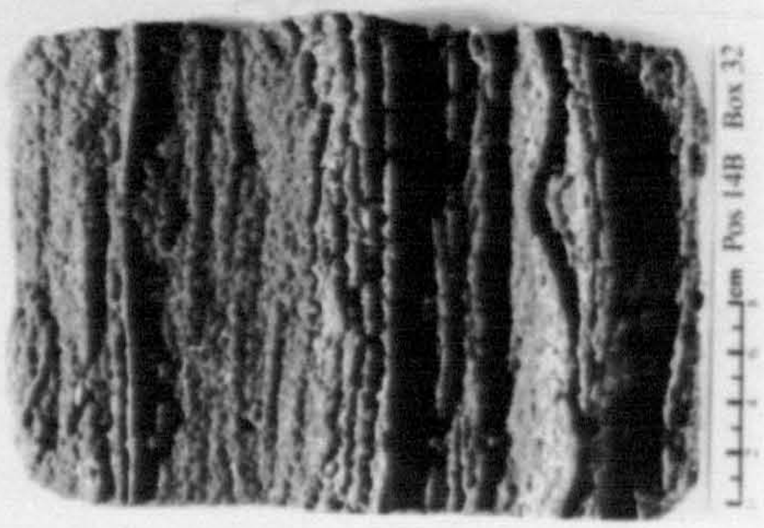

Fig: 7.17

Section of a sandwave at Position 14 according to box core sampling layout, showing internal structures.

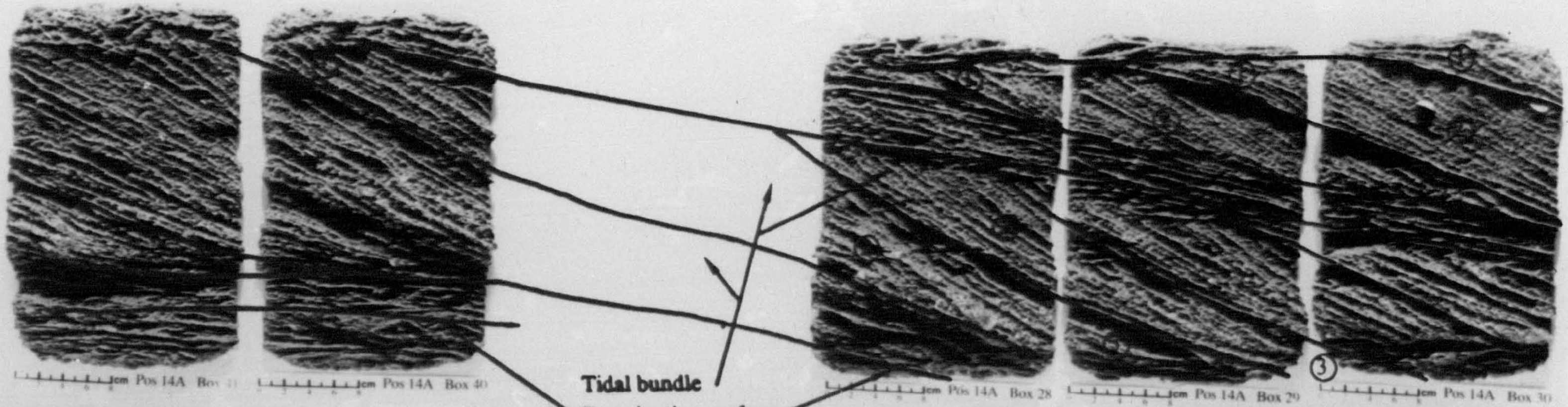

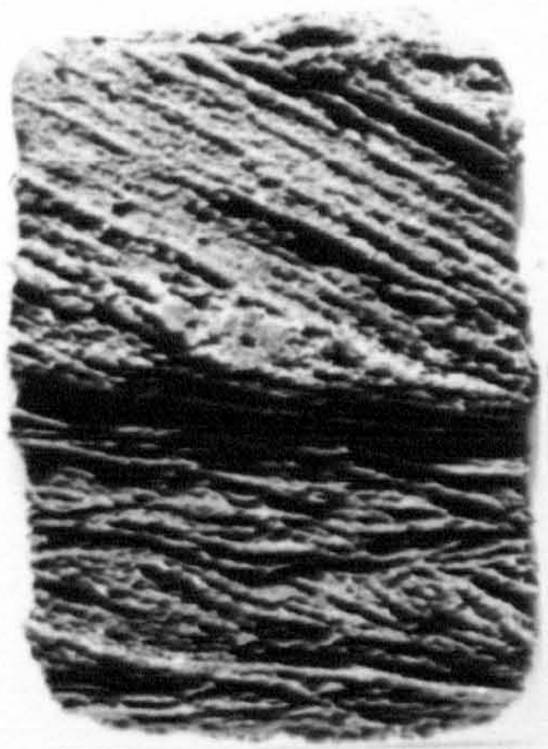

cm Pos 14A Box 33

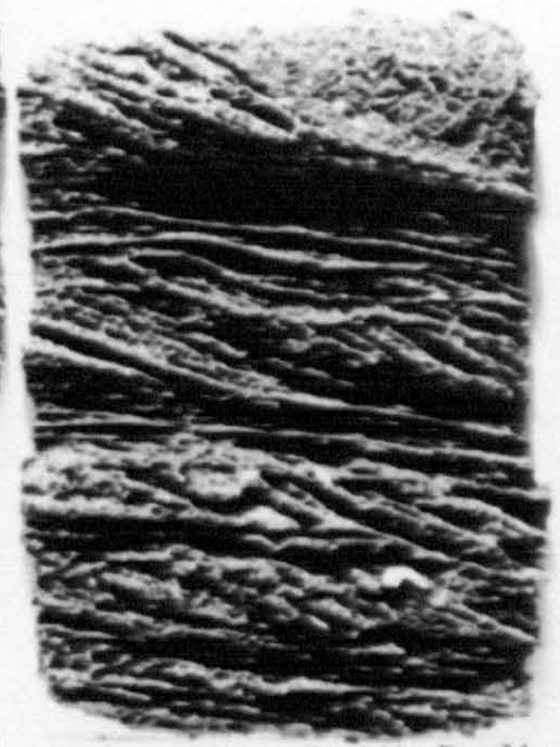

cm Pos 14A Box 34

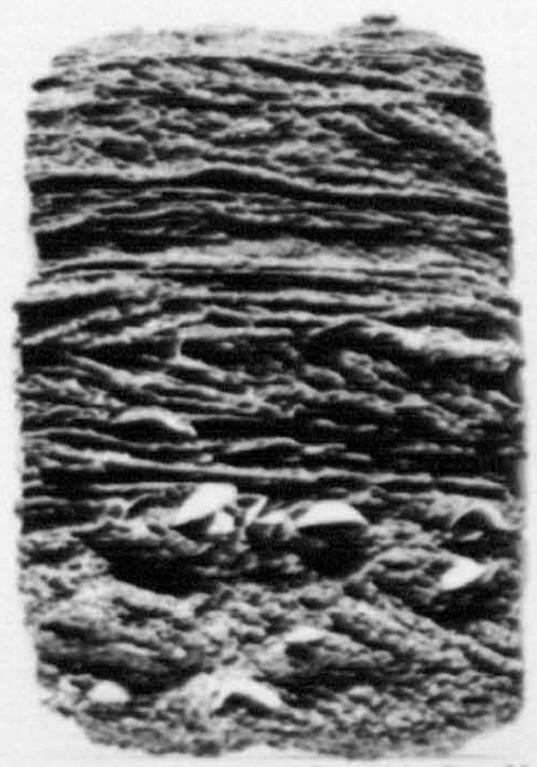

cm Pos 14A Box 35

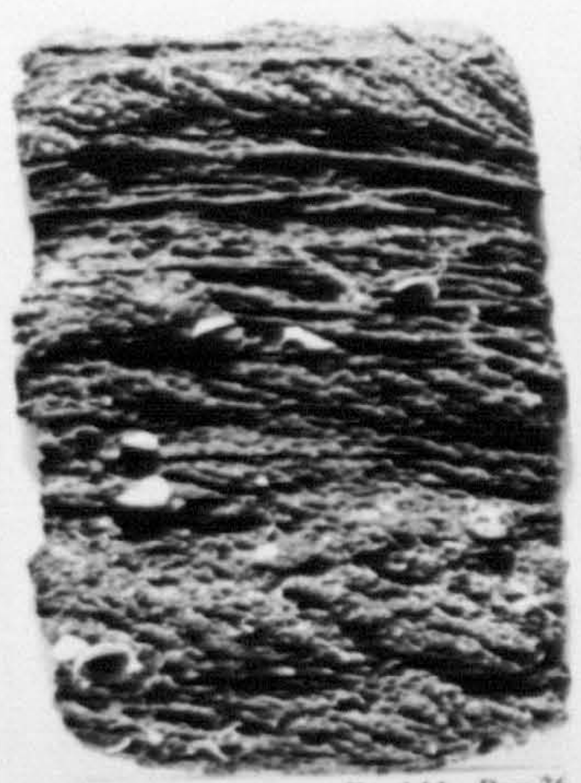

cm Pos 14A Box 36

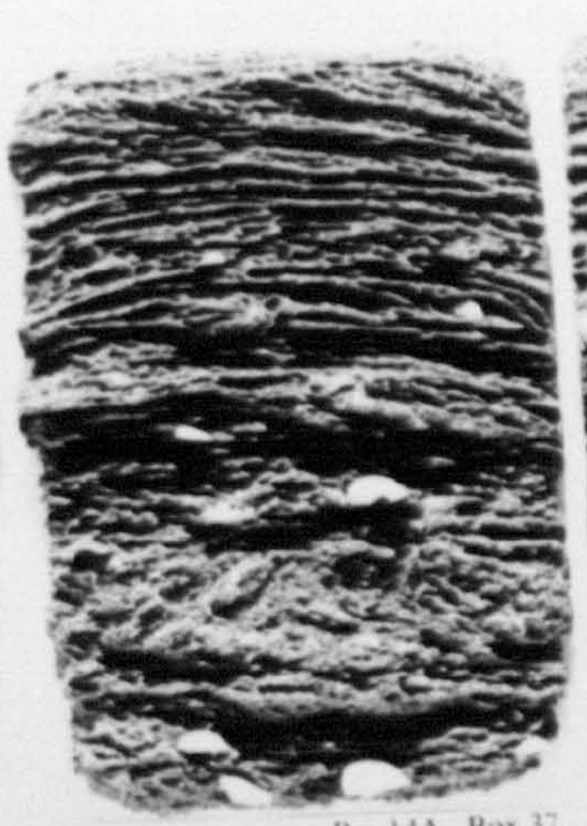

cm Pos 14A Box 37

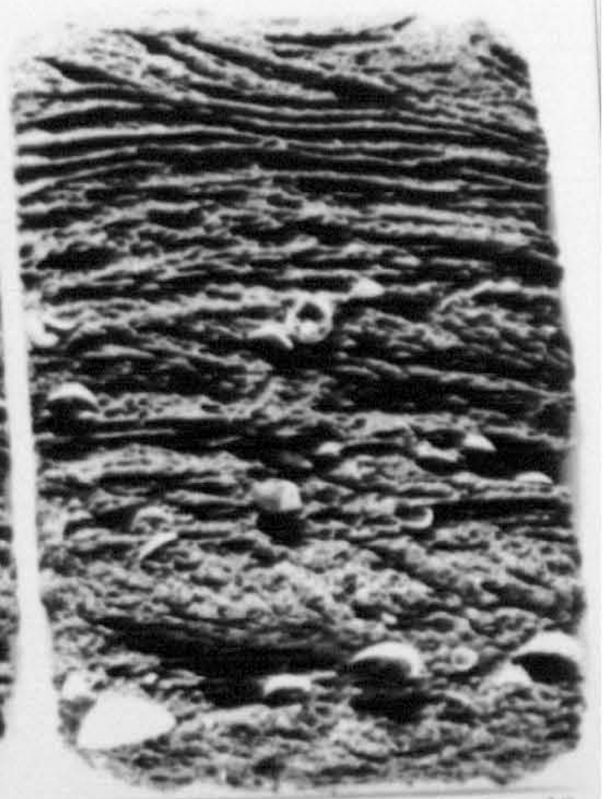

cm Pos 14A Box 38

cross bed dips on both stoss and lee sides indicate a bedform migration in the flood direction. In the trough (Boxes 35 - 38), the bedding was at a low angle; similar trough structures were noted by Jones [1984] on sandwaves at the other end of the Menai Strait, but with an ebb orientation. The interpretation of these structure is shown in Fig. 7.18.

The lateral variation in thickness of tidal bundles represents the spring/neap/spring sequence. From the left edge of the section (Fig. 7.18), the decrease in tidal bundle thickness shows part of the spring to neap tide sequence. Some of the bundles are marked with predicted tides with reference to the tide prior to sampling (ST-5). The bundle marked NT+6 is very different in shape from the adjacent bundles. The most probable reason is meteorological effects which can cause distortion in the neap/spring sequences [Langhorne, Malcolm & Read, 1985]. Daily weather summaries of the week prior to coring (4 September 1990), show a westerly front and a sudden change in weather over this area on 2 September (which was otherwise fair). So the flattened profile of tidal bundle NT+6 probably results from wind generated waves in the shallow water due to the aforementioned weather change [Daily Weather Summary 29th Aug. to 4th Sep. 1990].

The large scale cross bedding at position 14 shows a predominance of flood tide cross bedding and mostly forms on the lee side of the sandwaves as they migrate forward. On

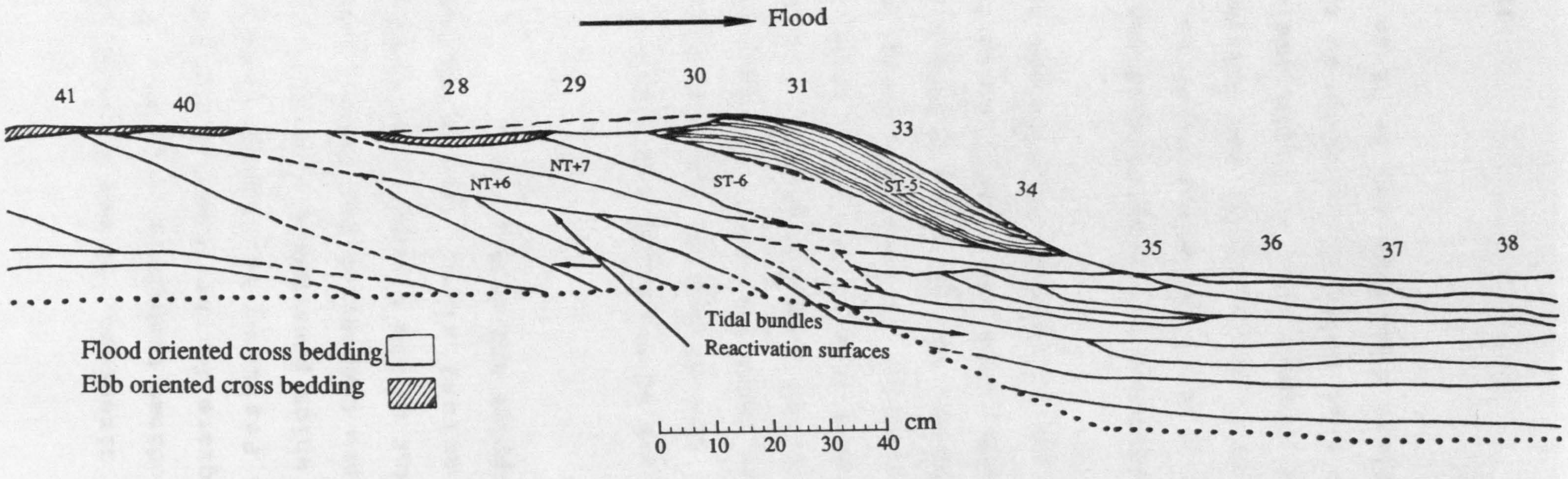

Fig: 7.18
Interpreted section showing internal structures at Position 14. Drawn from box peels; labels are box numbers.

the basis of cross bedding direction, it can be concluded that more than 97% of the bedload transport is in the flood direction. As bedforms migrate further towards the south west about 400m from the Position 14, these bedforms terminate in the channel, which presumably indicates that sediments are transported into Caernarfon Bay [Jones, 1984; Solangi, 1992]. On the flank of the channel, the bedforms show a reversal in migration; also, sandwaves have superimposed ebb oriented ripples and megaripples.

Position 15

Cross beds in this area are of the small scale type. In some sets of cross beds, the direction of dip of the foresets in adjacent sets are opposite; these structures are herringbone cross beds which are important for the interpretation of the sequences (Fig. 7.19; e.g., boxes 43, 48, 55 & 60). In the herringbone structures, other than estimation of bedload transport, the relative strength and duration of the flood and ebb tides can be determined from the comparison of the dips and thicknesses of adjacent sets of strata.

Lateral and vertical sequences of cross stratification in the interpreted section (Fig. 7.20) are similar to the *complex cross stratification* of Klein [1970] and Dalrymple [1984]. The quantitative computation of flood and ebb directed cross strata show that bedform migration in this location is 63.3% in the flood direction and 36.7% in the ebb direction.

Fig: 7.19
Section of a sandwave at Position 15 showing internal sedimentary structures (see also Fig. 7.20).

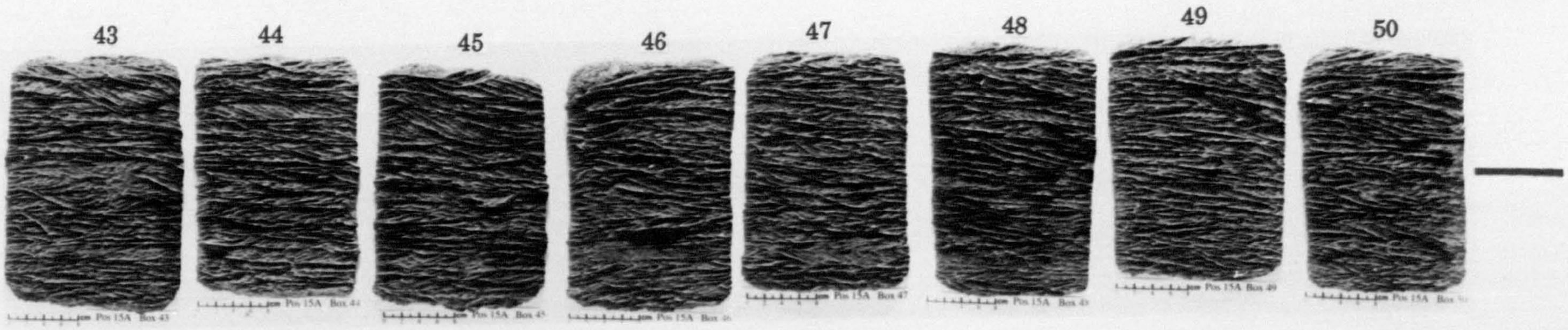

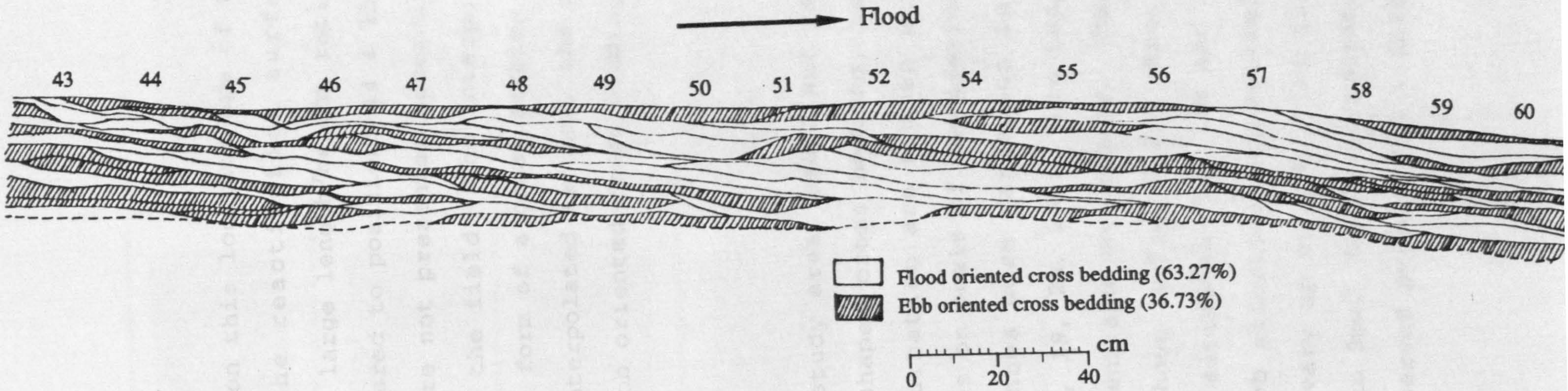

Fig: 7.20

Interpreted section on Position 15 showing small scale cross bedding. Section drawn from box peels; labels are box numbers.

Position 16

Sets of cross bedding on this location are of the large scale type. Most of the reactivation surfaces are erosional. Because of the large length/height ratio (27) of the covered transect, compared to positions 14 & 15, the box photographs (Fig. 7.21) are not presented according to the layout of box sampling in the field. The interpolation of internal structures in the form of a cross section are shown in Fig. 7.22. From the interpolated section, the calculated percentage of flood and ebb oriented cross bedding is 62.5% and 37.5%, respectively.

Positions 17 - 25

In this part of the study area, small and large scale cross bedding, festoon-shaped cross bedding, herringbone cross bedding and bioturbation are common structures. Compared to the structures on peels of the previous studied positions, this area shows more variation in vertical section (e.g., Positions, 19, 20, 23). This indicates the variability of tidal current and wave energy. The box peels of these positions are shown in Fig. 7.23. From the cross strata direction, it is estimated that 39% and 30% of the strata are flood and ebb oriented, respectively. These percentage figures may vary up to ±5%. The thickness of laminae varies from 0.5 to 3mm. Shell concentration in some of the peels is also observed periodically, which probably

Fig: 7.21

Sedimentary structures of a sandwave at Position 16 (see for sampling layout Figs. 7.14, 7.22).

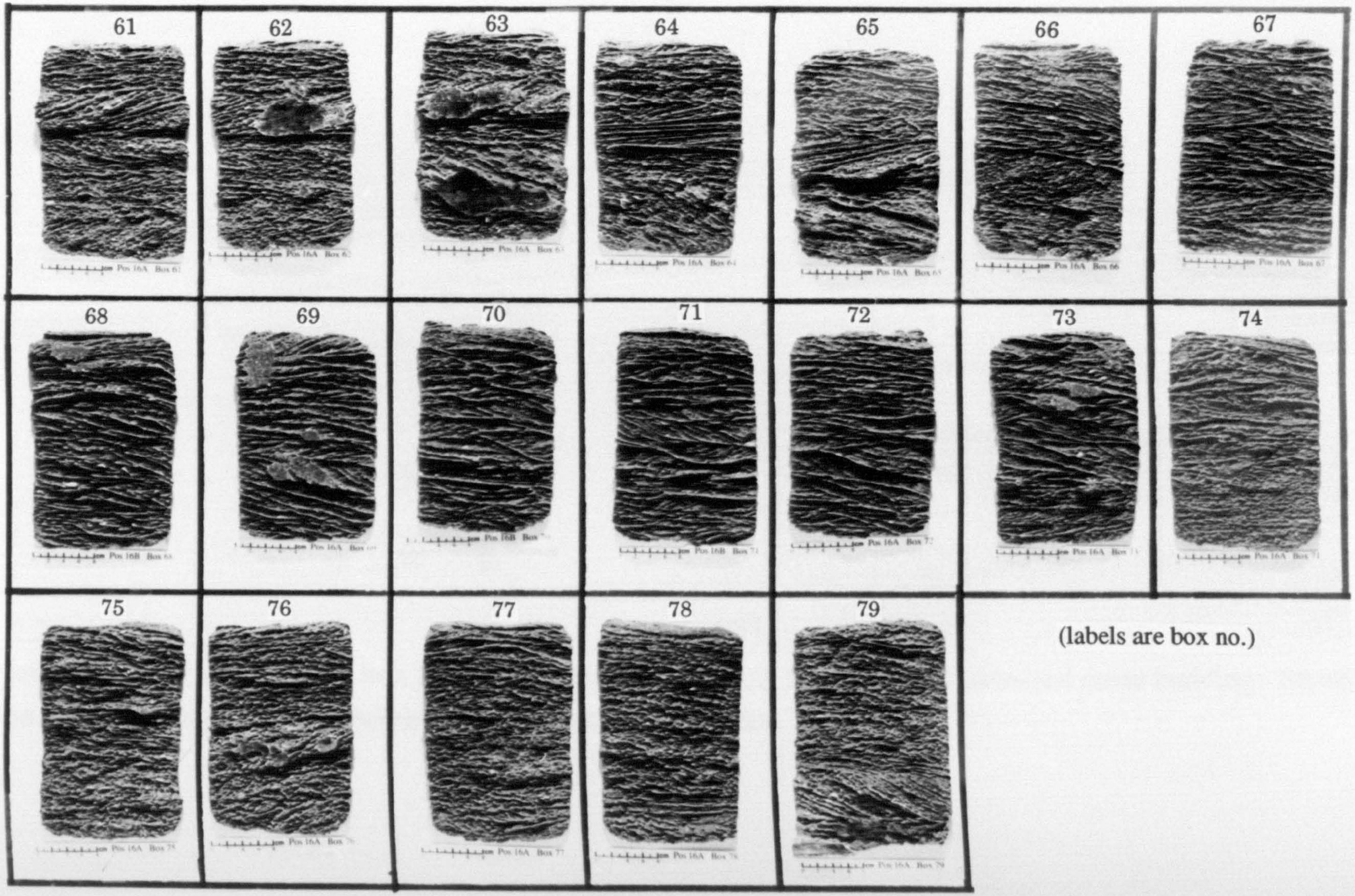

(labels are box no.)

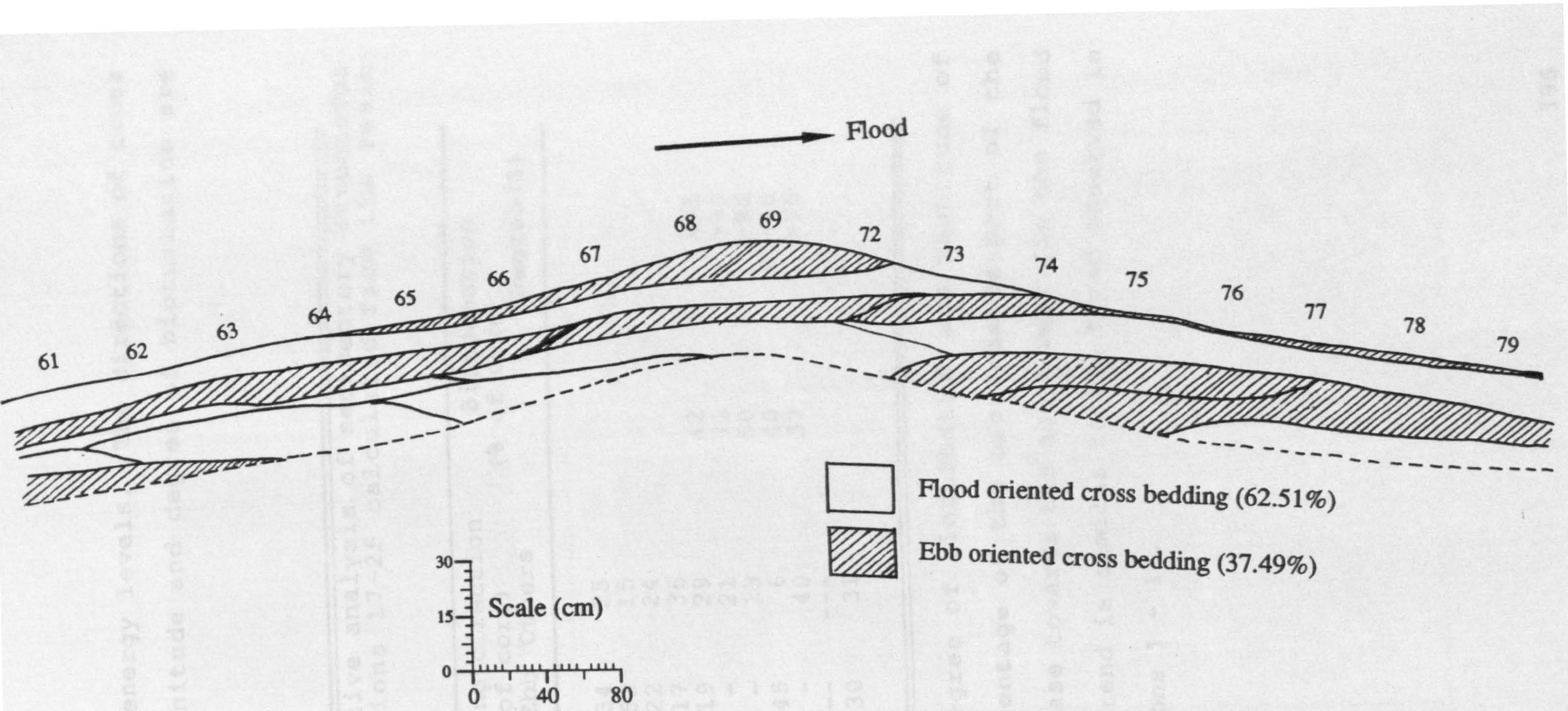

Fig: 7.22

Interpretation of structures from box peels at Position 16 showing flood and ebb oriented cross bedding. Structures in gaps between boxes are extrapolated. Labels are box numbers.

shows the different energy levels. The directions of cross bedding and the magnitude and degree of bioturbation are given in Table 7.3.

Table: 7.3 Quantitative analysis of sedimentary structures at Positions 17-25 calculated from the resin peels.

Pos. No.	Box No.	X-bedding direction (% of core) Flood	Ebb	Others	Bioturbation (% of core)	Degree(%)
17B	82	41	34	25		
18A	83	32	53	15		
19A	85	54	22	24		
20A	87	47	17	36		
21B	90	10	19	29	42	>95
22B	92	7	-	21	72	>95
23A	93	37	-	13	50	>95
24A	95	9	45	6	40	60-90
25A	97	23	-	40	37	>95
		39	30	31		

The measured degree of bioturbation and magnitude of bioturbation (percentage of the bioturbated part of the peel) show an increase towards the south west (in the flood direction). This trend is similar to the trend observed in the peels at Positions 1 - 13.

Fig: 7.23
Box peels showing sedimentary structures at Positions 17 - 25; labels are box number.

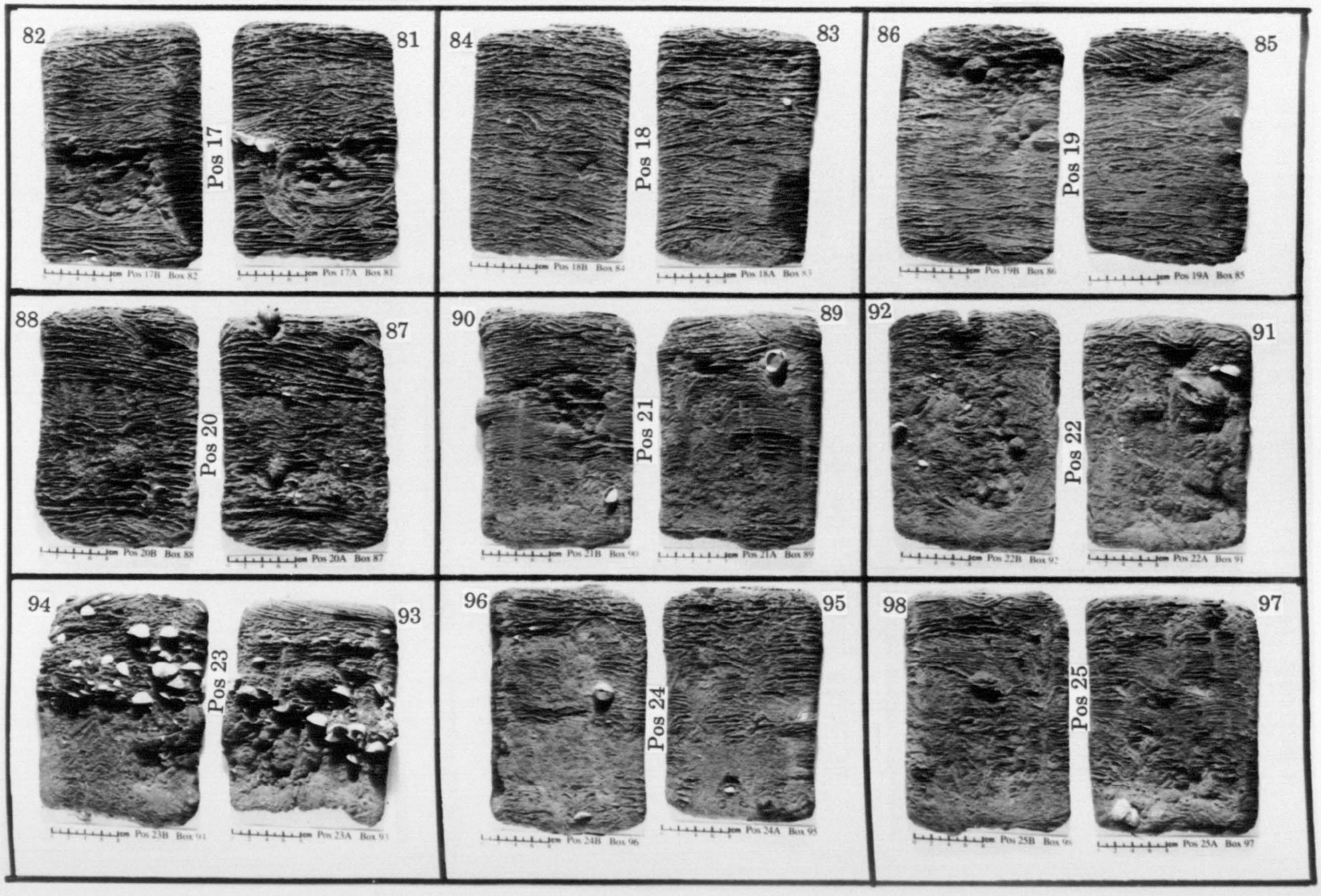

7.11 Conclusions

(1) From the box cores, the measured percentages of sediment transports show a pronounced flood dominance. The calculated percentage of bedload transport in the flood and ebb directions are given in Table 7.4 and the vectors of sediment transport are shown in Fig. 7.24.

Table: 7.4 Bedload transport in the flood and ebb directions.

Box Coring Positions	Bedload (percentage) Flood-directed	Ebb-directed
1 - 13	79.5	20.3
14	>97	<3
15	63.3	36.7
16	62.5	37.5
17 - 25	56.5	43.5

(2) The bedload transport in the flood direction is more in areas close to the main channel than in areas farther from the channel. The estimated sediment transport in the flood direction near the mainland of Arfon (Positions 17 - 25) is 1.3 times higher than the transport in the ebb direction. Nearer to the channel (Positions 1 - 13), the bedload transport ratio of flood and ebb directions is 3.9; whereas

Fig: 7.24

Sediment transport (%) in the Flood and Ebb directions estimated from the sedimentary structures of box cores.

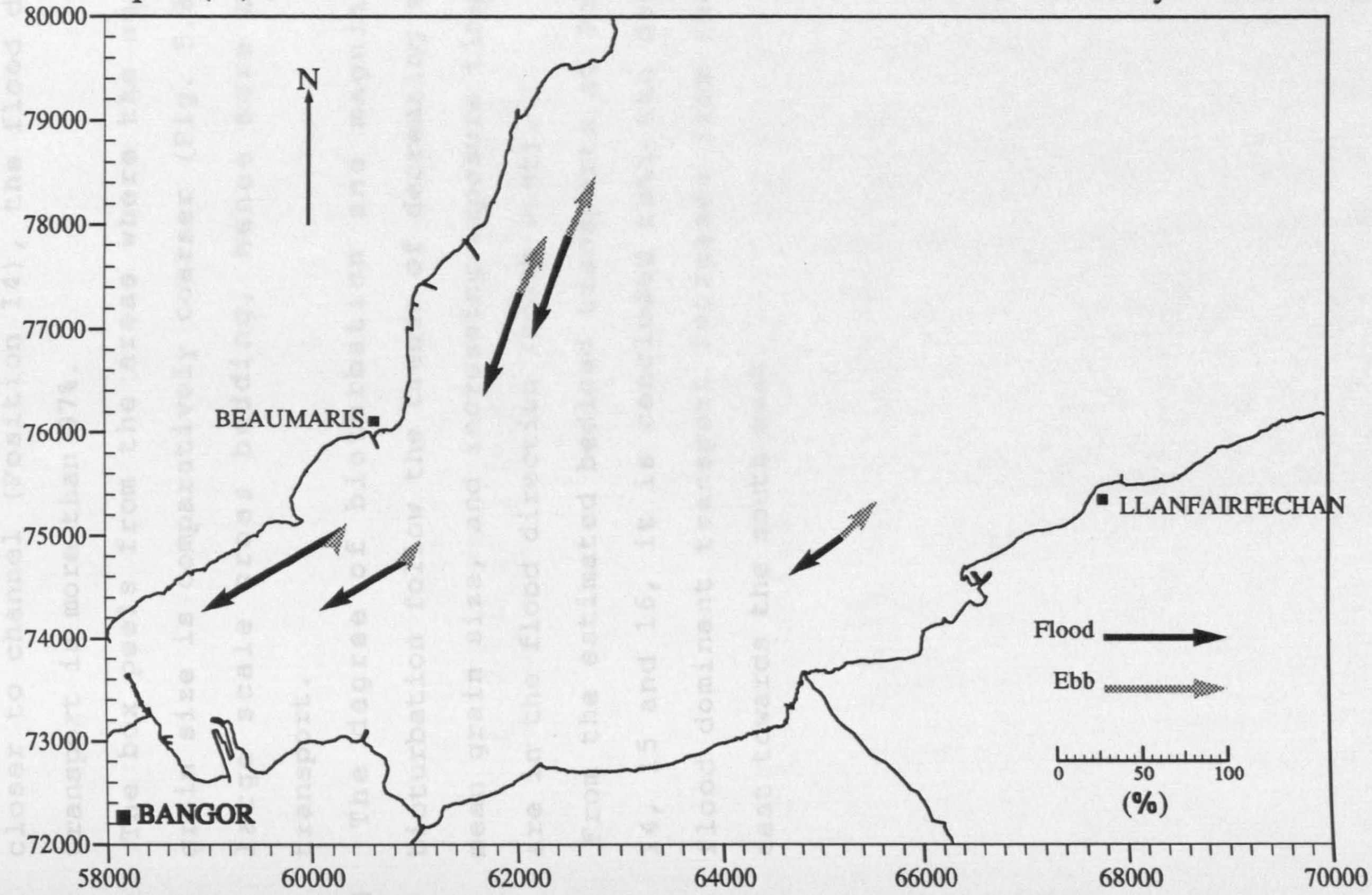

closer to channel (Position 14), the flood directed transport is more than 97%.

(3) The box peels from the areas where the surficial grain size is comparatively coarser (Fig. 5.8), show large scale cross bedding, hence more bedload transport.

(4) The degree of bioturbation and magnitude of bioturbation follow the trends of decreasing sediment mean grain size, and increasing exposure time, which are in the flood direction (south west).

(5) From the estimated bedload transports at Positions 14, 15 and 16, it is concluded that the degree of flood dominant transport increases from the north east towards the south west.

CHAPTER EIGHT

SUMMARY, CONCLUSIONS AND SUGGESTIONS

8.1 SUMMARY

8.1.1 Subbottom Seismic Stratigraphy

From the seismic sources (sparker, boomer and pinger), three main layers of sedimentary deposits are recorded in the area. These layers delineate glacial, postglacial and recent sedimentary deposits.

From the sparker records, a maximum depth of 99 metres relative to O. D. Newlyn is recorded to the north east of Puffin Island. The isopach maps (Fig. 3.33A, C, and Fig. 3.34A) show that the deposition of Quaternary sediments is largely influenced by the bedrock topography. Maximum thickness of glacial sediments occurs in the overdeepened depressions and decreases toward the coast.

A channel-fill structure with a NE-SW trend near Puffin Island is most probably an extension of the Dinorwic Fault. In Caernarfon Bay, similar features are reported by Al-Shaikh [1969, 1970], Bott [1964], Bott & Young [1971], and Solangi [1992]. From this evidence it appears that, although the origin of this buried valley which is incised into the bedrock is related to the Caledonian and subsequent Hercynian earth movements, its U-shaped glacial form suggests that its present form was generated by glacial action during the Quaternary glaciation. Blundell, Griffiths & King [1969] reported similar U-shaped buried valleys in Cardigan and Tremadoc Bays.

The results of the seismic survey show that the postglacial sediments in the area have thicknesses up to 31 metres and are deposited at a maximum depth of 45 metres below Ordnance Datum (Fig. 3.33B, D, and Fig. 3.34B). In Cardigan Bay, the deepest postglacial sediments are at about -30m O. D. [Blundell, Griffiths & King 1969]. Larcombe [1989] reported that in Barmouth Bay the transition between glacial and marine sedimentation occurs between -40m and -30m relative to O. D. Solangi [1992] reported the depth of postglacial deposits at about -30m in Caernarfon Bay. This suggests that when postglacial deposition commenced in these areas, sea level was about -30m to -40m relative to Ordnance Datum. According to the sea level curves of Shepard & Curray [1967] and Milliman & Emery [1968], sea level at about 9000 years B.P. was around 35 to 40 metres below the present sea level in this area. The depth of postglacial deposits in Cardigan, Barmouth, Caernarfon and Conwy Bays suggests that these sediments started to deposit in marine environments most probably c. 9000 years ago. Initial deposition must have taken place in relatively deeper channel areas and gradually the thickness of the postglacial sediments increased as sea level rose.

The thickness of the most recent sedimentary layer (Fig. 3.35) in the area is up to 12m. This thickness is again comparable to the thickness of modern sediments in Caernarfon, Barmouth and Cardigan Bays, where similar seismic techniques were used to identify the subbottom

sedimentary layers.

8.1.2 Tidal currents in the Area

According to the coastal classification of Davies [1964], Hayes [1979] and Davies & Hayes [1984] based on tidal range, the study area may be classified as a macrotidal coastal area. Tidal currents in the area are the most important hydraulic factor controlling sediment transport and deposition, the residual sediment transport paths, and the general morphology of the subtidal (Conwy Bay) and intertidal (Lavan Sands, Dutchman Bank, Irishman Spit) areas. From the results of 12 hydrographic stations (Fig. 4.14), it is clear that the currents are dominant in the flood direction at 11 stations, and only at Station 1 is the residual current in the ebb direction.

Waves must be important, especially in the shallow and intertidal areas, but are undoubtedly secondary relative to tidal currents.

8.1.3 Bedforms in the Area

Bedforms of different shape, size and orientation in marine environments are normally the result of different combinations of hydrodynamic conditions, surficial sediment grain size and water depth. Well developed bedforms are good indicators of bottom sediment migration paths.

Seabed features were studied using various techniques (i.e., side scan sonar survey, study of aerial photographs, field surveys and measurements) in different parts of the

study area. Aerial photographs from different sources were obtained (Chapter 7), and these revealed the presence of bedforms in the intertidal area at low tide. During field visits, terrains of different bedforms were identified on the basis of wavelength spacing measurements.

An integrated interpretation of seabottom features recorded by side scan sonar, photographs and field surveys is presented in Fig. 8.1.

Ripples are observed on Lavan sands, about 2.5 kilometres east of Beaumaris, on side scan sonar records. North east of Puffin Island and at Dutchman Bank, sonographs show the existence of ripples superimposed on sandwaves. From the aerial photograph study and field surveys, it was found that most of the central Lavan Sands is covered by ripples with wavelengths and heights less than 30cm and 10cm, respectively. The occurrence of ripples in this area is most probably due to the fineness of the surficial sediments and low current speeds compared to the other parts of the study area.

More than 90% of the megaripples recorded by side scan sonar are found in those areas where the water depth is between 9m and 11m and mean grain size more than 3.0 phi. Near Puffin Island, opposite the Lifeboat Station, and near Gallows Point at Lavan Sands, megaripples are found superimposed on the flanks of sandwaves. During the field surveys near Gallows Point, it was estimated that about 50% of the megaripple population is asymmetric in the flood

Fig: 8.1

Bedform spatial distribution based on results of sonographs, aerial photographs and field surveys.

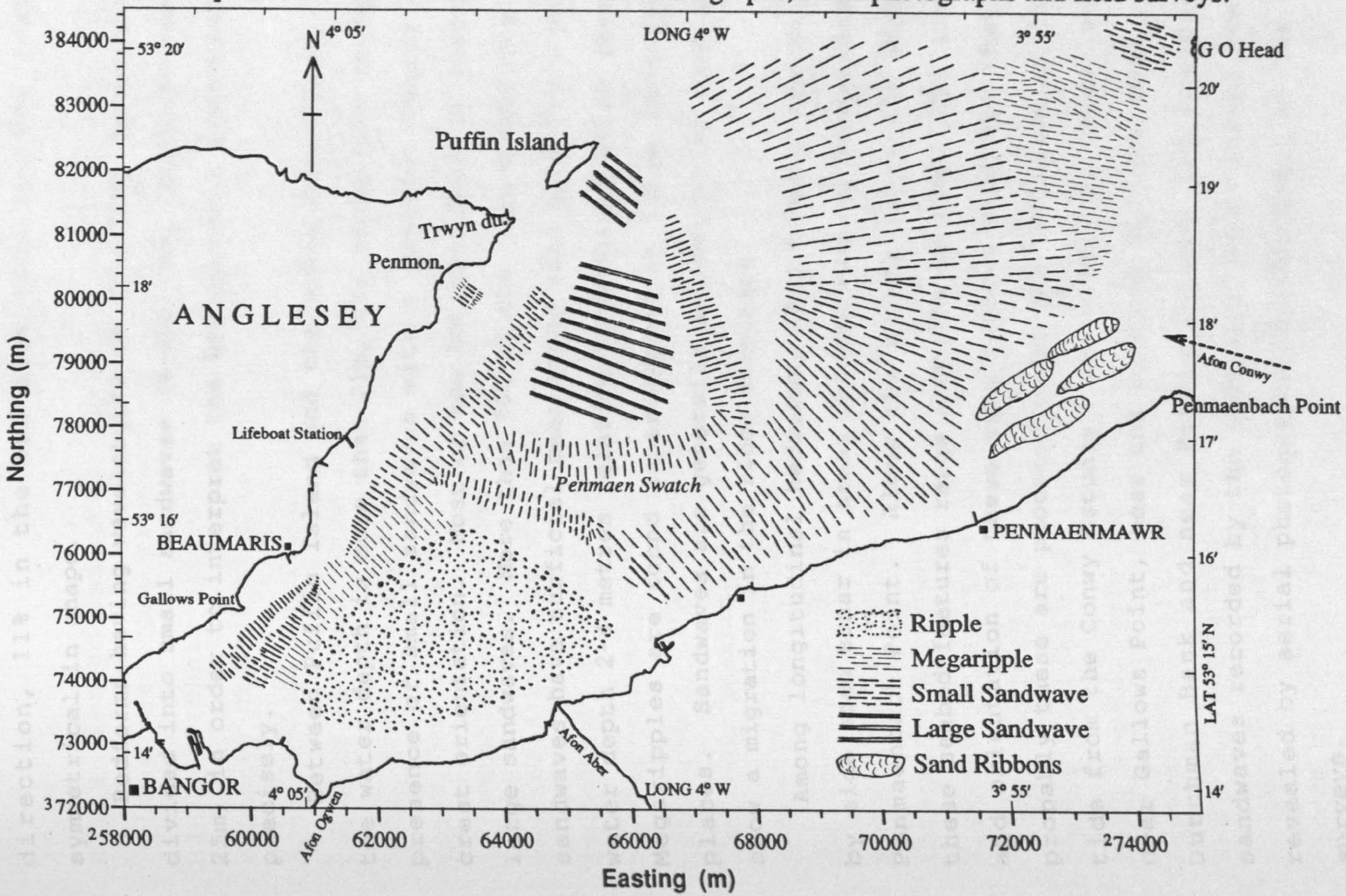

direction, 11% in the ebb direction and the rest are symmetrical in shape.

Bedforms having wavelengths of more than 6m are further divided into small sandwaves (6-25m) and large sandwaves (> 25m) in order to interpret the hydrodynamic processes more precisely.

Between Puffin Island and the Great Ormes Head, where the water depth is more than 11m, the sonographs reveal the presence of small sandwaves with a dominant nearly NE-SW crest orientation. Most of the Dutchman Bank is covered by large sandwaves. More than 90% of the area comprising large sandwaves have surficial mean grain size of 2.0-2.5 phi and water depth 2-4 metres relative to Ordnance Datum (Newlyn). Megaripples are found superimposed on large sandwaves in places. Sandwaves are generally asymmetric in profile and show a migration in the flood direction.

Among longitudinal bedforms, sand ribbons are recorded by side scan sonar in areas between east of Penmaenmawr and Penmaenbach Point. Along the survey lines the width of these seabed features range from 80m to 400m. The location and orientation of these sand ribbons indicate that most probably these are produced under the influence of the ebb tide from the Conwy Estuary. In intertidal areas, such as near Gallows Point, near the Lifeboat Station, most of the Dutchman Bank and near Puffin Island, the presence of sandwaves recorded by the side scan sonar survey are also revealed by aerial photographs and confirmed by the field surveys.

8.1.4 Seabed Sediments and Grain Size Distribution

The surficial sediments have been classified on the basis of their gravel, sand, and mud contents and their regional distribution is shown in Fig. 5.5. Sands are the most abundant surficial sediments in the area. The other types of sediment found in the area are gravely sand, muddy sand, sandy mud and mud. On the basis of surficial sediment types, the area is divided into 5 subareas (Fig. 5.6).

Detailed comparison of the textural parameters of the sediments of these subareas discriminates their prevailing sedimentary environments:

The sediments of *Area A* are very fine sand to medium silt, poorly to very poorly sorted, very positively skewed, and their peakedness is extremely leptokurtic. According to Visher's [1969] interpretation of lognormal cumulative curves (Fig. 5.21), 60% and 40% of the grain size populations in this subarea are deposited through intermittent suspension (saltation) and suspension modes of sediment transport, respectively.

The grain size results of 158 sediment samples from *Area B* show that the sediments are: unimodal, fine sand and very fine sands, very well sorted, positively skewed and leptokurtic. All the grain size populations in this area show a single mode of transportation (intermittent suspension) on interpretation of the probability cumulative curves of typical samples.

Because of the variable hydrodynamic conditions, the sediments from *Area C* demonstrate more variability in their textural parameters than other subareas. The majority of the sediment samples have a mean grain size within the gravel to fine sand grades according to the Wentworth size classification. Samples show nearly all classes of sorting [Folk & Ward 1957], and are very negatively skewed. Grain size distribution curves on a probability scale consist of two linear segments indicating two modes of sediment transport; traction (20% of the size population) and intermittent suspension (80% population).

Near Puffin Island, *Area D* comprises a gravelly sand type of surficial sediment. Grain size analysis shows that majority of the samples are poorly and very poorly sorted and skewness is negative to very negative. The cumulative weight percentage curves on lognormal paper show that the dynamics of sediment transport in this area are traction (35% of the grain size population), intermittent suspension (60%) and suspension (5%).

Area E is situated near Great Ormes Head and comprises dominantly sandy mud and mud types of surface sediments. The grain size analysis shows that most of the sediments are poorly to very poorly sorted, very positively skewed. Suspension is the dominant mode of transport in this area.

8.1.5 Sediment Transport

The results obtained from bedform characteristics (Chapter 3, Chapter 7), sediment size analysis (Chapter 5),

sediment transport rate calculation by empirical formulae (Chapter 6), and sediment transport estimated by analysis of internal sedimentary structures of bedforms (Chapter 7), are integrated to deduce the prevailing sediment transport pathways in the study area. The sediment transport pathways, based on calculated and predicted transport rates and directions, are shown in Fig. 8.2. As mentioned earlier, the sediment transport calculations are based on various methods/techniques (transport formulae, sedimentary structures analysis, bedform studies). So the rates and directions of sediment transport in Fig. 8.2 are divided into three categories based on the method of determination.

(i) Calculated sediment transport: The dark black arrows indicate the calculated amount and direction at 12 hydrographic stations in the subtidal area (using empirical formulae) and 5 stations in the intertidal area (using sedimentary structure analysis). The rates of transport shown at the box coring positions are derived from the calculated results of sediment transport percentage in the flood/ebb directions and from bedform type.

(ii) Direction observed; rate predicted: The light shaded arrows represent sediment transport vectors in those areas where the transport directions are determined from bedform asymmetry but the rates of transport are predicted. The transport rate prediction is based on the bedform size and interpolated from the calculated

Fig: 8.2 Sediment transport based on integrated results of bedform, grain size analysis, and transport estimated by empirical formulae and sedimentary structure analysis.

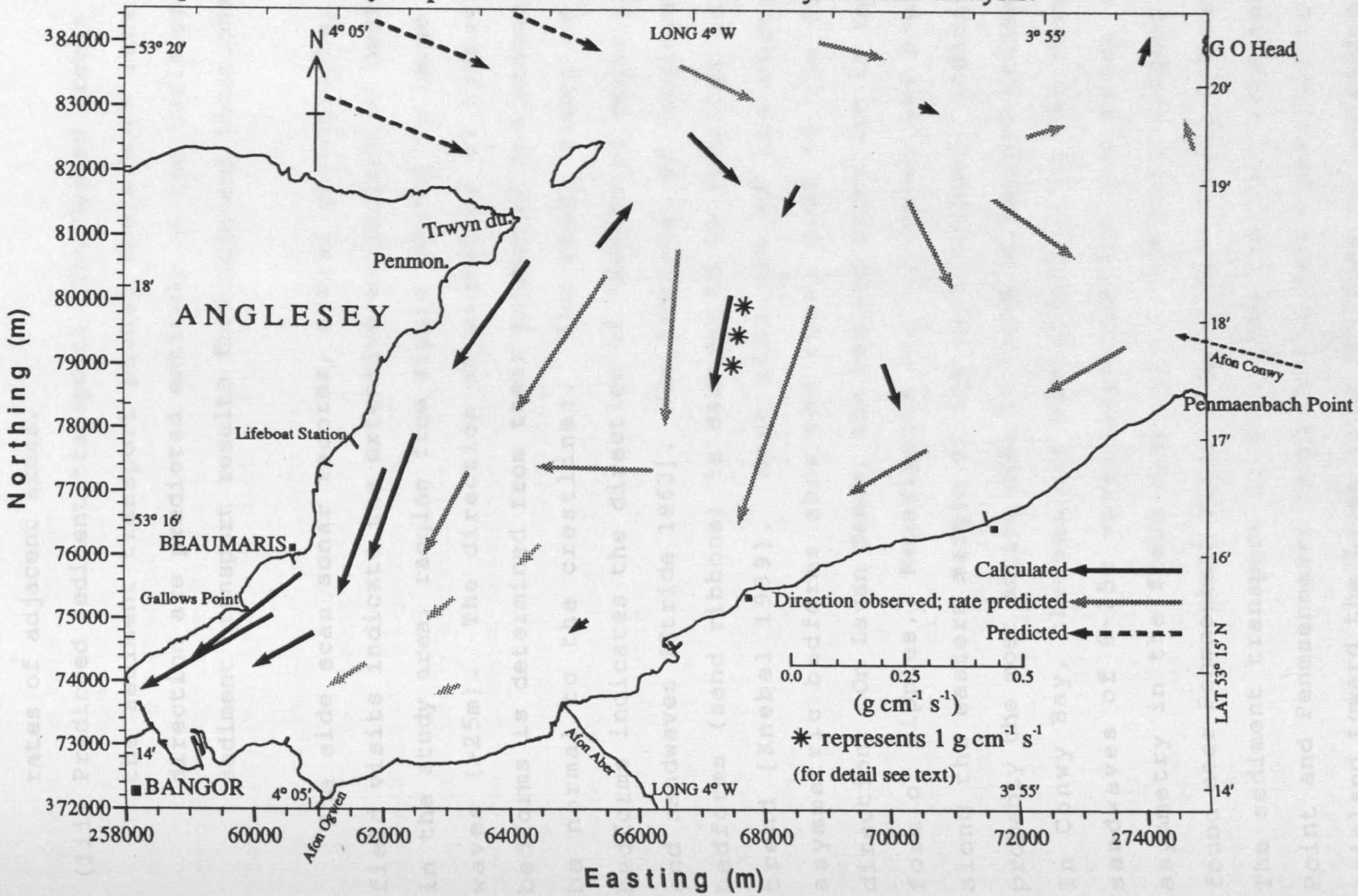

rates of adjacent areas.

(iii) Predicted sediment transport: The dashed arrows show the sediment transport paths, where both rate and direction are predicted entirely on the basis of the sediment transport results from adjacent locations.

The side scan sonar records, aerial photographs, and field visits indicate the extensive occurrence of bedforms in the study area, ranging from ripple (<0.6m) to large sand waves (>25m). The direction of migration of transverse bedforms is determined from their asymmetry and assumed to be normal to the crestlines. The steep sides of the bedforms indicates the direction of advance of megaripples and sandwaves [Stride 1963]. The transport of longitudinal bedforms (sand ribbons) is assumed to be parallel to the trend [Knebel 1989]. More than 95% of the observed asymmetric bedforms show the steep side in the flood direction. On Lavan Sands, the bedform migration is in the form of ripples. Megaripples and sandwaves are present along the eastern margin of the main channel, indicating probably the most active area in terms of bedload transport. In Conwy Bay, the bedform migration is in the form of sandwaves of 6-25m wavelength spacing and these show asymmetry in the flood direction. The sand ribbons are found near Penmaenbach Point indicating a nearly E-W trend. The sediment transport in this area (between Penmaenbach Point and Penmaenmawr) is predicted to be parallel to the mainland toward the Lavan Sands and then to Caernarfon Bay

through the Menai Strait.

Particle size distributions are commonly used to investigate sedimentary processes and environments. The progressive changes in numerical descriptors [Krumbein, 1939; McCave, 1978; Mclaren & Bowles, 1985; Dyer, 1986] and the interpretation of grain size distribution curves [Moss, 1962, 1972; Visher ,1969; Visher & Howard, 1974; Middleton, 1976; Walton, Stephens & Shawa, 1980; Bagnold & Barndorff-Nielson, 1980; Christiansen, Blaesild & Dalsgaard, 1984] have been used to determine the trends of sediment transport direction and modes of transport.

The regional distribution of mean grain size (Fig. 5.8) clearly shows the trend in fining of seabed sediments from the north towards the south and then southwest and it follows the trend of residual currents in the area. This progressive change in sediment size indicates that as coarse sediments are transported from the open sea to Conwy Bay and then Lavan Sands, the size of sediments decrease due to progressive sorting. The linear segments of grain size distribution curves show that in *Area D*, the sediment are deposited by traction and intermittent suspension transport modes; further south in *Area B*, the mode of transport is intermittent suspension; and in *Area A*, the sediments are transported by intermittent suspension and suspension. The regional distribution of mean grain size and the grain size distributions of individual sediments indicate that sediment transport is towards the south west of the area.

Sorting of the sediments also changes progressively from *Area D* to *Area B* and then to *Area A* (Fig. 5.9). Sediments transported from the Irish Sea by the flood tide are poorly sorted as they enter the area in its northwestern part (*Area D*). With further transport toward the southeast, then to the south and finally to the southwest, the sediments gradually become better sorted (small phi values) in the direction of transport. But as the sediments reach in the *Area A* towards south and in *Area E* towards northeast of the study area, their sorting worsen because of progressive transport for comparatively longer distance and suspension mode of deposition (Inman 1949).

Sediment skewness (Fig. 5.10) indicates a the similar trend of sediment transport in the area. North east of Puffin Island, the sediments are negatively skewed; samples in *Area B* are positively skewed, and very positively in *Area A*. This indicates that when coarser sediments from *Area D* are transported towards the south west i.e., towards *Area B* and then *Area A*, the finer population becomes progressively dominant, confirming the transport direction previously determined by the bedform orientation, mean grain size and sorting distribution of sediments.

Sediment transport rates in the area at 12 stations have been estimated by the formulae of Engelund & Hansen [1967] and Hardisty [1983] (see Chapter 6). Residual transport of sediments (Fig. 6.12) follows the residual tidal current trends. Only one station (Station 1) shows the transport in the ebb direction; at the other 11 stations, the calculated

net sediment transport is in the flood direction. The calculated transport directions agree well with the transport paths deduced from the bedform study and grain size analysis results (mean grain size, sorting, skewness).

Bedload transport has also been estimated from the internal sedimentary structures of bedforms (Chapter 7). In this method the percentages of bedload in the flood and ebb directions are calculated by measuring the areas (and hence, volumes) of flood and ebb oriented cross-strata in box cores sampled from different parts of the intertidal area. The results of 46 box cores from the Lavan Sands show that there is more flood-directed sediment transport in areas close to the main channel than in areas farther from the channel. The transport in the flood direction near the mainland of Arfon (positions 17-25 in Fig. 7.13) is 1.3 times higher than in the ebb direction, whereas near the channel (Positions 1-13) the flood transport is 3.9 times higher than sediment transport in ebb direction. At Position 14, about 97% of the cross-strata are flood-oriented. In the same way, the estimated ratio of flood and ebb directed bedload transport at Positions 15 and 16 is 3:2 (Table 7.4, Fig. 7.24).

The residual sediment transport to the south west (i.e., into the Menai Strait) is supported by Solangi [1992], who during a study of a Quaternary tidal delta at the south western end of the Menai Strait, concluded that" in Caernarfon Bay the sediment mainly enters from the northeast

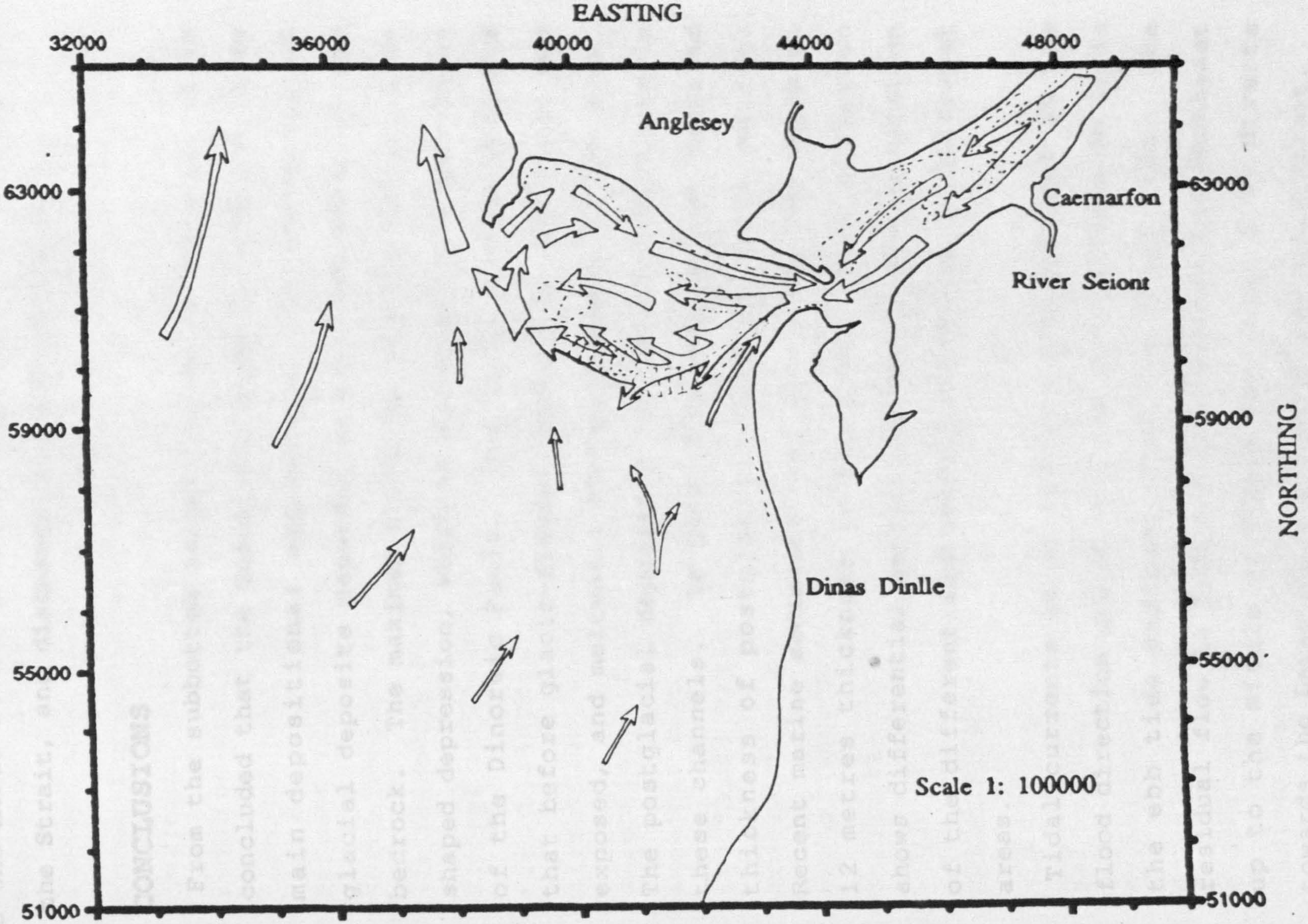

Fig: 8.3 proposed model of the sediment transport pathways in the study area (after Solangi 1992)

Sand bodies

side of the Menai Strait" (Fig. 8.3). Hence, sediment enters the Menai Strait from the north-east, is transported along the Strait, and discharge into Caernarfon Bay.

8.2 CONCLUSIONS

(1) From the subbottom seismic study of the area, it is concluded that the Quaternary deposits comprise three main depositional sequences. The thickness of glacial deposits depended on the topography of the bedrock. The maximum thickness was recorded in a U-shaped depression, which is a overdeepened expression of the Dinorwic Fault. Sea level curves indicate that before glacio-fluvial deposition, this area was exposed, and meltwater eroded channels in the area. The postglacial deposition has maximum thickness in these channels. In Conwy Bay the maximum recorded thickness of postglacial sediment is 31 metres. Recent marine sediments vary from about one metre to 12 metres thickness in the area. This variation shows differential deposition, which is an indication of the different sedimentary processes in different areas.

(2) Tidal currents at 11 stations are dominant in the flood direction and at only one station (Station 1) is the ebb tide dominant over the flood tide. The residual flow is from the northwest to the southeast up to the middle of Conwy Bay, then flow diverts towards the Lavan Sands and in to the Menai Strait.

(3) The results of grain size analysis of 235 seabed sediment samples demonstrate that the area can be divided into five subareas which indicate different prevailing sedimentary processes.

(4) Bedforms, grain size characteristics, and calculated sediment transport rates calculated (using transport formulae and internal structures of the bedforms) suggest that the source of sediment in Conwy Bay & North Eastern Menai Strait is the offshore region (Irish Sea). Bedforms at high water (sonographs) and exposed at low water (aerial photographic studies and field surveys) are asymmetrical in the flood direction, indicating migration in a south west direction. Trends of mean grain size, sorting and skewness also clearly indicate sediment transport in the flood direction. Flood dominance in bedload transport is confirmed by the transport calculations using transport equations and internal sedimentary structures of bedforms.

8.3 SUGGESTIONS

(1) In the main channel of the Menai Strait, current meter data for longer periods (spring-neap-spring cycle; preferably at three positions, between Trwyn-du and Penmon, between Lifeboat Station and Beaumaris, and near Bangor Pier) may provide a better indication of residual sediment transport towards

Caernarfon Bay.

(2) Seismic survey of Lavan Sands with sparker system is required to get more penetration to determine the presence and then thickness of glacial and postglacial deposits.

(3) Bore hole data will be useful to confirm the boundaries of the three main depositional units recorded during the present seismic survey and to provide further details of lithology of the Quaternary of the area.

BIBLIOGRAPHY

Abbe C.J. [1895]. Remarks on the cuspate capes of the Carolina coast. Bost. Soc. Natural Hist., Proc., 26:489-497.

Ackers P. & White W.R. [1973]. Sediment transport: new approach and analysis. Proc. Ame. Soc. Civ. Engrs., J. Hydraul. Div. HY11:2041-2060.

Allan D. [1985]. Seismic stratigraphic analysis of the North Eastern Menai Straits. M.Sc. Thesis, University of Wales, Bangor.

Allen J.R.L. & Friend P.F. [1976]. Changes in intertidal dunes during two spring-neap cycles, Lifeboat Station Bank, Wells-next-the-sea, Norfolk, England. Sedimentology, 23:329-346.

Allen J.R.L. [1965]. The sedimentation and palaeogeography of the Old Red Sand stone of Anglesey, North Wales. Proc. York Geol. Soc., 35:139-185.

Allen J.R.L. [1968a]. Current Ripples. North Holland, Amsterdam. 433p.

Allen J.R.L. [1968b]. The nature and origin of bed-form hierachies. Sedimentology 10:161-182.

Allen J.R.L. [1971]. Mixing at turbidity current heads, and its geological implications. J. Sed. Petrol., 41:97-113.

Allen J.R.L. [1978]. Polymodal dune assemblage: an interpretation in terms of dune creation-destruction in periodic flow. Sed. Geol., 20:17-28.

Allen J.R.L. [1980a]. Large transverse bedforms and the character of boundary-layers in shallow-water environments. Sedimentology, 27:317-323.

Allen J.R.L. [1980b]. Sandwaves: a model of origin and internal structure. Sed. Geol., 26:281-328.

Allen J.R.L. [1980c]. Sandwave immobility and the internal master bedding of the sandwave deposits. Geol. Mag. 117:437-446

Allen J.R.L. [1982a]. Sedimentary Structures: Their Character and Physical Basis. vol. 1 and 2. Elsevier,

Amsterdam.

Allen J.R.L. [1982b]. Simple models for the shape and symmetry of tidal sand waves. I. Statistically-stable equilibrium forms. Mar. Geol., 48:31-49.

Allen J.R.L. [1982c]. Simple models for the shape and symmetry of tidal sand waves. II. Dynamically-stable symmetrical equilibrium forms. Mar. Geol., 48:51-73.

Allen S.E, Grimshaw H.M., Parkinson J.A. & Quarmby C. [1974]. Chemical Analysis of Ecological Material. Blackwell, Oxford.

Al-Shaikh Z.D. [1969]. Geophysical results from Caernarvon and Tremadog Bays. Nature, 224:897-899.

Al-Shaikh Z.D. [1970]. Geophysical investigation in the northern part of Cardigan Bay (including a part of the central Irish Sea). Ph.D. Thesis, University of Wales, Aberystwyth.

American Society of Civil Engineers [1975]. Sedimentation Engineering (ed. by V.A. Vanoni) New York. 745p.

Amos C.L. & King E.L. [1984]. Bedforms of the Canadian eastern seaboard: a comparison with global occurrences. Mar. Geol., 57:167-208.

Anderson F.E. [1973]. Observation of some sedimentary processes acting on a tidal flat. Mar. Geol., 14:101-116.

Anikouchine W.A. & Sternberg R.W. [1973]. The World Ocean: an introduction to the oceanography. Prentice Hall, Inc., Englewood Cliffs, New York, 176-178.

Bagnold R.A. & Barndorff-Nielsen O. [1980]. The pattern of natural size distributions. Sedimentology, 27:199-207.

Bagnold R.A. [1955]. Some flume experiment on large grains but little denser than the transporting fluid and their implications. Proc. Inst. Civil Engng., 4(3):174.

Bagnold R.A. [1956]. The flow of cohesionless grains in fluids. Philos. Trans. Roy. Soc. London, 249:234-297.

Bagnold R.A. [1963]. Mechanics of marine sedimentation. In: M.N. Hill (ed.), The Sea, Wiley Interscience. 3:507-582.

Bagnold R.A. [1966]. An approach to the sediment transport

problem from general physics. U.S. Geol. Surv., prof. paper, 422-I.

Bagnold R.A. [1968]. Deposition in the process of hydraulic transport. Sedimentology, 10:45-56.

Bagnold R.A. [1973]. The nature of saltation and of bedload transport in water. Proc. Roy. Soc. 332:473-504.

Bagnold R.A. [1977]. Bedload transport by natural rivers. Water Resources Research, 13:303-312.

Banks N.I. [1973]. The origin and significance of some downcurrent-dipping cross stratification sets. J. Sed. Petrol., 43:423-427.

Barber A.J. & Max M.D. [1979]. A new look at the Mona Complex (Anglesey, North Wales). J. Geol. Soc. London, 136:407:432.

Bates D.E.B. [1968]. The lower Palaeozoic Brachiopod and trilobites faunae of Anglesey. Bull. British Mus. (Natural History), Geol., 16:127-199.

Bates D.E.B. [1972]. The stratigraphy of the Ordovician rocks of Anglesey. Geol. J., 8:29-58.

Bates D.E.B. [1974]. The structures of the lower Palaeozoic rocks of Anglesey, with special reference to faulting. Geol. J., 9:39-60.

Bedeus K. & Ivicsis L. [1963]. Observations of the noise of bedload. Proc. Int. Asso. Hydrologists., 65:384:390.

Belderson R.H., Johnson M.A. & Kenyon N.H. [1982]. Bedforms. In: A.H. Stride (ed.), Offshore tidal sands: processes and deposits. Chapman and Hall London. 27-58.

Belderson R.H., Kenyon N.H., Stride A.H. & Stubbs A.R. [1972]. Sonograph of the sea floor. Elsevier, Holland

Bengtsson L. & Enell M. [1986]. Chemical analysis. In: B.E. Berglund (ed.), Handbook of Holocene Palaeoecology and Palaeohydrology. 423-451, John Wiley & Sons.

Blundell J., Davey F.J. & Graves L.J. [1971]. Geophysical surveys over the South Irish Sea and Nymphe Bank. J. Geol. Soc. London, 127:339-375.

Blundell J., Griffiths D.H. & King R.F. [1969]. Geophysical

investigations braided river valleys around Cardigan Bay. Geol. J., 6:161-180.

Boersma J.R. & Terwindt J.H.R. [1981a]. Neap-spring tide sequences of intertidal shoal deposits in a mesotidal estuary. Sedimentology, 28:151-170.

Boersma J.R. & Terwindt J.H.R. [1981b]. Berms on an intertidal shoals: shape and internal structure. In: S.D. Nio, R.T.E. Schuttenhelm & Tj.C.E. van Weering (eds.), Holocene Marine Sedimentation in the North Sea Basin. Spec. Publ., Int. Asso. Sedimentologists, 5:39-49. Blackwell Sci. Publ., Oxford.

Boersma J.R. [1969]. Internal structures of some tidal megaripples on a shoal in the Westerschelde estuary, The Netherlands. Geologie Mijnb. 48:409-414.

Boomer Instructional Manual [1969]. Boomer record interpretation (Appendix). Instruction manual no TM69-152, A1-A9.

Boothroyd J.C. & Hubbard D.K. [1974]. Bedform development distribution pattern, Parker and Essex Estuaries, Massachusetts. U.S. Army Corps Engineers Coastal Engrs. Res. Centre Misc. Paper 1-74.

Boothroyd J.C. & Hubbard D.K. [1975]. Genesis of bedforms in mesotidal estuaries. In: L.E. Cronin (ed.), Estuarine Research, 2:217-234. Academic Press Inc., New York.

Bott M.P.H. & Young D.G.G. [1971]. Gravity measurements in the north Irish Sea. Quart. J. Geol. Soc. London, 126:413-434.

Bott M.P.H. [1964]. Gravity measurements in the north-eastern part of the Irish Sea. Quart. J. Geol. Soc. London, 120:369-396.

Bouma A.H. [1964]. Sampling and treatment of unconsolidated sediments for study of internal structures. J. Sed. Petrol., 34(2):349-354.

Bouma A.H. [1969]. Methods for Study of Sedimentary Structures. John Wiley & Sons, New York. 458p.

British Geological Survey [1979]. South Sheet, Anglesey

Sheet and Sheet 106. Inst. Geol. Sci., UK.

Brush L.M. [1965]. Sediment sorting in alluvial channels. In: G.V. de Middleton (ed.), Primary Sedimentary Structures and their Hydrodynamic Interpretation. Soc. Econ. Paleontologists Mineralogists, Spec. Publ. Tulsa Oklahoma, 12:25-33.

Bryant R.S. [1975]. Side scan sonar for hydrography. Int Hydrogr. Rev., 52(1):43-56.

Buller A.T. & McManus J. [1972a]. Simple metric sedimentary statistics used to recognise different environments. Sedimentology, 18:1-21.

Buller A.T. & McManus J. [1972b]. Nature of the Martian surface as determined from particle size distribution of lunar surface material - a discussion. Bull. Geol. Soc. Ame., 83:3833-3836.

Buller A.T. & McManus J. [1973a]. Modes of turbidite deposition deduced from grain-size analyses. Geol. Mag., 109:491-500.

Buller A.T. & McManus J. [1973b]. The quartile-deviation/median-diameter relationships of glacial deposits. Sed. Geol., 10:135-146.

Buller A.T. & McManus J. [1973c]. Distinction among pyroclastic deposits from their grain-size frequency distributions. J. Geol., 81:97-106.

Buller A.T. & McManus J. [1979]. Sediment sampling and analysis. In: K.R. Dyer (ed.), Estuarine Hydrography and Sedimentation. 87-130. Cambridge University Press.

Bullock S.J. [1988]. Future and present trends of navigations and positioning techniques in exploration geophysics. Geophysical J., 92(3):521.

Burton C.F. [1984]. Geotechnical/geophysical survey of Penmon Beach. North Wales. M.Sc. Thesis, University of Wales, Bangor.

Carling P.A. [1981]. Sediment transport by tidal currents and waves: observations from a sandy intertidal zone (Burry Inlet, South Wales). Spec. Publ., Int. Asso.

Sedimentologists., 5:65-80.

Carver R.E. [1971]. Procedures in Sedimentology Petrology. John Wiley & Sons, New York.

Chakrabarti A.K. [1971]. Studies on sediment movement at the entrance of a tidal river. Sed. Geol., 6:111-127.

Chakrabarti A.K. [1984]. Problems in making relief peels and certain remedial measures. Indian J. Earth Sci., 11:249-254.

Channon R.D. & Hamilton D. [1971]. Sea bottom velocity profiles on the continental shelf southwest of England. Nature, 231:383-385.

Charlesworth J.K. [1957]. The Quaternary Era with Special Reference to its Glaciation, II, Edward Arnold Ltd.

Chauhan O.S. & Chaubey A.K. [1989]. Comparative studies of moment, graphic and phi measures on the sands of East Coast beaches, India. Sed. Geol., 65:183-189.

Christiansen C., Blaesild P. & Dalsgaard K. [1984]. Reinterpreting 'segmented' grain size curves. Geol. Mag., 121:47-51.

Coastal Research Group, [1969]. Massachusetts Uni. Spec. Report 1969.

Collins M.B.C., Amos C.L. & Evans G. [1981]. Observation of some sediment transport processes over intertidal flats, The Wash, U.K. In: S.D. Nio, R.T.E. Schuttenhelm & Tj.C.E. van Weering (eds.), Holocene Marine Sedimentation in the North Sea Basin. Spec. Publ., Int. Asso. Sedimentologists, 5:81-98. Blackwell Sci. Publ., Oxford.

Collinson J.D. & Thompson D.B. [1982]. Sedimentary Structures. George Allen & Unwin, London, 194p.

Collinson J.D. [1970]. Bedforms of the Tana River, Norway. Geogr. Annlr., 52A:31-55.

Cornish V. [1914]. Waves of Sand and Snow and the Eddies which make them. T. Fisher. Unwin, London. 383p.

Costello W.R. & Southard J.B. [1981]. Flume experiments on lower-flow-regime bedforms in coarse sands. J. Sed. Petrol., 51:849-864.

Costello W.R. [1974]. Development of bed configuration in coarse sands. Mass. Inst. Techn. Dept. Earth Sci. Rep. 74(1):1-120.

Cronan D.S. [1972]. Skewness and kurtosis in polymodal sediments from the Irish Sea. J. Sed. Petrol., 42:102-106.

Daily Weather summary 28th Aug. to 4th Sep. [1990]. London Weather Centre, 284-286 High Holborn, London.

Dalrymple R.W., Knight R.J. & Lambiase J.J. [1978]. Bedforms and their hydraulic stability relationship in a tidal environment, Bay of Fundy, Canada. Nature, 275:100-104.

Dalrymple R.W. [1984]. Morphology and internal structure of sandwave in the Bay of Fundy. Sedimentology 31:365-382.

Davies R.A. Jr. & Hayes M.O. [1984]. What is a wave dominated coast ?. Mar. Geol., 60:313-329.

Davies R.A. Jr. [1964]. A morphologic approach to the World shore lines, Zeitfur Geomorph., 8:127-142.

De Boer P.L., Oost A.P. & Visser M.J. [1989]. The diurnal inequality of the tides as a parameters for recognising tidal influences. J. Sed. Petrol., 59(6):912-921.

De Vanssay de Blavous P. [1930]. Slope corrections for echo sounding. Hydrog. Rev., 36(1):29-42.

De Vanssay de Blavous P. [1933]. Slope corrections for echo sounding. Hydrog. Rev., 7(2):50-63.

Dean W.E. Jr. [1974]. Determination of carbonates and organic matter in calcarious sediments and sedimentary rocks by loss on ignition: comparison with other methods. J. Sed. Petrol., 44(1):242-248.

Decca Charts 1411, 1464, 1826, 1973, 1977, 1978 & 1986. Admiralty Hydrographic Dept. Taunton.

Doeglas D.J. [1946]. Interpretation of results of mechanical analysis. J. Sed. Petrol., 16:19-40.

Doeglas D.J. [1968]. Grain size indices, classification and environment. Sedimentology, 10:83-100.

Duane D.B. [1964]. Significance of skewness in recent sediments, Western Pamlico Sound, North Carolina. J. Sed.

Petrol., 34:864-874.

Dyer K.R. [1980]. Velocity profiles over a rippled bed and threshold of movement of sand. Estuarine Coastal Mar. Sci., 10:181-199.

Dyer K.R. [1986]. Coastal and Estuarine Sediment Dynamics. John Wiley & Sons. New York.

Edge M., Hart J.K. & Pointon W.K. [1990]. The sequences at Aber Ogwen and Glan-y-mor-isaf. In: K. Addison, M.J. Edge & R. Watkins (eds.), North Wales Field Guide. Quat. Res. Asso., 119:130.

Edwards W. [1905]. The Glacial Geology of Anglesey. Proc. of the Liverpool Geol. Soc., 10:26-37.

Einstein H.A. [1950]. The bed load function for sediment transportation in open channels. U.S. Dept. of Agriculture, Soil Conservation Serv., Tech. Bull. 1026.

Embleton C. & King C.A.M. [1968]. Glacial and Preglacial Morphology. Edward Arnold Ltd., London, 608p.

Embleton C. [1964]. The deglaciation of Afon and Southern Anglesey and the origin of the Menai Straits. Proc. Geol. Asso., 75(4):407-430.

Engelund F. & Hansen E. [1966]. Investigation of flow in alluvial streams. Acta Plytechnica Scandinavica, Bull. 9, Hydrog. Lab. Techn. Uni. of Denmark.

Engelund F. & Hansen E. [1967]. A monograph of sediment transport in alluvial streams. Technish Vorlag. Copenhagen, 62p.

Engstrom D.R. & Wright Jr. H.E. [1984]. Chemical stratigraphy of lake sediments as a record of environmental changes. In: E.Y. Harwarth & J.W.G. Lund (eds.), Lake Sedimentology and Environmental History. Leicester University Press, 11-67.

Evans G. & Collins M.B. [1975]. The transport and deposition of suspended sediments over the intertidal flats of the Wash. In: J.R. Hails & A. Carr (eds.), Nearshore Sediment Dynamics and Sedimentation. Wiley, Chichester.

Evans G. [1965]. Intertidal flat sediments and their environments of deposition in the Wash. Quart. J. Geol. Soc., London, 121:209-241.

Evans G. [1976]. Intertidal flat sediments and their environments of deposition in the Wash. In: G. de V. Klein, (ed.), Holocene Tidal Sedimentation. Benchmark Papers in Geology, vol. 30, Dowden, Hutchinson.

Fairbridge R.W. [1961]. Eustatic changes in the sea level. In: L.H. Ahrene (eds.), Physics and Chemistry of the Earth. 99-185. Pergamon, London.

Fenemore P.R. [1976]. Reflection and refraction seismic and the acoustically impeccable or 'turbid' nature of some sediments in Tremadog Bay, N Wales, M.Sc. Dissertation. University of Wales, Bangor.

Finley R.J. [1978]. Ebb tidal delta morphology and sediment supply in relation to seasonal wave energy flux, North Inlet, South Carolina. J. Sed. Petrol., 48(1):227-238.

Flemming B.W. [1976]. Side scan sonar: A practical guide. Inc. Hydrog. Rev., 53(1):65-92.

Flemming B.W. [1982a]. A historical introduction to underwater acoustics with special reference to echo sounding, sub-bottom profiling and side scan sonar. In: W.G.A. Russell-Cargill (ed.), Recent Development in Side Scan Sonar Techniques, 3-11.

Flemming B.W. [1982b]. Causes and effects of sonograph distortion and some graphical methods for their manual correction. In: W.G.A. Russell-Cargill (ed.), Recent Development in Side Scan Sonar Techniques, 103-141.

Folk R.L. & Ward W.C. [1957]. Brazos river bar: A study in the significance of grain size parameters. J. Sed. Petrol., 27(1):3-26.

Folk R.L. [1966]. A review of grain-size parameters. Sedimentology, 6:73-93.

Folk R.L. [1974]. Petrology of Sedimentary Rocks. Hemphill Publishing Co., Texas.

Forbes A.M.C [1969]. Electromagnetic monitoring of currents

in the Menai Strait. M.Sc. Thesis, University of Wales, Bangor.

Forrest O.J. & Clark N.R. [1989]. Characterising grain size distributions: evaluation of a new approach using a multivariate extension of entropy analysis. Sedimentology, 36:711-722.

Fouere J.F. [1966]. Sediments in the Menai Straits. M.Sc. Thesis, University of Wales, Bangor.

Frey R.W., Howard J.D., Han S. & Park B. [1989]. Sediments and sedimentary sequence on a modern macrotidal flat, Inchon, Korea. J. Sed. Petrol., 59(1):28-44.

Frey R.W., Howard J.D. & Dorjes J. [1989]. Coastal sediments and patterns of bioturbation, Eastern Buzzards Bay, Massachusetts. J. Sed. Petrol., 59(6):1022-1035.

Frey R.W. & Pemberton S.G. [1985]. Biogenic structures in outcrops and cores. I. Approaches to ichnology. Bull. Canadian Petrol. Geol., 33:72-115.

Friedman G.M. & Johnson K.G. [1982]. Exercises in Sedimentology. Wiley, New York.

Friedman G.M. [1961]. Distinction between dune, beach and river sands from their textural characteristics. J. Sed. Petrol., 31(4):514-529.

Friedman G.M. [1962]. On sorting, sorting coefficient, and the lognormality of grain-size distribution of sandstones. J. Geol., 70:737-753.

Friedman G.M. [1967]. Dynamic process and statistical parameters compared for size frequency distribution of beach and river sands. J. Sed. Petrol., 37(2):327-354.

Gadd P.E., Lavelle J.W. & Swift D.J.P. [1978]. Estimates of sand transport on the New York Shelf using near bottom current-meter observations. J. Sed. Petrol., 48:239-252.

Galle O.K. & Runnels R.T. [1960]. Determination of carbon dioxide in carbonate rocks by controlled loss on ignition. J. Sed. Petrol., 30:613-618.

Garrard R.A. [1977]. The sediments of the South Irish Sea and Nymhpe Bank area of the Celtic Sea. In: C. Kidson &

M.J. Tooley (eds.), The Quaternary History of the Irish Sea, Seel House Press. Liverpool, 69:92.

Gilbert G.K. [1914]. The transport of debris by running water. Prof. Pap. U.S. Geol. Surv., 86:1-263.

Glaister R.P. & Nelson H.W [1974]. Grain size distributions, an aid in facies identification. Bull. Canadian Petrol. Geol., 22:203-240.

Godwin H. [1943]. Coastal peat beds of the British Isles and North Sea. Presidential address to the British Ecological Society. J. Ecol., 31:199-247.

Graf W.H. [1971]. Hydraulics of Sediment Transport. McGraw-Hill Book Co., New York. p 513.

Greenly E. [1919]. The Geology of Anglesey. Memoirs of the Geological Survey of Great Britain, H.M.S.O., London.

Greenly E. [1928]. The Lower Carboniferous rocks of the Menaian region of Caernarvonshire. Quart. J. Geol. Soc. London, 84:382-439.

Greenly E. [1941]. Notes on the glacial phenomena of Arfon. Quart. J. Geol. Soc. London, 97:163-178.

Grim [1953]. Reference from W E Jr. Dean [1974]. Determination of carbonates and organic matter in calcarious sediments and sedimentary rocks by loss on ignition: comparison with other methods. J. Sed. Petrol., 44(1):242-248.

Groen P. [1969]. The Water of Sea. van Nostrand Reinbold Co. London.

Guy H.P., Simmons D.B. & Richardson E.V. [1966]. Summery of alluvial channel data from flume experiments, 1955-1961. Prof. Pap. U.S. Geol. Surv., 4621:1-96.

Hamilton E.L. & Bachman R.T. [1982]. Sound velocity and related properties of marine sediments. J. Acoustic Soc. Ame., 72:1891-1904.

Hardisty J. [1983]. An assessment and calibration of formulation for Bagnold's bedload equation. J. Sed. Petrol., 53(3):1007-1010.

Harms J.C., Southard J.B., Spearing D.R. & Walker R.G.

[1975]. Depositional environments as interpreted from primary sedimentary structures and signification sequences. Soc. Econ. Paleontologist Mineralogists Short Course 2:161p.

Harms J.C. [1969]. Hydraulic significance of some sand ripples. Bull. Geol. Soc. Ame., 80:363-369.

Harris P.T. [1988]. Large-scale bedforms as indicators of mutually evasive sand transport and sequential infilling of wide-mouthed estuaries. Sed. Geol., 57:273-298.

Hart J.K. [1990]. A re-interpretation of the Sequence at Dinas Dinlle. In: K. Addison, M.J. Edge & R. Watkins (eds.), North Wales Field Guide. Quat. Res. Asso., 63:70.

Harvey J.G. & Vincent C.E. [1977]. Observations of shear in near-bed currents in the Southern North Sea. Est. Coast. Mar. Sci., 5:715-731.

Harvey J.G. [1965]. Large sand waves in the Irish Sea. Mar. Geol., 4:49-55.

Harvey J.G. [1968]. The flow of water through the Menai Straits. Geophys. J. Roy. Astr. Soc., 15:517-528.

Hayes J.H. [1933]. Report on the sea trials of deep water echo sounding gear in H M S Challenger and Oromonde. Hydrog. Rev., 10(2):138-159.

Hayes M.O. (ed.), [1969]. Coastal Environments: NE Massachusetts and New Hamashire. Guidebook, Flied trip for Eastern Section of SEMP, May 9-11, 1969, 462p.

Hayes M.O. [1975]. Morphology and sand accumulation in estuaries: An introduction to the symposium. In: L.E. Cronin (ed.), Estuarine Research, 2:3-22, Academic Press Inc., New York.

Hayes M.O. [1979]. Barrier island morphology as a function of tidal and wave regime. In: S. Leatherman (ed.), Proceedings of the Coastal Symposium on Barrier Islands, Academic Press, New York.

Heathershaw A.D. & Carr A.P. [1977]. Measurements of sediment transport rate s using radioactive tracers. Ame. Soc. Civ. Engrs., Proc. Coastal Sediments, 77 Conf.,

Charleston, S.C., 399-416.

Heathershaw A.D. & Hammond F.D.C. [1979]. Swansea Bay (Sker) Project Topic Report, 6. Offshore sediment movement and its relations to observed tidal current and wave data. Inst. Oceanogr. Sci. Rep., 93:1-119.

Heathershaw A.D. & Thorne P.D. [1985]. Seabed noises reveal role of turbulent bursting phenomenon in sediment transport by tidal currents. Nature, 316:339-342.

Heathershaw A.D. [1981]. Comparisons of measured and predicted sediment transport rates in tidal currents. Mar. Geol., 42:75-104.

Helley E.J. [1969]. U.S. Geological Survey Prof. Paper, 562-G.

Henssion M.A. & Whittington R.J. [1987]. Aspects of Quaternary sediments of the Anglesey Sheet. Proc. Geol. Asso. 98:398-400.

Heward A.P. [1981]. A review of wave-dominated clastic shoreline deposits. Earth Sci. Rev., 17:223-276.

Hind D.R. [1974]. Sediments of Beaumaris and Conway Bays. A preliminary study. M.Sc. Thesis, University of Wales, Bangor.

Hine A.C. [1975]. Bedform distribution and migration on tidal deltas in the Chatham Harbour Estuary, Cape Cod, Massachusetts. In: L.E. Cronin (ed.), Estuarine Research, 2:235-252, Academic Press Inc., New York.

Hjulstrom F. [1935]. Studies of morphological activities of river as illustrated by the River Fyris. Bull. Geol. Inst. Uni. Uppsala, 25:221-527.

Hjulstrom F. [1955]. Transportation of detritus by moving water. In: P.D. Trask (ed.), Recent Marine Sediments: A symposium, Society of Economic Paleontologists and Mineralogists, Spec. Publ., 4, Tulsa, Oklahoma.

Howard J.D. & Reineck H.E. [1981]. Depositional facies of high-energy beach-to-offshore sequence: comparison with low energy sequence. Bull. Ame. Asso. Petrol. Geologists., 65:807-830.

Howarth M.J. [1982]. Tidal currents of continental shelf. In: A.H. Stride (ed.), Offshore tidal sands; processes and deposits. Chapman and Hall London. 10-26.

Hunter J.R. & Sherwin T.J. [1979]. The prediction of the motion of oil slicks around the coasts of Anglesey, North Wales. Report U79-3. UCES, Marine Science Laboratories, Menai Bridge.

Huws D.G. [1988]. A seismic survey of the Traeth Lligwy bay area: correlation of land and marine data. M.Sc. Thesis, University of Wales, Bangor.

Hydrographic Department, Admiralty [1960]. The West coast of England Pilot. Hydrographic Dept. Admiralty, London.

Imperato D.P., Sexton W.J. & Hayes M.O. [1988]. Stratigraphy and sediment characteristics of a mesotidal ebb-tidal delta, North Edisto Inlet, South Carolina. J. Sed. Petrol., 58(6):950-958.

Inman D.L. & Chamberlain T.K. [1955]. Particle-size distribution in nearshore sediments. In: J.H. Hough & H.W. Menard (eds.), Finding Ancient Shorelines. Spec. Publ., Soc. Econ. Paleontologists, 3:106-129.

Inman D.L. [1949]. Sorting of sediments in the light of fluid mechanics. J. Sed. Petrol., 19(2):51-70.

Inman D.L. [1952]. Measures for describing the size distribution of sediments. J. Sed. Petrol., 22(3):125-145.

Inokuchi M. & Takayama S. [1973]. Science Report, Tokyo Kyoiku Daigaku, C11:157-169.

Irani R.R. & Callis C.F. [1963]. Particle Size: Measurement, Interpretation, and Application. John Wiley & Sons, 165p.

Jago C.F. & Barusseau J.P. [1981]. Sediment entrainment on a wave graded shelf, Roussillon, France. In: C.A. Nittrouer (ed.), Sedimentary Dynamics of Continental Shelves. Mar. Geol., 42:279-299.

Jago C.F. & Hardisty J. [1984]. Sedimentology and morphodynamic of macrotidal beach, Pendine Sands, SW Wales. In: B. Greenwood & R.A. Davis Jr. (eds.),

Hydrodynamics and Sedimentation in Wave-Dominated Coastal Environments. Mar. Geol., 60:123-154.

Jago C.F. [1974]. The sedimentology of estuarine and coastal plain deposit between Pendine and Wharley points, Carmarthen Bay. Ph.D. Thesis, Dept. of Geology. Imperial College of Science and Technology, London.

Jago C.F. [1980]. Contemporary accumulation of marine sand in a macrotidal estuary, Southwest Wales. In: A.H. Bouma, D.S. Gorshine, C. Monty & G.P. Allen (eds.), Shallow Marine Processes and Products. Sed. Geol., 26:21-49.

Jago C.F. [1981]. Sediment response to waves and currents, North Yorkshire Shelf, North Sea. In: S.D. Nio, R.T.E. Schuttenhelm & Tj.C.E. van Weering (eds.), Holocene Marine Sedimentation in the North Sea Basin. Spec. Publ., Int. Asso. Sedimentologists, 5:283-301. Blackwell Sci. Publ., Oxford.

James J.W. & Wingfield R.T.R. [1987]. Aspects of the seabed sediments in the southern Irish Sea. Proc. Geol. Asso., 98:404-406.

Jasin B. [1976]. Pleistocene microfauna from submarine boreholes in Cardigan Bay. M.Sc. Thesis, University of Wales, Aberystwyth.

Jelgersma S. [1979]. Sea level changes in the North Sea Basin. In: E. Oele et. al. (eds.), The Quaternary History of the North Sea. Acta. Univ. Ups Symp. Univ Ups. Annum Quingentesimum Celebrantis, 2:235-248.

Jones K.P.N., McCave I.N. & Patel P.D. [1988]. A computer-interfaced sedigraph for model size analysis of fine-grained sediment. Sedimentology, 35:163-172.

Jones M.E. [1984]. The tidal stability of megaripples on an intertidal sandbank in the South-Western Menai Strait. M.SC. Thesis, University of Wales, Bangor.

Jones P.G.W. & Haq S.M. [1963]. The distribution of Phaeocystis in the Eastern Irish Sea. J. Cons. Perm. Int. Explor. Mer., 28(1):8-20.

Jones S.E. [1990]. Geophysical properties of surficial

sediments: Textural and Biological controls. Ph.D. Thesis, University of Wales, Bangor.

Jones S.J. [1978]. The sedimentary history of Gallows Point in the Menai Strait. M.Sc. Thesis, University of Wales, Bangor.

Jonys C.K. [1976]. Acoustic measurements of sediment transport. Dept. Fisheries and the Environment, Canada. Sci. Ser. No. 66, Inland Waters Directorate, CCIW Branch, Burlington, Ont., 114p.

Jopling V.A. [1963]. Hydraulic studies on the origin of bedding. Sedimentology, 2:115-121.

Jopling V.A. [1965]. Hydraulic factors controlling the shape of laminae in laboratory deltas. J. Sed. Petrol., 35(4):777-791.

Jopling V.A. [1967]. Origin of laminae deposited by movement of ripples along a streambed: A laboratory study. J. Geol., 75:287-305.

Kachel N.B. & Sternberg R.W. [1971]. Transport of bedload as ripples during an ebb current. Mar. Geol., 10:229-244.

Kelland N.C. & Bailey A. [1975]. An underwater study of sand wave mobility in Start Bay. Rep. Underwat. Asso. 1:74-80.

Kenyon N.H. [1970]. Sand ribbons of European tidal seas. Mar. Geol., 9:25-39.

Key W.H. [1984]. How commercial side scan sonar can help locate mines. Offshore Petrol., 1(6).

Kightley P.J. [1977]. A review of literature concerning the Menai Strait. M.Sc. Literature Review. University of Wales, Bangor.

Kindle E.M. [1917]. Recent and fossil ripple marks. Geol. Surv. Canada Mus. Bull., 25:56p.

Klein G. deV. [1970]. Depositional and dispersal dynamics of intertidal sand bars. J. Sed. Petrol., 40(4):1095-1127.

Klein M. [1982]. A modular sonar system for seabed mapping. In: W.G.A. Russell-Cargill (ed.), Recent Development in Side Scan Sonar Techniques, 11-47.

Knebel H.J. [1989]. Modern sedimentary environments in a large tidal estuary, Delaware Bay. Mar. Geol., 86:119-136.

Kohsiek L.H.M. & Terwindt J.H.J. [1981]. Characteristics of foreset and topset bedding in megaripples related to hydrodynamics conditions on an intertidal shoal. In: S.D. Nio, R.T.E. Schuttenhelm & Tj.C.E. van Weering (eds.), Holocene Marine Sedimentation in the North Sea Basin. Spec. Publ., Int. Asso. Sedimentologists, 5:27-37. Blackwell Sci. Publ., Oxford.

Koldijk W.S. [1968]. On environment-sensitive grain-size parameters. Sedimentology, 10:57-69.

Kolthoff I.M. & Sandell E.B. [1952]. Textbook of Quantitative Inorganic Analysis. The Macmillan Co., New York. 759p.

Komar, P.D. & Cui, B. [1984]. The analysis of grain-size measurements by sieving and settling-tube techniques. J. Sed. Petrol., 54:603-614.

Krenter F. [1921]. Der Flussbau (source is Leliovsky S. An Introduction to Fluvial Hydraulics. Dover Publ. Inc., 43p.

Krumbein W.C. & Pettijohn F.J. [1938]. Manual of Sedimentary Petrology. Appleton-Century-Croftd, Inc., New York, 549p.

Krumbein W.C. [1932]. History of mechanical analysis. J. Sed. Petrol., 2:89-124.

Krumbein W.C. [1934]. Size frequency distributions of sediments. J. Sed. Petrol., 4:65-77.

Krumbein W.C. [1936]. Applications of logarithmic moments to size frequency distributions of sediments. J. Sed. Petrol., 6:35-47.

Krumbein W.C. [1938]. Size-frequency distributions of sediments and the normal phi curve. J. Sed. Petrol., 8:84-90.

Krumbein W.C. [1939]. Graphic presentation and statistical analysis of sedimentary data. In: P.D. Trask (ed.), Recent Marine Sediments. Thos. Murby, London, 558-591.

Krumbein W.C. [1953]. Statical design for sampling Beach

sand. Trans. Ame. Geophys. Union, 34:857-868.

Lane E.W. [1955]. Design of stable channels. Trans. Ame. Soc. Civ. Engrs., 120:1234-1260.

Lane E.W. & Kalinske A.A. [1939]. The relation of suspended to bed material in rivers. Ame. Geophys. Union Trans., 20:637-641.

Langhorne D.N, Malcolm J.O. & Read A.A. [1985]. Observations of the changes of intertidal bedforms over a neap-spring tidal cycle. Institute of Oceanographic Sciences, Report 203, 101p.

Langhorne D.N. & Read A.A. [1986]. The evolution and mechanics of modern intertidal and subtidal bedforms: their relevance to geological structures. J. Geol. Soc. London, 148:957-962.

Langhorne D.N. [1981]. An evaluation of Bagnold's dimensionless coefficient of proportionality using measurements of sand movement. Mar. Geol., 43:49-64.

Langhorne D.N. [1982]. A study of the dynamics of a marine sandwave. Sedimentology, 29:571-594.

Lankford R.R. [1976]. Coastal lagoons of Mexico: their origin and classification. In: M. Wiley (ed.), Estuarine Process vol. II. Academic Press, New York, 182-215.

Larcombe P. [1989]. The post-glacial evolution and present-day processes of Mawddach Estuary. Ph.D Thesis, University of Wales, Bangor.

Leenhardt O. [1967]. Topics in seismic research at the Monaco Oceanographic Mus. Geophys. Pros., 257(6):1154-1544.

Leenhardt O. [1969]. Analysis of continuous seismic profiles. Int. Hydrog. Rev., 46(1):51-80.

Lees B.J. [1981]. Sediment transport measurements in the Sizewell-Dunwich Banks area, East Anglia, U.K. In: S.D. Nio, R.T.E. Schuttenhelm & Tj.C.E. van Weering (eds.), Holocene Marine Sedimentation in the North Sea Basin. Spec. Publ., Int. Asso. Sedimentologists, 5:269-281. Blackwell Sci. Publ., Oxford.

Lees B.J. [1983]. The relationship of sediment transport rates and paths of sandbank in a tidally dominated area off the coast of East Anglia, U.K. Sedimentology, 30:461-483.

Lewis D.W. [1984]. Practical Sedimentology. Hutchinson & Ross, Stroudsburg.

Ludwick J.C. [1972]. Migration of tidal sand waves in Chesapeake Bay entrance. In: D.J.P. Swift (ed.), Shelf Sediment Transport: Processes and Pattern, Dowden, Hutchinson & Ross, Stroudsberg, PA, 377-410.

Luskin B. & Israel H.G. [1956]. PDR Mk V. Tech. Rept. 15 ONRO 27124 Geol., Tech. Rept. 12 CU-35-56 no BSR 64547. Lamont Geol. Obs., Palisades, N. Y.

Maarse H. & Terwindt J.H.J. [1964]. A new method of making lacquer peel sections. Mar. Geol., 1:98-105.

Mahamod Y.B. [1989]. Sedimentary processes in the Dwyryd Estuary. Ph.D. Thesis, University of Wales, Bangor.

Maltman A.J. [1975]. Ultramafic rocks in Anglesey - Their non-tectonic emplacement. J. Geol. Soc. London, 131:593-606.

Marine Science Laboratories. [1976]. Geotechnical mapping of the sea-bed. Final report Part 1 - The Experimental area. NERC contact no. F60/4/22. UCNW, Menai Bridge, Gwynedd.

Mason C.C. & Folk R.L. [1958]. Differentiation of beach, dune and aeolian flat environments by size analysis - Mustang Island, Texas. J. Sed. Petrol., 28:211-226.

Matley C.A. [1928]. The Pre-Cambrian complex and associated rocks of the south-western Lleyn (Caernarvonshire), Quart. J. Geol. Soc. London, 84:440-504.

Mazel C.H. [1985a]. Side scan sonar record interpretation. Klein Associates, Inc., New Hampshire.

Mazel C.H. [1985b]. Side scan sonar : Training Manual. Klein Asso. Inc.

McCammon R.B. [1962]. Efficiencies of percentiles for describing the mean size and sorting of sedimentary

particles. J. Geol., 70: 453-465.

McCave I.N. & Geiser, A.C. [1978]. Megaripples, ridges and runnels on intertidal flats of the Wash, England. Sedimentology, 26:353-369.

McCave I.N. & Langhorne D.N. [1982]. Sound waves and sediment transport around the end of a tidal sand banks. Sedimentology, 29:95-110.

McCave I.N. [1971]. Wave effectiveness at the sea bed and its relationship to bedforms and depositions of mud. J. Sed. Petrol., 41:89-96.

McCave I.N. [1973]. Some boundary-layer characteristics of tidal currents bearing sands in suspension. Mem. Soc. R. des Sci. de Liege, 6:187-206.

McCave I.N. [1978]. Grain size trends and transport along beaches: examples from eastern England. Mar. Geol., 28:M43-M51.

McCave I.N. [1985]. Recent shelf clastic sediments. In: P.J. Brenchley & B.J.P. Williams (eds.), Sedimentology - Recent Development and Applied Aspects, 49-65. Blackwell Sci. Publ., Oxford.

McKee E.D. & Weir G.W. [1953]. Terminology for stratification and cross-stratification in sedimentary rocks. Bull. Geol. Soc. Ame., 64:381-390.

McKee E.D. [1957]. Flume experiments on the production of stratification and cross-stratification. J. Sed. Petrol., 27:129-134.

McKinney R.F., Stubblefield W.L. & Swift D.T.P. [1974]. Large-scale current lineations on the central New Jersey shelf: investigations by side scan sonar. Mar. Geol., 17:79-102.

McLaren P. & Bowles D. [1985]. The effects of sediment transport on grain-size distributions. J. Sed. Petrol., 55(4):457-470.

McLaren P. [1981]. An interpretation of trends in grain size measures. J. Sed. Petrol., 51(2):611-624.

McLaren P. [1982]. Hydraulic control of grain-size

distributions in a macrotidal estuary (Discussion). Sedimentology, 29:437-439.

McManus J. [1988]. Grain size determination and interpretation. In: M.E. Tucker (ed.), Techniques in Sedimentology. Blackwell Sci. Publ. Oxford. 63-85.

McMullen R.M. & Allen J.R.L [1964]. Preservation of sedimentary structures in wet unconsolidated sand using polyester resins. Mar. Geol., 1:88-97.

Meade R.H. [1969]. Landward transport of bottom sediments in estuaries of the Atlantic Coastal Plain. J. Sed. Petrol., 39:222-234.

Middleton G.V. & Southard J.B. [1978]. Mechanics of sediment movement. Short Course 3, Soc. Econ. Paleontologists Mineralogists, Tulsa. 242p.

Middleton G.V. [1976]. Hydraulic interpretation of sand size distributions. J. Geol., 84:405-426.

Miller M.C., McCave I.N. & Komar P.D. [1977]. Threshold of sediment motion under unidirectional currents. Sedimentology, 24:507-528.

Milliman J.D. & Emery K.O. [1968]. Sea level during the past 35,000 years. Science, 162:1121-1123.

MINITAB Statistical Software [1989]. Reference Manual - Release 7.2. PWS Publishers, Duxbury Press, Boston. (Minitab Inc. State College, USA).

Mitchum R.M. Jr. & Vail P.R. [1977]. Seismic stratigraphic interpretation procedure. In: C.E. Payton (ed.), Seismic Stratigraphy - Applications to Hydrocarbon Explorations. Ame. Asso. Petrol. Geologists, Memoir, 26:135-144.

Moss A.J. [1962]. The physical nature of common sandy and pebbly deposits. Part I. Ame. J. Sci., 260:337-373.

Moss A.J. [1963]. The physical nature of common sandy and pebbly deposits. Part II. Ame. J. Sci., 261:297-343.

Moss A.J. [1972]. Bed-load sediments. Sedimentology, 18:159-219.

Mukherjee K.K., Das S. & Chakrabarti A. [1987]. Common physical sedimentary structure in a beach-related open-sea

siliciclastic tropical tidal flat at Chendipur, Orissa, India, and evaluation of the weather condition through discriminate analysis. Senckenbergiana Marit., 19(7/6):261-293.

Newton R.D., Seibold E. & Werner F. [1973]. Facies distribution patterns on the Spanish Sahara continental shelf mapped with side-scan sonar. "Metero" Forsch. - Ergebnisse, Reihe C, 15:55-77.

Nittrouer, C.A. & Sternberg R.W. [1981]. The formation of sedimentary strata in an allochthonous shelf environment: the Washington continental shelf. Mar. Geol., 42:210-232.

Nowell A.R.M. [1983]. The benthic boundary layer and sediment transport. Rev. Geophys. Space Phys., 21:1181-1192.

Operating Manual RCM4/5. [1981]. Recording current meter. Models 4 & 5. Aanderaa Instruments Norway.

Ordnance Survey Sheets, SH 1:10,000; 77,67 (NE, SE, NW, SW), 78 (SE), 68 (SW), & 57 (SE).

Otto G.H. [1939]. A modified logarithmic probability graph for the interpretation of the mechanical analysis of sediments. J. Sed. Petrol., 9:62-76.

pattiaratchi C. & Collins M.B. [1987]. Mechanisms for linear sandbank formation and maintenance in relation to dynamical oceanographic observations. Prog. Oceanog., 19:117-176.

pickrill R.A. [1986]. Sediment pathways and transport rates through a tide-dominated entrance, Rangannu Harbour, New Zealand. Sedimentology, 33:887-898.

postma H. [1967]. Sediment transport and sedimentation in the estuarine environment. In: H.G. Lauff (ed.), Estuaries. 158-179. Ame. Asso. Adv. Sci., Publ. 83, Washington.

Ramsay A.C. [1860]. The Old Glaciers of Switzerland and North Wales. Longman, London.

Ramster J. [1965]. Circulation of the Irish Sea. I.C.E.S.,

Hydrographical Committee, 99p.

Raudkivi A.J. [1976]. Loose Boundary Hydraulics. Pergamon, Oxford.

Reineck H.E., Singh I.B. & Wunderlich F. [1971]. Einteilung der Rippeln uud anderer mariner Sandkorper. Senckenbergina. Marit., 3:93-101.

Reineck H.E. & Singh I.B. [1973]. Depositional Sedimentary Environment. Springer - Verlag Berlin, 439p.

Reineck H.E. & Wunderlich F. [1968]. Classification and origin of flasher and lenticular bedding. Sedimentology, 11:99-104.

Reineck H.E. [1957]. Stechkasten uud Deckweisz, Hilfsmittel des Meeresgeologen: Natur uud Volk, 87:132-134.

Reineck H.E. [1960]. Uber die Entstehung von Linsen uud Flaser Schichten. Abh. Deut. Akad. Wiss., 3:370-374.

Reineck H.E. [1961]. Versteinerte Nordsee: Natur uud Volk, 91:151-162.

Reineck H.E. [1967]. Layered sediments of tidal flats, beaches and shelf bottoms of the North Sea. In: G.H. Lauff (ed.), Estuaries. Ame. Asso. Adv. Sci., Spec. Publ., 83:191-206.

Reineck H.E. [1970]. Reliefgub uud projizierbarer Dickschliff. Senckenberginana. Marit., 2:61-66.

Reineck H.E. [1972]. Tidal flats. In: J.K. Rigby & W.K. Hamblin (eds.), Recognition of Ancient Sedimentary Environments. Soc. Econ. Paleontologists Mineralogists Spec. Publ., 16:146-159.

Reynolds J.M. [1990]. High-resolution seismic reflection surveying of shallow marine and estuarine environments. Mar. Geophys. Res. 12:41-48.

Rigler J.K., Collins M.B. & Williams S.J. [1981]. A high precision digital recording sedimentation tower for sands. J. Sed. Petrol., 51:642-644.

Ritter J.R. [1972]. Sediment transport in a tidal inlet. Proc. 13th Coastal Engng. Conf., Vancouver 1972. 832-842.

Roberts B. [1979]. The Geology of Snowdonia and Llyn: An

out line and field guide. Adam Hilger Ltd., Bristol.

Rouse H. [1938]. Fluid Mechanics for Hydraulic Engineers (Dover edition, 1961). Dover Publ., New York.

Rouse H. [1946]. Elementary Mechanics of Fluid. John Wiley & Sons, New York, 376p.

Rubin D.M. & Hunter R.E., [1982]. Bedform climbing in theory and nature. Sedimentology, 29:121-138.

Sagoe K.M.O. & Visher G.S. [1977]. Population breaks in Grain-size distributions of sand- a theoretical model. J. Sed. Petrol., 47(1):285-310.

Salge U. & Wong H.K. [1988]. Seismic stratigraphy and Quaternary sedimentation in the Skagerrak (northeastern North Sea). Mar. Geol., 81:159-174.

Sanford R.B. & Swift D.J.P. [1971]. Comparison of sieving an settling techniques for grain size analysis, using a Benthos rapid sediment analyser. Sedimentology, 7:257-264.

Schlee J. [1966]. A modified Woods Hole rapid sediment analyse. J. Sed. Petrol., 36:404-413.

Schmidt W. [1925]. Der Massenaustausch in freier Luft und verwandte Erschinungen. In: Probleme der Kosmischen Physik, Bd. 7. Hamburg.

Sedigraph 5000ET Instruction Manual [1986]. Sedigraph 5000ET Particle Size Analyser. Micromeritics Instrument Corporation, Norcoss, Georgia USA.

Sedimentation Seminar [1981]. Comparison of methods of size analysis for sands of the Amazon-Solimoes River, Brazil and Peru. Sedimentology, 28:123-128.

Sengupta S. & Veenstra H.J. [1968]. On sieving and settling techniques for sand analysis. Sedimentology, 11:83-98.

Sha L.P. [1989]. Sand transport patterns in the ebb-tidal delta off Texel Inlet, Wadden Sea, The Netherlands. Mar. Geol., 86:137-154.

Sha L.P. [1990]. Surface sediments and sequence models in the ebb-tidal delta of Texel Inlet, Wadden Sea, The Netherlands. Sed. Geol., 68:125-141.

Shackleton R.M. [1954]. The structure and succession of

Anglesey and Lleyn peninsula, X1 (4):106-108, Adv. Sci. London.

Shackleton R.M. [1956]. Note on the structure and relations of the Pre-Cambrian and Ordovician rocks of south-western Lleyn, Liverpool, Manchester. J. Geol., 1:400-409.

Shackleton R.M. [1969]. The Pre-Cambrian of North Wales. In: A. Wood (ed.), The Pre-Cambrian and Lower Palaeozoic rocks of Wales, 1-22, University of Wales Press, Cardiff.

Shaghude Y. [1990]. Investigation of transport and deposition of sediments in Christchurch Bay, Dorset. M.Sc. Thesis, Dept. of Oceanography, University of Southampton.

Shalowitz A.L. [1930]. Slops correction for echo sounding. Hydrog. Rev., 7(1):82-98.

Shepard F.P. & Curray J.R. [1967]. Carbon-14 determination of sea level changes in stable areas. In: M. Sears (ed.), Progress in Oceanography vol. 4 (The Quaternary History of the Ocean Basin). Pergamon Press Oxford.

Sheriff R.E. [1980]. Seismic Stratigraphy. Boston: International Human Resources Development Cooperation.

Sherwin T.J. & Williams A. [1988]. Menai Straits Tide Tables. UCES Marine Science Laboratories, Menai Bridge.

Sherwin T.J. & Williams A. [1989]. Menai Straits Tide Tables. UCES Marine Science Laboratories, Menai Bridge.

Sherwin T.J. & Williams A. [1990]. Menai Straits Tide Tables. UCES Marine Science Laboratories, Menai Bridge.

Sherwin T.J. & Williams A. [1991]. Menai Straits Tide Tables. UCES Marine Science Laboratories, Menai Bridge.

Sherwin T.J. [1988]. Measurements of current speed using an Aanderaa RCM4 current meter in the presence of surface waves. Continental Shelf Res., 8(2):131-144.

Shields A. [1936]. Application of similarity principles and turbulence research to bedload movement. (translated by W.P. Ott & J.C Van Uchelen), U.S. Dept. Agri. Soil Conservation Service, Coop, Lab. California Institute of Technology. 42p.

Side Scan Sonar mark 1B. [1982]. EG & G Environmental Equipment.

Side Scan Sonar Training Manual [1985]. Side scan sonar, record interpretation (Training Manual). Klein Asso. Inc. N Hampshire, USA.

Side Scan Sonar. [1984]. A comprehensive presentation (manual). EG & G Environmental Equipment Division. Mass., USA.

Simons B.D., Richardson E.V. & Nordin C.F. [1965]. Sedimentary structures generated by flow in alluvial channels. In: G.V. Middleton (ed.), Primary Sedimentary Structures and their Hydraulic Interpretation. Soc. Econ. Paleontologists Mineralogists, Spec. Publ., 12:34-52.

Simpkin P.G. [1976]. Geotechnical mapping of the seabed: Final Report, Part III - Acoustics. Marine Science Laboratories, Menai Bridge, University of Wales, Bangor.

Simpson J.H., Forbes A.M.G. & Gould W.J. [1971]. Electromagnetic observation of water flow in the Menai Straits. Geophys. J. Res. Astr. Soc., 24:245-253.

Sleath J.F.A. [1984]. Seabed Mechanics. John Wiley & Sons, New York.

Slot R.E. & Geldof H.J. [1986]. An improved settling tube system for sand. Delft University of Technology, Department of Civil Engineering, Report no. 86-4. The Netherlands.

Sly P.G., Thomas R.L. & Pelletier B.R. [1983]. Interpretation of grain size measurements derived from water-lain sediments. Sedimentology, 30:219-233.

Smith B. & George T.N. [1961]. British Regional Geology, North Wales, H.M.S.O., London.

Smith D.B. & Parsons T.V. [1965]. Silt movement investigation in the Oxcars spoil ground, Firth of Forth, using radioactive tracers, 1961 & 1964, AERER 4980 (HMSO, 1965).

Solangi S.H. [1992]. Geophysical/sedimentological studies of a Quaternary tidal delta system. Ph.D. Thesis,

University of Wales, Bangor.

Sonar Boomer System [1962]. EG & G Inc., Instructional Manual No. 2449.

Sorby H.C. [1859]. On the structures produced by the currents present during the deposition of stratified rocks. Geologist, 2:137-147.

Soulsby R.L., Atkins R. & Salkield A.P. [1987]. Observations of the turbulent structure of a suspension of sand in a tidal current. Euromech 215, Mechanics of Sediment Transport in Fluvial and Marine Environments.

Steidtmann J.R. [1982]. Size-density sorting of sand-size spheres during deposition from bedload transport and implications concerning hydraulic equivalence. Sedimentology, 29:877-883.

Stein R. [1985]. Rapid grain-size analysis of clay and silt fraction by Sedigraph 5000D: comparison with Coutler counter and Atterberg methods. J. Sed. Petrol., 55(4):590-593.

Stelczer K. [1981]. Bedload Transport: Theory and Practice. Water Resources Publ., PO Box 2841, Littleton, Colorado, USA.

Sternberg R.W. [1967]. Measurements of sediment movement and ripple migration in a shallow marine environment. Mar. Geol., 5:195-205.

Sternberg R.W. [1968]. Friction factors in tidal channels with differing bed roughness. Mar. Geol., 6:243-260.

Sternberg R.W. [1972]. Predicting initial motion and bedload of sediment particles in the shallow marine environment. In: D.J.P. Swift (ed.), Shelf Sediment Transport: Processes and Pattern. Dowden Hutchinson & Ross Stroudsberg, 61-79.

Sternberg R.W. [1976]. Measurements of boundary layer flow and boundary roughness over Campeche Bank, Yucatan. Mar. Geol., 20:M25-M31.

Steward Jr. H.B. [1958]. Sedimentary reflections of depositional environments in San Mignel Lagoon, Baja

California, Mexico. Ame. Asso. Petrol. Geologists Bull. 42:2567-2618.

Stride A.H. [1963]. Current swept sea floor near the southern half of the Great Britain. Quart. J. Geol. Soc. London, 119:175-199.

Stride A.H. [1988]. Preservation of marine sand wave structures. In: P.L. de Boer, A. van Gelder & S.D. Nio, (eds.), Tide-influenced Sedimentary Environments and Facies, 13-22, D. Reidel Publ. Co., Dordrecht (Holland).

Sundborg A. [1956]. The River Klarelven, a study of fluvial processes. Geografiska Annalen, Stockholm.

Taira A. & Scholle P.A. [1974]. Recognition of depositional environments in sediments using settling tube data. Ame. Asso. Petrol. Geologists, Soc. Econ. Paleontologists Mineralogists, Annu. Mtg. Abs., 1:88p.

Taira A. & Scholle P.A. [1979a]. Discrimination of depositional environments using settling tube data. J. Sed. Petrol., 49(3):787-800.

Taira A. & Scholle P.A. [1979b]. Origin of bimodal sands in some modern environments. J. Sed. Petrol., 49(3):777-786.

Taira A. [1973]. A new method for the recognition of sedimentary environments using photo-electric settling tube and stepwise discriminant analysis of sediments. Geol. Soc. Ame. Abs. with Programs, 5:833-834.

Taylor Smith D. [1975]. Geophysical assessment of seafloor sediment properties. Oceanology Int., 75:320-328.

Terwindt J.H.J. & Brouwer M.J.N. [1986]. The behaviour of intertidal sandwaves during neap-spring tide cycles and the relevance for palaeoflow reconstructions. Sedimentology, 33:1-31.

Terwindt J.H.J. [1971]. Sand waves in the southern bight of the North Sea. Mar. Geol., 10:51-67.

Terwindt J.H.J. [1981]. Origin and sequences of sedimentary structures in inshore mesotidal deposits of North Sea. In: S.D. Nio, R.T.E. Schuttenhelm & Tj.C.E. van Weering (eds.), Holocene Marine Sedimentation in the North Sea

Basin. Spec. Publ., Int. Asso. Sedimentologists, 5:4-26. Blackwell Sci. Publ., Oxford.

Thorne P.D., Williams J.J. & Heathershaw A.D. [1989]. In situ acoustic measurements of marine gravel threshold and transport. Sedimentology, 36:61-74.

Thorne P.D. [1986a]. Laboratory and marine measurements on the acoustic detection on sediments transport. J. Acoust. Soc. Ame., 80:899-910.

Thorne P.D. [1986b]. An intercomparison between visual and acoustic detection of seabed gravel movement. Mar. Geol., 72:11-31.

Trask P.D. [1932]. Origin and environment of source sediments of petroleum. Gulf Publ. Co., Houston, 68-76.

Tucker M.J. & Stubbs A.R. [1961]. A narrow-beam echo-ranger for fishery and geological investigations. Brit. J. Appl. Phys., 12:103-110.

Tywonivk N. & Warnock R.G. [1973]. Acoustic detections of bedload fluvial processes and sedimentation. Proc. 9th Canadian Hydrology Symp., Ottawa, Ont., 728-749.

Udden J.A. [1898]. Mechanical composition of wind deposits. Augustana Library Publ., 1:69p.

Udden J.A. [1914]. Mechanical composition of clastic sediments. Bull. Geol. Soc. Ame., 25:655-744.

UNIRAS User's Manual [1990]. User's Manuals; Umimap 2000, Unigraph 2000, Uniedit 2000, Picture Manager 2000, Rascon 2000. UNIRAS A/S, Sobrog, Denmark.

Vail P.R., Mitchum R.M. Jr. & Thompson S. [1977]. Relative changes of sea level from coastal onlap. In: C.E. Payton (ed.), Seismic Stratigraphy - Applications to Hydrocarbon Explorations. Ame. Asso. Petrol. Geologists, Memoir, 26:63-82.

Vail P.R., Todd R.G. & Sangree T.J. [1977]. Chronostartigraphic significance of seismic reflections. In: C.E. Payton (ed.), Seismic Stratigraphy - Applications to Hydrocarbon Explorations. Ame. Asso. Petrol. Geologists, Memoir, 26:99-116.

Van den Berg J.H. [1987]. Bedform migration and bed-load transport in some rivers and tidal environments. Sedimentology, 34:681-698.

Van Rijn L.C. [1984a]. Sediment transport, part 1: bedload transport. J. Hydraul. Engng., Ame. Soc. Civ. Engrs., 110:1431-1456.

Van Rijn L.C. [1984b]. Sediment transport, part III: bed forms and alluvial roughness. J. Hydraul. Engng., Ame. Soc. Civ. Engrs., 110:1733-1754.

Van Rijn L.C. [1986]. Applications of sediments pick-up functions. J. Hydraul. Engng. Ame. Soc. Civ. Engrs., 112(9):867-874.

Van Straaten L.M.J.V. & Kuenen, P.H. [1957]. Accumulation of fine grained sediments in the Dutch Wadden Sea. Geologie Mijnb., 329-354.

Van Straaten L.M.J.V. [1952]. Biogene texture and the formation of shell beds in the Dutch Wadden Sea. Proc. K. ned. Akad. Wet. B55:500-516.

Van Straaten L.M.J.V. [1954]. Sedimentology of recent tidal flat deposits and the psammites de Condroz (Devonian). Geologie Mijnb. 16:25-47.

Van Straaten L.M.J.V. [1959]. Minor structures of some Recent littoral and neritic sediment. Geol. en Mujnbouw, 21:197-216.

Van Straaten L.M.J.V. [1961]. Directional effects of winds, waves and currents along the Dutch North Sea coast. Geologie Mijnb., 40:333-346.

Viard J.P. & Breyer J.A. [1979]. Description and hydrodynamic interpretation of grain size cumulative curves from the Platte River system. Sedimentology, 26:427-439.

Vincent C.E., Young R.A. & Swift D.J.P. [1981]. Bed load transport under waves and currents. Mar. Geol., 39:71-80.

Vincent C.E., Young R.A. & Swift D.J.P. [1982]. On the relationship between bedload and suspended sand transport on the inner shelf, Long Island, New York. J. Geophys.

Res., 87(C6):4163-4170.

Visher G.S. & Howard J.D. [1974]. Dynamic relationship between hydraulics and sedimentation in the Altamaha Estuary. J. Sed. Petrol., 44:502-521.

Visher G.S. [1969]. Grain size distributions and depositional processes. J. Sed. Petrol., 39(3):1074-1106.

Visser M.J. [1980]. Neap-spring cycles reflected in Holocene subtidal large-scale bedform deposits: a preliminary note: Geology, 8:543-546.

Walker P.M. [1977]. A geotechnical survey of the Lavan Sands. M.Sc. Thesis, University of Wales, Bangor.

Walton E.K., Stephens W.E. & Shawa M.S. [1980]. Reading segmented grain-size curves. Geol. Mag., 117:517-524.

Wentworth C.K. [1922]. A scale of grade and class terms for clastic sediments. J. Geol., 30:377-392.

Wentworth C.K. [1929]. Methods of computing mechanical composition types in sediments. Bull. Geol. Soc. Ame., 40:771-790.

Werner F. & Newton R.S. [1975]. The pattern of large-scale bed forms in the Langeland Belt (Baltic Sea). Mar. Geol., 19(1):29-59.

White B.R. [1979]. Soil transport by winds o the Mars. J. Geophys. Res., 84:4643-4651.

Whittow J.B. & Ball D.F. [1970]. North West Wales. In: C.A. Lewis (ed.), The Glaciation of Wales and Adjoining Regions, Longman. London, 21-58.

Wijbenga J.H.A. & Klassen G.J. [1983]. Changes in bedforms under unsteady flow conditions is a straight flume. Spec. Publ., Int. Asso. Sedimentologists, 6:35-48.

Williams G.P. [1967]. Flume experiments on the transport of a coarse sand. U.S. Geol. Soc. Prof. Paper, 562B:31p.

Williams J.J., Thorne P.D. & Heathershaw A.D. [1989]. Comparisons between acoustic measurements and predictions of the bedload transport of marine gravels. Sedimentology, 36:973-979.

Wingfield R.T.R. [1987]. Giant sandwaves and relict

preglacial features on the sea bed west of Anglesey. Proc. Geologists Asso. 98:400-404.

Wright L.D., Coleman J.M. & Thomas B.G. [1975]. Sediment transport and deposition in a macrotidal river channel, Ord River, Australia. In: L.E. Cronin (ed.), Estuarine Research, 2:309-322, Academic Press Inc., New York.

Yalin M.S. [1963]. An Expression for bedload transportation. J. Hydraul. Div., Proc. Ame. Soc. Civ. Engrs., HY3:221-250.

Yalin M.S. [1972]. Mechanics of sediment transport. Pergamon, Oxford

Yang C.S. [1986a]. Estimation of sand transport in the Oosterschelde tidal basin using current meter. Mar. Geol., 72:143-170.

Yang C.S. [1986b]. On Bagnold's sediment transport equation in tidal marine environments and practical definition of bedload. Sedimentology, 33:465-486.

Zarillo G.A. [1982]. Stability of bedforms in a tidal environment. Mar. Geol., 48:337-351.

APPENDIXES

Appendix - I.

Current meter data from UCES.

Station 7			Station 8			Station 9		
Time hrs	Dir. (°)	Speed ms^{-1}	Time hrs	Dir. (°)	Speed ms^{-1}	Time hrs	Dir. (°)	Speed ms^{-1}
1033	128	0.40	1003	291	-0.37	1045	28	0.07
1102	128	0.33	1033	281	-0.33	1118	68	0.12
1134	134	0.18	1103	291	-0.35	1148	114	0.03
1203	188	0.04	1134	308	-0.25	1220	211	0.09
1235	234	0.03	1203	301	-0.24	1249	227	0.36
1303	304	0.10	1238	304	-0.18	1319	188	0.21
1333	308	0.13	1304	221	-0.02	1349	208	0.30
1403	311	0.35	1334	51	-0.07	1418	214	0.32
1433	331	0.44	1403	84	-0.15	1448	246	0.06
1504	304	0.47	1435	131	-0.10	1520	344	0.13
1534	304	0.52	1504	94	-0.22	1549	334	0.09
1605	311	0.39	1534	104	-0.24	1618	318	0.04
1635	301	0.29	1604	111	-0.33	1649	28	0.03
1705	301	0.22	1635	121	-0.28	1718	48	0.08
1735	121	-0.07	1705	131	-0.26	1749	38	0.11
1805	191	-0.06	1733	111	-0.13	1818	44	0.16
1904	318	-0.07	1805	101	-0.06	1847	34	0.26
1935	308	-0.24	1833	98	-0.07	1918	34	0.36
2004	308	-0.49	1904	206	-0.06	1950	28	0.52
2033	301	-0.54	1933	250	-0.04	2018	18	0.56
2105	308	-0.73	2007	274	-0.13	2049	21	0.50
2136	314	-0.75	2035	274	-0.17	2120	21	0.42
2205	314	-0.54	2103	278	-0.26	2149	24	0.34
2235	314	-0.60	2134	281	-0.27	2218	14	0.25
			2204	288	-0.35	2246	31	0.14

Appendix - II. Textural parameters of sediment samples.

A	B	C	D	E	F	G	H	I	J	K
1	12.0	0.00	6.29	93.71	11.32	8.58	8.95	2.65	-0.14	1.03
2	10.0	0.00	3.00	97.00	11.24	8.69	8.85	2.18	0.02	0.81
3	12.0	2.86	73.05	24.09	2.48	4.13	4.35	3.02	0.81	3.21
4	12.4	0.41	97.30	2.29	2.32	2.33	2.40	0.33	0.19	1.43
5	12.0	1.11	90.70	8.19	2.40	2.75	2.51	1.13	0.49	5.69
6	12.0	0.13	97.31	2.56	2.52	2.52	2.63	0.41	0.09	1.40
7	11.3	0.06	29.78	70.16	2.52	7.46	7.35	3.77	-0.19	0.51
8	8.0	0.00	8.86	91.14	11.28	9.47	9.76	2.68	-0.55	1.00
9	10.0	0.00	92.33	7.67	2.32	2.79	2.60	0.79	0.61	2.05
10	11.0	0.00	91.85	8.15	2.38	2.64	2.52	1.21	0.60	6.96
11	12.0	0.22	88.97	10.81	2.49	3.32	2.66	1.58	0.61	9.27
12	13.0	0.06	91.61	8.33	2.43	2.67	2.54	1.19	0.54	7.29
13	12.0	0.08	96.70	3.22	2.32	2.25	2.34	0.30	0.11	1.66
14	11.4	0.04	96.37	3.59	2.36	2.33	2.43	0.31	0.20	1.57
15	11.4	0.13	91.78	8.09	2.28	2.58	2.47	1.19	0.63	6.41
16	9.1	0.21	94.38	5.41	2.28	2.74	2.64	0.83	0.37	1.82
17	8.4	0.59	88.89	10.52	2.60	2.81	2.73	1.65	0.37	5.35
18	12.0	0.00	96.43	3.57	2.28	2.26	2.37	0.34	0.21	1.58
19	12.2	0.23	95.44	4.33	2.27	2.23	2.36	0.33	0.32	2.06
20	12.0	0.13	97.82	2.05	2.28	2.27	2.33	0.25	0.10	1.55
21	12.1	0.18	99.05	0.77	2.24	2.23	2.26	0.21	-0.03	1.28
22	13.0	0.16	96.84	3.00	2.20	2.11	2.19	0.29	0.08	1.41
23	12.8	0.30	99.06	0.64	2.40	2.46	2.48	0.23	0.12	1.43
24	11.0	0.93	96.12	2.95	2.47	2.46	2.59	0.37	0.15	1.51
25	8.0	0.67	96.27	3.06	2.47	2.51	2.64	0.40	0.23	1.38
26	8.0	0.30	94.56	5.14	2.68	2.85	2.80	0.57	0.40	2.90
27	10.2	0.36	97.07	2.57	2.47	2.51	2.61	0.33	0.28	1.43
28	12.0	0.35	92.97	6.68	2.36	2.65	2.42	0.56	0.47	4.63
29	14.0	0.13	97.54	2.33	2.24	2.21	2.28	0.20	0.18	1.73
30	13.0	0.12	97.37	2.51	2.08	2.01	2.09	0.27	-0.01	1.42
31	17.0	0.05	99.37	0.58	2.12	2.07	2.09	0.23	-0.04	1.12
32	16.0	0.28	97.95	1.77	2.08	2.03	2.09	0.24	0.02	1.29
33	14.1	0.80	97.23	1.97	2.24	2.20	2.26	0.23	0.06	1.80
34	11.0	0.27	96.27	3.46	2.44	2.33	2.44	0.33	0.12	1.78
35	10.0	0.47	95.39	4.14	2.56	2.76	2.72	0.34	0.35	1.53
36	7.2	0.00	98.95	1.05	2.76	2.86	2.91	0.27	0.28	1.13
37	7.0	0.11	97.02	2.87	2.76	2.80	2.94	0.31	0.25	1.14
38	11.0	0.30	95.37	4.33	2.44	2.71	2.62	0.38	0.36	1.72
39	13.0	0.52	97.47	2.01	2.32	2.32	2.37	0.22	0.21	1.86
40	15.0	0.94	97.19	1.87	2.16	2.16	2.21	0.25	0.17	1.46
41	19.0	0.87	92.04	7.09	2.20	2.40	2.20	1.10	0.32	7.89
42	20.0	2.02	95.96	2.02	2.08	2.00	2.07	0.30	-0.10	1.63
43	25.0	2.16	88.67	9.17	2.16	2.56	2.24	0.78	0.46	5.22
44	26.0	3.29	89.61	7.10	2.16	2.33	2.16	1.13	0.39	9.08
45	21.0	10.33	84.99	4.68	2.36	2.00	2.22	1.22	-0.42	4.55
46	15.0	2.74	94.05	3.21	2.32	2.07	2.14	0.57	-0.19	1.80

A= Sample no
B= Water depth (m)
C= Gravel % by Wt.
D= Sand % by Wt.
E= Mud % by Wt.
F= Modal grain diameter (Ø)
G= Mean grain size (Ø); moment
H= Mean grain size (Ø); Folk
I= Sorting (Ø)
J= Skewness
K= Kurtosis

cont.....

A	B	C	D	E	F	G	H	I	J	K
47	10.0	0.32	96.54	3.14	2.29	2.37	2.47	0.40	0.33	1.25
48	8.0	0.06	97.61	2.33	2.56	2.67	2.77	0.35	0.22	1.08
49	8.0	0.19	98.89	0.92	2.36	2.40	2.43	0.31	0.22	1.31
50	8.0	3.82	93.18	3.00	2.36	2.18	2.39	0.71	−0.16	1.68
51	9.0	27.69	68.42	3.89	2.40	1.00	0.79	2.44	−0.71	0.74
52	30.0	27.88	64.84	7.28	2.16	1.36	0.86	2.97	−0.40	1.12
53	26.0	24.29	70.72	4.99	2.20	1.35	0.72	2.28	−0.71	1.51
54	0.9	0.00	100.00	0.00	3.00	2.95	3.13	0.24	0.24	0.98
55	1.0	0.01	99.22	0.77	2.88	2.98	3.04	0.26	0.22	1.14
56	0.6	0.05	99.03	0.92	2.84	2.95	3.01	0.30	0.06	1.27
57	0.0	0.00	100.00	0.00	2.92	2.95	3.07	0.23	0.25	1.02
58	0.0	13.35	84.96	1.69	2.96	3.03	3.13	0.25	0.25	1.07
59	0.0	1.77	94.37	3.86	2.96	2.96	3.15	0.27	0.28	1.09
60	−1.0	1.70	96.24	2.06	2.99	3.03	3.13	0.26	0.26	1.06
61	−1.0	0.29	98.85	0.86	2.88	3.01	3.05	0.27	0.24	1.11
62	−1.0	0.27	97.84	1.89	2.92	2.98	3.07	0.28	0.20	1.18
63	0.0	7.40	91.27	1.33	3.00	3.07	3.13	0.29	0.22	1.03
64	−1.0	3.89	91.45	4.66	3.12	3.32	3.21	0.31	0.27	1.22
65	0.0	0.02	98.50	1.48	3.04	3.08	3.16	0.25	0.25	1.15
66	0.0	0.03	96.93	3.04	3.04	3.00	3.13	0.27	0.22	1.18
67	0.0	15.62	84.38	0.00	2.87	2.88	2.96	0.27	0.09	1.26
68	2.0	1.98	97.06	0.96	2.72	2.66	2.73	0.44	−0.17	1.59
69	4.0	0.01	99.62	0.37	2.72	2.74	2.79	0.28	0.16	1.09
70	5.0	0.30	96.85	2.85	2.68	2.68	2.79	0.31	0.19	1.17
71	5.0	0.77	98.14	1.09	2.16	2.18	2.21	0.26	0.12	1.61
72	7.0	5.68	94.32	0.00	1.76	1.65	1.66	0.40	−0.14	1.32
73	7.0	13.53	86.47	0.00	1.80	1.23	1.44	0.99	−0.52	2.03
74	7.0	1.67	98.33	0.00	1.60	1.62	1.64	0.34	0.05	1.19
75	8.0	14.22	84.98	0.80	1.80	1.11	1.28	1.11	−0.50	1.53
76	7.0	0.67	98.85	0.48	2.32	2.38	2.39	0.26	0.12	1.34
77	4.0	0.08	99.47	0.45	2.52	2.26	2.27	0.44	0.02	0.84
78	3.0	0.03	99.09	0.88	2.60	2.46	2.50	0.45	−0.16	0.97
79	2.7	0.33	99.34	0.33	2.16	2.18	2.20	0.44	0.01	1.22
80	2.0	0.09	99.55	0.36	2.16	2.15	2.16	0.48	0.07	0.93
81	2.0	0.14	99.61	0.25	2.32	2.33	2.35	0.43	−0.02	1.18
82	13.0	0.63	98.53	0.84	2.40	2.41	2.46	0.29	0.11	1.71
83	5.0	0.23	96.38	3.39	2.96	2.96	3.12	0.32	0.13	1.29
84	4.0	0.38	90.02	9.60	2.96	3.37	3.22	0.87	0.57	4.27
85	3.0	0.14	96.57	3.29	2.92	2.96	3.12	0.31	0.15	1.26
86	3.0	0.00	99.11	0.89	2.88	2.90	2.94	0.23	0.16	1.10
87	2.0	0.01	99.27	0.72	2.80	2.90	2.96	0.23	0.32	0.91
88	1.0	0.16	99.55	0.29	2.57	2.57	2.59	0.25	0.02	1.47
89	1.0	0.62	98.88	0.50	2.56	2.48	2.48	0.34	−0.08	1.16
90	2.0	0.11	99.45	0.44	2.40	2.46	2.56	0.37	0.12	1.11
91	4.5	6.53	92.14	1.33	2.56	2.26	2.54	1.11	−0.45	3.77
92	6.8	31.13	66.10	2.77	2.32	2.38	2.48	0.39	0.41	1.60
93	7.0	10.90	88.70	0.40	2.12	1.70	2.02	1.07	−0.56	6.97

A= Sample no
B= Water depth (m)
C= Gravel % by Wt.
D= Sand % by Wt.
E= Mud % by Wt.
F= Modal grain diameter (Ø)
G= Mean grain size (Ø); moment
H= Mean grain size (Ø); Folk
I= Sorting (Ø)
J= Skewness
K= Kurtosis

cont.....

A	B	C	D	E	F	G	H	I	J	K
94	7.0	1.17	98.74	0.09	1.84	1.76	1.82	0.26	−0.13	1.28
95	5.0	0.14	99.58	0.28	2.36	2.41	2.43	0.32	0.08	1.44
96	3.7	0.52	99.28	0.20	2.44	2.43	2.45	0.34	−0.08	1.32
97	4.0	0.04	99.68	0.28	2.36	2.36	2.39	0.34	−0.07	1.27
98	4.0	0.05	99.66	0.29	2.48	2.47	2.49	0.33	−0.03	1.22
99	7.0	0.83	87.65	11.52	2.88	3.14	3.05	1.37	0.54	6.27
100	5.0	0.11	94.07	5.82	2.80	3.08	3.00	0.63	0.50	3.80
101	4.0	0.01	99.08	0.91	2.80	2.79	2.89	0.30	0.14	1.05
102	3.5	0.02	96.89	3.09	2.91	2.93	3.06	0.25	0.33	1.20
103	2.5	0.27	99.18	0.55	2.64	2.67	2.69	0.16	0.18	1.36
104	25.0	14.73	83.32	1.95	2.08	1.21	1.73	1.32	−0.76	6.29
105	17.5	0.36	99.04	0.60	2.01	1.94	2.00	0.25	−0.11	1.23
106	13.0	0.04	99.96	0.00	1.97	1.94	1.97	0.25	−0.09	1.23
107	12.1	0.21	99.79	0.00	2.16	2.14	2.15	0.22	−0.04	1.27
108	13.0	0.41	98.85	0.74	2.16	2.03	2.16	0.24	−0.04	1.24
109	13.2	0.09	97.93	1.98	2.12	2.09	2.15	0.23	0.06	1.36
110	12.8	0.11	97.30	2.59	2.20	2.16	2.23	0.26	0.06	1.24
111	12.3	0.13	98.85	1.02	2.28	2.27	2.30	0.20	0.04	1.43
112	12.0	0.00	98.47	1.53	2.24	2.21	2.26	0.15	0.16	1.61
113	13.0	0.05	98.13	1.82	2.16	2.14	2.19	0.21	0.09	1.55
114	5.0	0.00	57.63	42.37	3.23	5.30	5.23	2.73	0.83	0.91
115	1.0	0.03	65.48	34.49	3.24	4.98	5.02	2.67	0.82	1.12
116	0.8	0.14	34.25	65.61	3.12	5.98	6.06	3.09	0.42	0.82
117	0.0	14.17	32.91	52.92	3.16	4.53	5.45	4.27	0.10	1.51
118	0.7	5.05	41.08	53.87	3.00	5.59	5.88	3.66	0.30	1.03
119	2.0	5.27	58.83	35.90	3.06	4.72	4.76	3.75	0.43	1.15
120	4.0	0.04	84.73	15.23	3.06	3.59	3.42	1.30	0.61	5.61
121	3.0	0.11	59.66	40.23	3.28	5.18	5.22	2.70	0.86	1.27
122	2.0	0.96	89.36	9.68	2.79	3.14	3.04	1.13	0.50	4.10
123	1.0	7.43	91.49	1.08	2.44	1.94	2.21	1.19	−0.57	3.45
124	0.0	0.00	98.73	1.27	2.80	2.85	2.92	0.30	0.17	1.26
125	0.0	0.00	99.65	0.35	2.68	2.82	2.85	0.24	0.27	1.08
126	1.0	0.08	99.92	0.00	2.32	2.35	2.38	0.21	0.16	1.53
127	3.0	3.70	96.30	0.00	2.12	2.14	2.14	0.23	0.16	1.65
128	0.5	2.40	82.15	15.45	3.12	3.59	3.42	1.38	0.59	6.43
129	0.0	0.02	90.72	9.26	3.28	3.42	3.42	1.11	0.40	6.09
130	−1.0	8.09	65.82	26.09	3.54	3.83	4.22	2.08	0.59	2.52
131	−1.0	0.28	94.25	5.47	3.04	3.40	3.29	0.39	0.29	1.66
132	−2.0	0.05	92.15	7.80	2.96	3.38	3.25	0.74	0.52	3.35
133	−2.0	0.00	95.82	4.18	3.00	3.06	3.24	0.30	0.28	1.17
134	−2.0	0.00	96.27	3.73	2.96	3.01	3.16	0.27	0.35	1.13
135	−2.0	0.19	96.94	2.87	3.15	3.20	3.34	0.28	0.20	0.94
136	−1.0	0.02	89.04	10.94	3.24	3.50	3.42	1.26	0.54	7.06
137	−1.0	0.30	96.57	3.13	2.32	2.27	2.35	0.42	0.21	2.47
138	1.0	0.37	99.63	0.00	2.24	2.12	2.20	0.29	−0.25	1.56
139	3.2	0.00	98.42	1.58	2.84	2.85	2.95	0.25	0.23	1.33
140	4.0	0.00	97.75	2.25	3.04	3.05	3.20	0.25	0.31	1.05

A= Sample no
B= Water depth (m)
C= Gravel % by Wt.
D= Sand % by Wt.
E= Mud % by Wt.
F= Modal grain diameter (Ø)
G= Mean grain size (Ø); moment
H= Mean grain size (Ø); Folk
I= Sorting (Ø)
J= Skewness
K= Kurtosis

cont.....

A	B	C	D	E	F	G	H	I	J	K
141	4.0	0.00	97.62	2.38	3.00	3.01	3.12	0.26	0.25	1.19
142	3.9	0.01	98.59	1.40	2.76	2.70	2.85	0.19	0.33	1.16
143	3.8	0.01	98.84	1.15	2.64	2.66	2.73	0.17	0.27	1.24
144	0.0	0.00	98.42	1.58	2.88	2.87	2.95	0.28	0.19	1.24
145	0.0	6.50	90.96	2.54	3.00	3.03	3.16	0.32	0.18	1.24
146	0.0	4.93	93.61	1.46	2.72	2.86	2.94	0.35	0.22	1.06
147	0.0	5.02	90.56	4.42	2.92	3.19	3.18	0.41	0.14	1.15
148	0.0	0.85	96.51	2.64	2.96	2.98	3.09	0.35	0.18	1.18
149	0.0	1.57	95.38	3.05	2.95	2.98	3.14	0.29	0.32	1.16
150	0.1	0.00	97.81	2.19	2.92	2.93	3.03	0.25	0.25	1.19
151	0.6	0.00	95.88	4.12	2.96	3.13	3.07	0.34	0.26	1.27
152	3.0	0.00	98.37	1.63	2.84	2.92	3.01	0.26	0.26	1.18
153	4.0	0.01	98.61	1.38	2.72	2.83	2.91	0.26	0.28	1.11
154	11.0	4.48	94.90	0.62	1.76	1.63	1.72	0.55	-0.03	2.00
155	1.6	0.52	98.89	0.59	2.24	2.24	2.25	0.28	0.03	1.44
156	0.8	2.72	96.66	0.62	2.39	2.39	2.43	0.30	0.05	1.59
157	0.3	0.01	98.71	1.28	2.76	2.79	2.86	0.37	0.09	1.18
158	0.0	4.34	94.68	0.98	2.60	2.75	2.81	0.38	0.14	1.09
159	0.5	2.21	96.51	1.28	2.40	2.64	2.70	0.41	0.11	1.01
160	0.4	3.88	93.90	2.22	3.04	3.06	3.23	0.30	0.07	1.42
161	0.8	4.26	94.57	1.17	3.00	2.96	3.05	0.30	0.12	1.32
162	2.0	0.01	99.17	0.82	2.60	2.76	2.81	0.36	0.17	1.15
163	2.0	4.25	95.19	0.56	1.84	1.76	1.78	0.45	-0.12	1.62
164	2.5	0.72	93.69	5.59	2.92	3.14	3.15	0.58	0.22	2.54
165	7.0	0.02	98.92	1.06	2.44	2.51	2.56	0.27	0.27	1.28
166	6.7	83.82	15.35	0.83	-5.08	-4.40	-4.22	3.12	0.39	1.48
167	8.0	33.22	43.67	23.11	2.12	1.80	1.68	4.65	0.06	1.17
168	4.0	26.82	70.78	2.40	2.00	0.38	0.19	2.53	-0.74	0.77
169	4.0	92.83	6.76	0.41	-5.16	-4.41	-4.70	1.63	0.49	2.34
170	6.0	90.13	9.14	0.73	-4.64	-3.26	-4.70	1.65	0.38	2.98
171	6.0	3.01	35.40	61.59	3.04	6.60	6.77	3.41	0.29	0.61
172	6.0	24.75	73.81	1.44	2.00	1.06	0.52	2.36	-0.84	1.72
173	2.0	0.00	96.35	3.65	2.48	2.62	2.76	0.40	0.35	1.02
174	6.0	0.69	68.29	31.02	3.04	4.81	4.94	2.83	0.82	1.30
175	6.0	0.00	34.64	65.36	3.20	6.64	6.73	3.34	0.34	0.59
176	6.0	0.17	33.96	65.87	3.20	6.65	6.76	3.34	0.33	0.59
177	6.0	25.58	38.53	35.89	3.00	2.97	2.54	6.12	-0.11	0.85
178	1.0	0.57	60.24	39.19	3.12	4.99	5.03	2.83	0.72	1.19
179	13.0	24.67	70.59	4.74	2.40	1.77	1.02	2.59	-0.72	0.87
180	8.0	9.32	86.59	4.09	2.46	2.25	2.37	1.17	-0.41	4.77
181	15.0	74.38	24.39	1.23	-4.60	-2.16	-1.89	2.65	0.69	0.67
182	7.0	6.06	92.10	1.84	2.12	1.86	2.09	0.91	-0.33	4.23
183	1.0	7.45	88.90	3.65	2.12	1.89	2.01	0.57	-0.20	1.47
184	6.0	0.08	97.71	2.21	2.64	2.68	2.80	0.29	0.25	1.30
185	3.0	0.50	94.21	5.29	2.76	2.99	2.99	0.58	0.22	1.99
186	3.0	0.64	90.68	8.68	2.60	3.00	2.89	1.08	0.56	4.38
187	3.0	0.01	98.14	1.85	2.56	2.64	2.76	0.34	0.31	1.15

A= Sample no
B= Water depth (m)
C= Gravel % by Wt.
D= Sand % by Wt.
E= Mud % by Wt.
F= Modal grain diameter (Ø)
G= Mean grain size (Ø); moment
H= Mean grain size (Ø); Folk
I= Sorting (Ø)
J= Skewness
K= Kurtosis

cont.....

A	B	C	D	E	F	G	H	I	J	K
188	3.0	0.14	98.53	1.33	2.58	2.67	2.74	0.31	0.24	1.10
189	5.0	0.36	98.64	1.00	2.32	2.23	2.27	0.40	−0.10	1.29
190	10.0	2.33	95.90	1.77	2.28	2.06	2.10	0.54	−0.25	1.26
191	6.5	45.24	53.28	1.48	2.68	2.65	2.76	0.79	−0.25	1.42
192	5.0	0.11	98.74	1.15	2.20	2.20	2.23	0.21	0.17	1.61
193	6.0	0.08	98.85	1.07	2.32	2.32	2.36	0.34	0.05	1.51
194	5.0	1.44	95.73	2.83	2.28	2.28	2.41	0.54	−0.04	1.33
195	3.9	0.00	97.02	2.98	2.75	2.66	2.77	0.34	0.04	1.43
196	3.7	0.25	98.35	1.40	2.44	2.51	2.57	0.26	0.27	1.27
197	3.0	13.98	83.00	3.02	2.12	1.51	1.84	1.43	−0.51	3.14
198	3.2	41.13	54.30	4.57	2.56	0.04	0.34	2.82	−0.50	0.58
199	5.0	0.07	98.63	1.30	2.44	2.59	2.64	0.33	0.22	1.04
200	5.0	0.59	98.30	1.11	2.20	2.19	2.22	0.35	0.07	1.31
201	5.0	3.08	94.69	2.23	2.16	1.94	2.02	0.50	−0.27	1.73
202	4.0	35.50	61.54	2.96	2.11	−0.31	0.07	2.74	−0.76	0.70
203	3.0	2.87	97.13	0.00	2.24	2.18	2.25	0.18	−0.20	1.56
204	4.0	42.27	57.19	0.54	2.00	1.95	1.98	0.34	−0.07	1.25
205	4.0	2.51	97.49	0.00	2.16	2.03	2.08	0.34	−0.42	1.99
206	6.0	0.06	95.76	4.18	2.80	2.76	2.94	0.39	0.10	1.59
207	5.0	0.57	99.43	0.00	2.28	2.29	2.31	0.16	0.01	1.27
208	4.0	0.07	99.93	0.00	2.28	2.17	2.24	0.24	−0.19	1.24
209	3.0	0.08	98.96	0.96	2.32	2.31	2.35	0.20	−0.02	1.51
210	6.0	0.09	99.91	0.00	2.32	2.31	2.32	0.27	0.02	1.55
211	7.5	0.08	97.90	2.02	2.72	2.76	2.85	0.38	0.17	1.04
212	7.0	0.19	97.56	2.25	2.84	2.82	2.92	0.35	0.14	1.07
213	5.4	0.07	98.06	1.87	2.68	2.72	2.80	0.24	0.22	1.22
214	6.0	0.01	97.10	2.89	3.00	2.91	3.05	0.29	0.12	1.14
215	6.5	0.18	95.97	3.85	2.84	2.85	3.03	0.31	0.29	1.24
216	5.8	0.00	95.90	4.10	2.91	3.08	3.03	0.30	0.24	1.30
217	5.7	0.02	98.42	1.56	2.64	2.66	2.73	0.26	0.19	1.24
218	7.0	1.31	95.72	2.97	2.24	2.23	2.35	0.44	0.14	1.67
219	9.0	0.55	93.07	6.38	2.72	2.72	2.77	1.06	0.44	4.93
220	6.0	0.41	96.09	3.50	2.60	2.61	2.75	0.37	0.13	1.71
221	6.0	0.06	98.78	1.16	2.48	2.44	2.48	0.35	−0.04	1.19
222	−1.0	0.00	96.80	3.20	2.76	2.83	2.96	0.30	0.37	1.24
223	0.8	0.00	97.23	2.77	3.01	3.03	3.16	0.29	0.19	1.17
224	0.0	9.40	87.32	3.28	2.88	2.85	2.99	0.28	0.22	1.30
225	0.6	3.65	94.17	2.18	3.00	3.03	3.15	0.28	0.13	1.15
226	1.5	0.43	99.57	0.00	2.28	2.31	2.31	0.32	0.03	1.35
227	9.0	0.35	99.65	0.00	2.12	2.10	2.13	0.20	−0.11	1.34
228	3.0	0.35	95.10	4.55	2.60	2.76	2.75	0.47	0.10	2.06
229	5.0	0.01	98.63	1.36	2.68	2.71	2.78	0.27	0.13	1.15
230	4.8	1.05	87.43	11.52	2.95	3.22	3.20	1.34	0.61	7.22
231	5.0	0.19	93.75	6.06	2.92	3.13	3.08	0.66	0.54	3.66
232	5.0	0.14	96.27	3.59	2.92	2.90	3.07	0.29	0.18	1.33
233	10.5	0.45	95.74	3.81	2.64	2.70	2.85	0.32	0.23	1.22
234	6.0	1.63	98.37	0.00	2.08	2.00	2.03	0.24	−0.16	1.33
235	2.0	0.54	95.82	3.64	2.08	2.06	2.18	0.44	0.20	1.49

A= Sample no
B= Water depth (m)
C= Gravel % by Wt.
D= Sand % by Wt.
E= Mud % by Wt.
F= Modal grain diameter (Ø)
G= Mean grain size (Ø); moment
H= Mean grain size (Ø); Folk
I= Sorting (Ø)
J= Skewness
K= Kurtosis

Appendix - III.

Loss-on-ignition results of selected sediment samples with nine samples; 3 each replicate analysis.

A	B	C	D	A	B	C	D
5	4.717	1.51	5.65	126	4.923	0.63	3.26
6	4.848	3.24	4.75	131	4.936	0.41	6.23
10a	4.049	0.99	5.54	134	4.538	0.56	5.64
10b	4.644	1.02	5.33	139	6.375	1.23	3.86
10c	3.994	1.21	4.14	144	5.041	0.55	4.53
14	5.366	0.80	4.54	145a	5.261	0.21	6.50
16	5.066	1.35	4.05	145b	5.009	0.22	6.42
20	4.625	0.85	3.31	145c	5.294	0.21	6.72
23	5.634	0.83	5.18	147	4.737	0.65	5.75
24	6.147	0.56	7.67	151	4.938	0.72	5.98
29	5.117	1.05	2.79	152	5.948	0.58	4.99
34	3.969	1.20	4.29	158	5.742	0.89	3.55
35	5.612	1.22	5.10	160	4.775	0.60	5.57
40	6.009	0.49	5.76	162	5.874	0.88	3.51
41a	3.836	2.44	7.46	163	5.905	0.68	8.41
41b	4.260	2.39	7.60	179a	4.639	2.45	10.43
41c	4.461	2.55	8.08	179b	5.641	2.36	10.92
46	5.456	0.82	9.47	179c	4.192	2.22	11.37
48	4.669	1.35	4.21	180	5.486	1.79	12.52
52	5.594	1.28	11.48	184	5.713	0.71	6.24
53	5.368	1.32	6.36	187a	4.857	0.31	4.78
56	4.886	1.27	3.61	187b	5.257	0.28	4.48
59	5.748	0.51	6.31	187c	5.025	0.27	4.66
71	5.758	0.70	4.18	189	6.537	0.66	5.33
74	5.836	1.00	6.99	192	5.521	0.64	2.79
79	5.365	0.86	4.63	199	5.929	0.34	4.13
85a	4.594	1.83	6.67	207	6.661	0.53	1.77
85b	5.125	1.82	6.48	211a	4.546	1.09	5.21
85c	5.346	1.88	6.92	211b	4.832	1.04	5.23
88	5.652	0.71	3.62	211c	5.094	1.12	5.42
93	4.473	1.15	5.79	213	5.870	0.42	4.55
96	5.568	0.70	4.37	215	4.914	1.63	4.72
99	5.009	0.32	6.42	219	5.971	1.61	6.45
105	6.037	0.81	4.43	223	4.589	0.36	5.82
107	5.167	0.48	3.65	225	5.364	1.24	5.13
109	4.384	0.64	3.31	227	5.797	0.85	4.83
113	5.675	0.62	3.51	229	5.799	1.02	4.05
114a	4.094	3.62	6.60	231	5.196	1.68	5.59
114b	4.471	3.71	6.16	235a	6.385	0.26	6.44
114c	4.326	3.56	6.64	235b	5.911	0.28	6.24
122	4.768	2.19	5.17	235c	5.356	0.29	6.42

A= Sample no.
B= Dry weight (g)
C= Percentage loss at 550°C
D= Carbonate contents (% by wt.)

Appendix - IV. Replicate analysis results of sediment grain size.

A	B	C	D	E	F	G	H	I	J	K
3	2.480	2.79	4.354	0.26	3.023	0.33	0.809	1.05	3.205	2.72
9	2.320	0.00	2.601	0.66	0.787	1.26	0.616	1.97	2.047	4.91
10	2.373	0.97	2.521	0.67	1.213	0.30	0.601	1.62	6.964	4.38
11	2.487	1.23	2.666	0.63	1.574	0.22	0.605	3.81	8.266	4.93
12	2.427	1.90	2.539	0.41	1.192	0.39	0.540	6.46	7.292	9.87
13	2.320	1.72	2.341	0.99	0.297	2.52	0.146	35.42	1.655	10.15
18	2.293	2.01	2.371	1.35	0.341	11.55	0.214	29.04	1.576	8.84
19	2.267	1.02	2.356	0.43	0.327	3.24	0.320	9.53	2.059	4.55
24	2.467	0.94	2.592	0.87	0.374	2.81	0.150	12.35	1.515	1.70
25	2.467	0.94	2.637	0.39	0.398	2.39	0.226	13.10	1.380	3.86
27	2.467	0.94	2.607	1.50	0.331	1.27	0.284	4.04	1.426	1.53
33	2.240	0.00	2.263	0.42	0.226	0.66	0.058	71.93	1.799	1.49
40	2.160	0.00	2.211	0.12	0.245	1.43	0.172	8.72	1.454	3.87
47	2.293	1.01	2.470	0.60	0.404	2.25	0.330	10.84	1.248	3.10
53	2.200	1.82	0.715	3.93	2.279	1.04	-0.713	3.97	1.515	4.89
60	2.987	0.77	3.134	0.43	0.267	5.74	0.261	13.37	1.055	4.19
67	2.867	0.81	2.960	0.56	0.271	4.62	0.085	51.42	1.263	5.63
74	1.600	0.00	1.637	0.31	0.340	0.29	0.049	9.72	1.192	1.39
81	2.320	1.72	2.350	0.43	0.428	1.75	-0.026	51.42	1.187	0.85
88	2.573	0.90	2.594	0.32	0.254	5.51	0.014	197.15	1.475	7.78
95	2.360	1.69	2.428	0.79	0.314	2.14	0.082	70.82	1.445	4.28
102	2.907	0.79	3.062	0.34	0.247	1.42	0.327	6.91	1.199	1.47
105	2.013	1.15	2.003	0.08	0.253	3.00	-0.104	18.01	1.227	2.40
106	1.973	1.17	1.967	0.36	0.246	3.05	-0.088	32.55	1.234	3.07
111	2.280	0.00	2.302	0.15	0.198	2.47	0.046	109.86	1.433	8.34
112	2.253	1.03	2.279	0.92	0.177	20.87	0.190	21.06	1.735	12.53
114	3.227	6.24	5.231	0.33	2.727	0.61	0.836	0.85	0.910	0.74
115	3.240	0.00	5.022	1.99	2.674	3.65	0.827	0.68	1.122	14.56
119	3.060	0.00	4.765	0.34	3.750	0.36	0.431	0.49	1.158	0.79
122	2.787	0.83	3.038	0.76	1.133	0.67	0.498	0.60	4.104	4.23
129	3.280	1.22	3.413	0.38	1.105	0.74	0.397	4.62	6.091	3.96
135	3.147	1.94	3.335	0.84	0.280	2.28	0.203	53.61	0.936	3.55
142	2.760	0.00	2.851	0.70	0.184	1.57	0.319	12.31	1.159	2.04
149	2.947	1.57	3.144	0.57	0.287	5.02	0.319	10.82	1.158	7.69
156	2.387	0.97	2.436	0.50	0.296	2.36	0.049	21.20	1.594	4.93
163	1.840	0.00	1.782	0.33	0.446	1.86	-0.121	20.46	1.615	2.35
172	2.000	0.00	0.515	1.18	2.359	0.32	-0.837	0.52	1.726	49.72
174	3.040	2.63	4.937	0.38	2.827	0.51	0.825	0.12	1.298	0.69
180	2.453	0.94	2.372	0.93	1.169	4.89	-0.412	5.47	4.770	3.04
188	2.587	1.79	2.742	0.81	0.312	4.29	0.236	30.50	1.098	1.24
195	2.747	0.84	2.771	0.45	0.337	0.62	0.039	142.72	1.430	9.79
202	2.113	0.54	0.070	7.25	2.742	2.94	-0.763	1.19	0.703	6.45
209	2.320	0.00	2.344	0.29	0.201	2.29	-0.020	315.60	1.513	6.87
216	2.907	3.46	3.031	0.56	0.295	4.10	0.242	24.29	1.298	8.40
223	3.013	0.77	3.164	0.44	0.290	1.07	0.183	34.80	1.163	4.31
230	2.947	0.78	3.197	0.31	1.336	0.11	0.611	3.28	7.219	3.92

A= Sample no.
B= average Mode
C= CV of Mode
D= average mean grain size
E= CV % of mean grain size
F= average sorting
G= CV % of sorting
H= average skewness
I= CV % of Skewness
J= average Kurtosis
K= CV % of kurtosis

Appendix - V

The total sediment transport load formula of Engelund & Hansen used/quoted by different research workers. Bold parameters were omitted in the originals, and double underlined parameters were incorrectly added in the originals.

Heathershaw [1981]

$$q_{st} = 0.05 p_s U^2 \left[\frac{d_{50}}{[(ps-p)/p)]g} \right]^{1/2} \left[\frac{\tau}{(ps - p) d_{50}\ g} \right]^{3/2}$$

Mahamod [1989]

$$\theta = \left[\frac{\tau}{(p_s - p) g d} \right]^{\underline{5/2}}$$

$$q = \frac{0.1}{C_f} \mathbf{ps} \left\{ \frac{p_s - p}{p} \mathbf{g} d^3 \right\}^{0.5} \left\{ \frac{\tau}{(p_s - p)\ gd} \right\}^{2.5}$$

Larcombe [1989]

$$jtot = 0.05 Ps U^2 \ (D50/g((Ps-P)/P))^{0.5} \ (T/((Ps-P) D50 \mathbf{g}))^{1.5}$$

Solangi [1992]

$$\theta = \left[\frac{\tau}{(p_s - p) g d} \right]^{\underline{5/2}}$$

$$q = 0.05 p_s U^2 \left[\frac{d_{50}}{[(ps-p)/p)]\mathbf{g}} \right]^{1/2} \left[\frac{\tau}{(\mathbf{ps}\ \underline{\mathbf{p}} - p) d_{50}\ \mathbf{g}} \right]^{3/2}$$